FACULDADE DE ENGENHARIA DA UNIVERSIDADE DO PORTO

Development of a machine to measure the impact strength of adhesive joints

André Filipe Lemos Antunes Palma Ramos

Mestrado Integrado em Engenharia Mecânica

Supervisor: Prof. António Mendes Lopes

Co-Supervisors: Inv. Carlos Moreira da Silva
Prof. Lucas FM da Silva

July 2016

Development of a machine to measure the impact strength of adhesive joints

André Filipe Lemos Antunes Palma Ramos

Mestrado Integrado em Engenharia Mecânica

July 2016

Resumo

O estudo e caracterização de adesivos e juntas adesivas é impulsionado na FEUP pelo ADFEUP (Grupo de Adesivos da Faculdade de Engenharia da Universidade do Porto). É do interesse do ADFEUP dispor de um dispositivo capaz de realizar ensaios ao impacto em juntas adesivas e dessa necessidade advém a criação deste projeto.

Este trabalho tem como objetivo o desenvolvimento e implementação de uma máquina para ensaios ao impacto em juntas adesivas. Esta máquina deverá ser capaz de medir e registar a força de impacto em função do deslocamento e a energia desse impacto. A conceção e desenvolvimento da máquina foi efetuada anteriormente em duas dissertações separadas, onde Carlos Castro desenvolveu o projeto mecânico e Rui Barbosa desenvolveu o projeto de automação.

Foi feita uma revisão do projeto mecânico e desenvolvidos os modelos necessários para as análises estáticas e dinâmicas da estrutura. As alterações necessárias para a maquinagem e montagem ser realizável foram também executadas. Foi também implementada a instrumentação em falta que garante o funcionamento correto da lógica de comando.

Por fim a lógica de comando, a interface gráfica de utilizador e sistemas de controlo foram redesenhados recorrendo às ferramentas do software *MATLAB GUIDE* e *Simulink*

Abstract

The study and characterization of adhesives and adhesive bonded joints is studied at FEUP by ADFEUP (Adhesives Group of the Faculty of Engineering of University of Porto). It is in the interest of ADFEUP to have a device capable of performing impact tests in adhesives in order to promote investigation on this subject.

This work has the purpose of develop and implement a machine capable of performing impact tests on adhesive joints. This machine should be able to measure and record the impact force in function of the deflection and energy of impact. The original design and development were performed by two past thesis, in which Castro developed the mechanical design and Barbosa developed the automation.

The mechanical design was revised and the necessary models to perform a static and dynamic analysis of the structure were developed. The necessary changes to ensure the manufacturing and assembly of the components were implemented. The necessary instrumentation that satisfies the command logic was also implemented.

Finally, the command logic, graphical user interface and control systems were redesigned using the MATLAB tools, GUIDE and Simulink.

Acknowledgements

Firstly, I wish to express my gratitude to Prof. António Mendes Lopes, Inv. Carlos Moreira da Silva and Prof. Lucas da Silva, supervisors of this thesis, for all the support, patience and availability during the development of this thesis, even at the most occupied times, and providing me with the opportunity to work in such an interesting project.

To Ricardo Carbas and Eduardo Marques, members of ADFEUP, for all the support and contributions made to the project.

To Prof. Dias Rodrigues, for his input and expertise.

To Fernando Pereira, for all the valuable discussions that, directly or indirectly, produced significant breakthroughs.

To Mr. José and Mr. Albino, for all the input and hard work in the workshop.

To Luís Sousa Martins, André Costa, Tiago Soares, Teresa Morim, Rita Marques, Inês Mesquita, Carolina Neves, Ricardo Castro and Fábio Fernandes for their friendship and company in this final moments of my academic life.

To Diogo Pereira, João Paulo Silva, João Carlos Nogueira and José Teixeira for their forever present friendship.

To my family, for always expecting the best of me.

Lastly, a very special thank you to my girlfriend, Cátia Batalha, for her patience and support in all the moments of my life.

André Ramos

"One day I will find the right words,
and they will be simple."

Jack Kerouac

Contents

Resumo i

Abstract iii

Acknowledgements v

Acronyms and Symbols xix

1 Introduction 1
- 1.1 Thesis motivation . . . 1
- 1.2 Thesis objectives . . . 1
- 1.3 Thesis layout . . . 2

2 Impact test of adhesive joints 5
- 2.1 Commercial machines . . . 5
  - 2.1.1 Rosand IFW5 . . . 5
  - 2.1.2 Zwick HIT230F . . . 5
  - 2.1.3 Instron Ceast 9350 . . . 5
  - 2.1.4 Imatek IM10T-25 . . . 6
  - 2.1.5 Summary . . . 6
- 2.2 Types of impact tests . . . 7
  - 2.2.1 Tensile impact test of SLJ . . . 7
  - 2.2.2 Mode I fracture . . . 8
  - 2.2.3 Mode II fracture . . . 8
  - 2.2.4 Cleavage fracture . . . 9

3 Mechanical design 11
- 3.1 Structure . . . 12
  - 3.1.1 Base . . . 14
  - 3.1.2 Guiding system . . . 15
  - 3.1.3 Static analysis . . . 19
  - 3.1.4 Dynamic analysis . . . 22
- 3.2 Lifting subsytem . . . 25
  - 3.2.1 Bellhousing . . . 26
  - 3.2.2 Barrel and screw . . . 27
  - 3.2.3 Axial connector, holders and shafts . . . 28
  - 3.2.4 Lifting subsystem base . . . 28
  - 3.2.5 Coupling and gears . . . 29
- 3.3 Carriage and release . . . 29

3.3.1 Carriage . . . 29
3.3.2 Linear ball bearings . . . 30
3.3.3 Cylinder-carriage connection . . . 30
3.3.4 Release clamp . . . 32
3.4 Drop-weight . . . 34
3.4.1 Configurations . . . 35
3.4.2 Hanging rod . . . 35
3.4.3 Anvil . . . 36
3.4.4 Clearance control . . . 38
3.4.5 Impactor and connections . . . 39
3.4.6 Top masses . . . 40
3.4.7 Lateral masses . . . 41
3.5 Impact velocity acquisition . . . 42
3.5.1 Supports . . . 42
3.5.2 Screw drive . . . 43

4 Actuation and instrumentation 45
4.1 Lifting subsystem . . . 45
4.2 Carriage and release subsystems . . . 47
4.2.1 Release . . . 47
4.2.2 Upper limit detector . . . 50
4.2.3 Drop-weight detector . . . 50
4.3 Drop-weight . . . 50
4.3.1 Accelerometer . . . 52
4.3.2 Signal condition and data acquisition unit . . . 52
4.4 Impact velocity acquisition subsystem . . . 52
4.4.1 Photoelectric detector . . . 54
4.4.2 Gearmotor . . . 56
4.4.3 Travel limit switch . . . 57

5 Command and control 59
5.1 State diagram . . . 59
5.1.1 Initialization routine . . . 60
5.1.2 Manual control . . . 61
5.1.3 Changing mass . . . 64
5.1.4 Changing tool or specimen . . . 64
5.1.5 Parameter input . . . 65
5.1.6 Release . . . 65
5.1.7 Results . . . 66
5.1.8 Emergency . . . 67
5.1.9 Auxiliary routines . . . 67
5.2 User interface . . . 70
5.2.1 Physical interface . . . 70
5.2.2 Graphical user interface . . . 70
5.3 Control . . . 75
5.3.1 Mathematical model of the system . . . 75
5.3.2 Velocity control . . . 79
5.3.3 Position control . . . 82

6 Conclusion **85**
6.1 Conclusions . . . 85
6.2 Future work . . . 86

A Drawings **89**
A.1 Assembly drawings . . . 89
A.2 Technical drawings . . . 95

B MATLAB code **137**
B.1 Solving a system of differential equations . . . 137
B.2 Computation of [x,F] . . . 140

C Datasheets **143**
C.1 Elesa+ganter leveling foot . . . 143
C.2 Ball bearings . . . 148
C.3 Linear ball bearings . . . 155
C.4 Locknut . . . 158
C.5 T-bolt . . . 160
C.6 Gears . . . 162
C.7 Rotex coupling . . . 164
C.8 Aluminum 7075 T651 properties . . . 168
C.9 Kistler K-Shear accelerometer . . . 170
C.10 Ruland coupling . . . 172
C.11 Transtecno Gearmotor ECM-100/040 . . . 174
C.12 Drive Electromen EM-12A . . . 182
C.13 Directional valve Parker B3R5BXXXXH . . . 185
C.14 Barrel inductive proximity sensor RS Pro 701-8253 . . . 189
C.15 Photoelectric sensor by diffuse reflection Omron E3FA-DN23 . . . 192
C.16 Kistler K-Shear Shock Accelerometer 5000g . . . 195
C.17 Charge amplifier and data acquisition unit Kistler LabAmp . . . 199
C.18 Photoelectric sensor through beam Omron EE-SX670-WR 1M . . . 205
C.19 DC gearmotor Como Drills 918D100112 . . . 211
C.20 Roller lever microswitch Cherry D459-V3RD . . . 214

References **217**

List of Figures

1.1 Rivet joint vs Adhesive joint . . . 2
1.2 Single Lap Joint (dimensions in mm) . . . 3

2.1 Illustrations of the several impact machines . . . 6
2.2 Instrumented Pendulum Test . . . 7
2.3 SLJ impact test using a drop weight machine . . . 8
2.4 Opening Mode I . . . 8
2.5 Carlberger Mode I setup . . . 8
2.6 Opening Mode II . . . 9
2.7 ENF specimen . . . 9
2.8 Wedge peel setup . . . 10
2.9 Wedge peel support and specimen . . . 10

3.1 Original Machine . . . 11
3.2 Original Structure . . . 13
3.3 Improved structure . . . 13
3.4 Base schematic . . . 14
3.5 Shoe . . . 14
3.6 Impactor area . . . 15
3.7 Elesa+Ganter leveling foot . . . 15
3.8 Guiding system . . . 16
3.9 Clamp and sleeve fit scheme . . . 17
3.10 Guiding system adjustment . . . 17
3.11 Guiding rod linearity worst case scenario . . . 18
3.12 Analogous guiding rod . . . 19
3.13 Structural layout . . . 20
3.14 Structural analysis . . . 22
3.15 Discrete model . . . 23
3.16 Force transmitted to the leveling foot . . . 25
3.17 Lifting subsystem . . . 26
3.18 Lifting subsystem comparison . . . 26
3.19 Bellhousing . . . 27
3.20 Barrel and screw renders . . . 27
3.21 Barrel recess (dimensions in mm) . . . 28
3.22 Lifting subsystem base . . . 28
3.23 Rotex 19 . . . 29
3.24 Gear . . . 29
3.25 Carriage and release subsystem comparison . . . 29

3.26 Carriage schematic (dimensions in mm) . . . 30
3.27 Cylinder-carriage connection schematic . . . 30
3.28 Stress . . . 31
3.29 Displacement . . . 32
3.30 Release clamp assemble . . . 32
3.31 Original release clamp functionality description . . . 33
3.32 Original energy profile . . . 34
3.33 Cylinder-carriage connection simulation . . . 34
3.34 Drop-weight configurations . . . 35
3.35 Hanging rod . . . 36
3.36 Anvil . . . 37
3.37 Base and feet spring system representation . . . 37
3.38 Anvil impact simulation . . . 38
3.39 Clearance control (dimension in mm) . . . 38
3.40 Original impactor . . . 39
3.41 Impactor attach method . . . 39
3.42 Connecting part . . . 39
3.43 Impactor and connecting part simulation . . . 40
3.44 Top extensions assembly . . . 41
3.45 Lateral extensions assembly . . . 41
3.46 Impact velocity acquisition subsystem . . . 42
3.47 Bottom support . . . 43
3.48 Top support . . . 43
3.49 Optical detector support . . . 43
3.50 igus drylin® screw drive . . . 43
3.51 Lead screw connections . . . 44

4.1 Parvalux PM60G . . . 45
4.2 Gearmotor Transtecno ECM-100/040 . . . 46
4.3 Drive Electromen EM-12A . . . 47
4.4 Solenoid Kuhnke V45 . . . 47
4.5 Pneumatic system . . . 48
4.6 Pneumatic cylinder SMC C85N25-25S . . . 48
4.7 Directional valve Parker B3R5BXXXXH . . . 49
4.8 L-shped flow regulator G $^1/_8$ to 4 mm . . . 49
4.9 Silencer G $^1/_8$ . . . 49
4.10 Male stud coupling G $^1/_8$ to 4mm . . . 49
4.11 Barrel inductive proximity detector RS Pro 701-8253 . . . 50
4.12 Distance between top extension and carriage at the coupling . . . 51
4.13 Photoelectric detector Omron E3FA-DN23 . . . 51
4.14 Piezoelectric load cell Kistler 9361B . . . 51
4.15 Kistler K-Shear Shock Accelerometer 5000g . . . 52
4.16 Signal conditioning and data acquisition unit Kistler LabAmp . . . 52
4.17 Velocity acquisition subsystem . . . 53
4.18 Actual velocity evolution $v(t)$ compared to measured velocity v_m . . . 53
4.19 Photoelectric detector through beam Omron EE-SX670-WR 1M . . . 55
4.20 Interfering part . . . 55
4.21 DC gearmotor Como Drills 918D100112 . . . 56
4.22 Motor control circuit . . . 57

4.23 Roller lever microswitch Cherry D459-V3RD 57
4.24 Path limit switch assemble circuit 58

5.1 State diagram 60
5.2 Flowchart key 60
5.3 Initialization routine state flowchart 61
5.4 Manual control state flowchart 63
5.5 Changing mass state flowchart 64
5.6 Changing tool or speci. state flowchart 64
5.7 Parameter input state flowchart 65
5.8 Release state flowchart 66
5.9 Results state flowchart 67
5.10 Set impact point routine flowchart 68
5.11 Picking routine flowchart 69
5.12 Velocity acquisition routine flowchart 69
5.13 Physical panel mockup 70
5.14 Welcome panel mockup 71
5.15 Initialization routine dialog boxes 71
5.16 Manual control panel mockup 72
5.17 Changing mass dialog box 73
5.18 Parameter input panel mockup 73
5.19 Release panel mockup 74
5.20 Results panel mockup 74
5.21 Positioning model of discrete parameters 75
5.22 Screw free body diagram 78
5.23 Proportional motor velocity control system 80
5.24 Velocity ramp response 81
5.25 m_z position evolution 81
5.26 Proportional motor position control system 82
5.27 Angular position response to half sinusoidal wave signal 83
5.28 Mass m_z position response to half sinusoidal wave signal 83

List of Tables

2.1 Summary of impact test machines 6

3.1 Profile properties 21
3.2 Load weight 21
3.3 Coefficient values 24
3.4 Mass and energy range of each configuration 35

4.1 Transtecno ECM-100/040 properties 46
4.2 Relative error between v_m and v_i 54
4.3 H-bridge control summary 57

5.1 Lifting subsystem inertia properties 76

Acronyms and Symbols

FEUP	Faculdade de Engenharia da Universidade do Porto
ADFEUP	Adhesives Group at FEUP
SLJ	Single Lap Joint
DCB	Double Cantilever Beams
ENF	End-Notch Flexure
LET	Laboratório de Ensaios Tecnológicos
DEMec	Departamento de Engenharia Mecânica
ϕ	Diameter
ξ	Damping ratio
F_{max}	Maximum clearance
$T_{\odot}$	Concentricity tolerance
H	Column height
I	Second-area moment
E	Modulus of elasticity
m_i	Mass of element i
k_i	Spring constant of element i
c_i	Damping coefficient of element i
v_I	Impact velocity
m_I	Impact mass

Chapter 1

Introduction

In this first chapter, the subject of study is introduced by exposing the thesis motivation, the objectives and the thesis layout.

1.1 Thesis motivation

Adhesive joints exhibit many advantages over classical mechanical joints, namely the ones that use bolts and rivets. First and foremost, the adhesive area is spread over a larger surface than the classical joints without the need to drill holes, where it creates a stress concentration, as shown in Figure 1.1. Other advantages include reduction in structural weight, higher fatigue resistance and vibration damping. On the other hand, these adhesives joints also show poor chemical resistance and vulnerability to hostile environments, needing proper surface preparation, process control and maintenance repairs.

Currently, the use of structural adhesives joints is expanding in many industries, specifically in the automotive industry in order to decrease weight and therefore, reduce the fuel consumption. Figure 1.2 shows the Single Lap Joint (SLJ) that due to its simplicity and efficiency, is the most common type of adhesive joint.

In vehicles, the joint will often be exposed to impact and although the behaviour of the SLJ is well understood in static conditions, its impact behavior is still a subject needing of considerable investigation.

1.2 Thesis objectives

This thesis aims to develop an experimental machine able to measure the impact resistance of adhesive joints. The device will be based on the past two thesis, where the automation [1] and mechanical design [2] were developed.

On a first stage, the mechanical and automation projects ought to be revised and their missing subsystems are required to be designed (rebound and security). Secondly, it is necessary to order the chosen components, elaborate the technical drawings, manufacture several parts and finally,

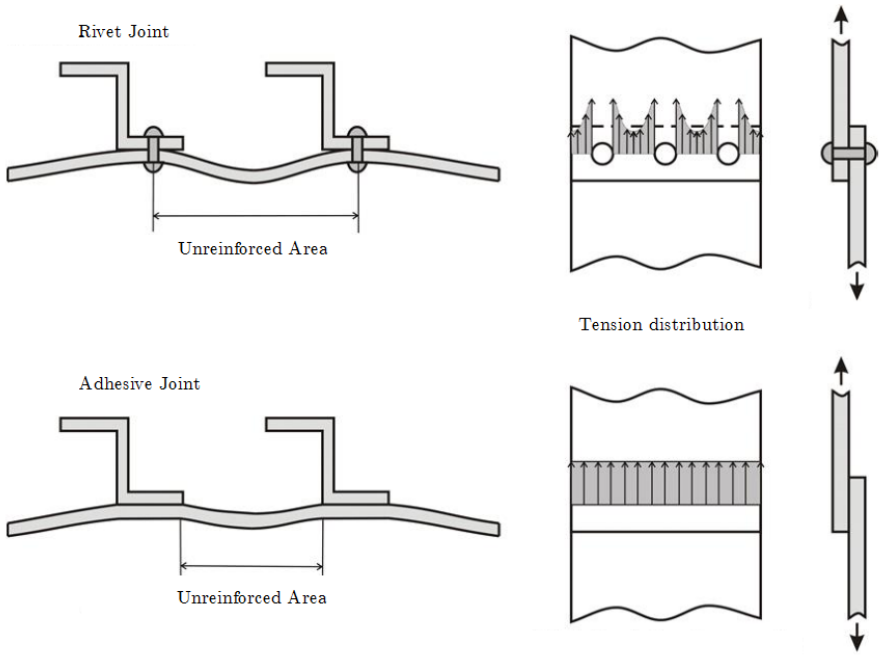

Figure 1.1: Rivet joint vs Adhesive joint

assemble the device. Thirdly, the command application must be developed in agreement with the specification. Finally, some experimental validation should be acquired through the testing of some samples.

1.3 Thesis layout

This thesis is organized by chapters that address different topics that are considered relevant to understand the machine importance, functionality or implementation.

Chapter 2 introduces some commercial models able to perform impact tests, as well as the types of tests that these models should be able to accomplish on adhesive joints.

Chapter 3 comprises the structural and design changes made to the machine to guarantee the assemble, manufacture and implementation of every component.

Chapter 4 encompasses the selection of electrical and electromechanical components needed to automate the machine.

Chapter 5 discusses the command logic and control system needed to comply with the specification.

Chapter 6 concludes with the current state of the implementation and proposed future work.

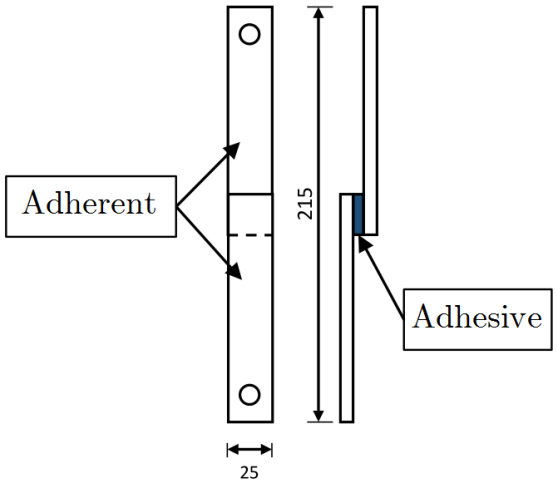

Figure 1.2: Single Lap Joint (dimensions in mm)

Chapter 2

Impact test of adhesive joints

Along this chapter, several commercially available impact test machines will be presented, as well as the tests that they should be able to perform.

2.1 Commercial machines

Currently there are several manufacturers that provide drop-weight impact test machines although not all of them are intended to be used for testing adhesive bonded joints specifically. In this section will be presented and compared the specifications for the commercially available machines that most resemble the desired machine, along with the existing impact machine in the faculty facilities.

2.1.1 Rosand IFW5

Currently, in the *Laboratório de Ensaios Tecnológicos* (LET) at *Departamento de Engenharia Mecânica* (DEMec) sits the impact test machine Rosand IFW5, shown in Figure 2.1a. Through the years the machine has suffered several adaptations to improve its performance but it is still limited to 300 J and 4 m/s which is not acceptable in the implementation of several test types [2]. The force acquisition period is based on the total time of acquisition (from impact moment onward), as the machine has a fixed value of 1000 samples per test.

2.1.2 Zwick HIT230F

The ZWICK HIT230F has the simplest design of the machines mentioned in [1] and [2] as it can be inferred from Figure 2.1b, altough it comes at the expense of functionality. The Zwick HIT230F is only to function up to 230 J and 4.4 m/s. Despite this, the acquisition rate is able to go up to 4 MHz.

2.1.3 Instron Ceast 9350

Amongst several commercial machines available in the market, there are two that are fairly similar to the machine presently under development. One of them is the Instron Ceast 9350 (Figure 2.1c).

This machine is capable of testing the desired materials in the 0.59 to 757 J range, allowing a maximum speed of 5.0 m/s. It is able to acquire the force intensity during the impact at a frequency of 2 MHz and has the option of having a temperature chamber added to perform the test in a controlled temperature environment.

2.1.4 Imatek IM10T-25

Finally, there is the Imatek IM10T-25, shown in Figure 2.1d. This model works in the 2.5 to 735 J range, up to 7 m/s and with an acquisition rate of 3 MHz. Although this machine does not come with a temperature chamber, it does have the electrical parts separated from the structure, which seems interesting from the impact induced vibrations point of view.

2.1.5 Summary

In Figure 2.1 the previously mentioned machines are illustrated and in Table 2.1 it is shown a summary of the main differences between them.

(a) Rosand IFW5 (b) Zwick HTI230F (c) Instron Ceast 9350 (d) Imatek IM10T-25

Figure 2.1: Illustrations of the several impact machines

Table 2.1: Summary of impact test machines

Machine	IFW5	HTI230F	CEAST 9350	IM10T-25
Energy [J]	up to 300	up to 230	0.59 – 757	2.5 – 735
Maximum velocity [m/s]	4	4.4	5.0	7.0
Force acquisition frequency [MHz]	Variable[1]	4	2	3
Temperature chamber	No	No	Yes	No

[1] See Section 2.1.1

2.2 Types of impact tests

In this section it will be thoroughly discussed the current implementation of impact tests.

Although the Izod and Charpy impact tests are specified for both metallic materials and thermoplastics, these are not suitable for adhesive testing since the results produced are of difficult interpretation and consequently of difficult application [3].

2.2.1 Tensile impact test of SLJ

As referenced in Section 1.1 the SLJ is the most common adhesive joint and therefore it is paramount to better understand its behavior when subject to an impact induced dynamic load. To answer this, Harris and Adams [4] developed the Instrumented Pendulum Test, shown in Figure 2.2.

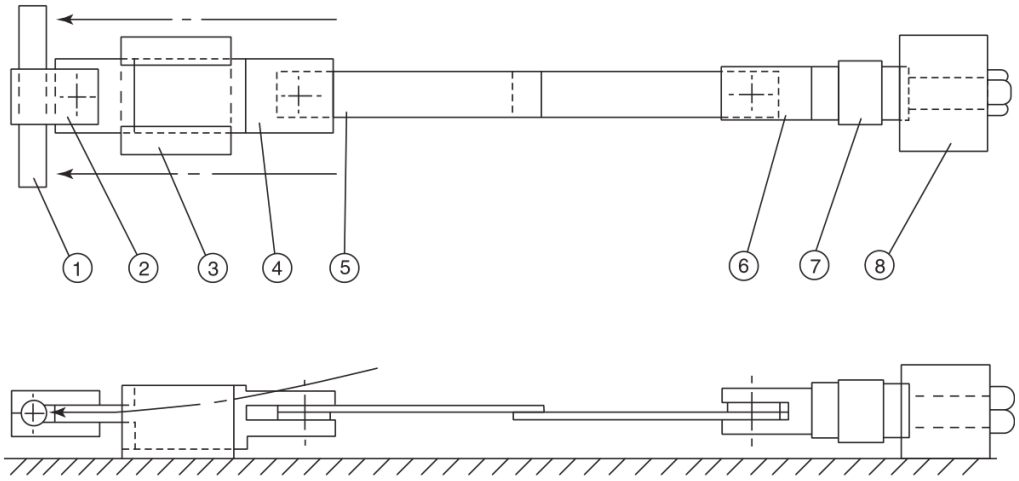

1. Impacted bar
2. End clamp
3. Journal bearing block
4. Bearing shaft and specimen clamp
5. Specimen
6. Specimen clamp
7. Force transducer
8. Fixed end block

Figure 2.2: Instrumented Pendulum Test [3]

With this tool, the pendulum should impact the bar (No. 1 in Figure 2.2), moving the bearing shaft (No. 4) frictionless through the journal bearing block (No. 3) causing a dynamic force to be read by the force transducer (No. 7).

This method has the downside of inducing a significant amount of vibration in the specimens that can difficult the interpretation of the data collected [3]

In recent past, Liao, Sawa and Huang [5] developed an alternative test using a drop weight machine. In Figure 2.3 it is portrayed the solution adopted, which is constituted by two separated bodies that when exposed to an impact stress, transmit the load to the SLJ and the strain is measured by the strain gauges A & B. At the time, this was considered to be the most effective method to test SLJ to tensile impact loads.

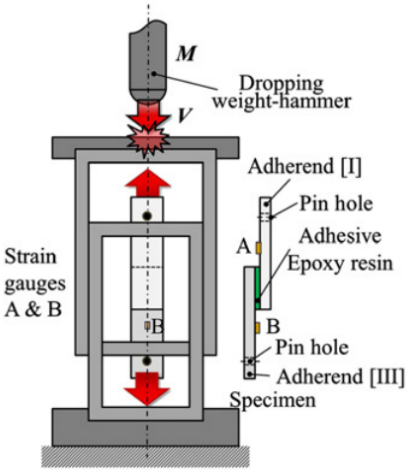

Figure 2.3: SLJ impact test using a drop weight machine [5]

2.2.2 Mode I fracture

In joint design, mode I, is the opening mode in which the loads are normal to the crack, exemplified in Figure 2.4.

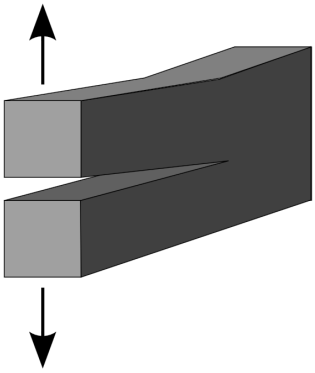

Figure 2.4: Opening Mode I

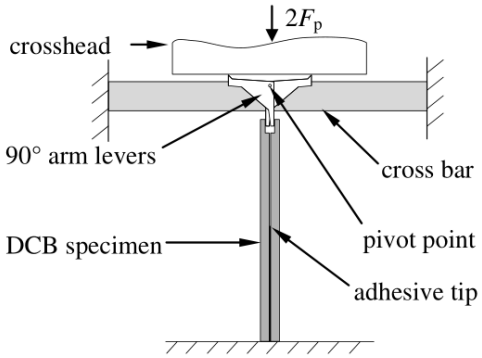

Figure 2.5: Carlberger Mode I setup [6]

In 2009, Carlberger [6] used the setup shown in Figure 2.5 to test double cantilever beams (DCB) specimens do dynamic forces using a servo-hydraulic testing machine. The same concept should be able to be applied to a drop weight machine.

2.2.3 Mode II fracture

Opening Mode II, illustrated in Figure 2.6, is an in-plane shear opening mode where the crack surfaces slide over one another in a direction perpendicular to the leading edge of the crack and is typically tested using an end-notch flexure (ENF) specimen [3]. The adhesive thickness t_A shown in Figure 2.7a causes the adherents to slide in the long axis when they curve under the influence

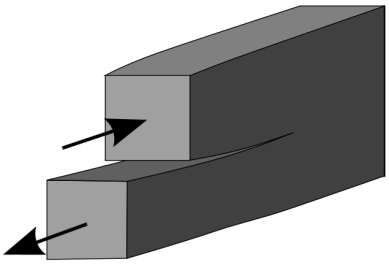

Figure 2.6: Opening Mode II

of the load P. This test can be done by dynamic forces, such as impact, without any adaptations (Figure 2.7b).

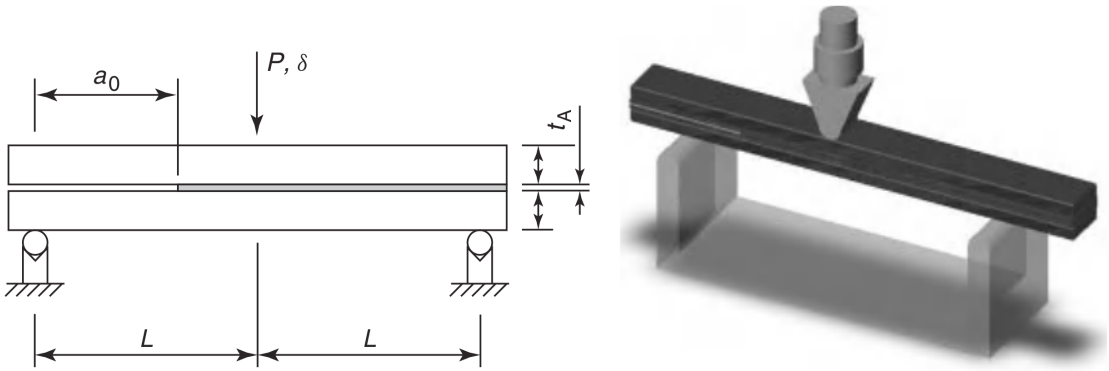

(a) Testing setup [3] (b) 3D Model [3]

Figure 2.7: ENF specimen

2.2.4 Cleavage fracture

Finally, it is also interesting to measure the cleavage fracture resistance by performing a wedge-peel impact test. In Figure 2.8 it is illustrated the setup of the test, where it is shown that the specimen should be shaped like a tuning fork, and a wedge is drawn through the bonded portion of the specimen [7]. In Figure 2.9 it is shown a real life application of the setup to be used in a drop weight machine.

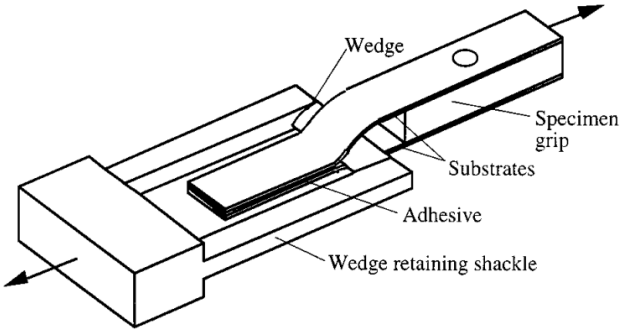

Figure 2.8: Wedge peel setup [7]

Figure 2.9: Wedge peel support and specimen [8]

Chapter 3

Mechanical design

Impact test machines are used to measure the energy absorbed by the specimen in a controlled impact situation. These tests cause sudden load variations and a considerable peak impact force. As a result, along with the ability to create an impact situation and measure the relevant physical properties, the machine should have a robust structure adequate to handle the stress caused by the aforementioned tests.

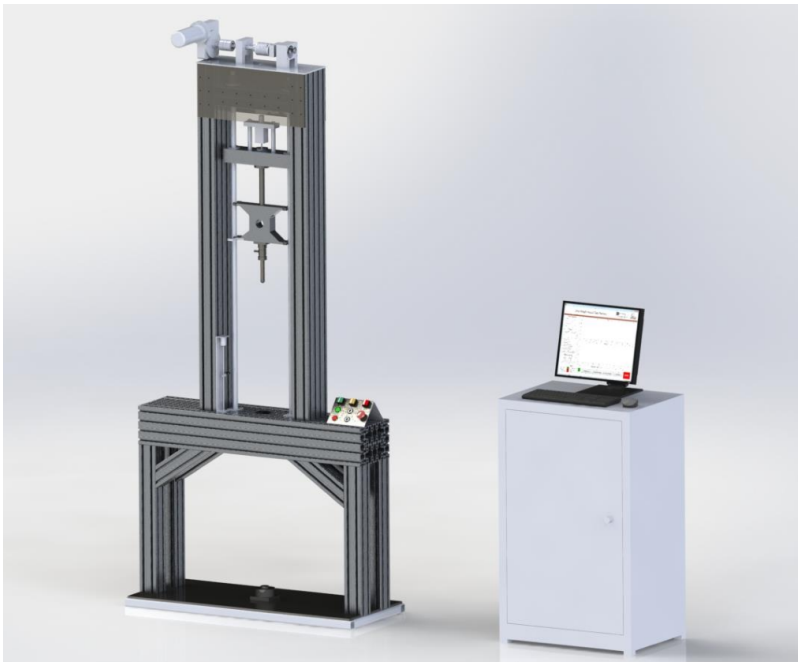

Figure 3.1: Original Machine

The machine conceived by Barbosa [1] and Castro [2] (Figure 3.1) uses the drop-weight method, which consists in lifting a given mass to a specified height, followed by a free fall, causing the mass itself to collide with the tool connected to the specimen with an energy $E = mgh$, where m is the mass, g is the gravitational acceleration and h the drop height.

The specification established in the past theses between the authors and ADFEUP was as follows:

- Maximum energy at the moment of impact: 700 J;
- Maximum speed at the moment of impact: 5 m/s;
- Drop height positioning resolution: 1 mm;
- Positioning speed: 0.1 m/s;
- High acquisition rate during the moment of impact.
- A minimum energy at the moment of impact of 50 J, at maximum speed.

In order to implement the machine developed in the prior theses, some changes had to be performed and these are explained in the subsequent sections, one for each of the following subsystems:

- Structure (Section 3.1)
- Lifting (Section 3.2)
- Carriage and release (Section 3.3)
- Drop-weight (Section 3.4)
- Impact velocity acquisition (Section 3.5)

3.1 Structure

The original structure shown in Figure 3.2 had an excessive number of profiles that complicated the structure assembly and increased the error in verticality of the final assembly.

To address this problem, the upper columns were extended to the base and spaced to 600 mm (Figure 3.3 – 2), allowing enough working space to accommodate the tools and specimens intended to be used by ADFEUP. The lateral supports were replaced by a 15 mm thick steel support and the tables for UNP180 steel profiles.

These changes are detailed in the assembly and technical drawings exhibited in Appendix A.2 (0–E and E–1 to E–9 respectively)

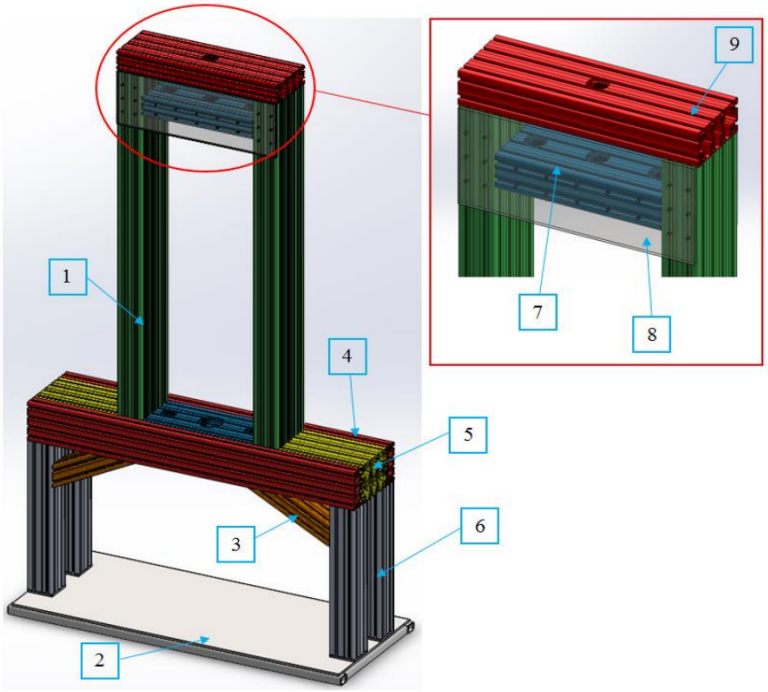

1. Upper column
2. Base
3. Reinforcement
4. Lateral support
5. Outer table
6. Inferior column
7. Table
8. Upper plate
9. Top profile

Figure 3.2: Original Structure [2]

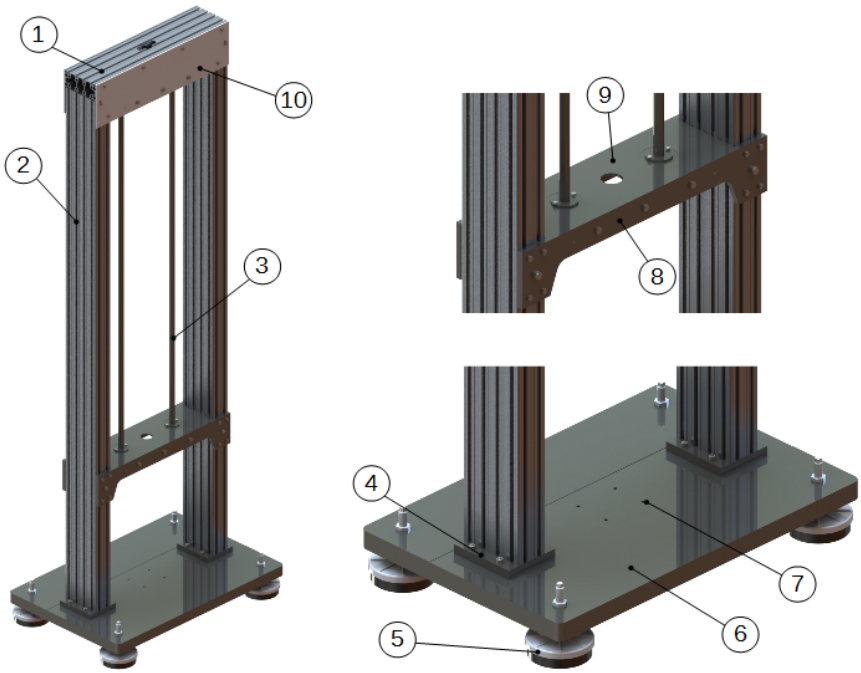

1. Top profile
2. Column
3. Guiding rod
4. Shoe
5. Feet
6. Base
7. Tool connection
8. Lateral support
9. Table
10. Top plate

Figure 3.3: Improved structure

3.1.1 Base

The base was intended to be a welded structure (Figure 3.2 – 2), but due to the difficulty in welding structures in FEUP, a part was designed as solid steel plate (Figure 3.3 – 6). This part would only need to have 4 sets of 4 holes: 1 for the feet, 2 to connect to the columns and 1 to connect to the tool (Figure 3.3 – 7). The connection surface would need to have a considerable flatness, achieved by milling a lengthwise band (Figure 3.4).

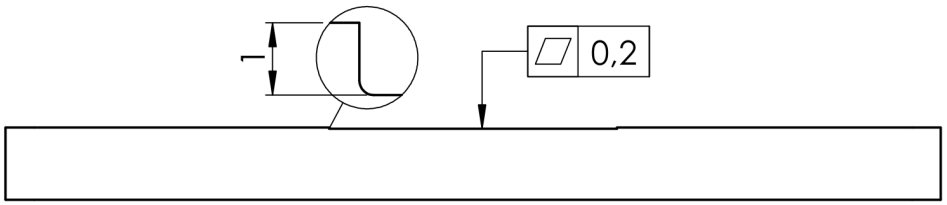

Figure 3.4: Base schematic

In order to facilitate the assemble and, if necessary, the disassemble, a shoe (Figure 3.5) was conceived to change the assemble orientation.

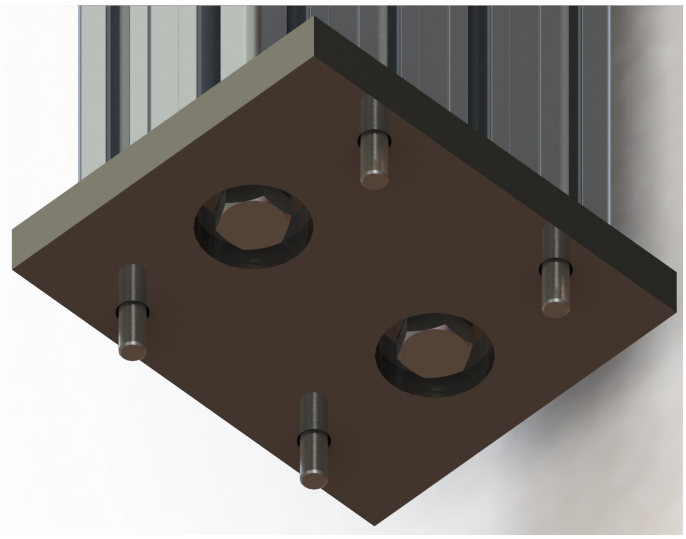

Figure 3.5: Shoe

The simulation in Section 3.4.5.1 indicates a maximum stress of 1160 MPa in the area of impact, painted in red in Figure 3.6. According to SolidWorks [9], this area equals 28.27 mm^2.

This leads to,

$$F = \sigma A = 33.44 \text{ kN}$$

where F is the resulting force, σ is the normal stress and A is the area where the stress is applied.

That consequentially, led to choosing the Elesa+Ganter LW.A-160-M20x1.5x170 leveling foot. These are able to function up until a max load of 80 kN. Assuming an inflationed total mass for the machine of 1500 kg (the entire structure subsystem has under 450 kg) that generates

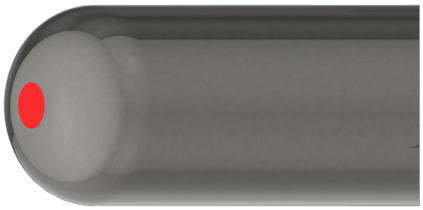

Figure 3.6: Impactor area

a maximum load of 48.1 kN, well under the admissible 80 kN. It also has good damping properties, beneficial for managing the shock induced vibrations.

Outer ϕ	Thread	Max load	Max deflection	Stiffness	ξ
160 mm	M20 $\times$ 1.5	20 kN	2.2 mm	9000 N/mm	0,1 [10]

Figure 3.7: Elesa+Ganter leveling foot [11]

3.1.2 Guiding system

To ensure a correct guiding function, several aspects had to be carefully envisioned.

To prevent buckling on the guiding rods, caused by its own weight, they should only be secured by the top side and guided in the bottom side (Figure 3.8a). It also deals with the problems caused by different thermal expansion coefficients of the aluminum structure and steel guides.

By machining the UNP profiles as illustrated in Figure 3.8b the lodging holes are ensured to be lined up and the profiles are ensured to have the same length. The faces where the clamp and sleeve are mounted should have a specified flatness to ensure the guiding rods parallelism, and consequently the verticality by adjusting the feet.

To guarantee the correct assembly of the system, an asymmetric tolerance scheme was considered.

On the left, both the clamp and the sleeve should have a slight interference fit and on the right a free running fit, as exhibited in Figure 3.9. In the assemble, the left guiding rod should

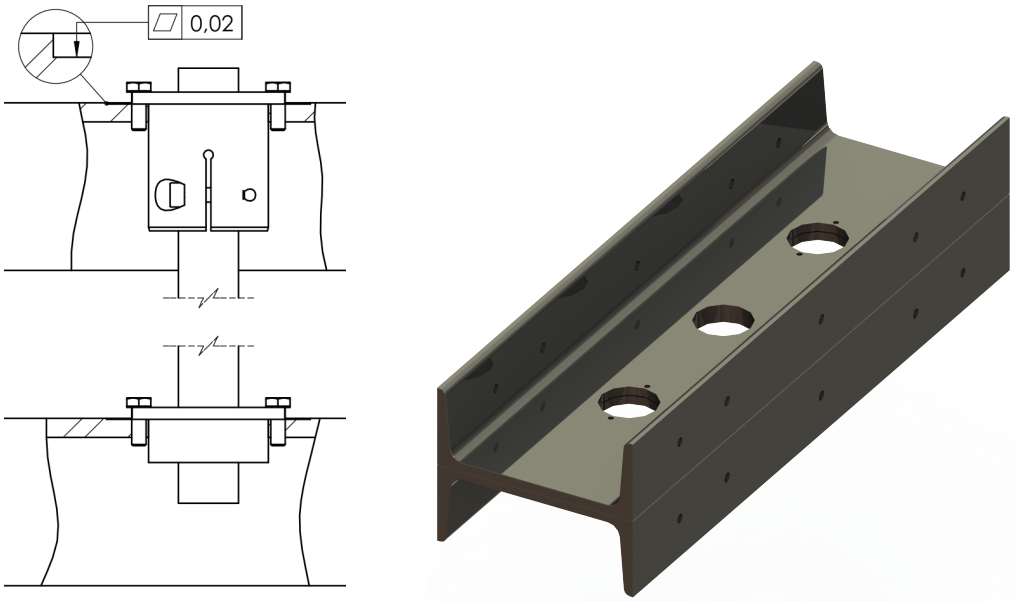

(a) Guiding rod assemble (b) UNP machining

Figure 3.8: Guiding system

be tightened first and subsequently, the carriage (Section 3.3.1) should be used to adjust the right guiding rod.

Although the parallelism is assured this way, the linearity of the left guiding rod, is still not ensured. To comply with the other functional elements, namely the clearance control and linear ball bearing (Sections 3.4.4 and 3.3.2 respectively), the guiding rod should be:

- Under 0.3 mm of axial center deviation to ensure friction-less free-fall
- Under $30'$ of angle deviation since this is the maximum misalignment compensation provided by the linear ball bearings

To accomplish these points, the guiding rod mounting hole was given a perpendicularity tolerance of ϕ 0.01 mm in relation to the support surface and a concentricity tolerance of ϕ 0.01 mm relative to the outside surface center axis, was chosen (Drawings E–2 and E–4 in Appendix A.2).

Since α, β and $\theta \ll \pi/12$ (Figure 3.11)

$$\tan \alpha, \beta, \theta = \sin \alpha, \beta, \theta = \alpha, \beta, \theta$$

The tolerance values were check against worst case scenario illustrated in Figure 3.11

The δ is the maximum distance between the clamp and sleeve axis and is equal to,

$$\delta = 2 \cdot \frac{F_{max}}{2} + \frac{T_{\odot}}{2} \tag{3.1}$$

where F_{max} is the maximum clearance between the outside surface and the table hole and $T_{\odot}$ is the concentricity tolerance.

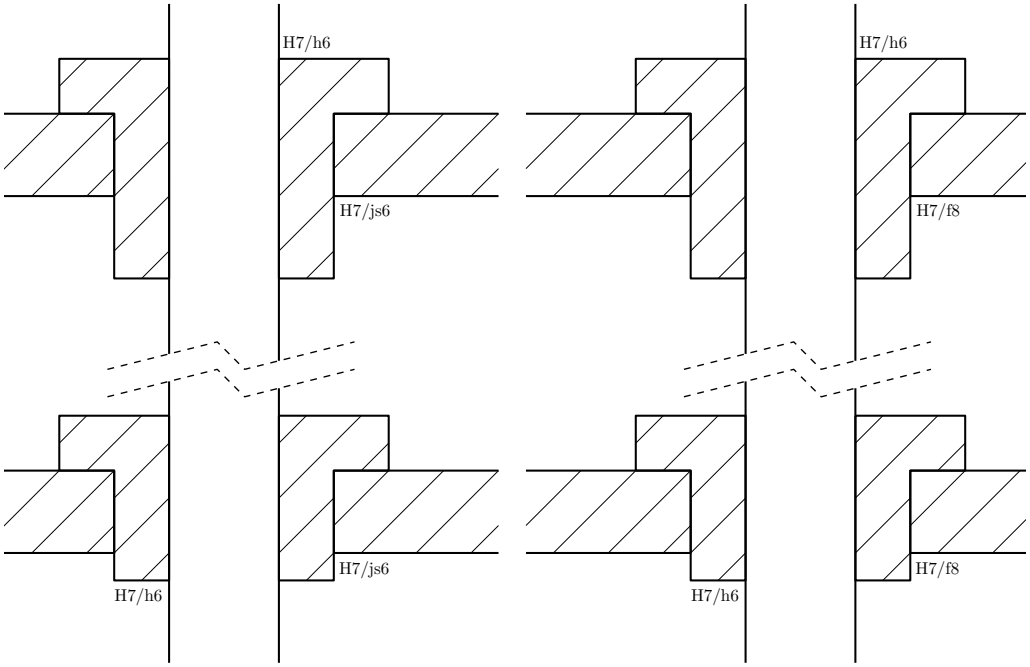

Figure 3.9: Clamp and sleeve fit scheme

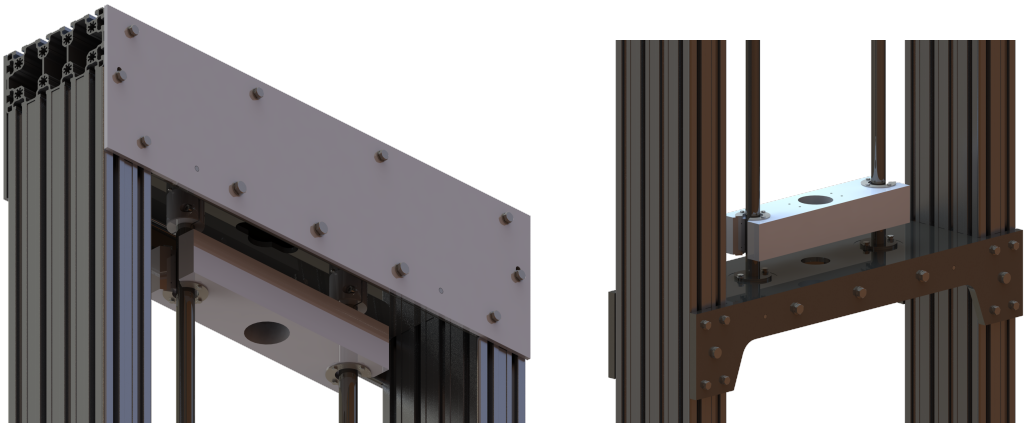

Figure 3.10: Guiding system adjustment

According to Simões Morais [12],

$$F_{max} = D_{max} - d_{min} = \text{IT7} + \frac{\text{IT6}}{2} = 33\ \mu\text{m}$$

where D_{max} is the maximum diameter of the hole, d_{min} the minimum diameter of the shaft, IT7 and IT8 are the respective tolerance classes and es is the shaft upper deviation.

Returning to Equation 3.1,

$$\delta = 38\ \mu\text{m}$$

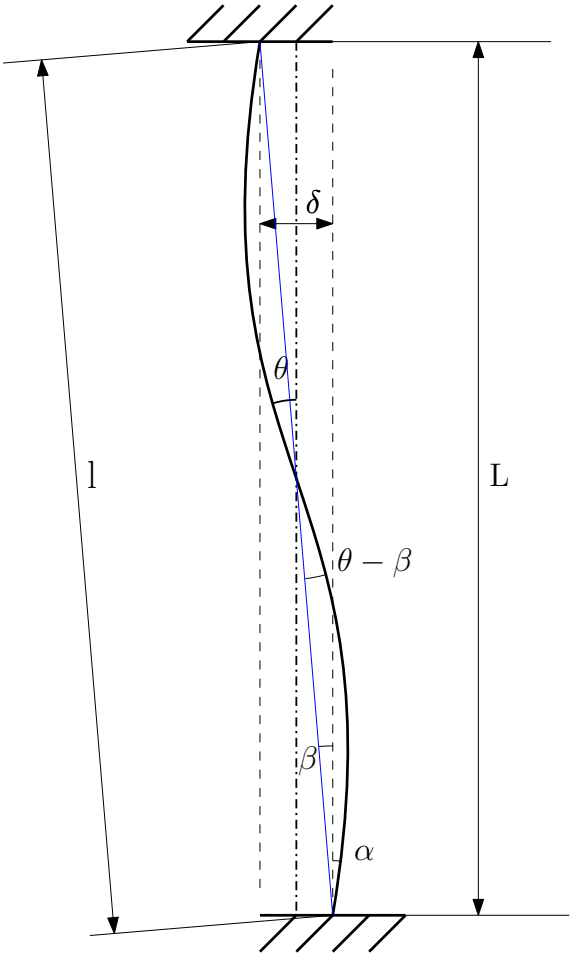

Figure 3.11: Guiding rod linearity worst case scenario

By the definition of perpendicularity tolerance, the angle α that the guiding rod forms with the normal vector of the support surface is,

$$\alpha = \frac{0.01}{23} = 1.72 \times 10^{-4} \text{ rad}$$

And β is the angle made by the blue line in Figure 3.11 and the support surface normal vector,

$$\beta = \frac{\delta}{L} = \frac{0.038}{1737} = 2.19 \times 10^{-5} \text{ rad} \tag{3.2}$$

To ease the calculations, Figure 3.11 was rotated and the scenario in Figure 3.12 was achieved. It is important to notice that, because $\delta \ll l$, implies,

$$l = \sqrt{L^2 + \delta^2} \approx L$$

Defining $y(x)$ as the transverse position alongside the x axis and using an approximation,

$$y(x) = a \sin \frac{2\pi}{L} x \tag{3.3}$$

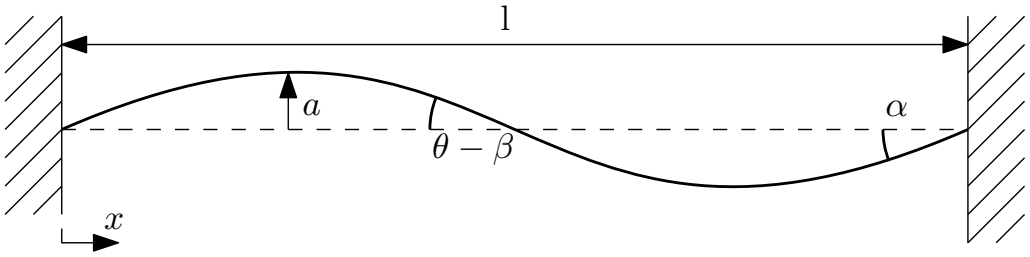

Figure 3.12: Analogous guiding rod

Differentiating Equation 3.3, yields

$$\frac{\mathrm{d}y}{\mathrm{d}x} = \frac{2\pi d}{L}\cos\frac{2\pi}{L}x \tag{3.4}$$

knowing that,

$$\left.\frac{\mathrm{d}y}{\mathrm{d}x}\right|_{x=0} = \alpha \tag{3.5}$$

and combining Equations 3.4 and 3.5,

$$a = \frac{\alpha L}{2\pi} \tag{3.6}$$

On the other hand,

$$\theta - \beta = \left.\frac{\mathrm{d}y}{\mathrm{d}x}\right|_{x=\frac{L}{2}} = \frac{2\pi}{L}\cdot\frac{\alpha L}{2\pi} \tag{3.7}$$

that results in,

$$\theta = \alpha + \beta = 1.94\times10^{-4}\,\mathrm{rad} = 0.7' \tag{3.8}$$

which in turn is much lower than the admissible $30'$.

Despite being difficult to calculate, the maximum transverse deviation, A, is easy to estimate:

$$A = \left(a + \frac{\delta}{4}\right)\cdot 2 = 112\ \mu\mathrm{m} \tag{3.9}$$

Which is also lower than the 0.3 mm given by the clearance control.

3.1.3 Static analysis

Considering all the structural changes that were made, the static analysis was also revised.

The structure was modeled as shown in Figure 3.13. All the component properties are defined in Table 3.1 where A is the cross section area, I_y the second-area moment about the y axis, z_G the distance to the center of mass about the z axis and E the elastic modulus.

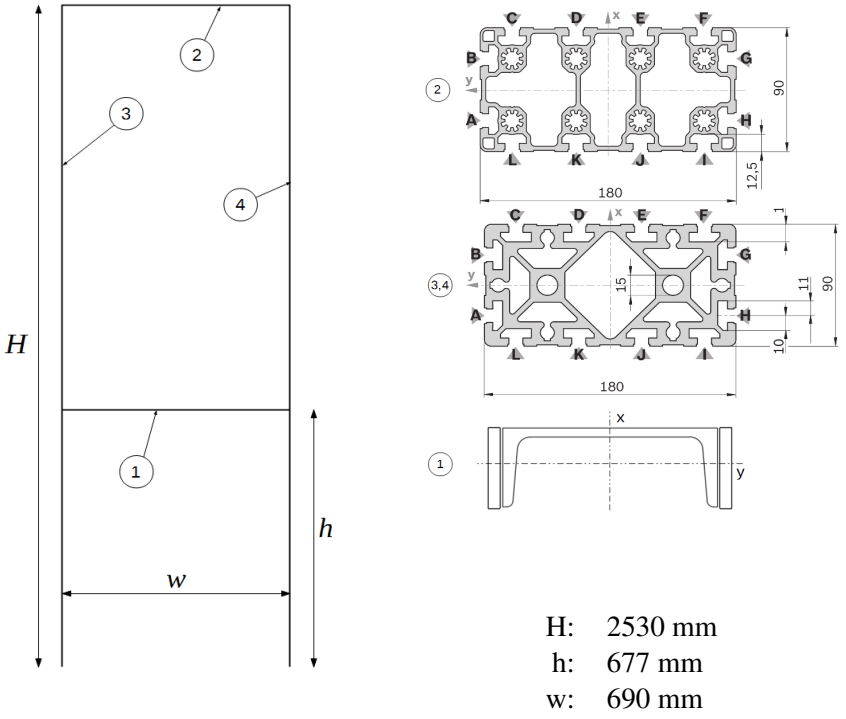

H: 2530 mm
h: 677 mm
w: 690 mm

Figure 3.13: Structural layout

The UNP 180 and lateral support ensemble I_y were determined the following manner,

$$z_G = \frac{2 \cdot A^{lat} \cdot z_G^{lat} + A^u \cdot z_G^u}{2} = 3.31 \text{ cm} \tag{3.10}$$

Huygens–Steiner theorem states that,

$$I_y = I_y^G + A \cdot d^2 \tag{3.11}$$

Thus,

$$I_y^u = I_y^{u_G} + A^u \cdot \left(z_G - z_G^u\right)^2 = 168.1 \text{ cm}^4 \tag{3.12}$$

and knowing that,

$$I_y^{lat_G} = \frac{b\, h^3}{12} = 42.9 \text{ cm}^4 \tag{3.13}$$

the lateral support second-area moment about the y axis, I_y can now be calculated

$$I_y^{lat} = I_y^{lat_G} + A^{lat} \cdot \left(z_G - z_G^{lat}\right)^2 = 43.3 \text{ cm}^4 \tag{3.14}$$

Being on the same axis these can now be added,

$$I_y = 2 \cdot I_y^{lat} + I_y^u = 254.7 \text{ cm}^4 \tag{3.15}$$

Table 3.1: Profile properties

Nr	Profile	A (cm^2)	I_y^G (cm^2)	z_G (cm)	E (GPa)
-	UNP 180	28	114	1.92	210
-	Lateral support	10.5	42.9	3.5	210
1	Ensemble	38.5	254.7	3.31	210
2	90×180L	42.8	401	4.5	70
3, 4	90×180	63.6	544.3	4.5	70

Additionally, the structure will be loaded with the weight of the Lifting subsystem (Section 3.2), the Positioning subsystem (Section 3.3), the Drop-weight subsystem (3.4) and the top profile. The mass and weights of these subsystems as discriminated in Table 3.2.

Table 3.2: Load weight

Component	Mass (est.) [kg]	Weight [N]
Lifting	50	490.5
Positioning	10	98.1
Drop-weight	56	549.4
Top profile	9	88.3
Total	125	1226.1

Using a total of 2000 N applied on the top profile center, this gives in the worst case scenario a 1.63 security coefficient.

Applying the 2-D frame analysis software Ftool [13], it was revealed a maximum torque of 273 Nm (Figure 3.14a) and a maximum deflection of 3.04 μm (Figure 3.14b).

And according to Shigley's [14],

$$\sigma_{max} = \frac{M_{max} \cdot z}{I_y} = 3.06 \text{ MPa} \tag{3.16}$$

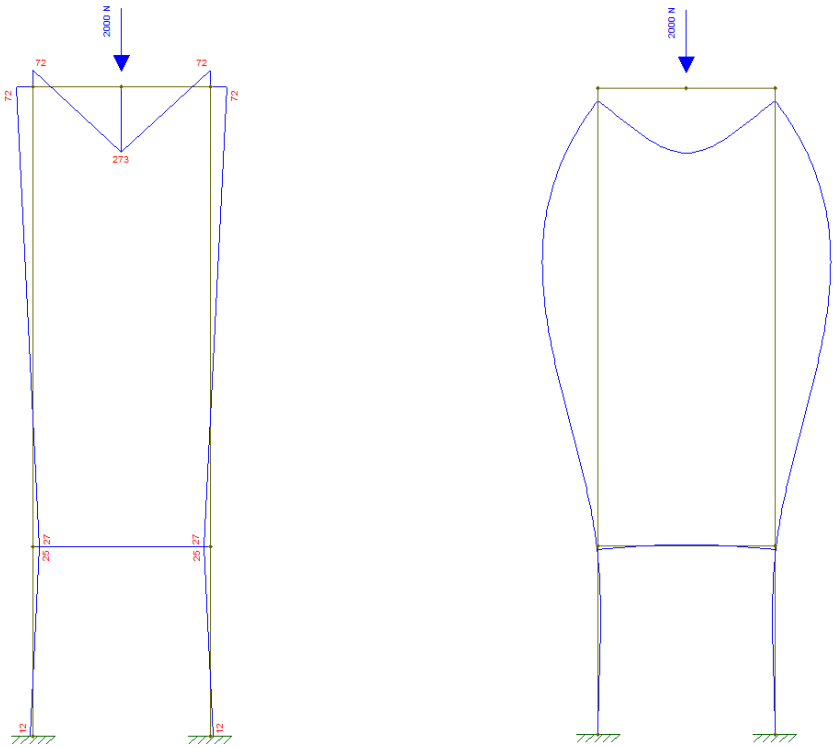

(a) Structural moments distribution (b) Structural displacement

Figure 3.14: Structural analysis

3.1.4 Dynamic analysis

Considering the impact loads that will be enforced onto the structure, it is crucial to consider the dynamics of the system. In order to calculate the influence of the impact in the structural integrity, the system was discretized as exposed in Figure 3.15.

The lifting mechanism and the top profile were modeled as a concentrated mass, m_l, at the top. The columns were modeled as a spring-mass-spring (k_c-m_c-k_c), the base and tool as a mass-spring (m_b-k_b and m_t-k_t respectively) and the leveling feet as a mass-spring-damper (m_a-k_a-c_a). The origin of the degrees of freedom x_i are considered without the static compression. These coefficients are calculated using the following expressions and condensed in Table 3.3.

$$k_c = \frac{EA}{H/2} = 3.52 \times 10^8 \text{ N/m} \tag{3.17}$$

$$k_b = \frac{48EI}{l^3} = 1.15 \times 10^8 \text{ N/m} \tag{3.18}$$

The tool spring constant, k_t, was estimated by excess and the mass, m_t, was predicted to be around 20 kg.

For the leveling feet, the spring constant, k_a is equal to 4×9000 N/mm and the mass m_a is equal to 4×2.65 kg.

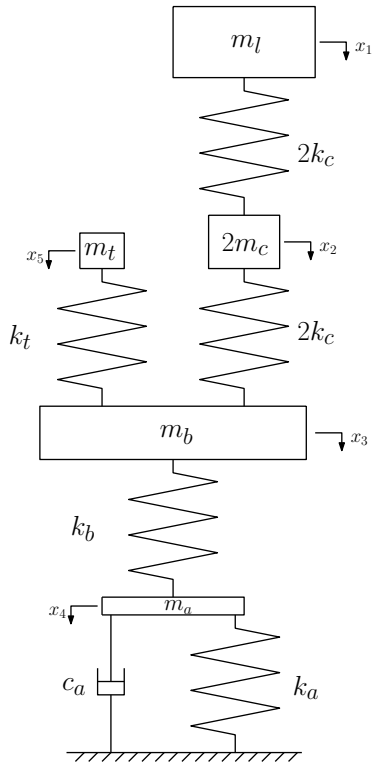

Figure 3.15: Discrete model

As for the damper constant, c_a, it needs to be calculated using the damper ratio, ξ [15]

$$\xi = \frac{c_a}{2m_a w_{n_a}} \tag{3.19}$$

and,

$$w_{n_a} = \sqrt{\frac{k_a}{m_a}} = 1843 \text{ rad/s} \tag{3.20}$$

resulting in,

$$c_a = 3.91 \times 10^3 \text{ Ns/m} \tag{3.21}$$

According to Newton's second law,

$$\left[m\right]\left\{\ddot{x}\right\} + \left[c\right]\left\{\dot{x}\right\} + \left[k\right]\left\{x\right\} = \left\{f\right\} \tag{3.22}$$

Where $\left[m\right]$, $\left[c\right]$, $\left[k\right]$ are the mass, damping and stiffness matrices and $\left\{x\right\}$ and $\left\{f\right\}$ are the displacement and force vectors. The initial displacement due to the structure own weight is already taken into account in the origin selection.

Table 3.3: Coefficient values

Constant	Value	Units
m_l	59	kg
k_c	$3,52 \times 10^8$	N/m
m_c	43,5	kg
k_b	$1,15 \times 10^8$	N/m
m_b	246	kg
k_t	10^9	N/m
m_t	20	kg
k_a	$3,6 \times 10^7$	N/m
m_a	10,6	kg
c_a	$3,91 \times 10^3$	Ns/m

$$\left[m\right] = \begin{bmatrix} m_l & 0 & 0 & 0 & 0 \\ 0 & 2m_c & 0 & 0 & 0 \\ 0 & 0 & m_b & 0 & 0 \\ 0 & 0 & 0 & m_a & 0 \\ 0 & 0 & 0 & 0 & m_t \end{bmatrix} \qquad \left[c\right] = \begin{bmatrix} 0 & 0 & 0 & 0 & 0 \\ 0 & 0 & 0 & 0 & 0 \\ 0 & 0 & 0 & 0 & 0 \\ 0 & 0 & 0 & c_a & 0 \\ 0 & 0 & 0 & 0 & 0 \end{bmatrix}$$

$$\left[k\right] = \begin{bmatrix} 2k_c & -2k_c & 0 & 0 & 0 \\ -2k_c & 4k_c & -2k_c & 0 & 0 \\ 0 & -2k_c & 2k_c + k_b + k_t & -k_b & -k_t \\ 0 & 0 & -k_b & k_b + k_a & 0 \\ 0 & 0 & -k_t & 0 & k_t \end{bmatrix} \qquad \left\{f\right\} = \begin{Bmatrix} 0 \\ 0 \\ 0 \\ 0 \\ 0 \end{Bmatrix}$$

The impact load imposed to the system can be mathematically represented as an initial velocity $\dot{x}_{0_5}$ applied in the tool.

Defining v_{impact} as the maximum impact velocity of 5 m/s and m_{impact} as the maximum impact mass of 56 kg, and considering the linear momentum preservation,

$$\dot{x}_{0_5} = \left(\frac{2m_{impact}}{m_{impact} + m_t} \right) \cdot v_{impact} = 7.37 \text{ m/s} \tag{3.23}$$

With this, the initial conditions vectors result in:

$$\left\{x_0\right\} = \begin{Bmatrix} 0 \\ 0 \\ 0 \\ 0 \\ 0 \end{Bmatrix} \qquad \left\{\dot{x}_0\right\} = \begin{Bmatrix} 0 \\ 0 \\ 0 \\ 0 \\ 7.37 \end{Bmatrix}$$

In this analysis it is relevant to calculate the maximum force transmitted to the leveling feet, to

ensure that they can withstand the force transmitted. In order to calculate these, Equation 3.22 was solved numerically using MATLAB [16] as described in Appendix B. As result, $\left\{x\right\}$ and $\left\{\dot{x}\right\}$ are now known.

The force transmitted to each leveling foot is define as $f_{40}(t)$ and is given by,

$$f_{40}(t) = \frac{1}{4}\left(k_a \cdot x_4(t) + c_a \cdot \dot{x}_4(t)\right) \tag{3.24}$$

The response is plotted in Figure 3.16.

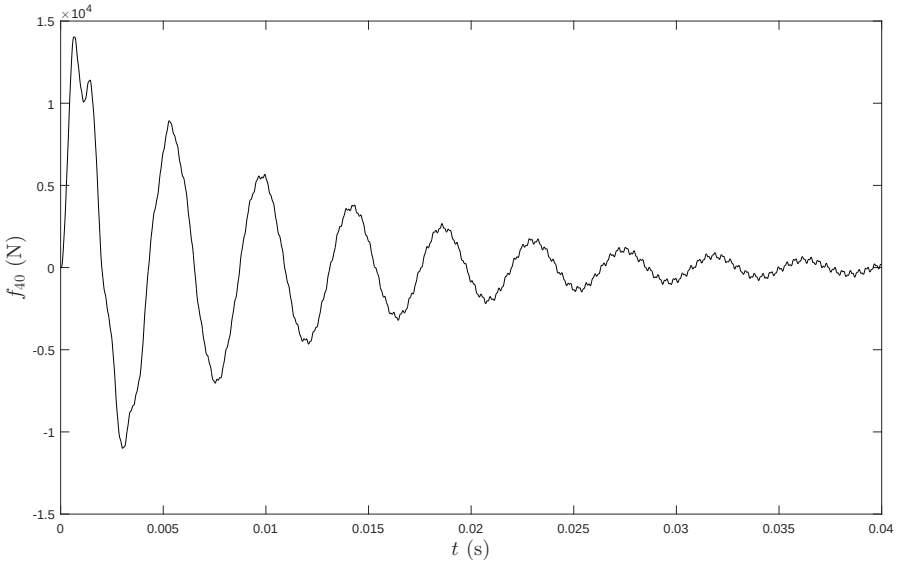

Figure 3.16: Force transmitted to the leveling foot

The maximum force of $f_{40}(t)$ is equal to 18.2 kN which is inferior than the maximum load allowed by the leveling foot [11].

3.2 Lifting subsytem

The Lifting subsystem is responsible to position the carriage (Section 3.3) at the appropriate height to release the drop-weight (Section 3.4) and induce an impact at a specific velocity or energy. This is implemented the way shown in Figure 3.17. The steel cable responsible to lift the carriage will be rolled up in the barrel and will be further rolled or unrolled by the gearmotor. The gears transmit the movement to the screwe shaft with a 2:1 ratio and since the barrel has a pitch of 7 mm and the screw a pitch of 3,5 mm, and the axial movement is synchronized, the cable is able to be unrolled in a permanent vertical line.

The complete assembly drawing is represented in Drawing 0–L in Appendix A.2. The technical drawings are numbered L–1 to L–9.

This solution was proposed by Castro [2] but some changes had to be produced (Figure 3.18).

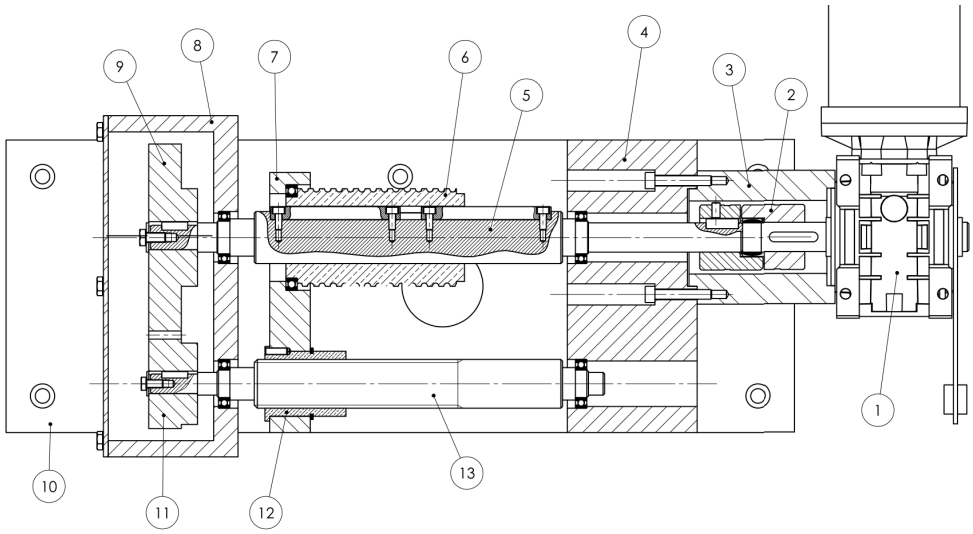

1. Worm gearmotor
2. Rotex coupling
3. Bellhousing
4. Motor holder
5. Barrel shaft
6. Barrel
7. Axial connector
8. Gear holder
9. Pinion
10. Lifting base
11. Gear
12. Screw
13. Screwed shaft

Figure 3.17: Lifting subsystem

A base plate was added to facilitate the assemble and disassemble the whole mechanism from the structure. The gearmotor had to be changed, as described in Section 4.1 and consequently its connection to the motor holder. Several other changes were also made to accommodate the workshop limitations.

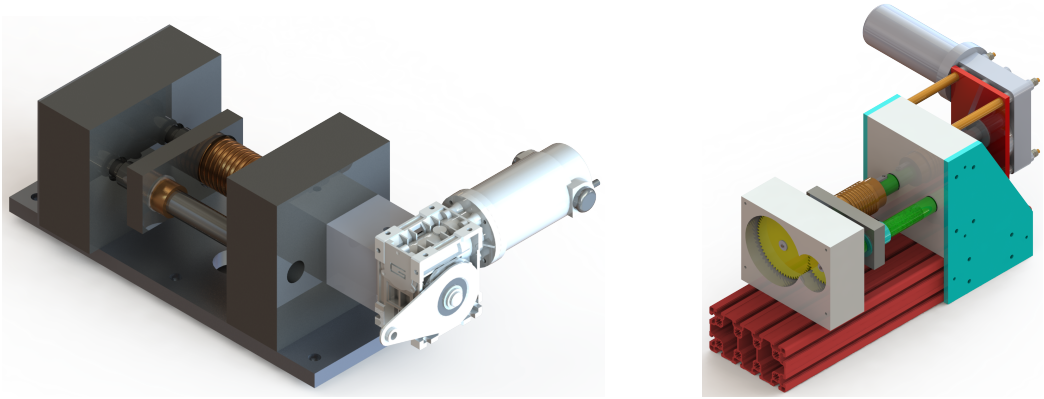

Figure 3.18: Lifting subsystem comparison

3.2.1 Bellhousing

The bellhousing (Figure 3.19) connects and centers the gearmotor with the motor holder. Its connecting function is achieved by two sets of holes, offsetted by 45 degrees to house bolts in both

directions (one set for each direction). Its center function is achieved by the ϕ 60 hole/sleeve at both extremities. Its complete technical drawing is documented in Drawing L–6 in Appendix A.2.

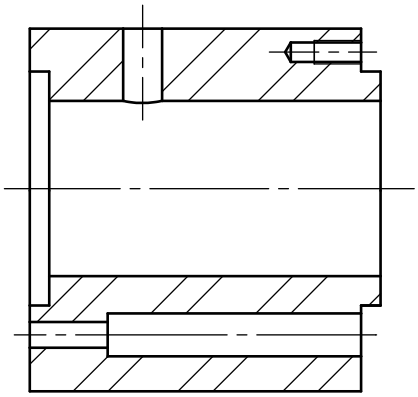

Figure 3.19: Bellhousing

3.2.2 Barrel and screw

The barrel (Figure 3.20a) and screw (Figure 3.20b) materials were changed to bronze to reduced friction between them and the shafts.

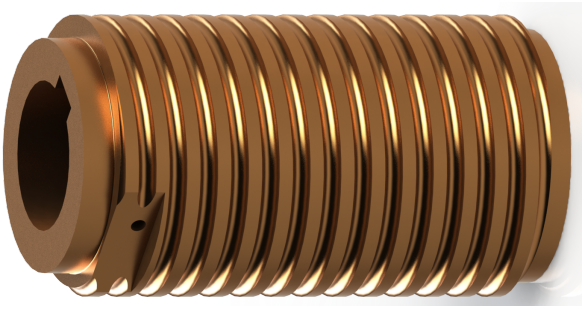

(a) barrel

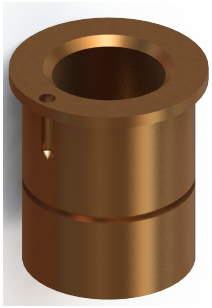

(b) screw

Figure 3.20: Barrel and screw renders

The barrel thread was extended to both ends to facilitate the machining, as the flat surface where the cable end is going to be attached.

As shown in Figure 3.21, a recess was included due to the key slotter tool length being only 90 mm long.

Chamfers were added to both screw ends to ease the assemble.

These parts drawings are represented in Drawings L–4 (screw) and L–8 (barrel) in Appendix A.2.

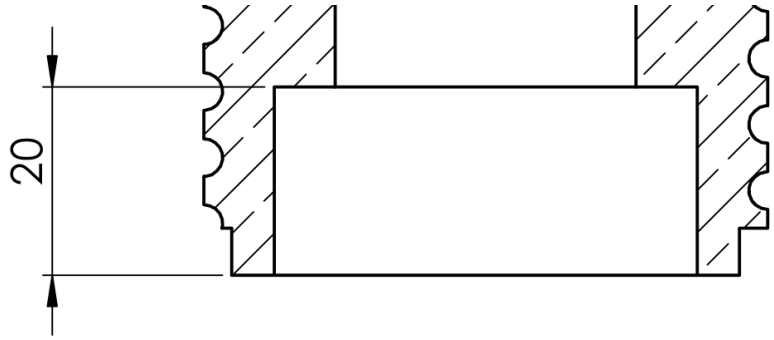

Figure 3.21: Barrel recess (dimensions in mm)

3.2.3 Axial connector, holders and shafts

There were no functional changes to any of these parts, but the technical drawings had to be elaborated and are shown in Drawings L–5, L–1, L–2, L–3 and L–7 respectively in Appendix A.2.

3.2.4 Lifting subsystem base

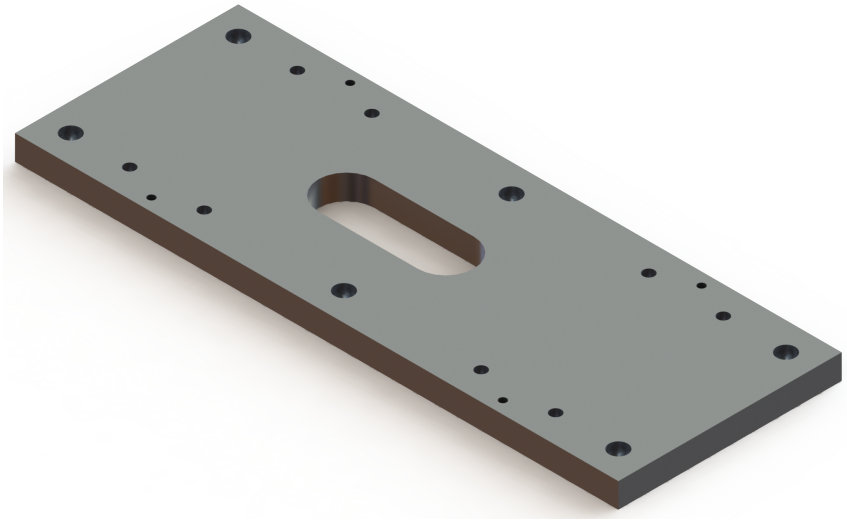

Figure 3.22: Lifting subsystem base

The lifting subsystem was conceived to be assembled in the top profile and attached using t-bolts (Appendix C.5). This implied that either the lifting subsystem would be assembled prior to the structure or that the mechanism had to be assembled on the top of the structure. Neither of these were convenient in the project implementation so a base (Figure 3.22) was created which also introduced a relative location between the supporting blocks.

3.2.5 Coupling and gears

Both the coupling and gears remained unchanged but their datasheet it is included in Appendix C.6 and C.7 for future reference.

Figure 3.23: Rotex 19

Figure 3.24: Gear

3.3 Carriage and release

The carriage and release subsystem (Figure 3.25) is responsible for securing the drop-weight while this is positioned by the lifting mechanism. The changes made to this subsystem are mostly a consequence of changing the actuation technology, as described in Section 4.2. The technical drawings for all the machined parts are displayed in Appendix A.2 where the drawing number has a configuration of T–[1-8].

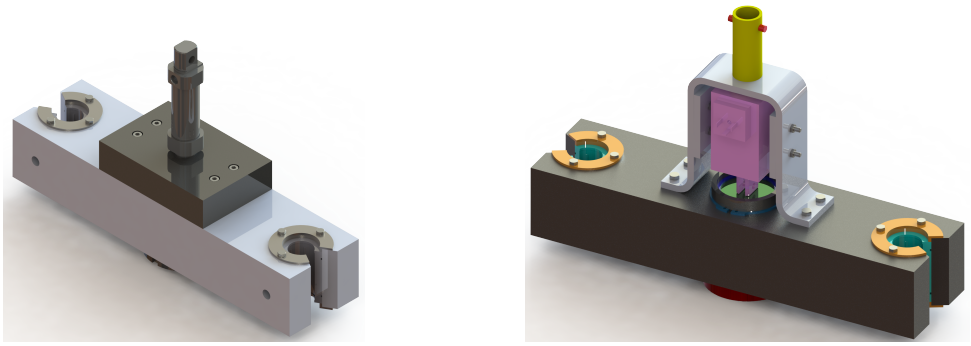

(a) New (b) Old

Figure 3.25: Carriage and release subsystem comparison

Each part will be thoroughly described ahead.

3.3.1 Carriage

The carriage geometry was mostly maintained (Figure 3.26), only being added a threaded hole M3 to ensure that the linear ball bearings don't rotate.

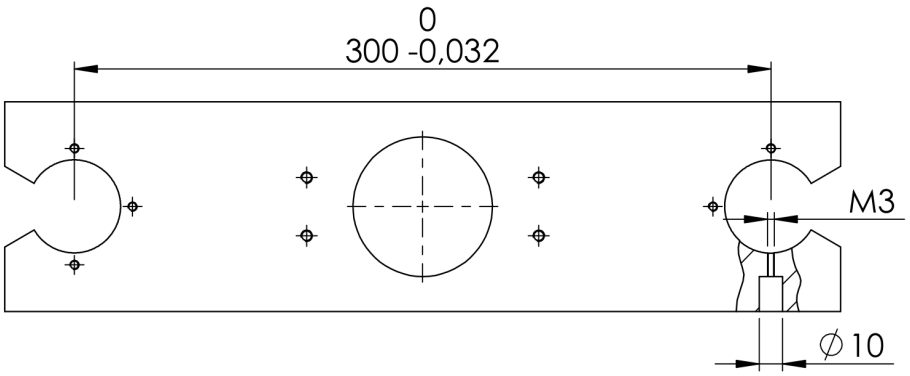

Figure 3.26: Carriage schematic (dimensions in mm)

The material was changed to Aluminum 7075 to reduce the load that the motor chosen in Section 4.1 will be subject to.

Finally it was given a tolerance between the linear ball bearing holes to provide a correct interaction with the guiding rods.

This part drawing number is T–1 and is shown in Appendix A.2.

3.3.2 Linear ball bearings

The linear ball bearings were already selected by Castro [2] and they were preserved in the project since there was no reason to change.

The maximum misalignment allowed by these is 30' [17] and its datasheet it is given in Section C.3.

3.3.3 Cylinder-carriage connection

Since the solenoid was replaced with a pneumatic cylinder, as explained in Section 4.2, its connection to the carriage had to be redesigned.

It was decided to use a steel cage, connected to the cylinder thread in one end and by four screws M5 to the other end (Figure 3.27). Its technical drawing is described in drawing T–3 in Appendix A.2.

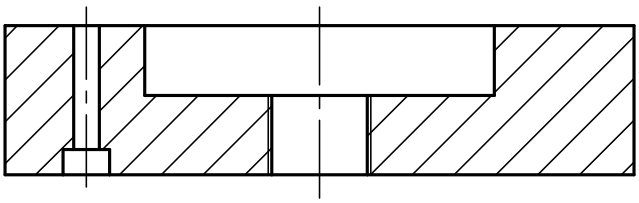

Figure 3.27: Cylinder-carriage connection schematic

To safeguard the integrity of this part, a worst case scenario analysis was made.

$$F - P = m \cdot a \tag{3.25}$$

Where F is the upward force made by the lifting subsystem, P is the weight of the carriage and maximum drop-weight, m the mass and a is the maximum acceleration during the upward movement.

According to Barbosa [1], the acceleration would be 0.32 m/s^2. Since the gearmotor (Section **??**) was altered, this value was majored to 0.4 m/s^2.

Using SolidWorks [9] mass evaluation function and using a security multiplier of 1.5 results in a load of

$$F \approx 950\text{N} \tag{3.26}$$

Using SolidWorks Simulation, a mesh of 17289 tetrahedral elements with an average size of 5.43 mm was created. Applying the load defined in Equation 3.26 in the screw's housing and fixating the central thread produces a von Mises maximum stress of 23.6 MPa and a maximum displacement of 6 μm as exhibited in Figures 3.28 and 3.29

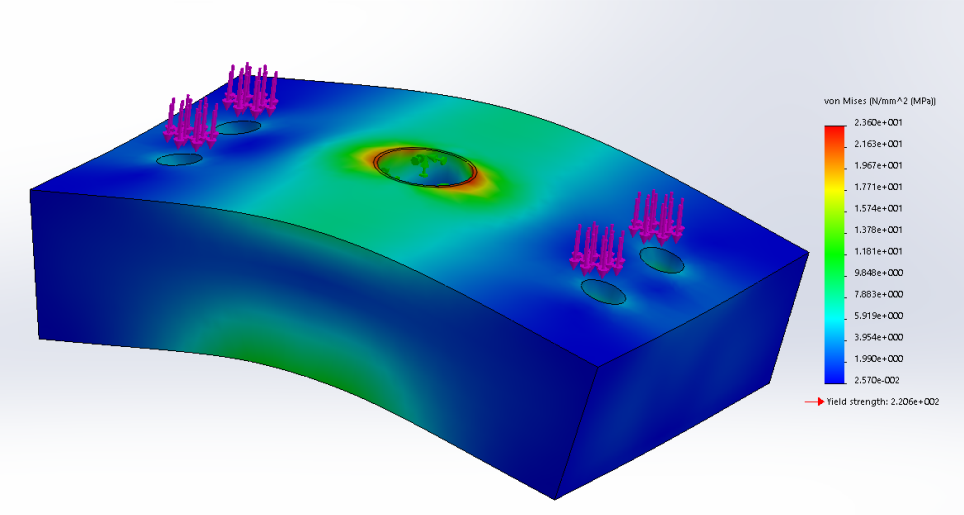

Figure 3.28: Stress

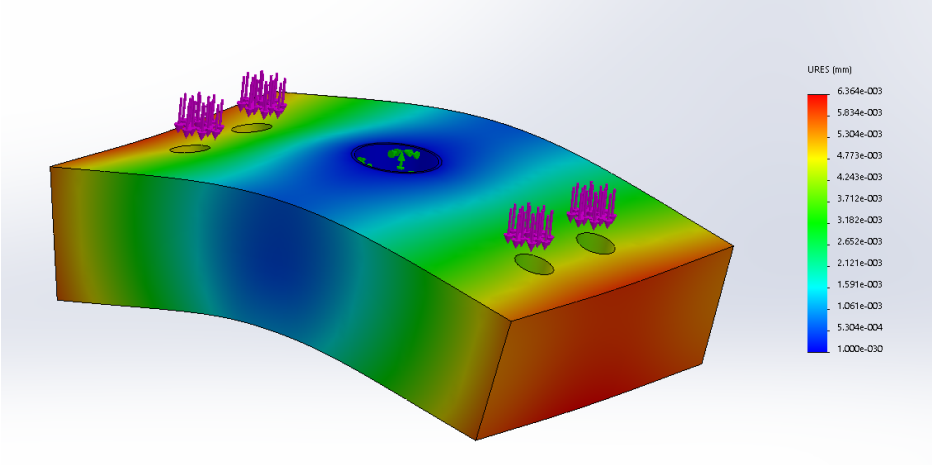

Figure 3.29: Displacement

3.3.4 Release clamp

The release clamp is responsible to release the drop-weight once its height is set by the lifting subsystem. Its technical drawings are comprised in Appendix A.2, drawings T–[4-8]

Its function was developed by Castro [2], as described in Figure 3.31. The first stage represents the approach, the second the coupling. In the third stage the drop-weight is secured and it is released in the fourth stage.

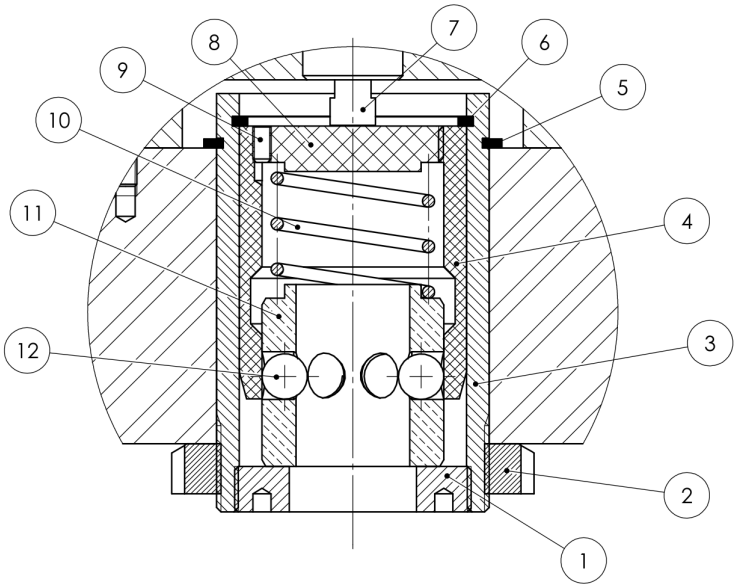

1.	Bottom cover	4.	Sleeve	7.	Cylinder	10.	Spring
2.	Locknut	5.	Outer retaining ring	8.	Sleeve cover	11.	Ball carrier
3.	Exterior part	6.	Inner retaining ring	9.	Position screw	12.	Ball

Figure 3.30: Release clamp assemble

The functionality was kept as is, but several changes were made to guarantee the assemble and function. Chamfers were made in all parts, a sleeve cover was introduced to simplify the

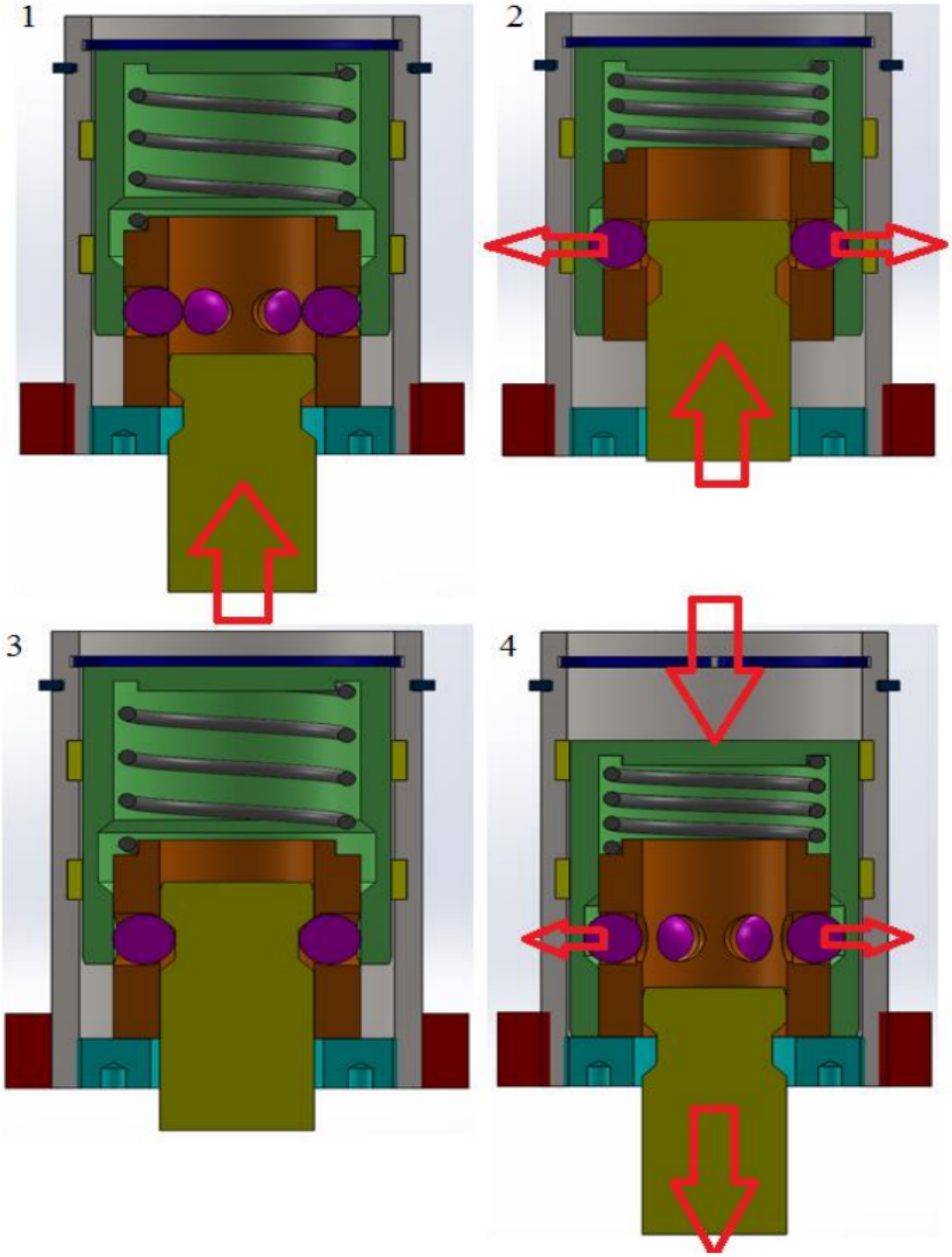

Figure 3.31: Original release clamp functionality description [2]

construction and the materials were replaced to reduce friction between the moving parts resulting in the disappearance of the guide ring between the sleeve and exterior part. Slight interferences were also fixed.

These changes can be appreciated in Figure 3.30.

3.4 Drop-weight

The drop-weight consist in all the parts that will be in free fall during the moments prior to the test and went through several changes for two main reasons: excessive mass and economic reasons.

The original design (Figure 3.33a) had a mass of 8.7 kg which leads to a energy profile as is shown in Figure 3.32 which was incompatible with the energy range ADFEUP wanted.

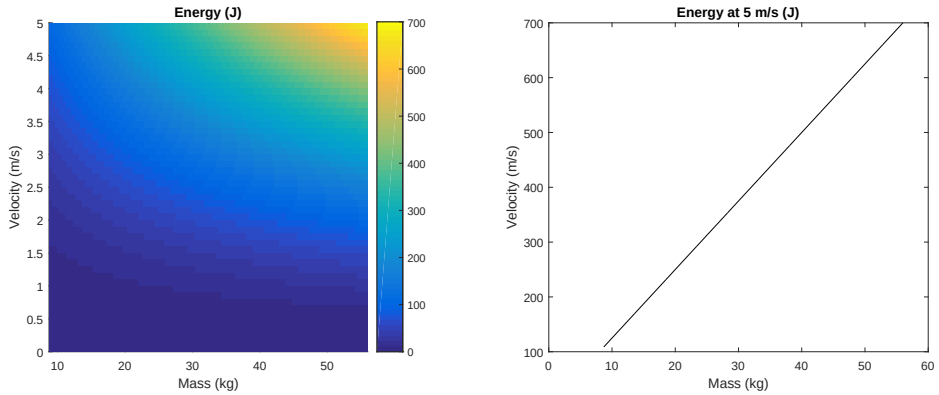

Figure 3.32: Original energy profile

At 5 m/s, the impact energy without additional mass attached to the anvil is 109 J and ADFEUP wanted to be able to test adhesive joints at 5 m/s with approximately 50 J.

This led to severe design changes to the anvil and anvil hanger.

The economical aspect led to the substitution of the load cell for an accelerometer that will be further discussed in Section 4.3.1. This also had an impact in all the connection parts.

The assembly drawing is displayed in Appendix A.1 as Drawing 0–M.

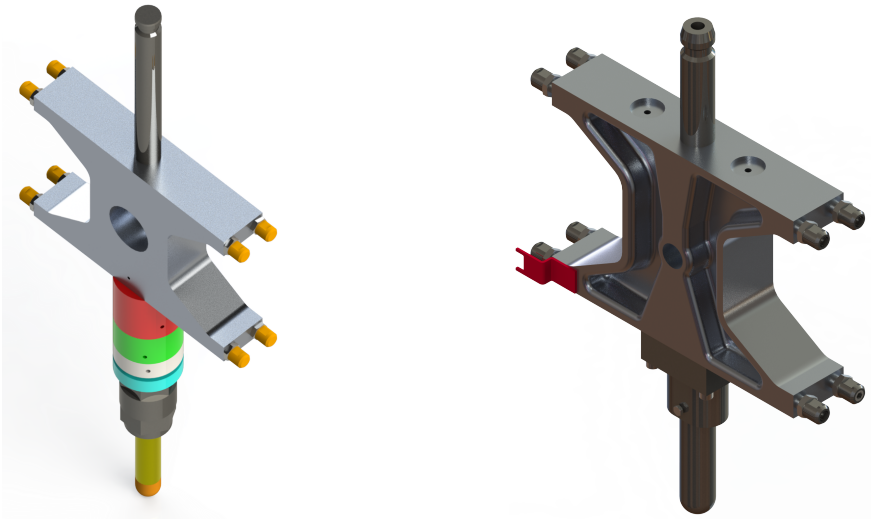

(a) Original (b) Current

Figure 3.33: Cylinder-carriage connection simulation

3.4.1 Configurations

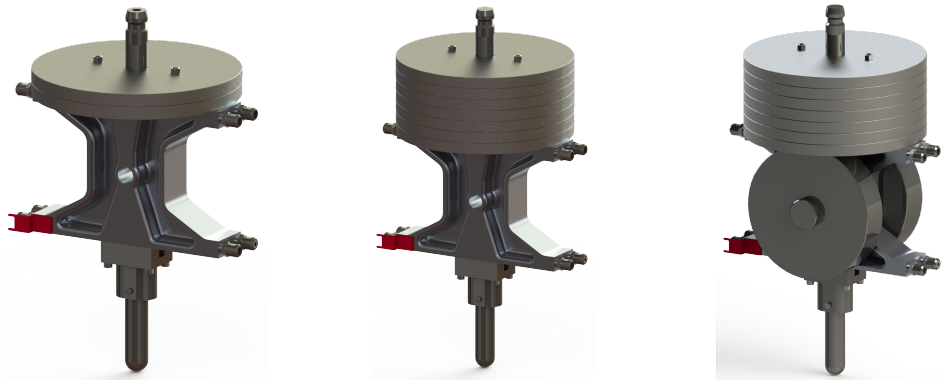

(a) Minimum configuration (b) Medium configuration (c) Maximum configuration

Figure 3.34: Drop-weight configurations

To guarantee the minimum energy at 5 m/s and the structural integrity at the maximum energy, it was chosen to divide the the drop-weight subsystem in three different configurations (Figure 3.34). This allowed to fulfill the specification, leaving the configuration modification to the user. The energy range that each configuration is able to achieve is condensed in Table 3.4.

Table 3.4: Mass and energy range of each configuration

Configuration	Mass (kg)	Energy (J)
Minimum	4–14,3	50–179
Medium	4.5–40	56.3–500
Maximum	20.4–56	255–700

3.4.2 Hanging rod

The rod is responsible for connecting the anvil to the release clamp (Section 3.3.4) and centering the top masses (Section 3.4.6). Originally these was achieved by a single part for all the functional range of the machine, but due to the introduced specification this was no longer possible. In Figure 3.35 are shown the two instances that will be used in the possible configurations.

Castro [2] specified that this part should be manufactured from a guiding rod. This line of reasoning was maintained to accomplish the centering function. The top chamfer was prolonged to assure a smooth picking (Section 5.1.9.2).

The changes can be fully appreciated in Appendix A.2, Drawings M–1 and M–2.

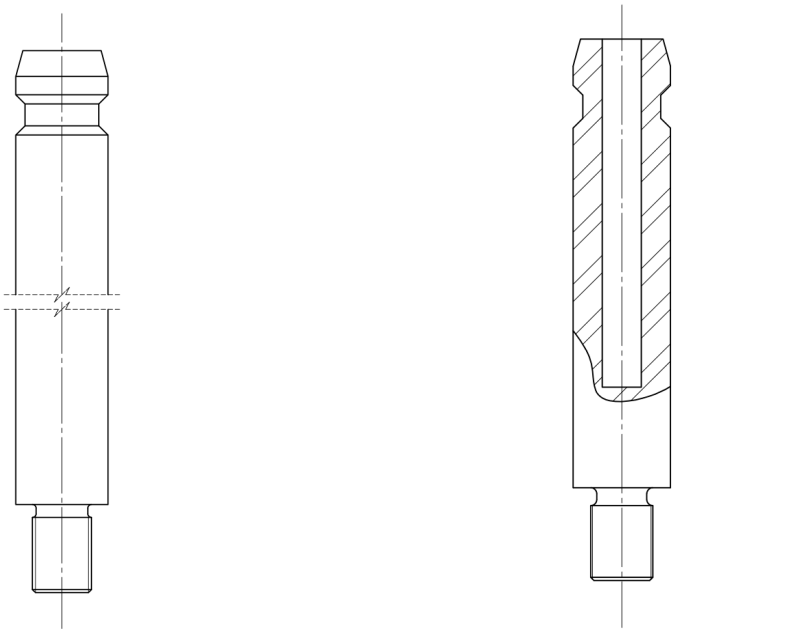

(a) Medium/Maximum configuration rod (b) Minimum configuration rod

Figure 3.35: Hanging rod

3.4.3 Anvil

The anvil is the central part of the subsystem. It holds all the external masses (Sections 3.4.6 and 3.4.7) that allow the machine to operate properly, it is coupled with the clearance control (Section 3.4.4) and connected to the impactor through its connection.

To function correctly, it needs to be symmetrical with respect to the central axis.

In Figure 3.36 is represented the current state of the anvil and its complete technical drawing is exhibited in Drawing M–3 (Appendix A.2).

The first and second features were maintained from the original project. The third was added and is used to secure the top extension. Since the load cell was exchanged for an accelerometer, the connection had to reflect that change. Feature number four was designed to center the impactor connection with the anvil and number five to fasten that same part.

Several recesses were added to reduce the mass and to ensure that its structural integrity was not compromised, an impact simulation was performed.

Its length was shortened to allow the anvil to be disassembled without disassembling the guiding rods.

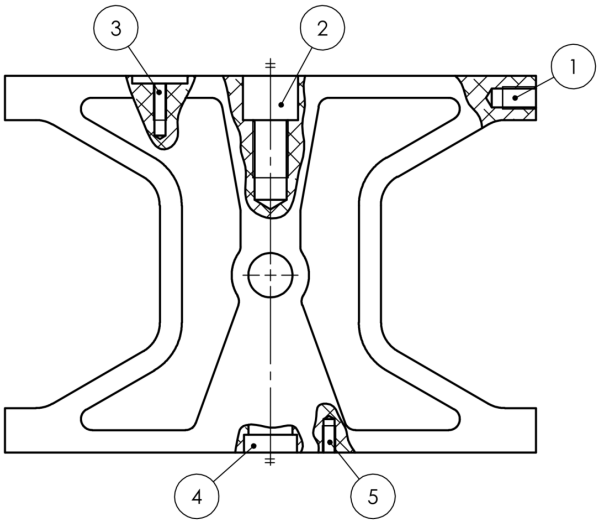

1. Clearance control threaded hole
2. Hanging rod centering surface
3. Mass extension threaded hole
4. Center sleeve centering surface
5. Connecting part threaded hole

Figure 3.36: Anvil

3.4.3.1 Simulation

The simulation was carried out using SolidWorks [9] drop-test simulation.

To reduce the computational work a simplified model of both the lateral and top extensions was modeled, as well of the impactor connection.

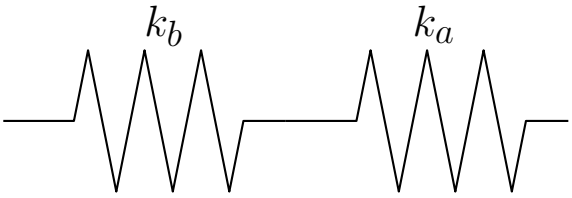

Figure 3.37: Base and feet spring system representation

The mesh was generated with 59024 tetrahedral elements with a size of 5.97 mm to 29.89 mm.

As presented in Figure 3.38, the maximum von Mises stress for the duration of the impact fluctuates between 4 and 35 MPa which is less than 10% of the yield strength of the material, 455 MPa (Appendix C.8).

As for the setup, it was assumed that the tool would be perfectly rigid in a worst case scenario, so the stiffness would be equal to the equivalent spring of the base and feet in series, as represented in Figure 3.37. The equivalent stiffness is then expressed by

$$k_{eq} = \frac{1}{\frac{1}{k_a} + \frac{1}{k_b}} = 2.74 \times 10^7 \text{ N/m} \tag{3.27}$$

Since SolidWorks defines the target rigidity per unit of area, k_{eq} was divided by the area of the surface of impact, $A = 50.27 \times 10^{-6}$ m^2.

Finally the impact velocity was established as the maximum velocity allowed, 5 m/s.

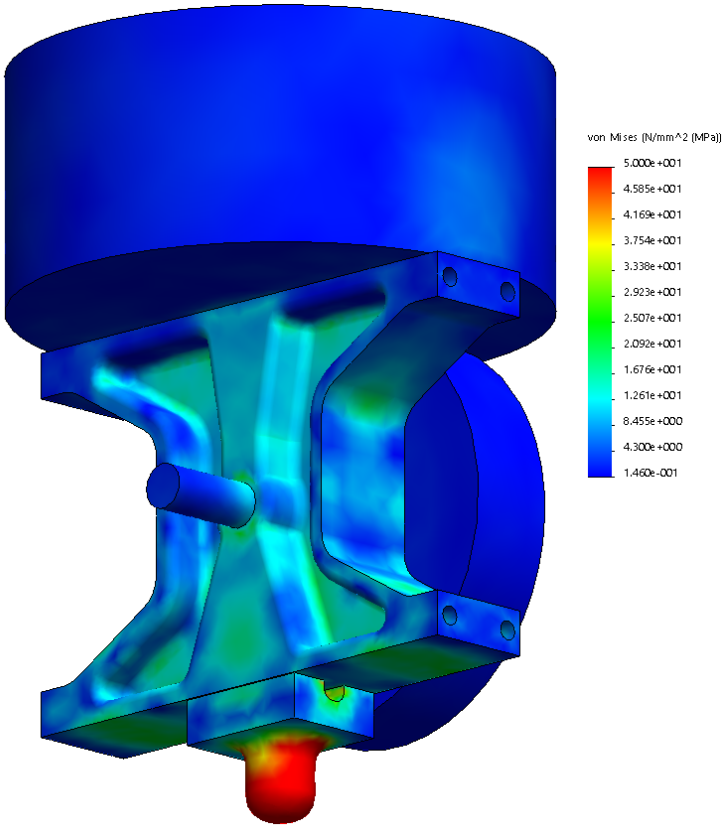

Figure 3.38: Anvil impact simulation

3.4.4 Clearance control

The clearance control is designed to maintain a clearance of 0.3 mm between the clearance nut and the guiding rod, as defined be Castro [2]. This will allow to detect slight deviations in the structure verticality compensate them by adjusting the leveling feet.

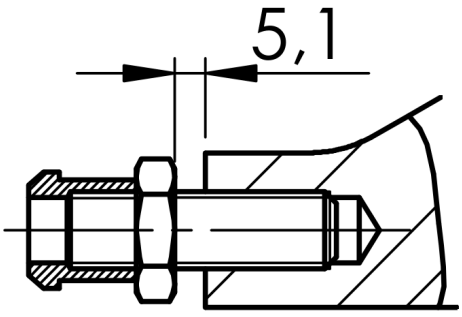

Figure 3.39: Clearance control (dimension in mm)

It is composed by 3 elements: an hex socket set screw, a thin nut and the clearance nut.

The screw should be screwed until the end of the thread and bonded with the anvil using Loctite® Epoxy Weld™ Bonding Compound. The nuts should be fastened against each other at

approximately 5.1 mm from the anvil to guarantee the aforementioned 0,3 mm clearance.

3.4.5 Impactor and connections

The impactor is the part that will be in contact with the tool at the moment of impact. It was designed to be easily substituted since that might be a need of different geometries of impact according to the tool used.

Originally this function was carried out by two different parts, fastened together (Figure 3.40), where the body was to be made in titanium and the tip in tool steel Böhler K600 (DIN 1.2767). This was done to reduce the tensile force applied to the load cell, in order to obtain better test result by eliminating that component. Since the load cell was swapped by an accelerometer, it was no longer necessary to use titanium in the impactor and it was change to a single part of K600.

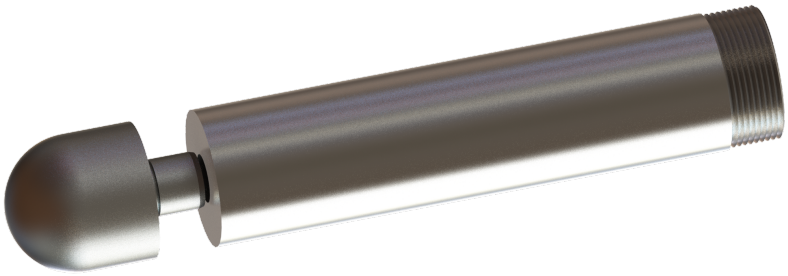

Figure 3.40: Original impactor

The attach method was simplified from a screw to a notch, as displayed in Figure 3.41 and Drawing M–5 in Appendix A.2.

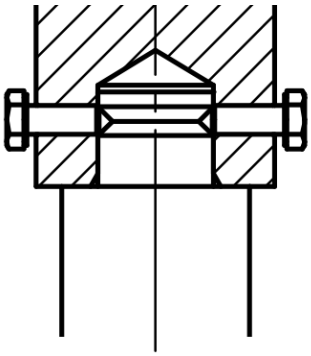

Figure 3.41: Impactor attach method

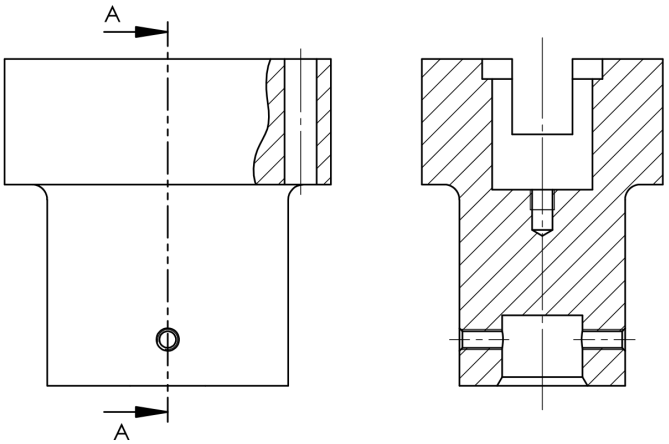

Figure 3.42: Connecting part

The connecting part (Figure 3.42) serves as an interface between the anvil, impactor and accelerometer. Besides that, it was required, as the anvil, to be symmetrical with respect to the central axis and to be centered in relation to the anvil and impactor, hence the bottom and top holes with guiding tolerance (Drawing M–4, Appendix A.2).

The surface and hole in contact with the accelerometer were designed according its datasheet (Appendix C.9).

3.4.5.1 Simulation

Both the impactor and the connecting part were submitted to a drop-test simulation in SolidWorks [9].

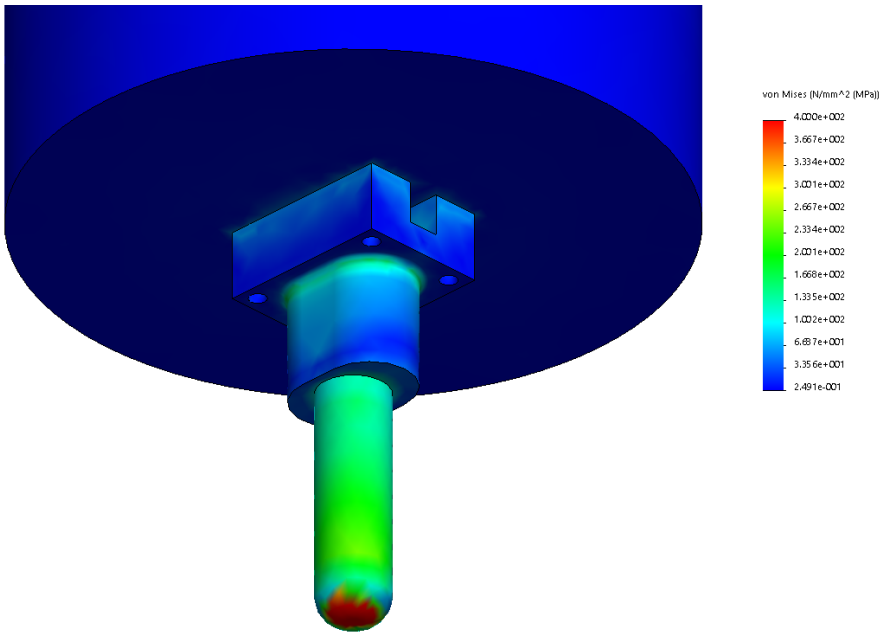

Figure 3.43: Impactor and connecting part simulation

The setup was the same used in Section 3.4.3.1 with the exception of the target rigidity, that was adjusted to this area of impact.

The mesh was generated with 28959 tetrahedral elements with a size of 3.87 mm to 19.33 mm.

This led to the following maximum von Mises maximum stresses: 244 MPa for the impactor (excluding the tip, in which the stress will tend to infinity) and 171 MPa for the connection. Both are well under the yield strength of the material, 1150 MPa.

3.4.6 Top masses

The top mass extensions needed for all configurations were designed from scratch. It was designed to allow 1 kg increments so its configuration will be a combination of up to seven 5 kg extensions (Drawing M–9 in Appendix A.2), one or two 2 kg extensions (Drawing M–10 in Appendix A.2) and one 1 kg extension (Drawing M–11 in Appendix A.2).

As displayed in Figure 3.44, all the extensions will be centered on the hanging rod surface and secured by a conjunction of two nuts and a threaded rod. The jam nut fastens the threaded rod to the anvil and the top nut secures the extensions.

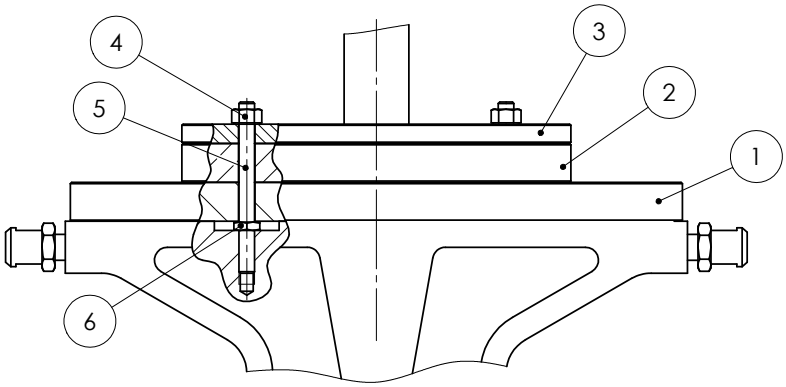

1. 5 kg extension
2. 2 kg extension
3. 1 kg extension
4. Top nut
5. Threaded rod
6. Jam nut

Figure 3.44: Top extensions assembly

3.4.7 Lateral masses

The lateral extension is needed for the maximum configuration and it is assembled as shown in Figure 3.45

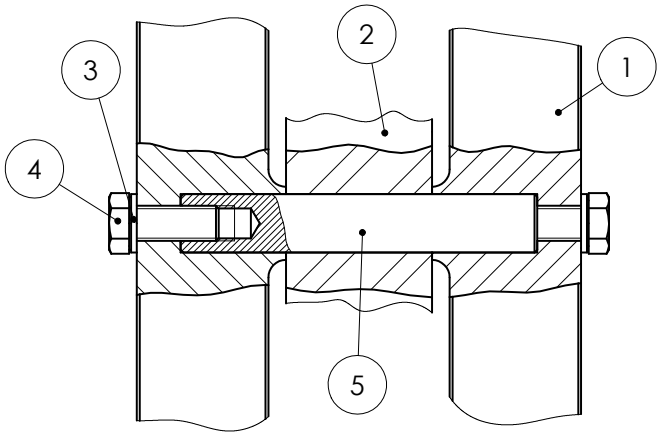

1. Lateral extension
2. Anvil
3. Washer
4. Hex bolt
5. Central shaft

Figure 3.45: Lateral extensions assembly

To ensure that the center of mass is kept in the center while allowing a proper fastening of the elements, the central shaft length was toleranced with an upper deviation of -10 μm and a lower deviation of -20 μm. These parts drawing are compiled in Appendix A.2 as Drawings M–13 and M–7.

3.5 Impact velocity acquisition

The impact velocity acquisition subsystem (Figure 3.46) is responsible for acquiring the velocity as close to the moment of impact as possible. Since the point of impact varies with the tool used, it was selected a screw drive system to compensate for that height change. Its assembly is detailed in Drawing 0–V in Appendix A.1.

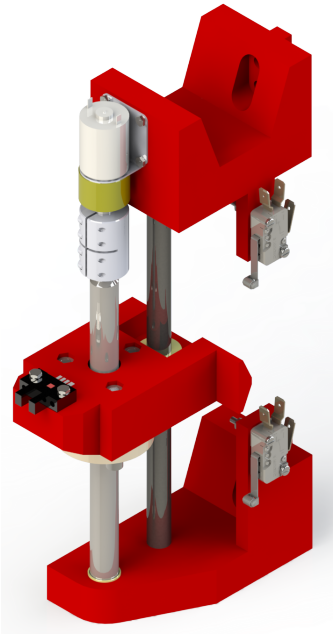

Figure 3.46: Impact velocity acquisition subsystem

3.5.1 Supports

The bottom and top supports (Figures 3.47 and 3.48) connect the subsystem to the structure. Considering that any of these parts will not be susceptible to significant forces, they were designed to be manufactured by additive manufacturing, as the optic detector support. This allowed the design of a somewhat more complex geometries to be implemented like the lugs that hold the limit switches and the nut lodgers.

Since the manufacturing process only needs a 3D CAD model to manufacture the parts, no technical drawings were elaborated.

To connect the top and bottom supports to the structure (Section 3.1) a nut was designed (Drawing V–1 in Appendix A.2).

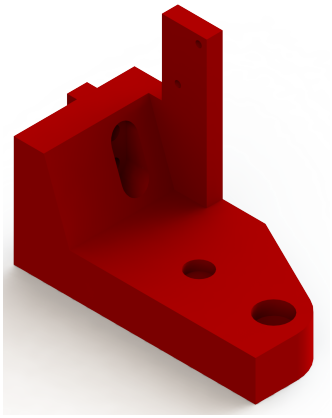

Figure 3.47: Bottom support

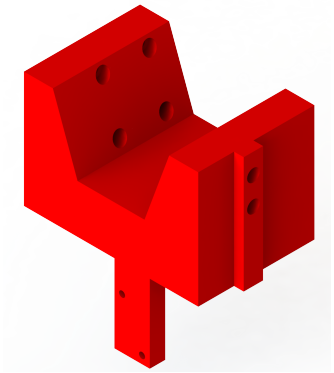

Figure 3.48: Top support

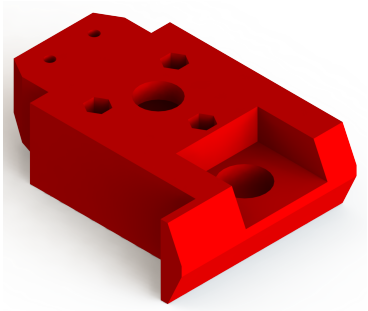

Figure 3.49: Optical detector support

3.5.2 Screw drive

To accomplish the vertical translation, a screw drive system was used. Since there will be no significant loads applied, a igus drylin® screw drive (Figure 3.50) was chosen.

Figure 3.50: igus drylin® screw drive

At this point, the only constrain given is the lead screw geometry. By choosing a trapezoidal screw, it allows the system to self sustain itself vertically without securing the lead screw.

Given this, a trapezoidal lead screw in stainless steel, with 14 mm diameter and 4 mm pitch was chosen.

Using the inclined plane analogy,

$$T_{ac} \cdot \frac{2}{d} \cos\alpha - m\, g \sin\alpha - F_a = 0 \tag{3.28}$$

where T_{ac} is the starting torque, d is the diameter, mg is the weight being lifted, F_a is the friction force and is equal to

$$F_a = \mu \left(m\, g \cos\alpha + T_{ac} \cdot \frac{2}{d} \sin\alpha \right) \tag{3.29}$$

And μ is the friction coefficient between the the nut and screw materials and α is the screw angle and is equal to

$$\alpha = \arctan \frac{p}{\pi d} \tag{3.30}$$

where p is the screw pitch.

By overestimating the mass to 1 kg, considering the friction coefficient μ equal to 0.18 [18] and reorganizing Equations 3.28, 3.29 and 3.30

$$T_{ac} = \frac{d\ m\ g}{2} \cdot \frac{\sin\alpha - \mu\cos\alpha}{\cos\alpha - \mu\sin\alpha} = 0.02 \text{ Nm} \tag{3.31}$$

This value will be relevant when selecting the gearmotor in Section 4.4.2.

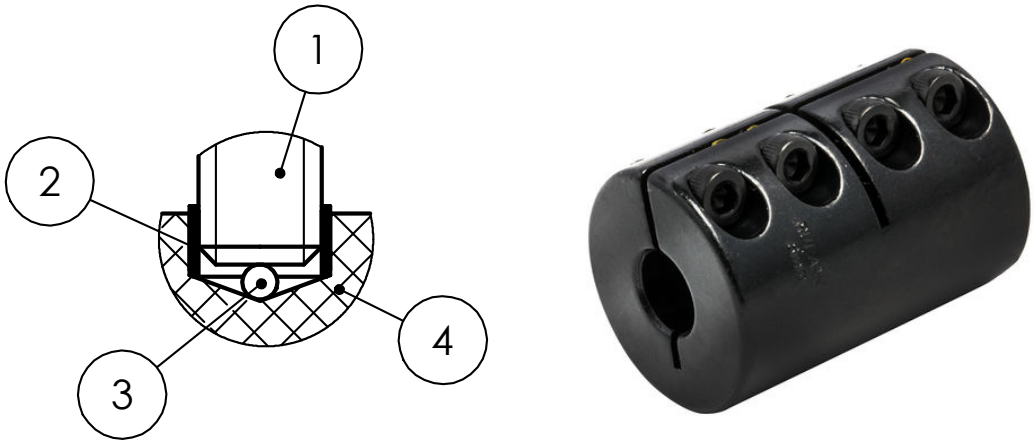

(a) Bottom connection

(b) Top coupling

Figure 3.51: Lead screw connections

The lead screw was chosen to be connected to the gearmotor specified in Section 4.4.2 using a rigid coupling Ruland MCLX-8-8-F(Appendix C.10).

To separate the weight between the top and bottom (No. 4) supports, the lead screw (No. 1) was projected to be supported on top of a roller bearing sphere (No. 3), as shown in Figure 3.51a, maintaining a reduced friction on the bottom surface. As for the lateral surface, this will wrapped around a igus® dry bushing (No. 2).

To lock the optic support rotation, a guiding rod in conjunction with another dry bushing was used.

Chapter 4

Actuation and instrumentation

To properly automate the machine as specified in Chapter 5, several electrical and electromechanical components had to be chosen.

In this chapter, the process regarding the selection of these components is explained.

4.1 Lifting subsystem

For the lifting subsystem only a motor was needed to power the barrel shaft (Section 3.2.3) and to position the carriage (Section 3.3) and the drop-weight (Section 3.4). A direct current worm gearmotor was chosen by Barbosa [1] to fulfill this purpose.

The original worm gearmotor was the permanent magnet DC motor Parvalux PM60G (Figure 4.1).

Figure 4.1: Parvalux PM60G [19]

Since the motor is used to lift a gravitic load, the system must be able to sustain the load in case of a power failure. This led to the choice of a worm gearmotor, due to its irreversibility. The selection of the particular motor is detailed by Barbosa [1].

Because of difficulties in buying the motor from Parvalux representatives in Portugal, an alternative had to be found.

Figure 4.2: Gearmotor Transtecno ECM-100/040 [20]

It was selected the Transtecno ECM-100/040 (Figure 4.2) with 80:1 reduction, and the properties shown in Table 4.1, retrieved from the datasheet posted in Appendix C.11.

Table 4.1: Transtecno ECM-100/040 properties

I (A)	U (V)	T (Nm)	n (min^{-1})
8.4	24	21	38

where I is the maximum input current for non-continuous service, U the supply voltage, T the output torque and n the output velocity.

Since,

$$F = \frac{T}{r} \tag{4.1}$$

where F is the necessary force to lift the load, T the output torque and r the barrel (Section 3.2.2) radius. The gearmotor is then able to lift the carriage with a total mass of up to 71 kg, which is over the 64.5 kg required.

Moreover, as

$$v = \omega \cdot r \tag{4.2}$$

where v is the linear velocity, ω the angular velocity and r is the barrel radius. The carriage is then able to reach a linear velocity of 0.12 m/s, which is in accordance with the specification.

The motor drive is an electronic device that serves as a power amplifier, converting a voltage reference signal to a current signal that drives the motor.

It was selected by Barbosa [1] and it's only included in this thesis for future reference. Its properties are shown in the datasheet, in Appendix C.12.

Compatibility with the new gearmotor was assured.

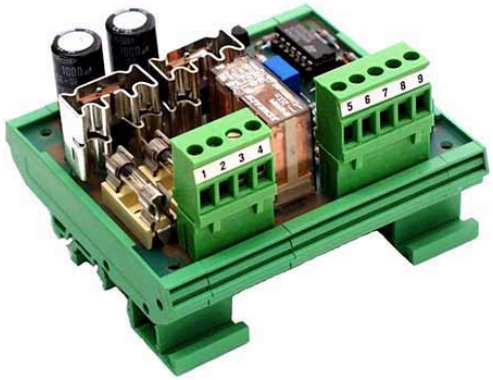

Figure 4.3: Drive Electromen EM-12A [21]

4.2 Carriage and release subsystems

For the machine to perform as intended, the carriage and release subsystem must be equipped with a component able to transmit a linear compression force to release the drop-weight. An upper limit switch to protect the integrity of the system and a detector to identify if the drop-weight is attached to the carriage are included.

4.2.1 Release

Originally, the release actuation was to be performed by a solenoid Kuhnke V45 (Figure 4.4). However, due to its cost, it was changed to a pneumatic system.

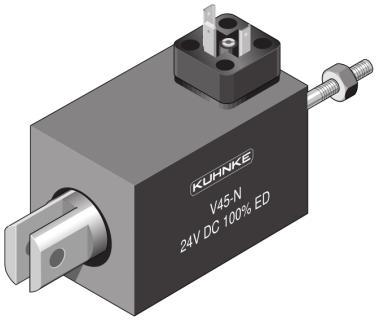

Figure 4.4: Solenoid Kuhnke V45

Since the anti-rebound subsystem to be developed is pneumatic, the machine will operate with access to a pneumatic source. Knowing this, the solenoid was replaced by a pneumatic system constituted by a normally closed 3/2 directional valve, solenoid operated with spring return and a single action pneumatic cylinder, coupled with a flow regulator. The corresponding scheme is displayed in Figure 4.5.

When the input S1 is actuated, pressure line P is connected to port A and consequently, the cylinder primary chamber is pressurized. Its advance velocity is manually set by adjusting the flow regulator valve. Once S1 resets, the spring returns the cylinder to its rest position.

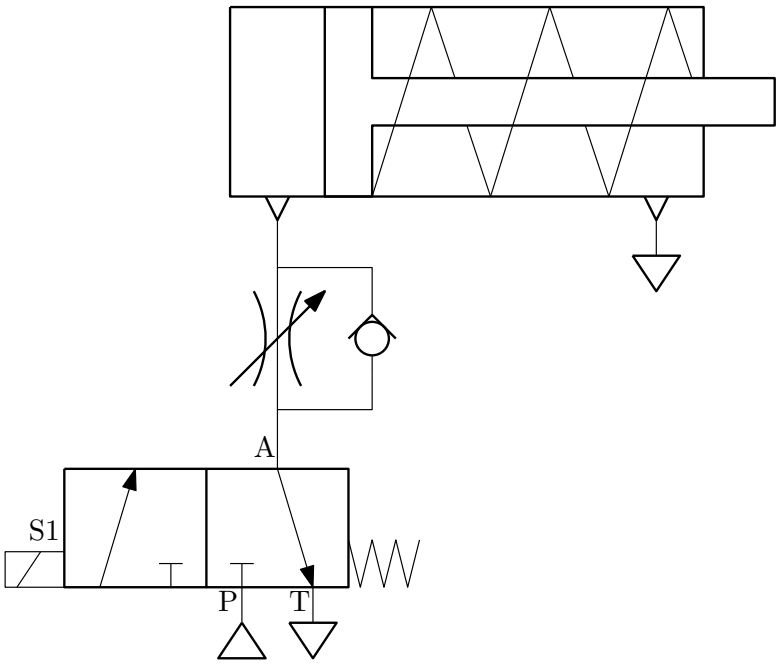

Figure 4.5: Pneumatic system

4.2.1.1 Pneumatic cylinder

Figure 4.6: Pneumatic cylinder SMC C85N25-25S [22]

As Castro [2] stated, the spring maximum force is 60 N. Considering that most pneumatic grids feed its components with a pneumatic pressure ranging from 6-8 bar, that results in,

$$F = p\,A \qquad \equiv \qquad A = \frac{F}{p} \qquad \equiv \qquad d = \sqrt{\frac{4\,F}{\pi\,p}} = 11.3 \text{ mm} \tag{4.3}$$

where F is the resulting force, p the pressure intensity and A the cylinder area subjected to the pressure with a diameter d.

Since the carriage (Section 3.3) and drop-weight (Section 3.4) will be supported by the cylinder body, a roundline cylinder with a piston of 25 mm (intentionally over dimensioned so it can

withstand the tensile forces generated by the weight that it must carry) and sufficient stroke, was chosen. This led to the selection of SMC C85N25-25S (Figure 4.6). Its connection screw is G $^1/_8$.

4.2.1.2 Directional valve

Because of its low cost and identical connection in relation to the cylinder (Section 4.2.1.1), the Parker B3R5BXXXXH was chosen and its datasheet is attached in Appendix C.13.

Figure 4.7: Directional valve Parker B3R5BXXXXH [22]

4.2.1.3 Flow regulator and connection components

To limit the advance velocity, a flow regulator was selected. Due to geometric constrains, an L-shaped device was chosen, with an G $^1/_8$ screw to connect to the cylinder. Since there were a low flow demand, the 4 mm tube was chosen.

The selected accessories to complete the pneumatic circuit were the Legris flow regulator 7668 (Figure 4.8), silencer 0675 (Figure 4.9) and male stud coupling 3175 (Figure 4.10).

Figure 4.8: L-shped flow regulator G $^1/_8$ to 4 mm [23]

Figure 4.9: Silencer G $^1/_8$ [23]

Figure 4.10: Male stud coupling G $^1/_8$ to 4mm [23]

4.2.2 Upper limit detector

To safeguard the carriage (Section 3.3.1) from hitting the upper structure during manual control, a travel limit detector had to be implemented. Because the carriage is made from aluminum, a proximity inductive detector was the obvious choice, due to its reliability.

Figure 4.11: Barrel inductive proximity detector RS Pro 701-8253 [22]

Because of its easy of assemble, a barrel body was chosen. Since there were no other constrains, the RS Pro barrel inductive proximity detector 701-8253 was selected based on its price. The detector datasheet is shown in Appendix C.14.

4.2.3 Drop-weight detector

To accomplish the functionality detailed in Chapter 5, the machine has to autonomously verify if the drop-weight (Section 3.4) is attached to the carriage (Section 3.3).

Due to the proximity between the carriage and the top extensions, during the coupling (Figure 4.12), an inductive detector can not be used, so a photoelectric detector was the next best choice.

The photoelectric detector by diffuse reflection Omron E3FA-DN23 (Appendix C.15) was selected due to its convenient price and flexibility. Its non-invasive installation does not interfere with any subsystems.

Being a diffuse reflection, it can possibly have problems detecting the rod (Section 3.4.2) due to the rod rectified surface, but the alternative would be a through beam detector, that would cost approximately twice the selected component.

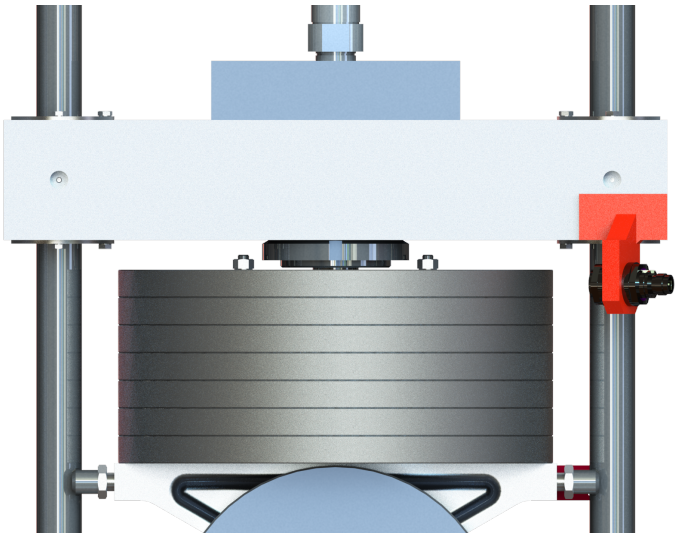

Figure 4.12: Distance between top extension and carriage at the coupling

Figure 4.13: Photoelectric detector Omron E3FA-DN23 [22]

4.3 Drop-weight

Since the machine has to be able to register the force evolution during the impact, the drop-weight (Section 3.4) subsystem needs to be instrumented accordingly.

Barbosa [1] suggested a piezoelectric load cell Kistler 9361B (Figure 4.14), but its high cost prevented it to be acquired.

Figure 4.14: Piezoelectric load cell Kistler 9361B [24]

4.3.1 Accelerometer

Since the drop-weight will be moving during the impact, the load cell could be replaced by an accelerometer. Specifically by the K-Shear Shock Accelerometer 5000g (Figure 4.15), developed for impact application, as stated in its datasheet (Appendix C.16).

Figure 4.15: Kistler K-Shear Shock Accelerometer 5000g [24]

As stated in Section 3.1.1, the maximum force that needs to be measured is 33.44 kN and since,

$$F = m\,a \tag{4.4}$$

then the maximum acceleration will be 597 m/s^2, which is within the accelerometer range.

4.3.2 Signal condition and data acquisition unit

The signal conditioning and data acquisition unit, Kistler LabAmp (Figure 4.16), is provided in conjunction with the accelerometer.

Figure 4.16: Signal conditioning and data acquisition unit Kistler LabAmp [24]

As stated in the datasheet (Appendix C.17), it possesses Ethernet connection capabilities and an application to process the acquired data. The application is equipped with an API to further process the data externally if necessary.

4.4 Impact velocity acquisition subsystem

Regarding the velocity acquisition subsystem, its main purpose is providing the machine with the ability to measure the velocity of the drop-weight right before the moment of impact in order to estimate with great precision the energy of the impact.

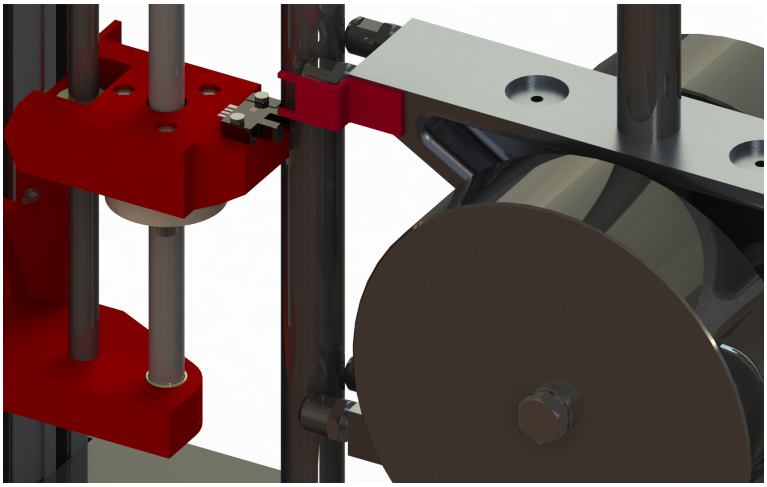

Figure 4.17: Velocity acquisition subsystem

In Figure 4.17 is illustrated the velocity acquisition subsystem. Essentially, a through beam photoelectric detector will be interrupted twice as the drop-weight falls. The first interruption starts a counter and the second stops it. Knowing the distance l, the increment frequency, f, and being n the final counter value, the average velocity can be expressed by,

$$v_m = \frac{f \cdot l}{n} \tag{4.5}$$

and according to Newton's law of motion,

$$v(t) = v_0 + a\,t \tag{4.6}$$

The acceleration originates a slight discrepancy between $v(t)$ and v_m that is shown in Figure 4.18.

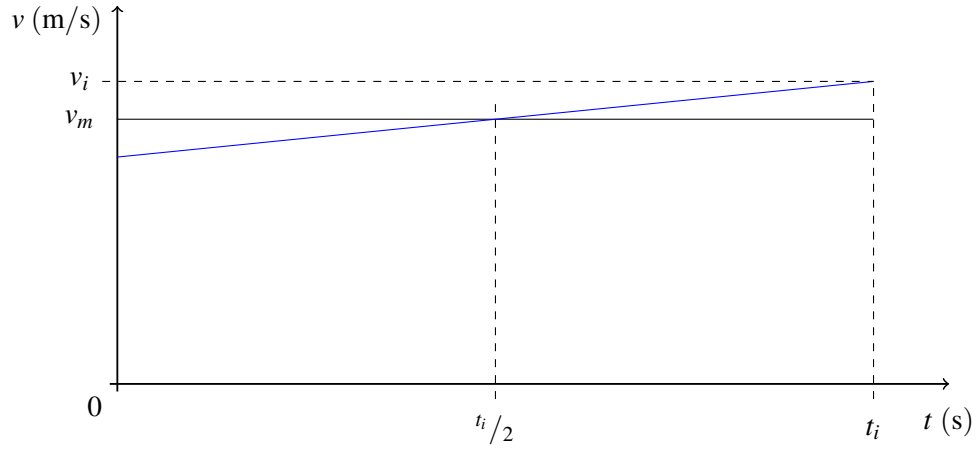

Figure 4.18: Actual velocity evolution $v(t)$ compared to measured velocity v_m

The velocity of impact v_i can be computed considering v_0 equal to v_m and the initial time to be $\frac{t_i}{2}$.

$$v(t_i) = v_m + g \cdot \frac{t_i}{2} \tag{4.7}$$

where t_i is the time passed between both interruptions.

Since l is a fixed value, determined in Section 4.4.1,

$$t_i = \frac{l}{v_m} \tag{4.8}$$

v_i can be computed, alongside its error in relation to v_m (Table 4.2).

As demonstrated, the measurement error for low impact velocity is too high to be neglected and v_i has to be computed by software, based on v_m.

Table 4.2: Relative error between v_m and v_i

v_m (m/s)	t_i (ms)	v_i (m/s)	error (%)
1.5	9.3	1.55	3.0
1.6	8.8	1.64	2.6
1.7	8.2	1.74	2.3
1.8	7.8	1.84	2.1
1.9	7.4	1.94	1.9
2	7.0	2.03	1.7
2.1	6.7	2.13	1.5
2.2	6.4	2.23	1.4
2.3	6.1	2.33	1.3
2.4	5.8	2.43	1.2
2.5	5.6	2.53	1.1
2.6	5.4	2.63	1
>2.6	—	—	< 1

4.4.1 Photoelectric detector

The photoelectric detector (Figure 4.19) is able to detect the interfering part (Section 4.4.1.1) and was already selected by Barbosa [1] and there was no reason to change it.

Figure 4.19: Photoelectric detector through beam Omron EE-SX670-WR 1M [22]

The interfering part however was yet to be designed. Since the detector is to be actuated multiple times, it's important to note that it has a response frequency of 1 kHz (Appendix C.18).

4.4.1.1 Interfering part

The interfering part (Figure 4.20a) is the part attached to the anvil (Section 3.4.3) that will interrupt the photoelectric detector to start and stop the counter, providing the necessary information to calculate the velocity at the moment of impact.

It had to be light, to maintain the center of mass of the drop-weight in the vicinity of its geometric center, and it could not surpass the detector maximum operating frequency at maximum velocity.

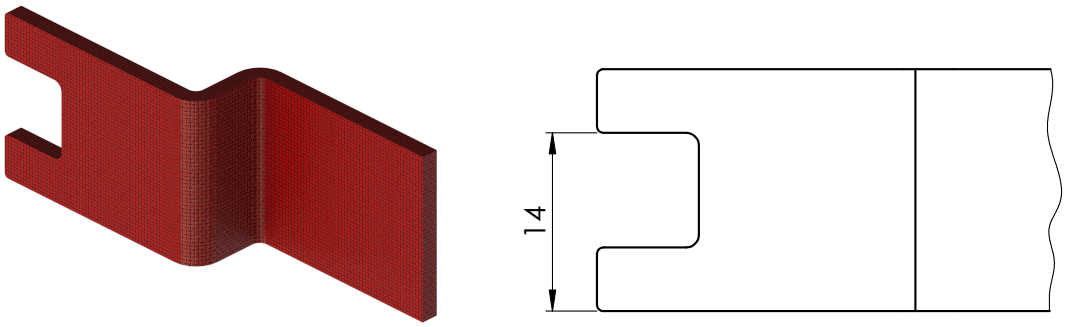

(a) Photo realistic render (b) Schematic (dimensions in mm)

Figure 4.20: Interfering part

Knowing that,

$$v_{max} = \frac{d_{min}}{t} \tag{4.9}$$

and,

$$t = \frac{1}{f} \tag{4.10}$$

where v_{max} is the maximum impact velocity of 5 m/s, d_{min} is the minimum functional distance, t the time passed between both detector interruptions and f the detector response frequency. resulting in,

$$d_{min} = 5 \text{ mm} \tag{4.11}$$

As shown in Figure 4.20b the part was designed to have 14 mm between both ledges.

4.4.2 Gearmotor

The gearmotor is responsible for powering the screw drive (Section 3.5.2) that transforms the angular movement in linear movement, necessary to position the photoelectric detector (Section 4.4.1.

Considering that,

$$\omega = v \cdot \frac{2\,\pi}{p} \tag{4.12}$$

where ω is the motor angular velocity, v the correspondent linear velocity and p is the screw pitch, then using the information provided in Section 3.5.2 and choosing a linear velocity of approximately 10 mm/s, results

$$\omega \approx 15.71 \text{ rad/s} \approx 150 \text{ rpm} \tag{4.13}$$

The necessary torque was calculated in Section 3.5.2 and is 0.02 Nm.

Figure 4.21: DC gearmotor Como Drills 918D100112 [22]

The DC gearmotor selected was the Como Drills 918D100112 (Figure 4.21), capable of providing 0.098 Nm at 168 rpm, being supplied at 24 VDC (Appendix C.19).

4.4.2.1 Reversibility

Because the motor is to be commanded directly by the computer, in both directions, a circuit capable of reversing the direction of the current going through the motor, based on digital signals had to be designed.

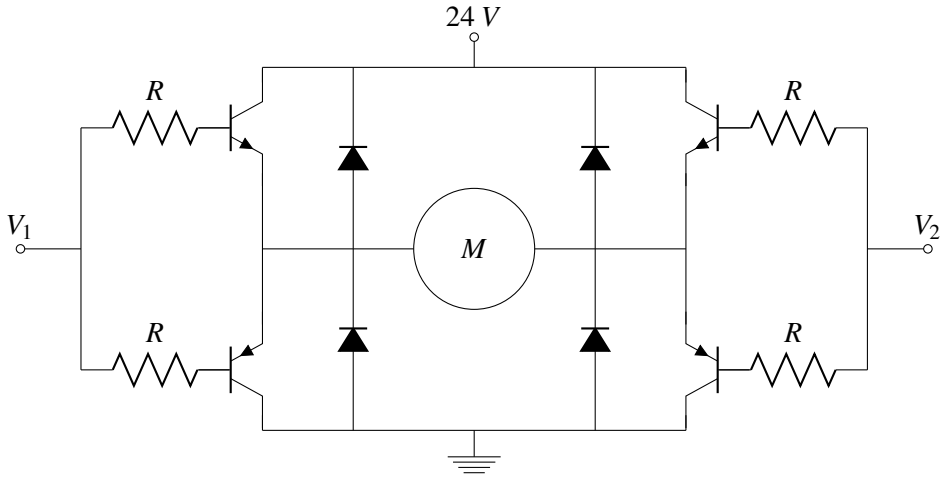

Figure 4.22: Motor control circuit

In Figure 4.22 is represented the implementation of a common circuit known as an H-bridge. To reverse the current, V_1 and V_2 are set, as shown in Table 4.3. The diodes were included to protect the circuit from voltage spikes caused by the motor (which an inductive load) once supply voltage is removed.

4.4.3 Travel limit switch

The travel limit switch is necessary to prevent the system from trying to overextending past its geometric limits.

Table 4.3: H-bridge control summary

V_1	V_2	Motor
0	0	Stops
1	0	Forward
0	1	Backward
1	1	Stops

Functionally, these behave like a microswitch and since there are no high voltages or currents, any kind would suffice.

Figure 4.23: Roller lever microswitch Cherry D459-V3RD [22]

The Roller lever microswitch Cherry D459-V3RD (Figure 4.23) was selected and its datasheet is attached in Appendix C.20.

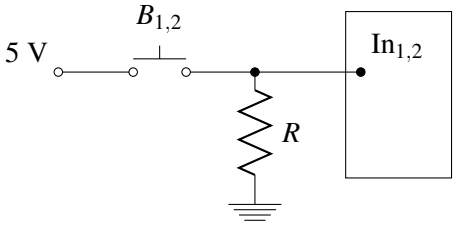

Figure 4.24: Path limit switch assemble circuit

Figure 4.24 shows the electrical scheme for connecting the microswitches. The contact $B_{1,2}$ represents both path limit switches, $\text{In}_{1,2}$ are the respective digital input channels and R is a resistor.

Chapter 5

Command and control

For the machine to function properly, its command logic and control systems have to be well defined and implemented. All of its functioning must be well characterized and it must not present unexpected behavior due to changes in the surrounding environment.

This Chapter addresses the states in which the machine can operate, outlined in its state diagram. It presents the graphical user interface (GUI) created using MATLAB Graphical User Interface Development Environment (GUIDE) to allow the user to operate the machine and, finally, it presents the control requirements and controller design.

It is presumed that the safety mechanisms described in future work (Section 6.2) are already implemented.

5.1 State diagram

The machine operates between 8 different macro states shown in Figure 5.1.

The *initialization routine* is run every time the machine is powered on, or when it leaves the *emergency state*.

Manual control is the state where the user is allowed to manually set the height of the carriage (Section 3.3), or release the drop-weight (Section 3.4). Mass or tool and specimen substitution is done under the *changing mass or change tool and specimen* states. These can only be accessed from *manual control*.

Parameter input is where the test parameters, height, energy or velocity of impact, are introduced.

From *manual control* and *parameter input* the user is allowed to access the *release* state. This works both as a security measure, by requiring a second confirmation to release the drop-weight and allows the user to setup any kind of recording mechanism more accurately.

The *results* state is where the user has access to the test results.

All states allow the transition to the *emergency* state when the emergency button is pressed or when a safety condition is breached.

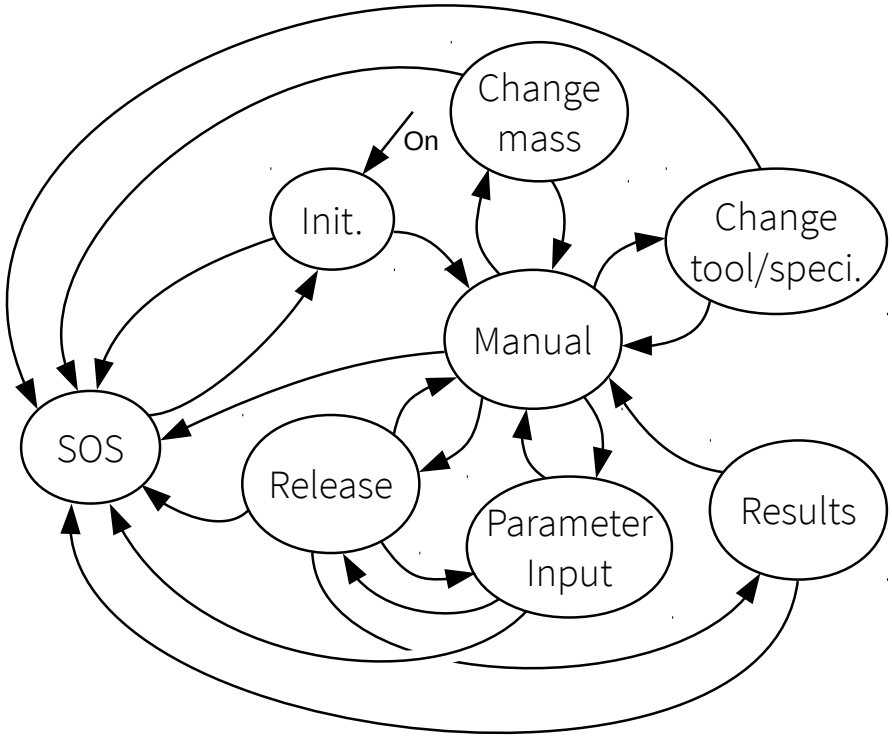

Figure 5.1: State diagram

In the following sections, the individual steps essential in each state will be detailed in flowcharts with the key shown in Figure 5.2.

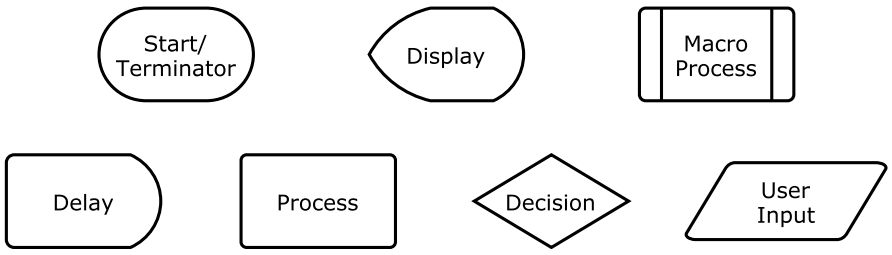

Figure 5.2: Flowchart key

5.1.1 Initialization routine

The *initialization routine* is at the start of every session and ideally it is only run once.

It starts by checking the safety doors detectors and, in case they're open, loops the routine until they're closed.

Secondly, it checks if the anvil is attached to the carriage and if it isn't, it starts the picking (Section 5.1.9.2) sub-routine.

Finally, is sets the impact point through its sub-routine (Section 5.1.9.1). This is necessary since the worm gearmotor (Section 4.1) only possesses an incremental encoder, the current position is unknown at start up.

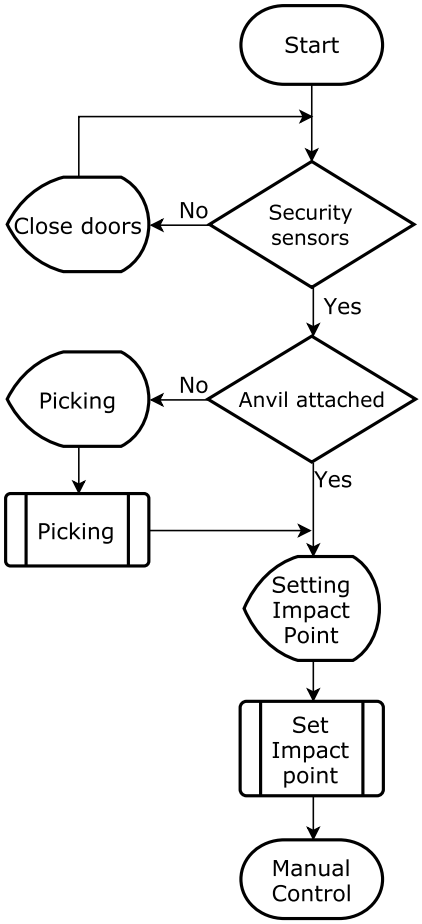

Figure 5.3: Initialization routine state flowchart

5.1.2 Manual control

Manual control is the most used state in any session. It can be accessed from any state (except *emergency*) and is often used for pivoting between states.

As demonstrated in *manual control* flowchart (Figure 5.4) the carriage (Section 3.3) position can be adjusted, between maximum and minimum values, in velocity control (Section 5.3.2), using the up or down physical buttons (Section 5.2.1). If top or bottom limits are reached the motor (Section 4.1) is stopped and the user receives feedback indicating the reason the carriage is stopped. During this process, the safety mechanism is turned on.

If no physical button is pressed, the program stays in an infinite loop until the user presses a button in the GUI (Section 5.2.2.2) to either change mass (Section 5.1.3), change tool or specimen (Section 5.1.4), release the drop-weight (Section 5.1.6) or input new test parameters (Section 5.1.5).

To *change mass*, the user must make sure that the drop-weight is not hanged by the carriage, but rests against the safety stop mechanism (Section 6.2) to avoid accidents in case of steel cable failure.

To *change the tool or specimen*, the drop-weight must be hanged by the carriage and positioned above the safety mechanism. This must be turned on before entering the change tool or specimen state.

In order to enter the *parameter input* state, the drop-weight must be attached to the carriage. If the user tries to enter *parameter input* from *manual control* without the drop-weight attached it will be prompted by a dialog allowing him to either cancel the action or to automatically pick up the drop-weight and change state.

If either the physical emergency button or any door is open the system should enter to the *emergency* state.

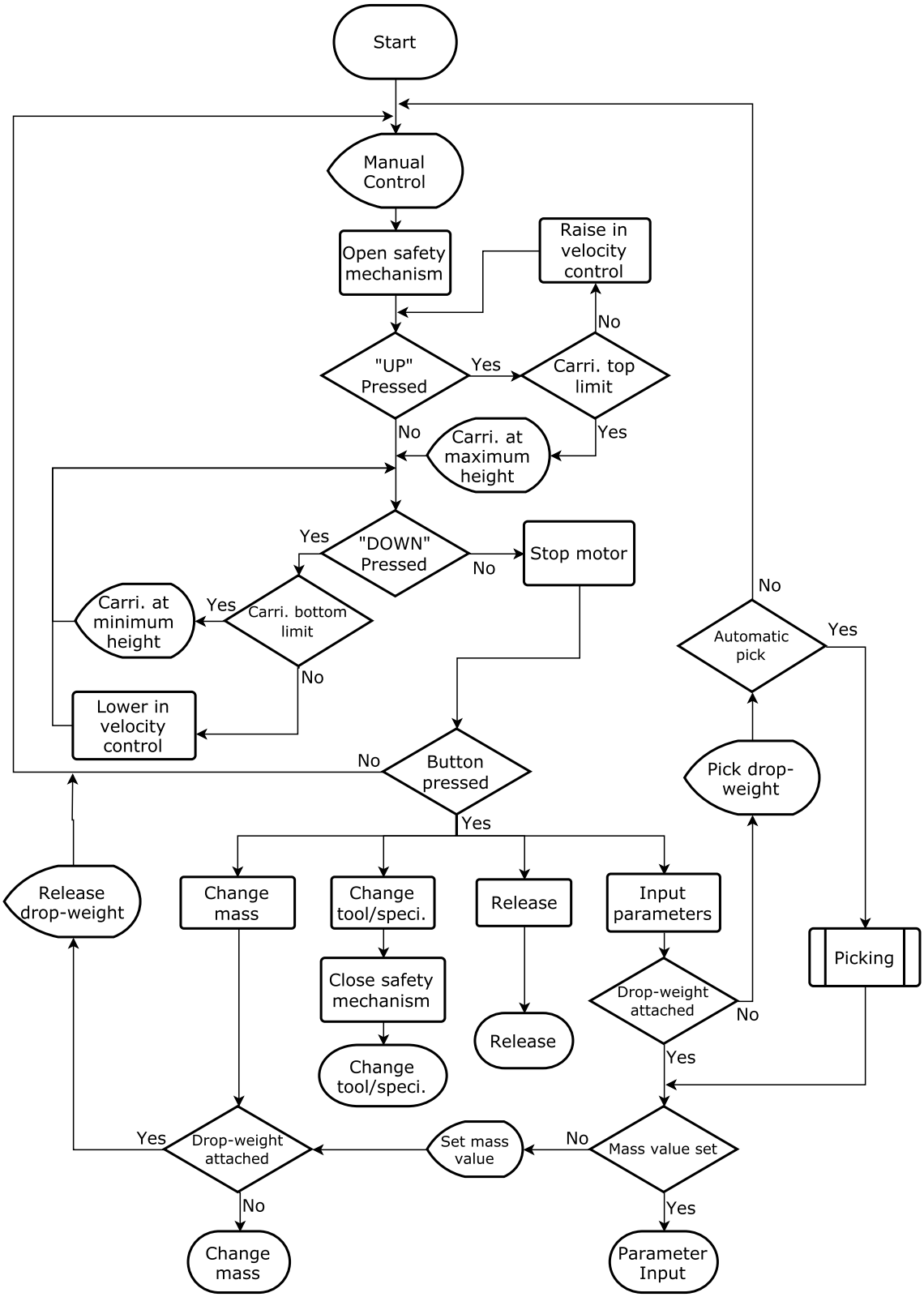

Figure 5.4: Manual control state flowchart

5.1.3 Changing mass

The *changing mass* routine (Figure 5.5) starts by unlocking the top door, allowing the user to open the door without triggering an emergency transition. Once the user is done setting up, the system checks if the doors are closed and locks the door, returning to its default state. Finally it prompts the user for the current mass of the drop-weight.

5.1.4 Changing tool or specimen

The *changing tool or specimen* routine (Figure 5.6) shares most the logic of the changing mass routine, but instead of unlocking/locking the top door, it unlocks/locks the bottom door, and instead of asking the user for the mass value it sets a new impact point.

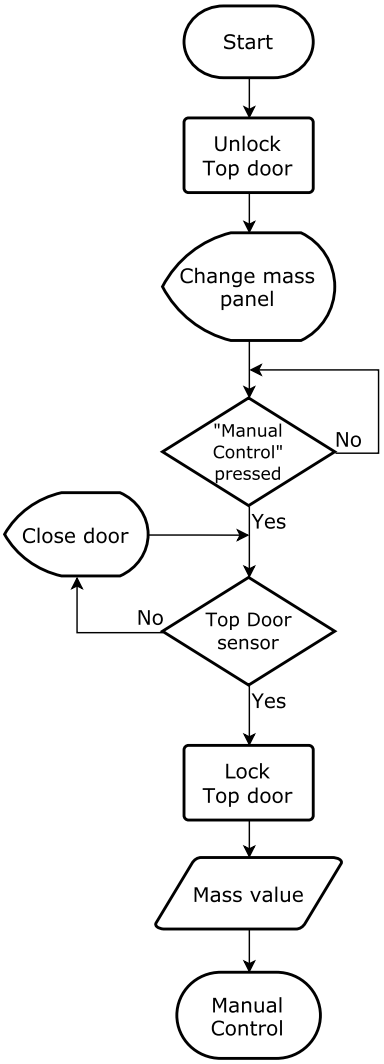

Figure 5.5: Changing mass state flowchart

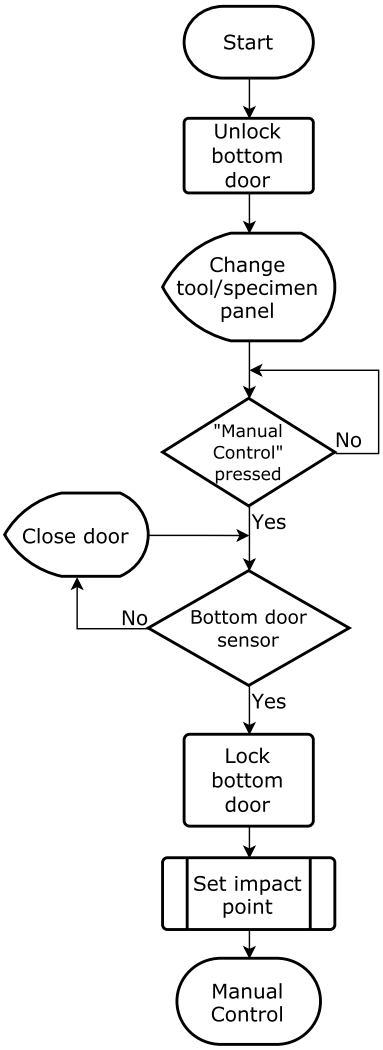

Figure 5.6: Changing tool or speci. state flowchart

5.1.5 Parameter input

The *parameter input* state (Figure 5.7) allows the user to introduce the test parameters. It allows the user to revert back to *manual control* until the ready button is pressed.

Once the ready button is pressed the *positioning* routine is initiated. It starts by setting a flag informing the system that the drop-weight is positioned and reads the input parameters from the GUI (Section 5.2.2.3). In case the *parameter input* is either velocity or energy, the height is computed and passed to the position control routine.

As in *manual control*, if either the physical emergency button or any door is open the system should enter to the emergency state.

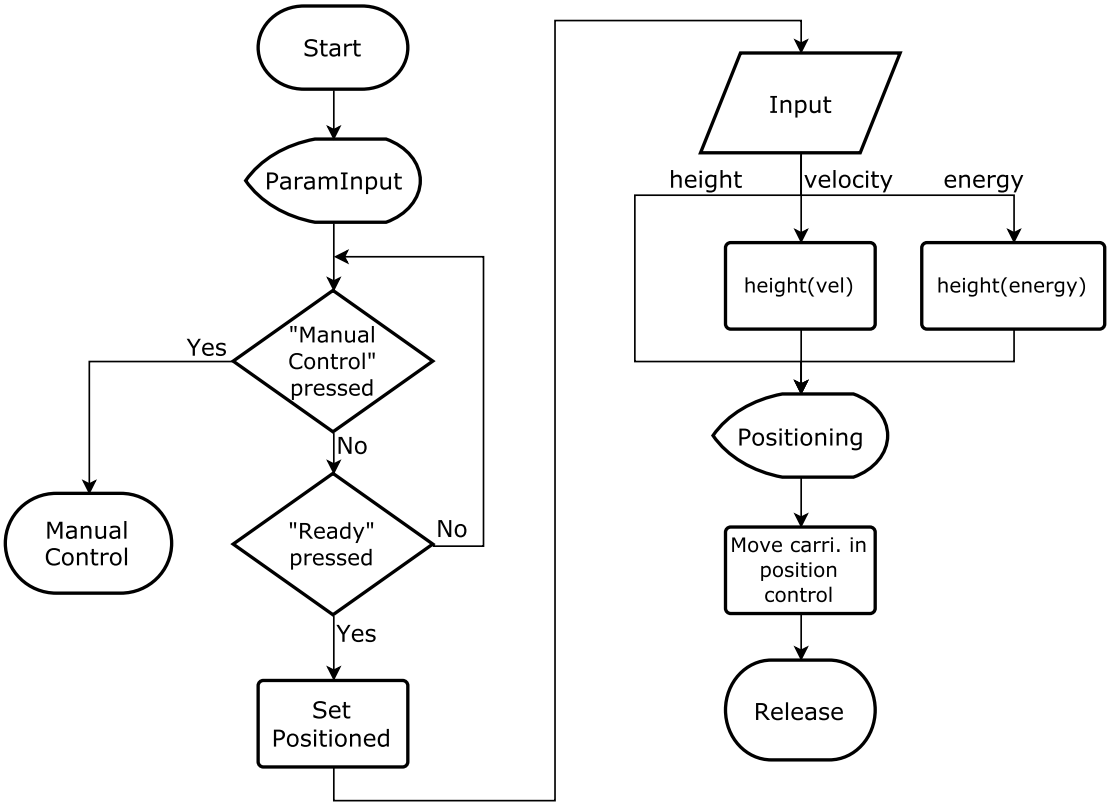

Figure 5.7: Parameter input state flowchart

5.1.6 Release

The *release* state (Figure 5.8) serves as a confirmation state and as an acquisition state.

In the first stage it prompts the user with the option to return to either *manual control* or to change the test parameters in the *parameter input* state. If the user confirms the release, this is delayed so that the user can setup a recording method. Currently this delay is set to 3 seconds but it should be adjusted after real-life usage.

Secondly, if the user sets for release from *manual control*, the positioned flag is not set and the machine would return to *manual control*. If the user sets the release from *parameter input*, the system would start the data acquisition.

Finally, the system starts acquiring the velocity of impact and once it is done, it starts reading and storing the acceleration data in an array, `[t_accel, acceleration_value]`.

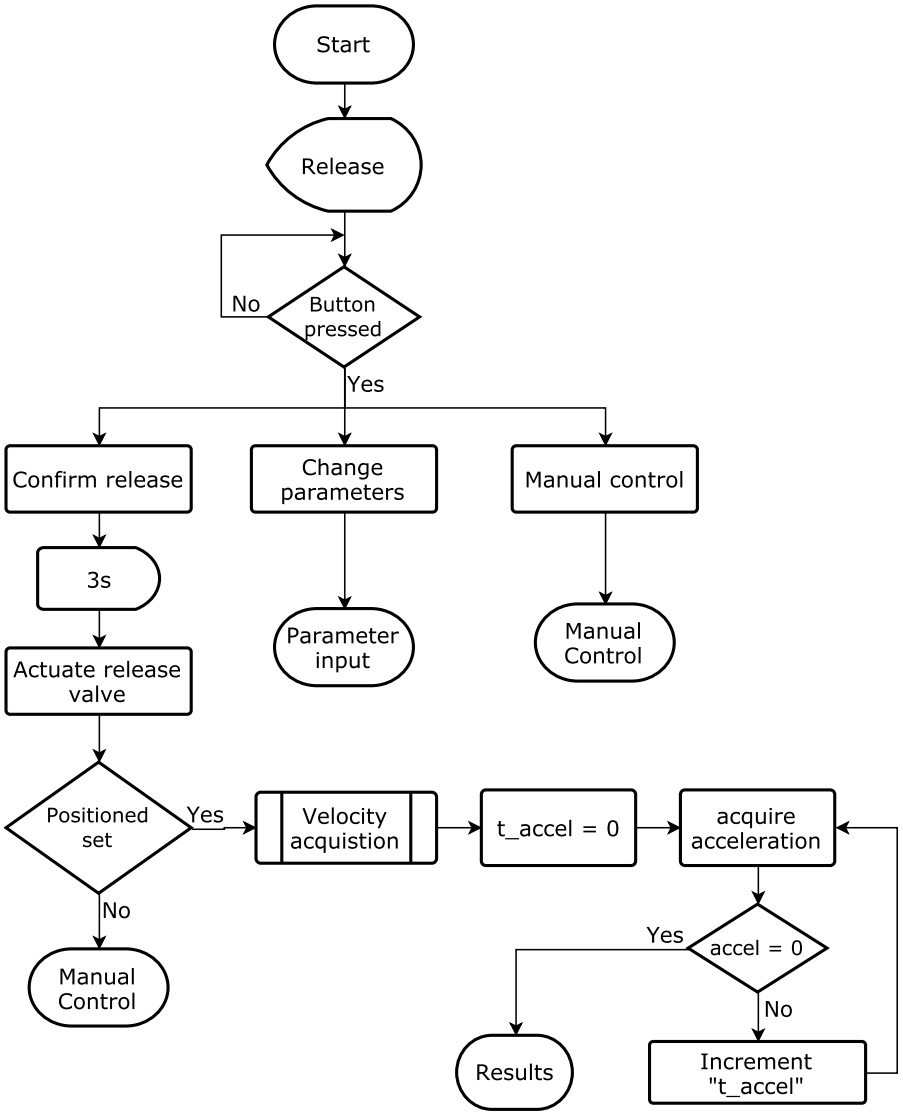

Figure 5.8: Release state flowchart

5.1.7 Results

Results state (Figure 5.9) is where the user gets the feedback from the acquired data.

It starts by computing and plotting the data relevant to the user, explained in Appendix B.

While the user examines the output data the system will pick the drop-weight and reset the impact point. This is done to prevent the user to loosen the cable by trying to lower the drop-weight past its impact point, if the machine is set to return to *manual control*.

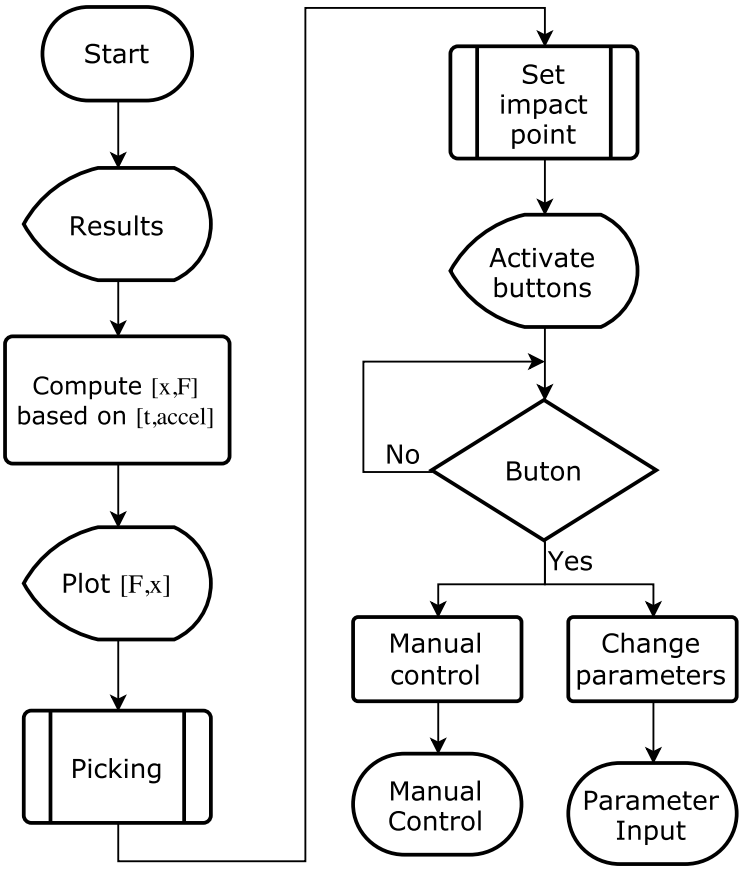

Figure 5.9: Results state flowchart

Finally it activates the buttons and waits in an infinite loop until the user presses one of the buttons and the system is taken to the respective state.

5.1.8 Emergency

The *emergency* state, as envisioned by Barbosa [1], is a particular state because the actions associated with it are focused on the panelboard where the energy is cut from both gearmotors and the pneumatic directional valve (Sections 4.1, 4.4.2 and 4.2).

Its transition is triggered either by pressing the emergency physical button or a breach detected by the security detectors.

In order to return to its normal function the machine must be reinitialized by going through the initialization routine, in which the security conditions must be verified.

5.1.9 Auxiliary routines

The routines encapsulated within a macro process (set impact point, picking and velocity acquisition) are described in this section.

5.1.9.1 Set impact point

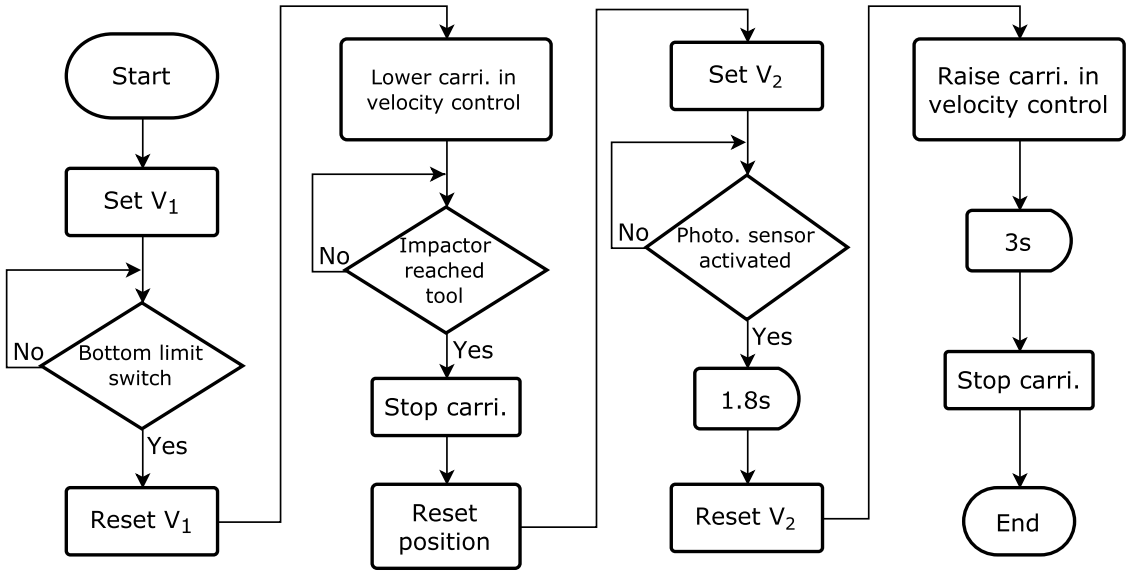

Figure 5.10: Set impact point routine flowchart

The set impact point routine (Figure 5.10) positions the photoelectric detector (Section 4.4.1) and resets the lower reference.

First it lowers the photoelectric detector to its lowest position to avoid collision with the carriage (Section 3.3) by setting V_1 already defined in Section 4.4.2.1 as the action that lowers the detector. Once the bottom limit switch is reached, the system stops the velocity acquisition gearmotor and starts lowering the carriage in velocity control until a sudden change in the acceleration is noticed. Then it stops the carriage and resets the bottom reference.

Then it sets V_2 to raise the photoelectric detector until it is activated, and after 1.8 seconds, it stops the gearmotor. This value is obtained by dividing the length of the interfering part (Section 4.4.1.1), of 19 mm by the linear velocity of the photoelectric detector, 11.1 m/s.

Finally, it raises the carriage in velocity control for 3 seconds positioning the carriage at around 300 mm from the impact point.

5.1.9.2 Picking

The picking routine (Figure 5.11) lowers the carriage (Section 3.3) in velocity control until the release clamp (Section 3.3.4) locks onto the drop-weight, approximately 75 mm below the drop-weight detector (Section 4.2.3), and raises again in velocity control to around 200 mm, so it can be better integrated with the other routines.

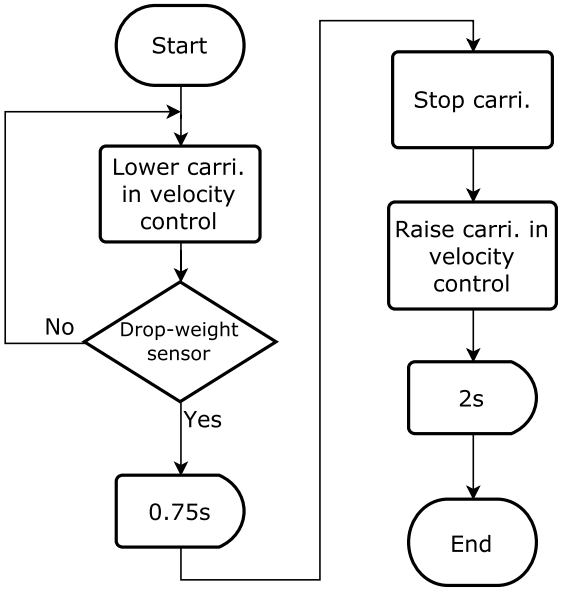

Figure 5.11: Picking routine flowchart

5.1.9.3 Velocity acquisition

On the hardware level, the velocity acquisition translates to a counter that starts with the signal edge of the photoelectric detector, increments with each clock cycle and stops with the next signal edge.

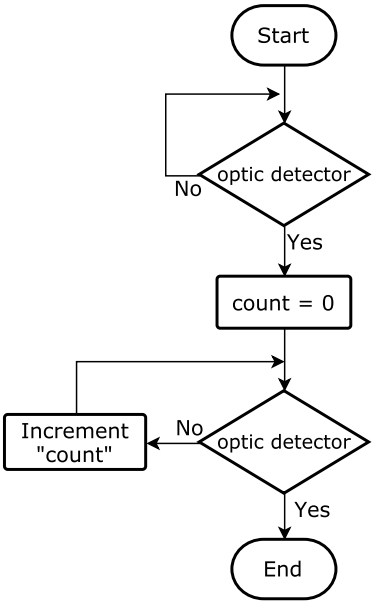

Figure 5.12: Velocity acquisition routine flowchart

5.2 User interface

This section refers to the design of the user interface, either physical or graphical, that allows the user to interact with the system, as described in Section 5.1.

5.2.1 Physical interface

The physical interface simply of four buttons.

An on/off button to power the machine that acts directly on the panelboard, two directional push buttons to be used in manual control (Section 5.1.2), connected to the data acquisition board and an emergency button that also acts directly on the panelboard, as state in Section 5.1.8.

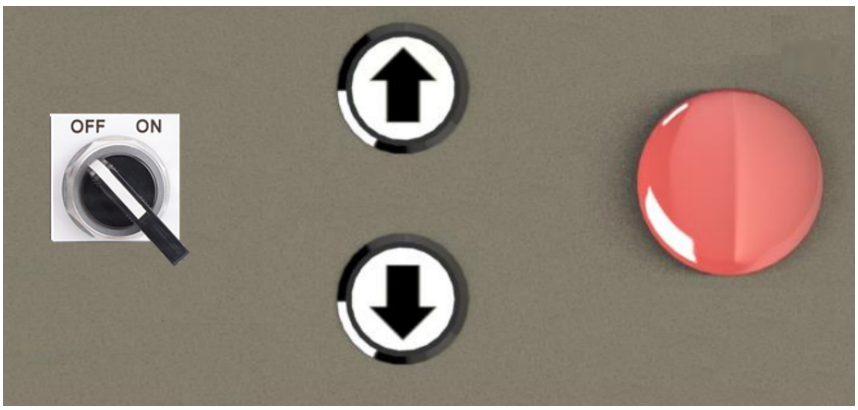

Figure 5.13: Physical panel mockup

5.2.2 Graphical user interface

The graphical interface, developed using MATLAB [16] GUIDE, allows the user to interact with the machine from the computer and is composed by 5 different panels and several dialog boxes.

The welcome panel (Figure 5.14) serves as the entry point of the GUI. Once the start button is pressed the initialization routine (Section 5.1.1) should start.

5.2.2.1 Initialization routine

The feedback about the current stage of the initialization routine would be given through wait bar boxes indicating the progress in the picking and set impact point subroutine (Figures 5.15b and 5.15a).

The feedback about the state of the doors is given through the use of a dialog box (Figure 5.15c).

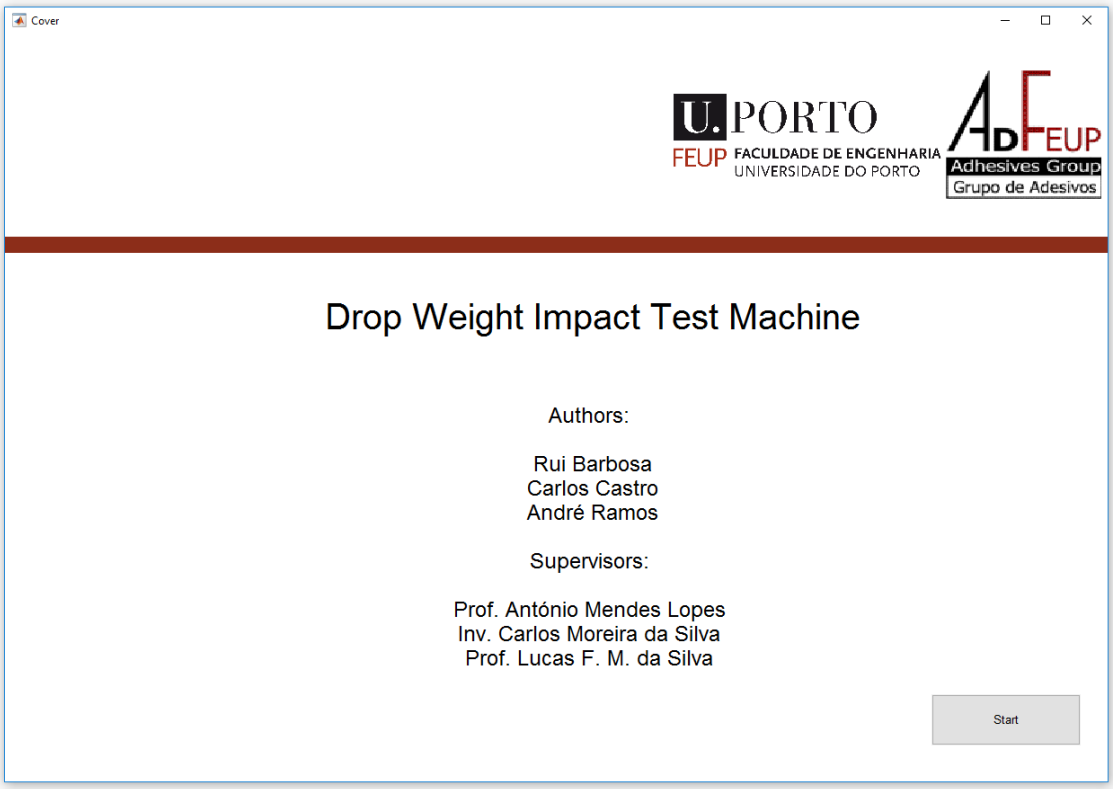

Figure 5.14: Welcome panel mockup

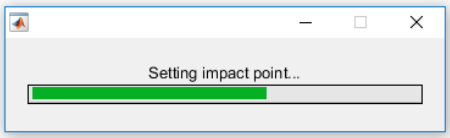

(a) Set impact point wait bar box

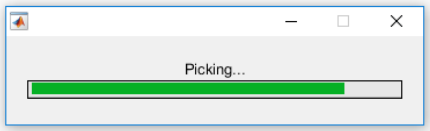

(b) Picking wait bar box

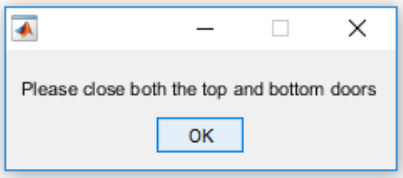

(c) Close doors dialog box

Figure 5.15: Initialization routine dialog boxes

5.2.2.2 Manual Control

Manual control needs a minimal GUI (Figure 5.16) since both the up and down buttons are in the physical interface and the feedback should be done through dialog boxes.

It is required to have four buttons to access the states defined in Section 5.1.2. In addition, it needs four different dialog boxes, similar to Figure 5.15c, to inform the user that:

- The carriage is at its top position
- The carriage is at its bottom position
- The drop-weight needs to be picked in order enter the parameter input state
- The drop-weight needs to be release to enter the changing mass state

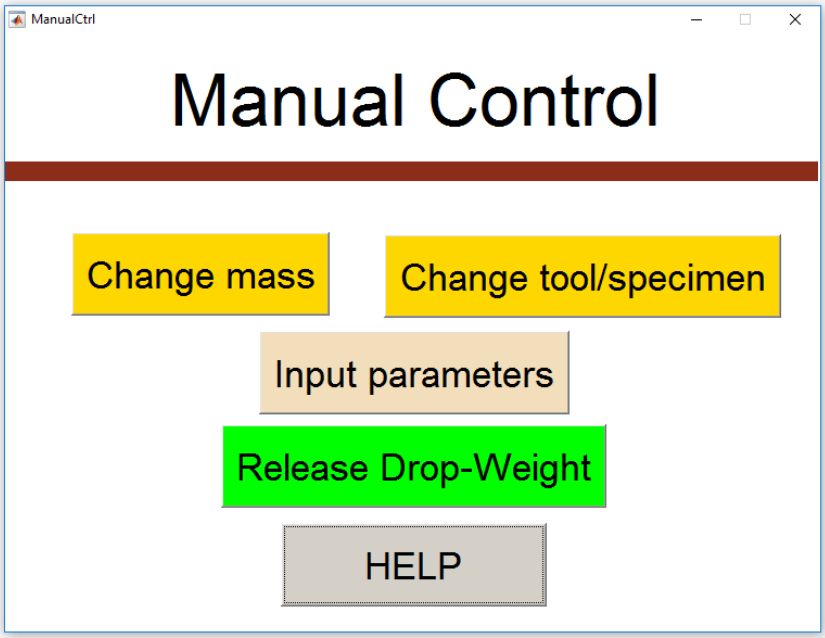

Figure 5.16: Manual control panel mockup

Since the changing mass and changing tool or specimen states are not complex enough to require their own panels, the desired functionality can be achieved also trough dialog boxes, with the *OK* button disabled until the the door detector are activated.

The mass dialog box needs an additional input parameter for the mass value as illustrated in Figure 5.17.

Finally, although not mandatory, it would have a help button to guide the user through the software.

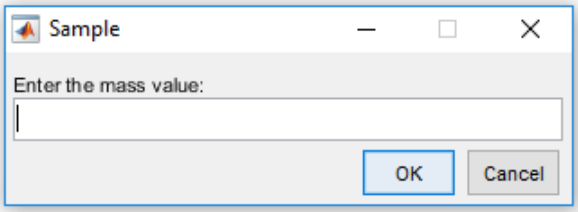

Figure 5.17: Changing mass dialog box

5.2.2.3 Parameter input

The parameter input panel needs to gather from the user which type of parameter he wants to introduce and its respective value.

As shown in Figure 5.18, this is achieved with the use of a radio button in conjunction with the respective editable text box.

It also allows the user to change states through the use of the release and manual control buttons.

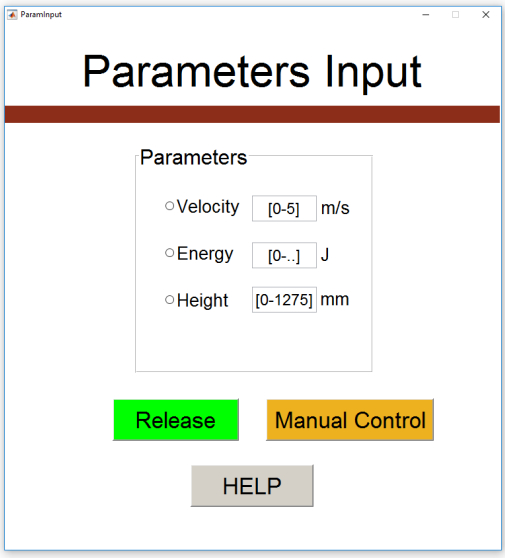

Figure 5.18: Parameter input panel mockup

As in the *manual control* GUI, this panel would also possess a help button to guide the user.

5.2.2.4 Release

The release panel (Figure 5.19) needs to allow the user to change back and forth between the manual control and parameter input states implemented with the use of push buttons.

By pressing the confirm button the user triggers a wait bar that is completed after 3 seconds, as defined in Section 5.1.6.

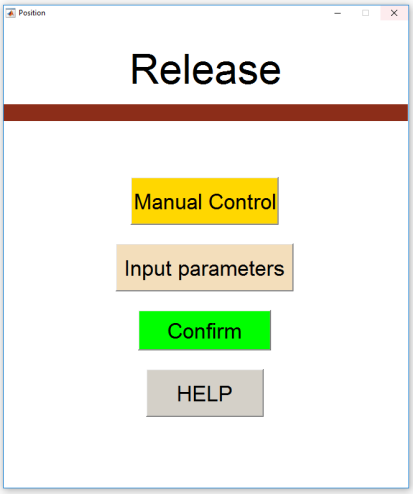

Figure 5.19: Release panel mockup

5.2.2.5 Results

The results panel needs primarily to provide the user with the test data, calculated according to Appendix B.2. This is easily achieved using the Axes tool to create an interactive plot provided in MATLAB GUIDE as shown in Figure 5.20.

Additionally, it should present the user with the measured velocity and respective energy and allow him to leave the results panel to either manual control to modify the mass, tool or specimen, or to introduce new parameters while maintaining the current setup.

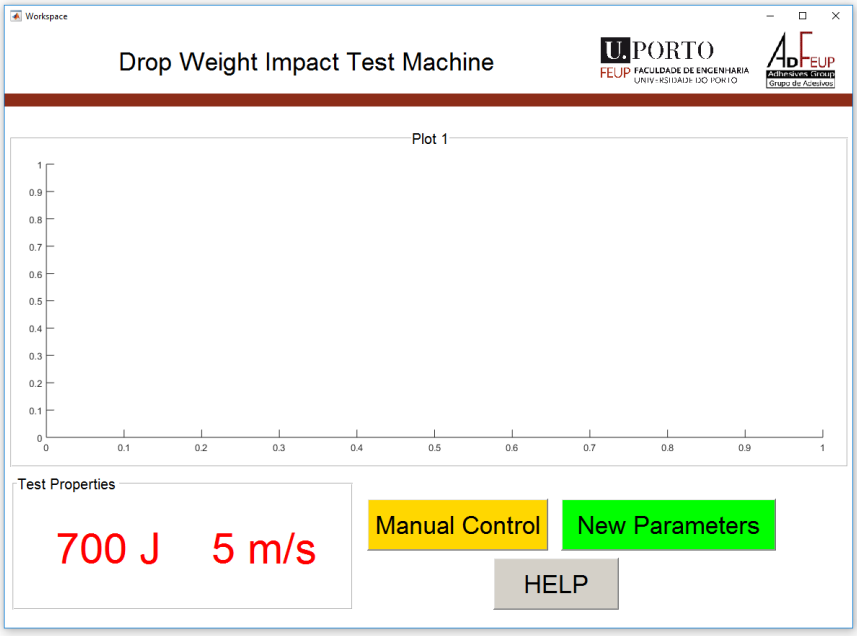

Figure 5.20: Results panel mockup

5.3 Control

As stated in Section 5.1, the carriage (Section 3.3.1) needs to be controlled in velocity and in position for different purposes. Velocity control to be used while in manual control since is up to the user to choose when to start moving upwards or downwards and the system must maintain a constant velocity. Position control for positioning the carriage (Section 3.3) through an input, prior to any test. In order to achieve this a physical model of the system must be defined.

This physical model was accomplish by considering only the dominating properties of the system, as displayed in Figure 5.21.

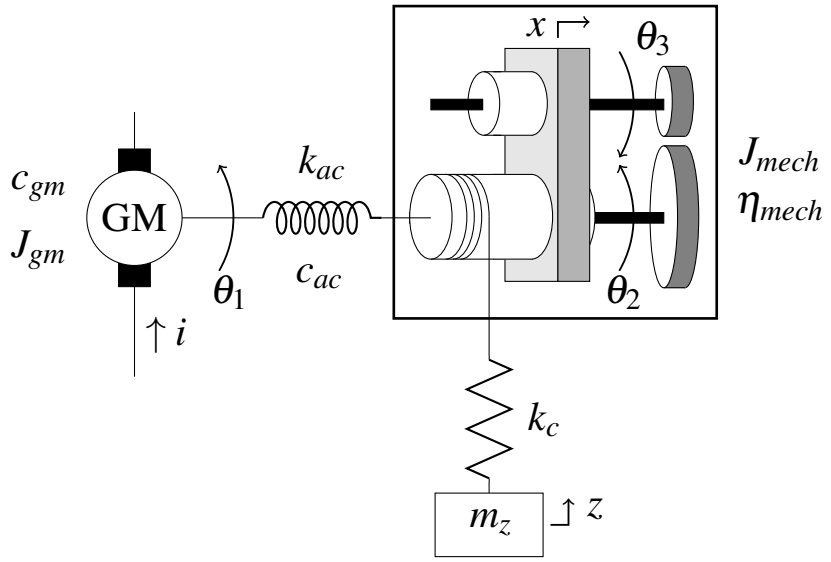

Figure 5.21: Positioning model of discrete parameters

The gearmotor possesses an inertia J_{gm} and a damping coefficient c_{gm}, seen from the gear output shaft. It is supplied by an electrical current i and rotates with an angular velocity $\dot{\theta}_1$.

The coupling possesses a damping coefficient c_{ac} and a stiffness k_{ac}.

The lifting mechanism is modeled as a subsystem with an inertia J_{mech} and an efficiency η_{mech} due to power losses generated by friction, the steel cable possesses a stiffness k_c, and finally, the drop-weight and carriage (Sections 3.4 and 3.3) are modeled as a concentrated mass m_z.

5.3.1 Mathematical model of the system

The gearmotor powers the system with an angular velocity ω and a torque T that is proportional to the current i. Since the torque constant is not supplied directly by the manufacturer, it was calculated using the motor performance curves shown in Appendix C.11.

Defining T_m as the torque provided by the electrical motor, before the reduction,

$$k_{t_m} = \eta_e \frac{\Delta T_m}{\Delta i} \tag{5.1}$$

and,

$$T = \eta_m \cdot n \cdot T_m \tag{5.2}$$

where η_e is the motor efficiency, η_m is the worm drive efficiency and n is the reduction ratio. This leads to,

$$k_t = \eta_e \cdot \eta_m \cdot n \cdot \frac{\Delta T_m}{\Delta i} = 2.462\,\text{Nm/A} \tag{5.3}$$

As for the lifting mechanism, the equivalent inertia, seen from θ_2, had to be calculated. Considering K the kinetic energy of the mechanism,

$$K = \frac{1}{2}\left(J_1 + J_b + J_{g_1}\right)\dot{\theta}_2^2 + \frac{1}{2}\left(J_2 + J_{g_1}\right)\dot{\theta}_3^2 + \frac{1}{2}\left(m_s + m_b + m_c\right)\dot{x}^2 \tag{5.4}$$

where the $\dot{\theta}_3$ is the screw shaft (Section 3.2.3) angular velocity and $\dot{x}$ is the axial linear velocity of the barrel, screw and axial connector. The inertia of the parts with the respective values are presented in Table 5.1, determined using SolidWorks [9].

Table 5.1: Lifting subsystem inertia properties

Label	Component	Value
J_1	Barrel shaft	1.56×10^{-2} kgm^2
J_b	Barrel	1.76×10^{-1} kgm^2
J_{g_1}	Gear barrel shaft	1.66×10^{-1} kgm^2
J_2	Screw shaft	1.22×10^{-2} kgm^2
J_{g_2}	Gear screw shaft	1.59×10^{-2} kgm^2
m_s	Screw	0.319 kg
m_b	Barrel	1.56 kg
m_c	Axial connector	1.68 kg

Since,

$$\dot{\theta}_3 = 2\dot{\theta}_2 \tag{5.5}$$

and,

$$\dot{x} = \frac{p_2}{2\pi}\dot{\theta}_3 = \frac{p_2}{\pi}\dot{\theta}_2 \tag{5.6}$$

where p_2 is the screw (Section 3.2.2) step. Combining Equations 5.4, 5.5 and 5.6 yields,

$$K = \frac{1}{2}\left(J_1 + J_b + J_{g_1} + 4\left(J_2 + J_{g_1}\right) + \frac{p_2^2}{\pi^2}\left(m_s + m_b + m_c\right)\right)\dot{\theta}_2^2 \tag{5.7}$$

Which in turn implies that

$$J_{mech} = \left(J_1 + J_b + J_{g_1} + 4\left(J_2 + J_{g_1}\right) + \frac{p_2^2}{\pi^2}\left(m_s + m_b + m_c\right) \right) = 0.365 \text{ kgm}^2 \tag{5.8}$$

As for the the lifting subsystem power losses, this are due to the existence of Coulomb friction between the barrel and the barrel shaft, and between the screw and the screw shaft.

Given

$$P = F \cdot v \tag{5.9}$$

the useful output power P_{out}, when velocity reaches steady state, is equal to

$$P_{out} = \dot{z} \cdot m_z \, g \tag{5.10}$$

The efficiency is determined by,

$$\eta_{mech} = \frac{P_{out}}{P_{out} + P_b + P_s} \tag{5.11}$$

where P_b and P_s are the power losses to friction in the barrel and screw respectively.

The axial friction force F_μ can be expressed by the Coulomb's law of friction,

$$F_\mu = \mu \cdot R = \mu \cdot m_z \, g \tag{5.12}$$

where μ is the friction coefficient between greased steel and bronze, with the adimensional value of 0.16.

Considering that, in steady state, $\dot{z}$ and $\dot{\theta}_2$ can be related by

$$\dot{\theta}_2 = \frac{\dot{z}}{r_1} \tag{5.13}$$

where r_1 is radius of the barrel.

Resorting to Equation 5.6 once again,

$$\dot{x} = \frac{p_2}{r_1 \, \pi} \dot{z} \tag{5.14}$$

resulting in

$$P_b = \mu \cdot m_z \, g \cdot \frac{p_2}{r_1 \, \pi} \dot{z} \tag{5.15}$$

As for P_s, in an ideal case, the linear force that the screw shaft must overcome is F_μ. Resorting to the inclined plane analogy, the free body diagram can be drawn as displayed in Figure 5.22 where r_2 is the screw radius, p_2 is the screw step, F is the force transmitted by the screw shaft and $F_{\mu t}$ is the tangential friction force between shaft and screw.

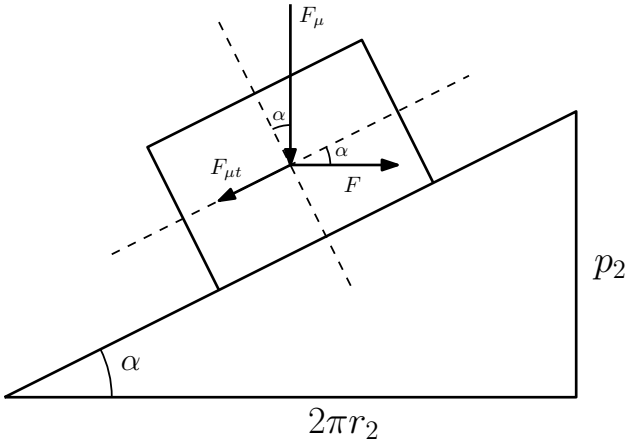

Figure 5.22: Screw free body diagram

Knowing that in steady state,

$$\sum F_{ext} = 0 \tag{5.16}$$

results in,

$$F\cos\alpha = F_\mu \sin\alpha + F_{\mu t} \tag{5.17}$$

and resorting once more to Coulomb's law of friction, it yields

$$F_{\mu t} = \mu\left(F_\mu \cos\alpha + F\sin\alpha\right) \tag{5.18}$$

Combining Equations 5.17 and 5.18, then

$$F_{\mu t} = m_z\, g \cdot \mu^2\, \frac{\cos\alpha + \sin\alpha\tan\alpha}{1-\mu\tan\alpha} \tag{5.19}$$

resulting in,

$$P_s = m_z\, g \cdot \mu^2\, \frac{\cos\alpha + \sin\alpha\tan\alpha}{1-\mu\tan\alpha} \cdot r_2 \cdot \dot{\theta}_3 \tag{5.20}$$

and combining with Equations 5.5 and 5.13

$$P_s = m_z\, g \cdot \mu^2\, \frac{\cos\alpha + \sin\alpha\tan\alpha}{1-\mu\tan\alpha} \cdot \frac{2r_2}{r_1}\dot{z} \tag{5.21}$$

Returning to Equation 5.11, replacing P_{out}, P_b and P_s and dividing both the numerator and denominator by $m_z\, g\, \dot{z}$ results in,

$$\eta_{mech} = \frac{1}{1+\mu\frac{p_2}{r_1\pi} + \mu^2\,\frac{\cos\alpha+\sin\alpha\tan\alpha}{1-\mu\tan\alpha}\cdot\frac{2r_2}{r_1}} = 96.9\ \% \tag{5.22}$$

The steel cable stiffness k_c can be estimated by default using

$$k_c = \frac{E\,A}{l} \tag{5.23}$$

where E is the Young's modulus, A the area of the rope and l the length of the cable. Since the wire has a 4 mm diameter and is 2.42 meters long, k_c is equal to 1.091×10^6 N/m.

Finally, m_z varies between 12.84 kg and 64.84 kg depending on the drop-weight mass. These values were retrieved from SolidWorks [9].

5.3.1.1 Subsystem model

With every parameter well defined, the subsystem can be modeled with a set of differential equations,

$$\begin{cases} i\,k_t = J_{gm}\,\ddot{\theta}_1 + c_{gm}\,\dot{\theta}_1 + c_{ac}\left(\dot{\theta}_1 - \dot{\theta}_2\right) + k_{ac}\left(\theta_1 - \theta_2\right) & (5.24) \\ c_{ac}\left(\dot{\theta}_1 - \dot{\theta}_2\right) + k_{ac}\left(\theta_1 - \theta_2\right) = \dfrac{1}{\eta_{mech}}\left(J_{mech}\,\ddot{\theta}_2 + r_1\,k_c\left(r_1\,\theta_2 - z\right) - r_1\,m_z\,g\right) & (5.25) \\ k_c\left(r_1\,\theta_2 - z\right) - m_z\,g = m_z\,\ddot{z} & (5.26) \end{cases}$$

To simplify the model, the coupling was considered a rigid body since the difference between θ_1 and θ_2 will hardly be relevant to the carriage vertical positioning.

The gearmotor supplier does not provide the inertia J_{gm} nor c_{gm} however, by considering the coupling as a rigid body, θ_1 is equal to θ_2 (and from this point on referred as only θ) and J_{gm} can be neglected in relation to the lifting mechanism inertia J_{mech}

This results in a simplified version of the model,

$$\begin{cases} i\,k_t = \dfrac{1}{\eta_{mech}}\left(J_{mech}\,\ddot{\theta}_2 + r_1\,k_c\left(r_1\,\theta_2 - z\right)\right) & (5.27) \\ k_c\left(r_1\,\theta_2 - z\right) - m_z\,g = m_z\,\ddot{z} & (5.28) \end{cases}$$

5.3.2 Velocity control

The system requirements for velocity control are reduced being only expected to follow a reference while being allowed to present a constant error in steady state. Because of this, a proportional controller was chosen.

To simulate the system behavior, MATLAB Simulink was used.

From Equations 5.27 and 5.28 a block diagram was created in Simulink as shown in Figure 5.23.

Since both the position feedback from the motor and the control action, done by computer, will happen in discrete time, a sample frequency must be well defined.

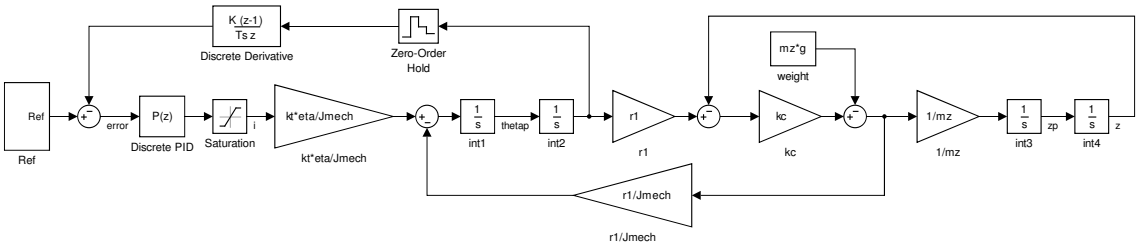

Figure 5.23: Proportional motor velocity control system

Considering the natural frequencies of the mechanism and the minimum mass m_z, results in

$$\omega_{n_{mech}} = \sqrt{\frac{k_c\ r_1^2}{J_{mech}}} = 45.7 \text{ rad/s} \tag{5.29}$$

$$\omega_{n_{m_z}} = \sqrt{\frac{k_c}{m_z}} = 291.4 \text{ rad/s} \tag{5.30}$$

Since the Nyquist rate is by definition twice the maximum component frequency being sampled and that is good practice choosing a sample rate 10 times the Nyquist rate, then

$$f_s = 20 \cdot \frac{\omega_{n_{m_z}}}{2\ pi} = 927 \text{ Hz} \tag{5.31}$$

so a sample rate of 1 kHz was chosen.

This sample rate is used on the zero-order hold, that simulates the motor angular position acquisition, the discrete derivative, and discrete control action.

The discrete derivative is used to differentiate the discrete signal from the encoder, to obtain its angular velocity that is used to calculate the error between the reference and current angular velocity.

The saturation block is used to assure that the motor is not overloaded with an excessive current, above 8.4 A.

Because the system is not static when $z = 0$ and $\theta = 0$, a z_0 initial condition had to be defined in integrator block, `int4` to correspond to the static extension of the wire rope due to the weight of m_z,

$$z_0 = \frac{m_z\ g}{k_c} \tag{5.32}$$

Because the control system feedback is done at the motor, the controller cannot act based on the error of linear velocity. Then the reference must be provided as an angular velocity correspondent to the desired linear velocity.

It was chosen an angular velocity of 3.6 rad/s, below the motor maximum velocity of 3.98 rad/s that corresponding to 108 mm/s, which is according to the specification.

In Figure 5.24 is displayed the velocity ramp response signal for both the minimum and maximum mass.

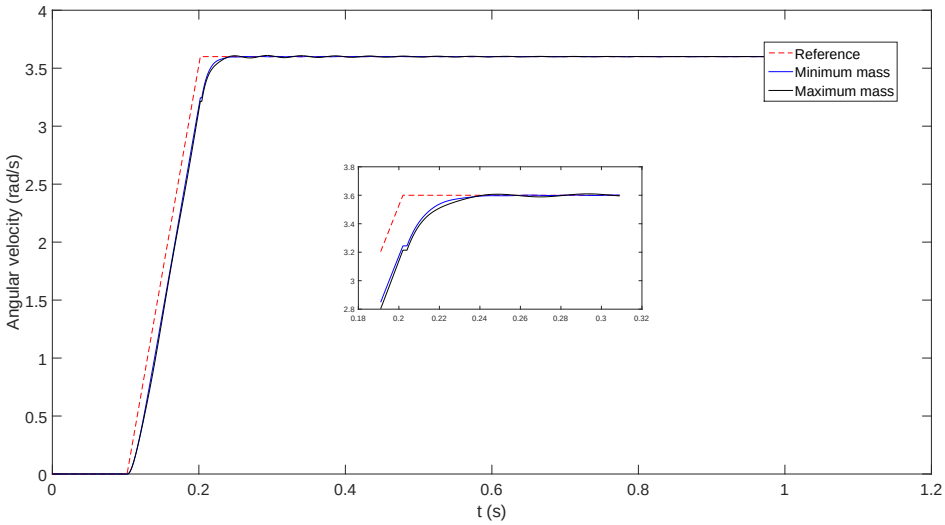

Figure 5.24: Velocity ramp response

By feeding the system with a ramp reference (red dashed line) (Figure 5.24) for 0.1 seconds with a slope of 36 rad/s^2 the desired velocity reference of 3.6 rad/s is achieved, without sudden movements that cause the mass m_z to oscillate.

After iteratively adjusting the proportional gain to 19.5 As/rad, a settling time of 0.12 seconds was achieved without compromising the stability of m_z (Figure 5.25).

It is noted in both responses that the variation in mass does not produce relevant shifts in the response.

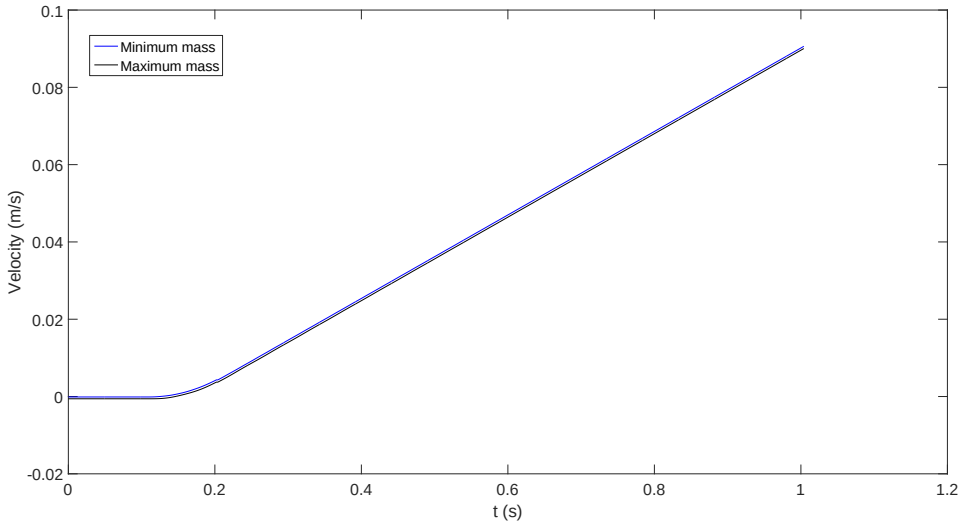

Figure 5.25: m_z position evolution

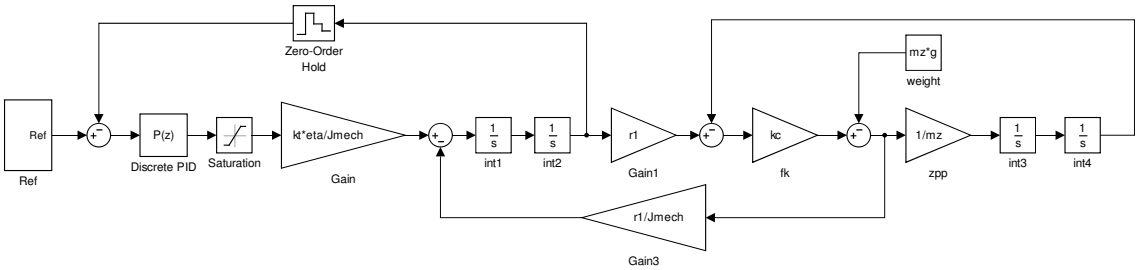

Figure 5.26: Proportional motor position control system

5.3.3 Position control

Position control, although more demanding than velocity control, can also be accomplished with a proportional controller. As perceived in Figure 5.24, the velocity control system presents a constant steady state error to the ramp signal, which implies a type 1 system. By introducing an integrator, the system becomes of type 2 and presents null error to both the step and ramp signals and constant error to the parabola signal.

In Figure 5.26 it is displayed the MATLAB/Simulink model, almost identical to the velocity control model, excluding the discrete derivative block, that is no longer needed since the position is measured directly.

To accomplish a smooth movement while achieving the desired average velocity, an half sinusoidal wave was adopted as the reference signal. This should be shaped as,

$$\begin{cases} \dfrac{\theta_A}{2}\left(1-\cos\dfrac{\pi\dot{\theta}_r}{\theta_A}t\right), \ 0<t<\dfrac{\theta_A}{\dot{\theta}_r} & (5.33) \\ \theta_A \qquad\qquad , \ t\geq\dfrac{\theta_A}{\dot{\theta}_r} & (5.34) \end{cases}$$

where $\dot{\theta}_r$ is the desired velocity of 3.6 rad/s and θ_A is the reference amplitude. Feeding this reference to the system, after adjusting the proportional gain to 50 A/rad produces the results shown in Figure 5.27 are produced.

The controller was simulated against both the angle that produces the maximum displacement (red dashed), with the maximum (black) and minimum (blue) masses, and an average angle that produces a 200 mm displacement (magenta dashed), also with both mass edge cases (gray and cyan).

In Figure 5.28 are illustrated the mass, m_z, displacement results. In the 4 cases, the simulation shows that the mass oscillates in the 1 mm range, which is according to the specification. The real-life usage is expected to present an oscillation even lower since this model doesn't contemplate the energy dissipation in the steel wire nor drag.

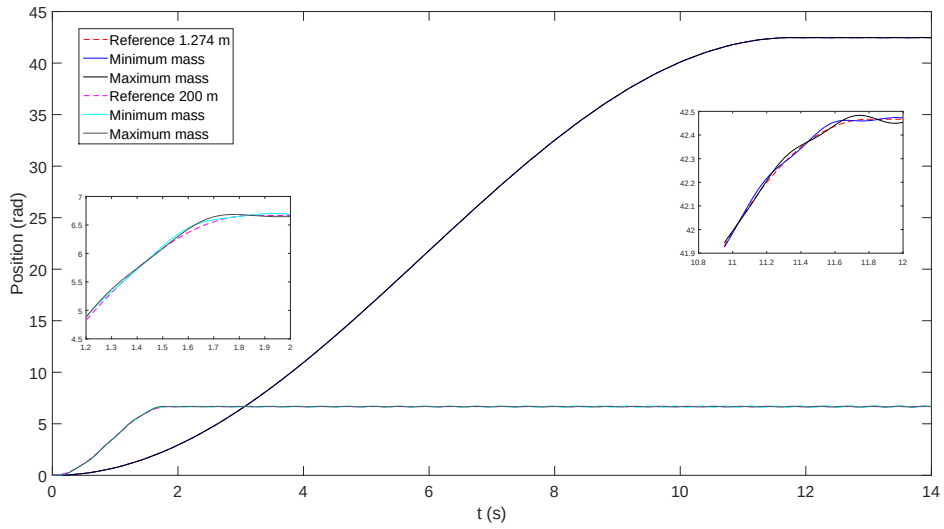

Figure 5.27: Angular position response to half sinusoidal wave signal

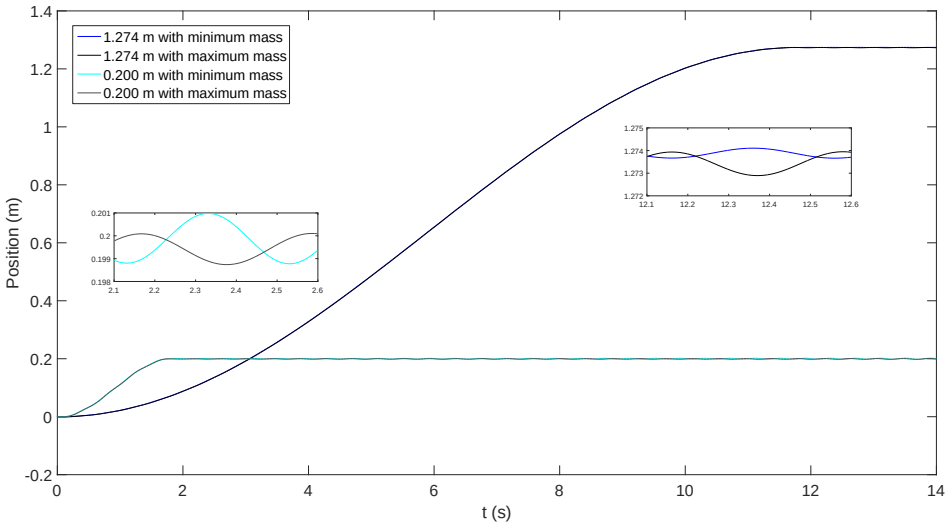

Figure 5.28: Mass m_z position response to half sinusoidal wave signal

Chapter 6

Conclusion

This chapter is intended to summarize the main conclusions of the thesis, reporting the main developments and results achieved. The current state of implementation and the future work to be done to improve the system are also addressed.

6.1 Conclusions

On a first stage, it was sought to understand the requirements needed for the machine. To achieve this a study of available commercial models was completed, accompanied by a study of the types of tests that these models are able to accomplish and that the developed machine must also be able to do.

Subsequently it was sought to improve the existing machine structure since several components were over engineered that would lead to an increased financial burden. In addition to this, a base structure was conceived and a static analysis was done to revalidate the improved structure along with a frequency analysis to validate the newly conceived structure.

The drop-weight suffered a profound structural revamp to reduce its weight in order to accommodate the low energy, and high velocity impact specifications that were not contemplated in past work.

The technical and assembly drawings were elaborated for all the machined parts. This implied to revise and calculate the tolerances to ensure the assembly of all parts. Due to manufacturability limitations, several designs had to be tweaked to accommodate said limitations.

The velocity acquisition subsystem, fundamental to validate every test done by the impact machine, was conceived.

Due to supplier limitations, some components had to be substituted by their equivalents, namely the lifting gearmotor and the release solenoid. Even though a suitable gearmotor replacement was found, and the release solenoid was replaced by a pneumatic system.

Two detectors had to be implemented, the drop-weight presence detector and the top inductive detector. The drop-weight presence detector checks if the rod is attached to the carriage and the top

inductive detector signals the control system that the carriage is at the top limit, so it can respond accordingly.

Because of financial reasons, the load cell for measuring the impact force profile was replaced with a suitable accelerometer, able to achieve the same functionality while being a less expensive.

The command logic was completely redone, since its design had some inconsistencies. For performing the desired functionality, it was divided in 8 different states:

1. Initialization routine
2. Manual control
3. Changing mass
4. Changing tool or specimen
5. Parameter input
6. Release
7. Results
8. Emergency

The *initialization routine* checks the safety detectors and resets the drop-weight reference position. *Manual control* allows the user to manually move the drop-weight. *Changing mass, tool or specimen* states allow the user to modify the respective test components. *Parameter input* grants the user with the ability to set the test parameters. The *release* state allows to release the drop-weight, either from *manual control* or after a test setup. *Results* provides the user with the test data to be analyzed. Finally the *emergency* state locks all movements of the machine for safety reasons.

A graphical user interface mockup was created, for machine operation. The control systems for both position and velocity were completely redesigned to comply with to the aforementioned changes. Mathematical control models of the relevant components of the systems were obtained for controller design.

In parallel with this work, most of the components were acquired, and are currently being assembled.

6.2 Future work

This thesis presented a progress in the design, development and implementation of a drop-weight machine.

The safety layer is still lacking from the project. A physical safeguard needs to be implemented with the necessary instrumentation to protect the user from projectiles caused by the impact. Moreover, a protection mechanism needs to be conceived to protect the user from a possible steel wire failure while replacing the tool or specimen.

The electrical project must be concluded and the panelboard conceived by Barbosa [1] must be adapted to the changes carried throughout this work.

The graphical user interface serves only as a mockup and needs further developments.

It would also be interesting, although not mandatory to implement the following subsystems:

- An anti-rebound subsystem, to prevent multiple impacts in case of rebound after the first impact.
- A controlled temperature chamber for testing adhesive bonded joints at different temperatures, since the adhesive mechanical properties wildly vary with temperature.

Finally, the machine needs experimental validation both in terms of hardware and software.

Appendix A

Drawings

A.1 Assembly drawings

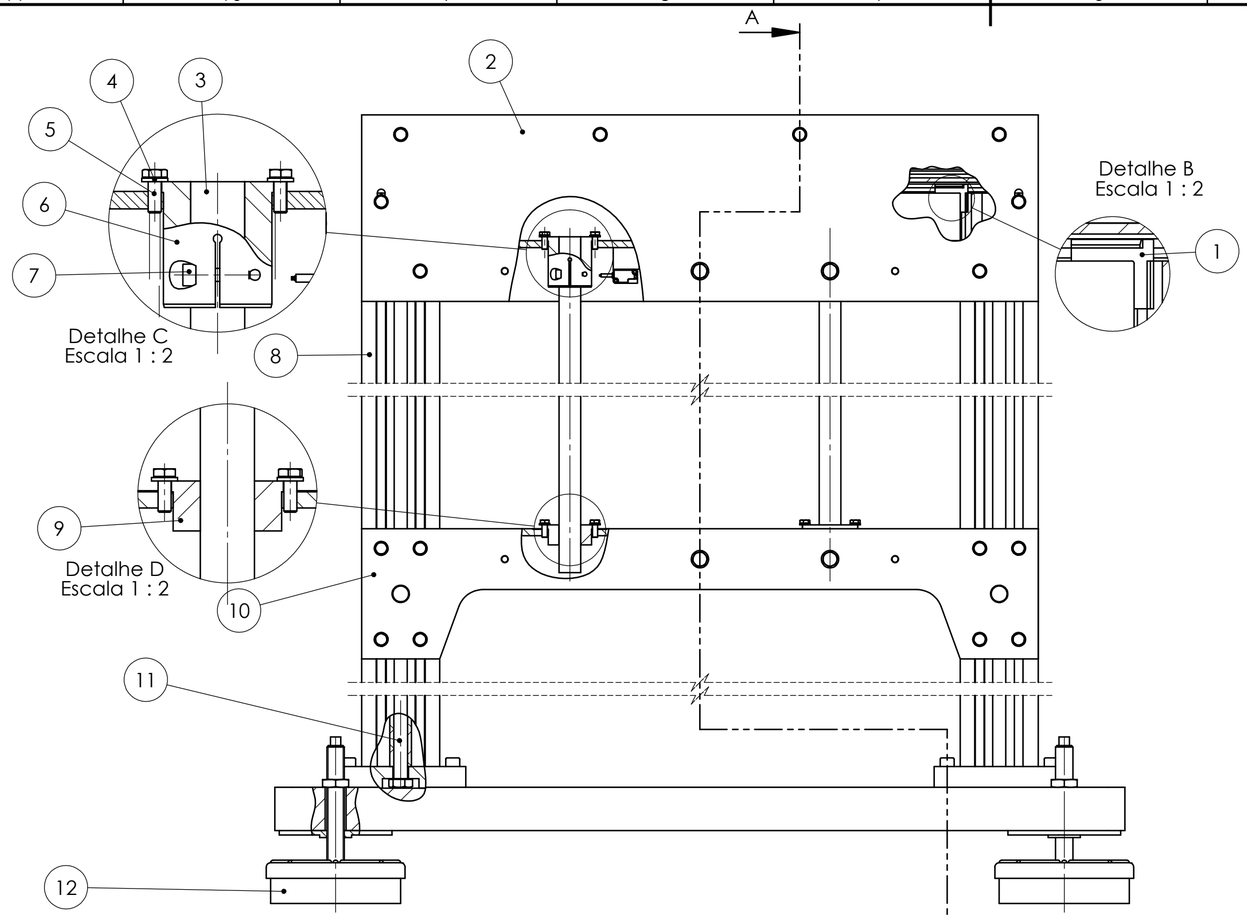

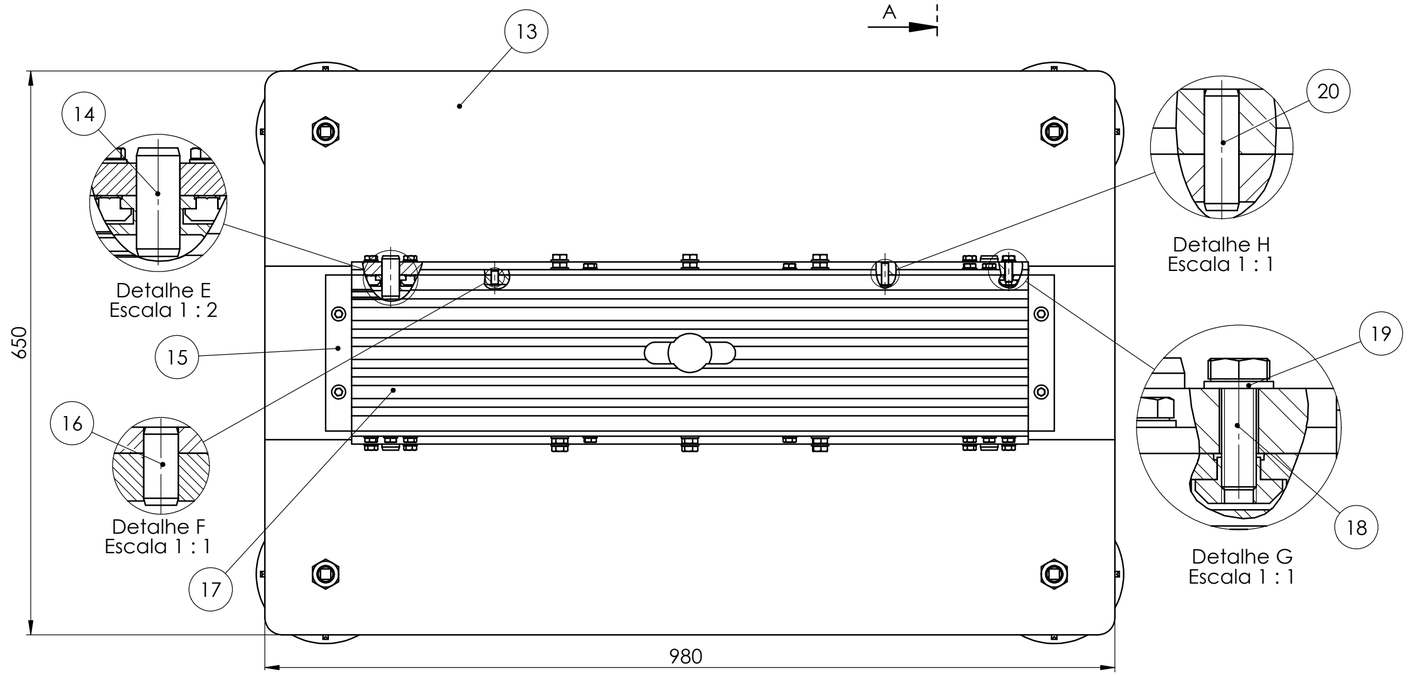

Rf nº	Designação	Norma ou Des Nº	Material	Nº	Massa	Observações
28	Porca corrediça	-	Aço	32	0,096	
27	Parafuso de cabeça hexagonal - M8 x 16	ISO 4017	Aço 8.8	16	-	
26	Mesa superior	E-10	Aço St. 37	1	12,64	
25	Parafuso de cabeça hexagonal - M10 x 20	ISO 4017	Aço 8.8	6	-	
24	Mesa inferior	E-5	Aço St. 37	1	12,64	
23	Anilha plana - M - M10	ISO 7089	Aço Inox 140 HV	12	-	
22	Parafuso de cabeça hexagonal - M10 x 30	ISO 4017	Aço 8.8	6	-	
21	Parafuso CHC - M10 x 70	ISO 4762	Aço 8.8	8	-	
20	Pino cilíndrico 8 m6 x 28	ISO 2338	Aço	4	-	Para posicionamento da mesa inferior
19	Anilha plana - M - M8	ISO 7089	Aço Inox 140 HV	32	-	
18	Parafuso de cabeça hexagonal - M8 x 25	ISO 4017	Aço 8.8	8	-	
17	Topo	E-11	Al 6063-T3	1	8,81	Perfil Bosch-Rexroth 90x180L L=780 mm
16	Pino cilíndrico 8 m6 x 18	ISO 2338	Aço	4	-	Para posicionamento da mesa superior
15	Sapata	E-8	Aço DIN Ck45	2	4,88	
14	Pino cilíndrico 20 m6 x 60	ISO 2338	Aço	4	-	
13	Base	B-1	Aço S275	1	246	
12	Pé nivelador	-	-	4	2,65	Pé nivelador Ganter+elesa LW.A-160-M20x1,5x170
11	Parafuso de cabeça hexagonal - M16 x 40	ISO 4017	Aço 8.8	4	-	
10	Suporte lateral	E-6	Aço DIN Ck45	2	8,19	
9	Casquilho inferior	E-1	Aço DIN Ck45	2	0,31	Do lado dt. deve ser montada a peça equiv. E-2
8	Montante	E-9	Al 2017 T451	2	43,45	Perfil Bosch-Rexroth 90x180 L=2530 mm
7	Parafuso CHC - M6 x 25	ISO 4762	Aço 8.8	4	-	
6	Casquilho superior	E-3	Aço DIN Ck45	2	0,67	Do lado dt. deve ser montada a peça equiv. E-4
5	Parafuso de cabeça hexagonal - M6 x 16	ISO 4017	Aço 8.8	8	-	
4	Anilha plana - M - M6	ISO 7089	Aço Inox 140 HV	8	-	
3	Guia	-	Aço	2	6,66	Veio rectificado INA-FAG L=1850 mm
2	Chapa lateral superior	E-7	Al 2017 T451	2	2,70	
1	Esquadro Interior	-	Aço	4	0,054	

FEUP

Escala 1:5

	Nome	Assinatura	Data
Desenho	André Ramos		
Verif	Inv. Carlos M. Silva		

Título:
Estrutura

Revisão:
A

Desenho Nº
C-E

A2

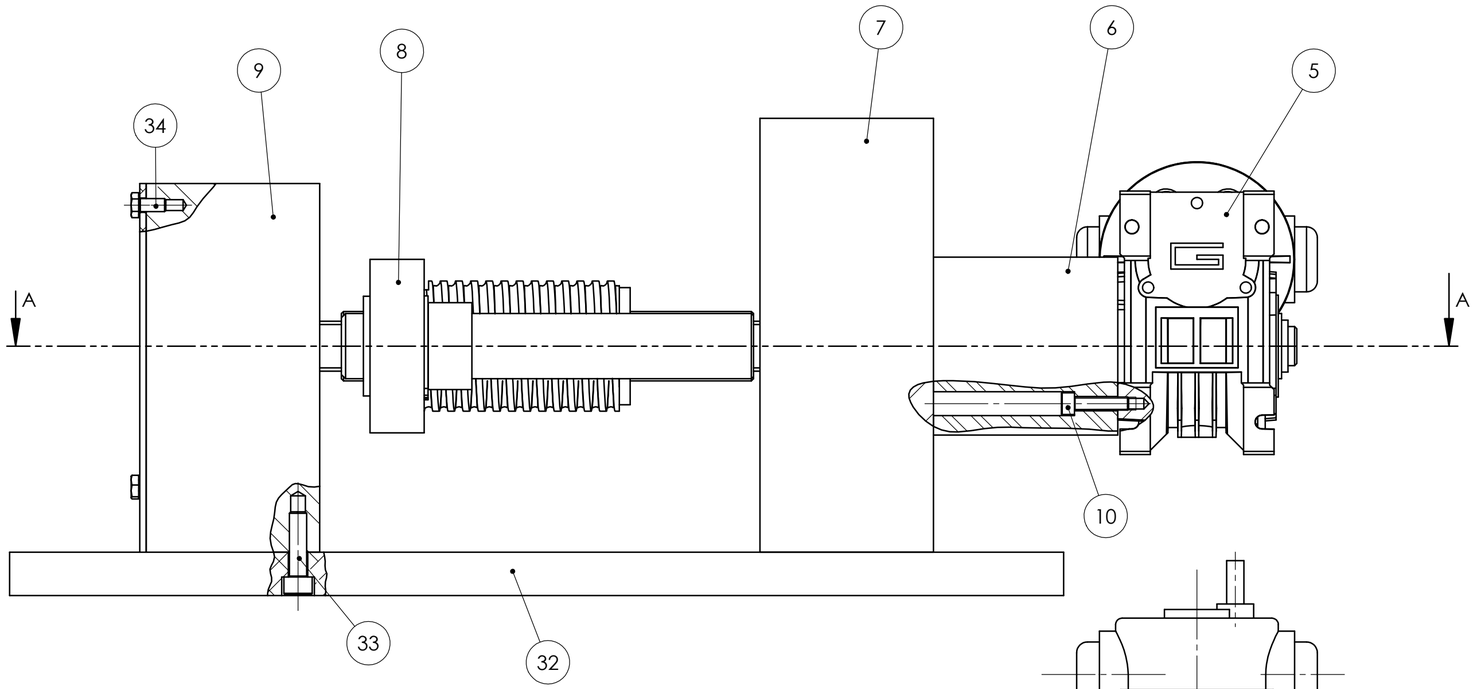

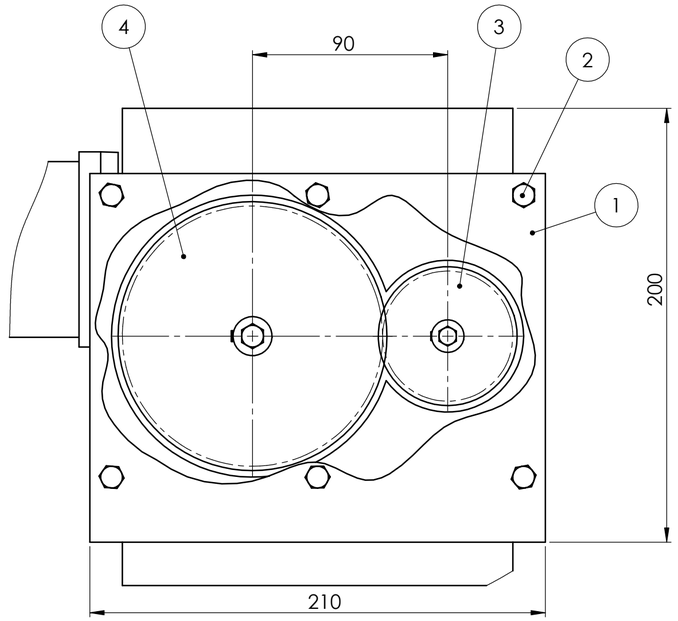

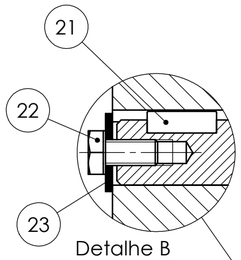

Detalhe B
Escala 1 : 1

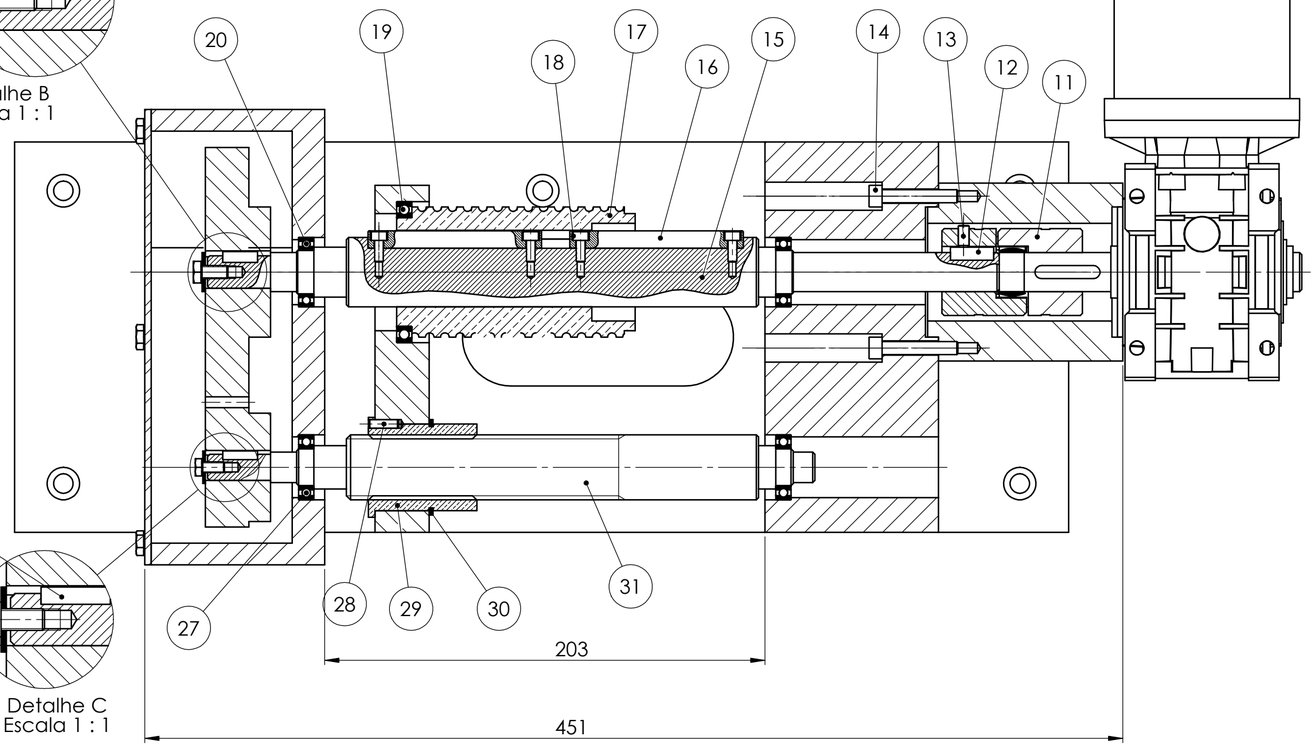

Detalhe C
Escala 1 : 1

Nº	Designação	Norma ou Des Nº	Material	Rf nº	Massa	Observações
6	Parafuso de cabeça hexagonal - M6 x 12	L-7	Aço 8.8	34	-	
8	Parafuso CHC - M8 x 30	ISO 4762	Aço 8.8	33	-	
1	Base elevação	L-10	Al 5083	32	4,53	
1	Veio translação	L-7	Aço DIN Ck45	31	1,18	
1	Anel elástico - 40 x 1,75	DIN 471	Aço	30	-	
1	Porca Motora	L-8	Bronze CuSn12	29	0,32	
1	Pino cilíndrico - 4 m6 x 14	EN ISO 2338	Aço	28	-	
2	Rolamento radial de esferas - 61903-2RZ	ISO 15	-	27	-	
1	Anilha plana - L - M5	ISO 7093	Aço 140HV	26	-	
1	Parafuso de cabeça hexagonal - M6 x 12	ISO 4017	Aço 8.8	25	-	
1	Chaveta paralela - A - 4 x 4 x 16	ISO/R 773	Aço	24	-	
1	Anilha plana - L - M6	ISO 7093	Aço 140HV	23	-	
1	Parafuso de cabeça hexagonal - M6 x 12	ISO 4017	Aço 8.8	22	-	
1	Chaveta paralela - A - 5 x 5 x 16	ISO/R 773	Aço	21	-	
2	Rolamento radial de esferas - 61804-2RZ	ISO 15	-	20	-	
1	Rolamento radial de esferas - 61810-2RZ	ISO 15	-	19	-	
4	Parafuso CHC - M4 x 10	ISO 4762	Aço 8.8	18	-	
1	Tambor	L-4	Bronze CuSn12	17	1,72	
2	Chaveta paralela - A - 10 x 8 x 80	ISO/R 773	Aço	16	-	
1	Veio tambor	L-3	Aço DIN Ck45	15	1,48	
4	Parafuso CHC - M6 x 35	ISO 4762	Aço 8.8	14	-	
2	Parafuso sem cabeça, oco HC - M5 x 10	ISO 4026	Aço 14H	13	-	
1	Chaveta paralela - A - 6 x 6 x 20	ISO/R 773	Aço	12	-	
1	Acopolamento	-	-	11	0,45	Acopolamento Rotex 19
4	Parafuso CHC - M6 x 25	ISO 4762	Aço 8.8	10	-	
1	Caixa posterior	L-2	Aço DIN Ck45	9	13,52	
1	Ligação tambor-porca	L-5	Aço DIN Ck45	8	1,74	
1	Caixa anterior	L-1	Aço DIN Ck45	7	21,24	
1	Luneta	L-6	Al 7075	6	1,15	
1	Motorredutor	-	-	5	2,7	Motorredutor Transtecno ECM 100/040 u 80
1	Roda dentada de dentes paralelos	-	Aço EN8	4	-	z = 60 m = 2
1	Roda dentada de dentes paralelos	-	Aço EN8	3	-	z = 30 m = 2
6	Parafuso de cabeça hexagonal - M6 x 12	ISO 4017	Aço 8.8	2	-	
1	Tampa engrenagens	L-9	Al 5083	1	0,29	

FEUP

Escala 1:2

	Nome	Assinatura	Data
Desenho	André Ramos		
Verif	Inv. Carlos M. Silva		

Título:

Elevação

Revisão: F

Desenho Nº C-L

A2

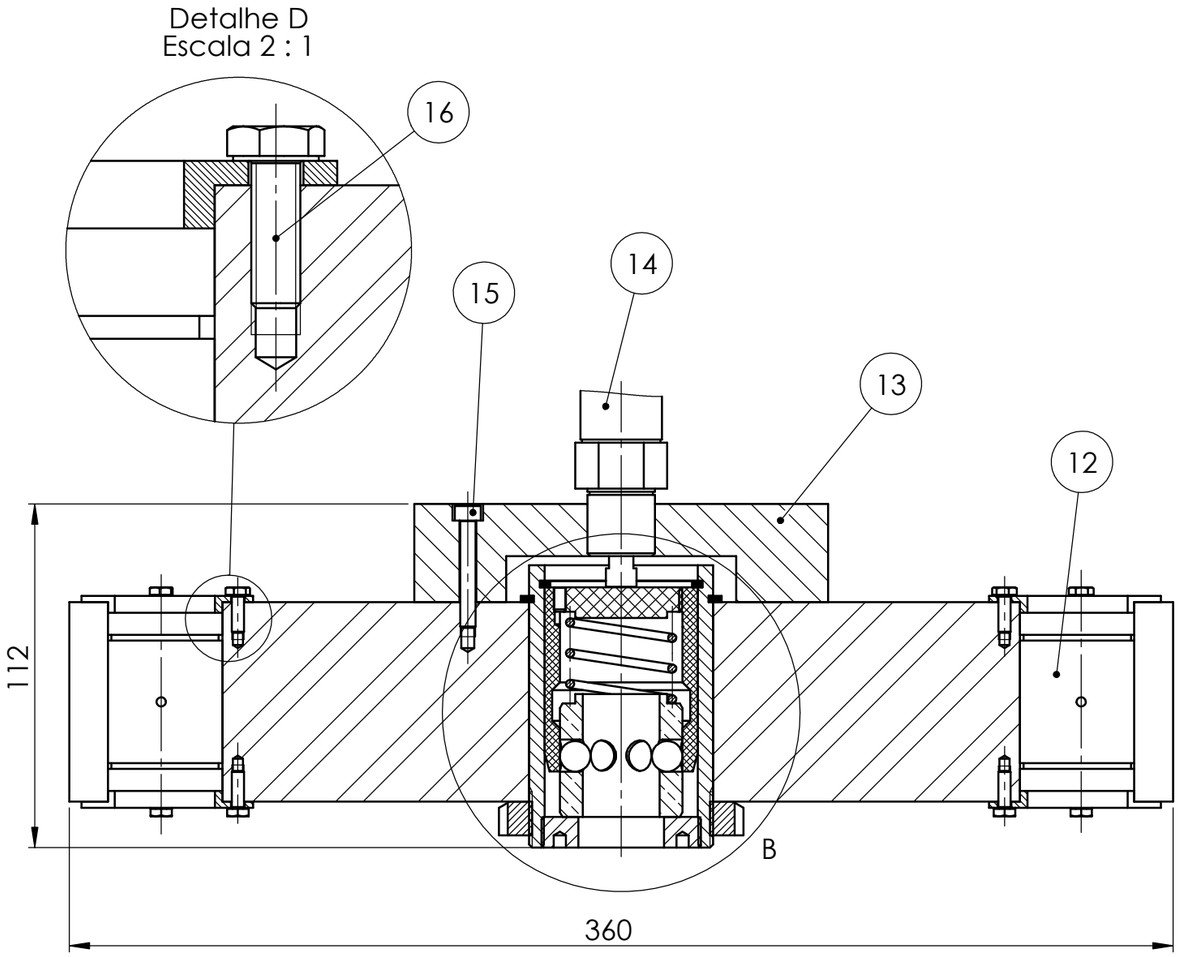

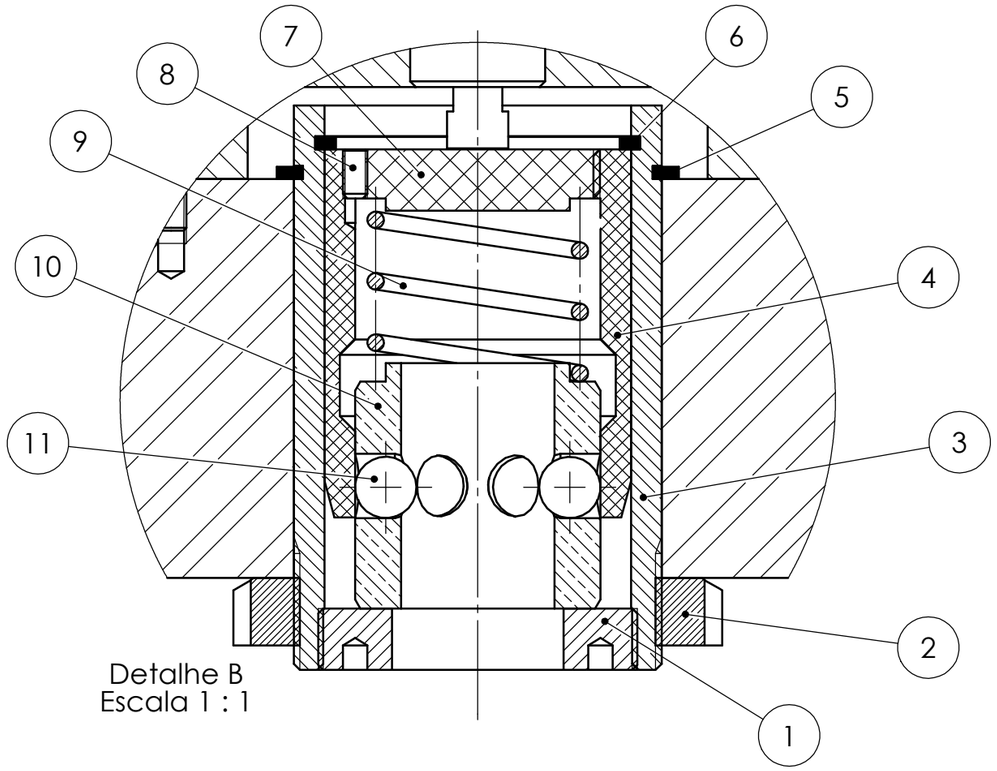

Detalhe B
Escala 1 : 1

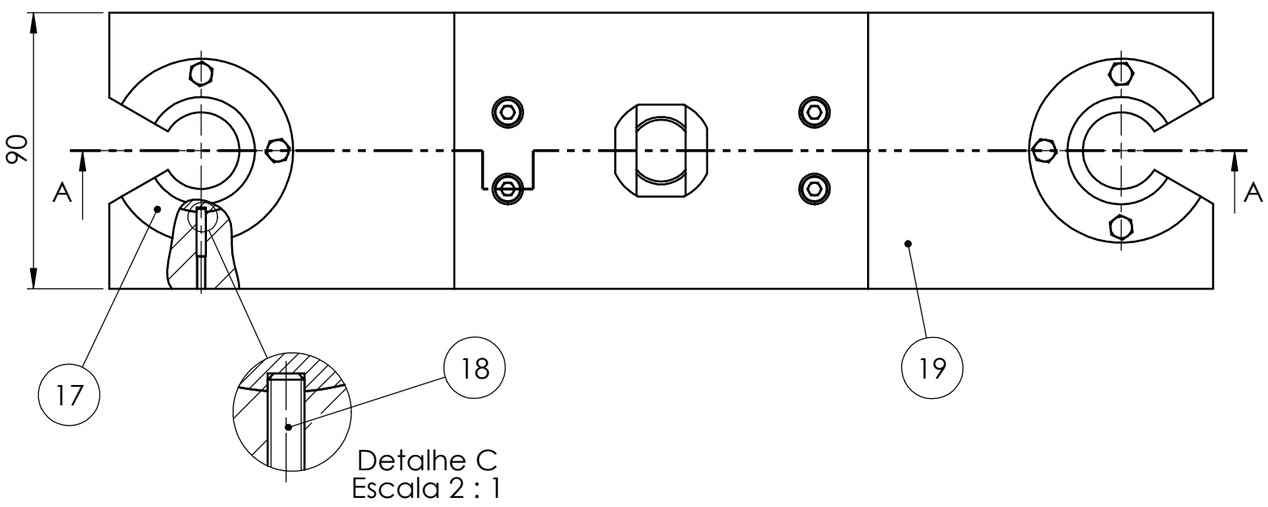

Detalhe C
Escala 2 : 1

Nº	Designação	Norma ou Des Nº	Material	Rf nº	Massa	Observações
1	Carro	T-1	Al 7075	19	4,63	
2	Parafuso sem cabeça, oco HC - M3 x 16	ISO 4026	Aço 14H	18	-	
4	Tampa rolamento	T-2	Aço DIN Ck45	17	0,03	
12	Parafuso de cabeça hexagonal - M4 x 12	ISO 4017	Aço 8.8	16	-	
4	Parafuso CHC - M5 x 16	ISO 4762	Aço 8.8	15	-	
1	Cilindro Pneumático	-	-	14	-	SMC C85N25-25S
1	Ligação carro-cilindro	T-3	Aço Ck45	13	2,41	
2	Rolamento linear de esferas	-	-	12	0,15	INA-FAG KBO25-PP
6	Esfera de rolamento	-	-	11	-	d=10
1	Porta esferas	T-8	Bronze CuSn12	10	0,22	
1	Mola	-	Aço Inox R302	9	-	L0=35 x De=36 x P=10 x d=2.7
2	Parafuso sem cabeça, oco HC - M4 x 8	ISO 4026	Aço 14H	8	-	
1	Tampo camisa esferas	T-6	igdur A180	7	0,02	
1	Anel elástico - 50 x 2	DIN 472	Aço	6	-	
1	Anel elástico - 60 x 2	DIN 471	Aço	5	-	
1	Camisa esferas	T-5	igdur A180	4	0,06	
1	Peça exterior	T-4	Aço Inox R304	3	0,61	
1	Porca ranhurada - M60 x 2	DIN 981	Aço Inox R304	2	-	
1	Tampa interior	T-7	Aço Inox R304	1	0,12	

	Nome	Data	Assinatura
Desenho	André Ramos		
Verif.	Inv. Carlos M. Silva		

Revisão: CMS

Número: 0-P

FEUP

Titulo: Posicionamento

A3

ESCALA:1:2

FOLHA 1 de 1

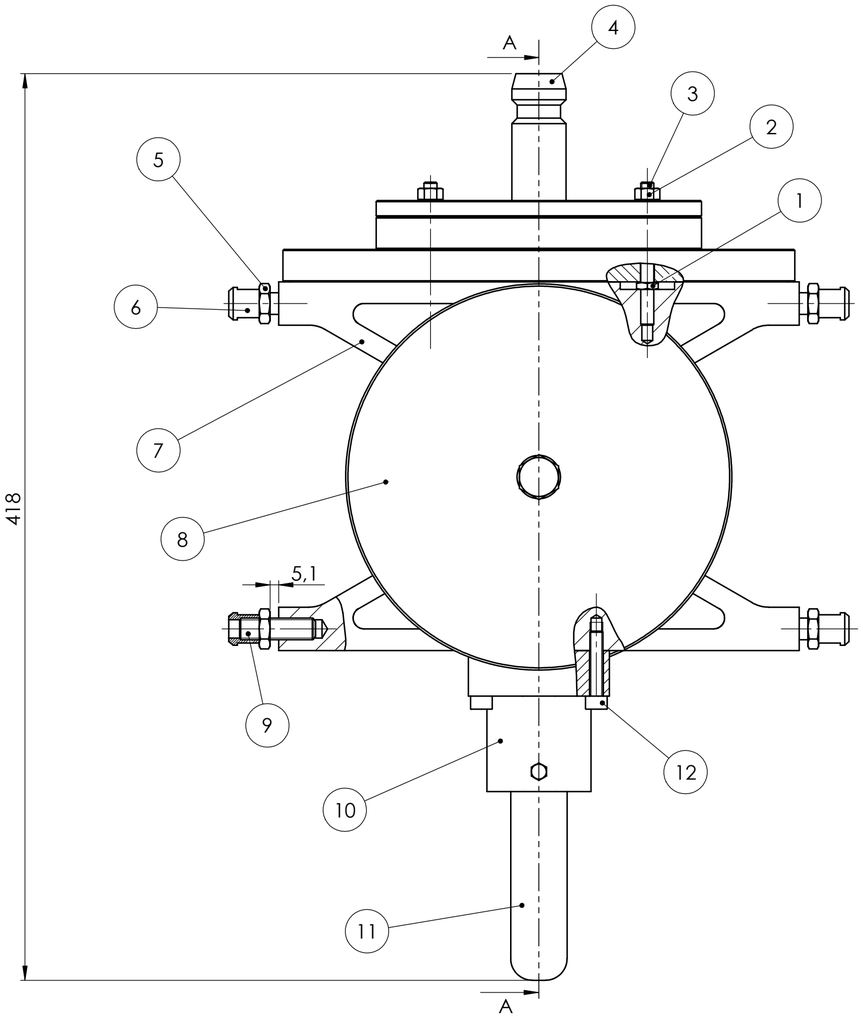

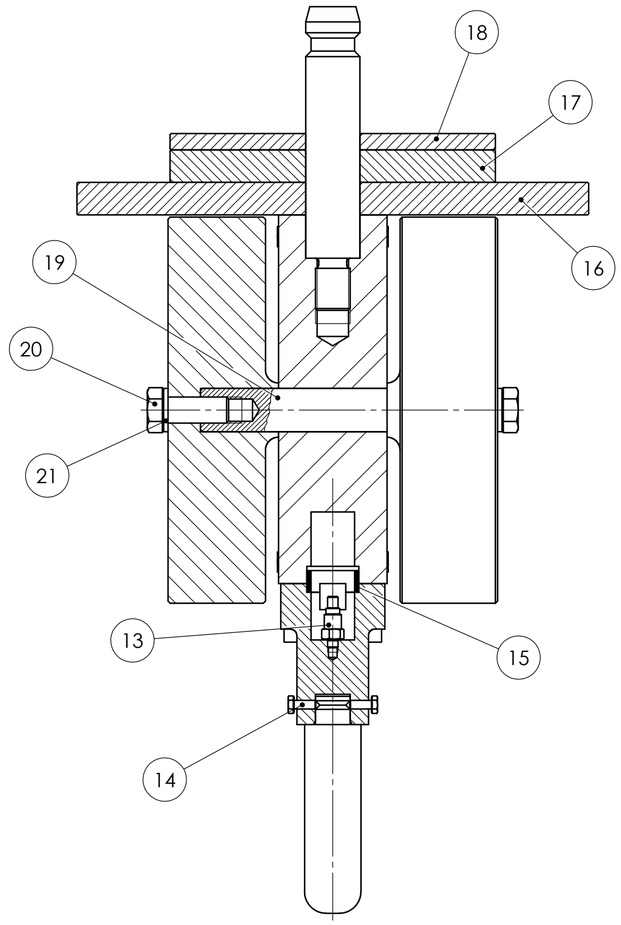

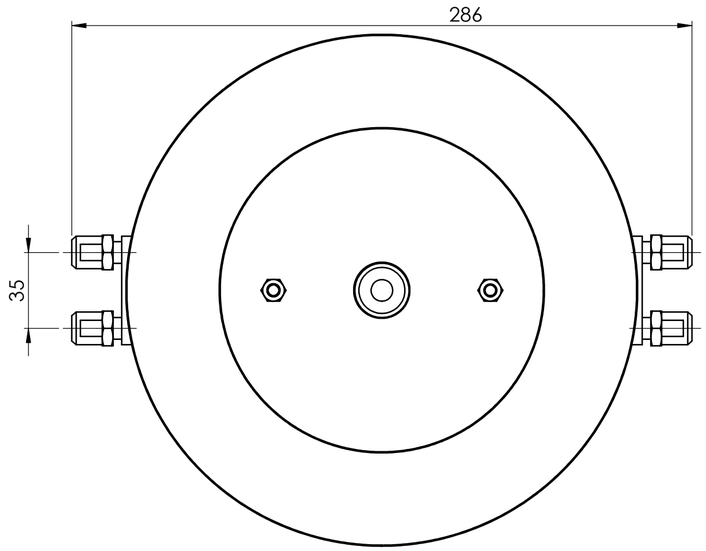

Rf nº	Designação	Norma ou Des Nº	Material	Nº	Massa	Observações
21	Anilha plana - M - M12	ISO 7089	Aço Inox 140 HV	2	-	
20	Parafuso de cabeça hexagonal - M12 x 30	ISO 4017	Aço 8.8	2	-	
19	Veio central	M-13	Aço DIN Ck45	1	0,266	
18	Extensão superior 1 kg	M-11	Aço DIN Ck45	1	1,029	
17	Extensão superior 2 kg	M-10	Aço DIN Ck45	1	2,023	
16	Extensão superior 5 kg	M-9	Aço DIN Ck45	1	5,038	
15	Manga centragem	M-12	Aço DIN Ck45	1	0,005	
14	Parafuso de cabeça hexagonal - M4 x 10	ISO 4017	Aço 8.8	2	-	
13	Acelerometro	-	-	1	0,005	Acelerometro Kistler K-shear 8742A
12	Parafuso CHC - M6 x 30	ISO 4762	Aço 8.8	4	-	
11	Impactador	M-5	Aço K600	1	0,361	
10	Alojamento acelerometro	M-6	Aço K600	1	0,775	
9	Parafuso sem cabeça, oco HC - M10 x 35	ISO 4026	Aço 14 H	8	-	
8	Extensão lateral	M-8	Aço DIN Ck45	2	5,770	
7	Bigorna	M-3	Al 7075	1	2,345	
6	Controlador de folga	M-4	Aço DIN Ck45	8	0,012	
5	Porca hexagonal - M10	ISO 4032	Aço 8	8	-	
4	Suporte massa	M-1	Aço Ceax	1	0,944	
3	Varão roscado - M6 x 70	-	Aço 5.8	2	-	
2	Porca hexagonal - M6	ISO 4032	Aço 5	2	-	
1	Porca hexagonal baixa - M6	ISO 4035	Aço 05	2	-	

FEUP

Escala 1:2

	Nome	Assinatura	Data
Desenho	André Ramos		
Verif	Inv. Carlos M. Silva		

Título: Drop-weight

Revisão: F

Desenho Nº 0-M

A2

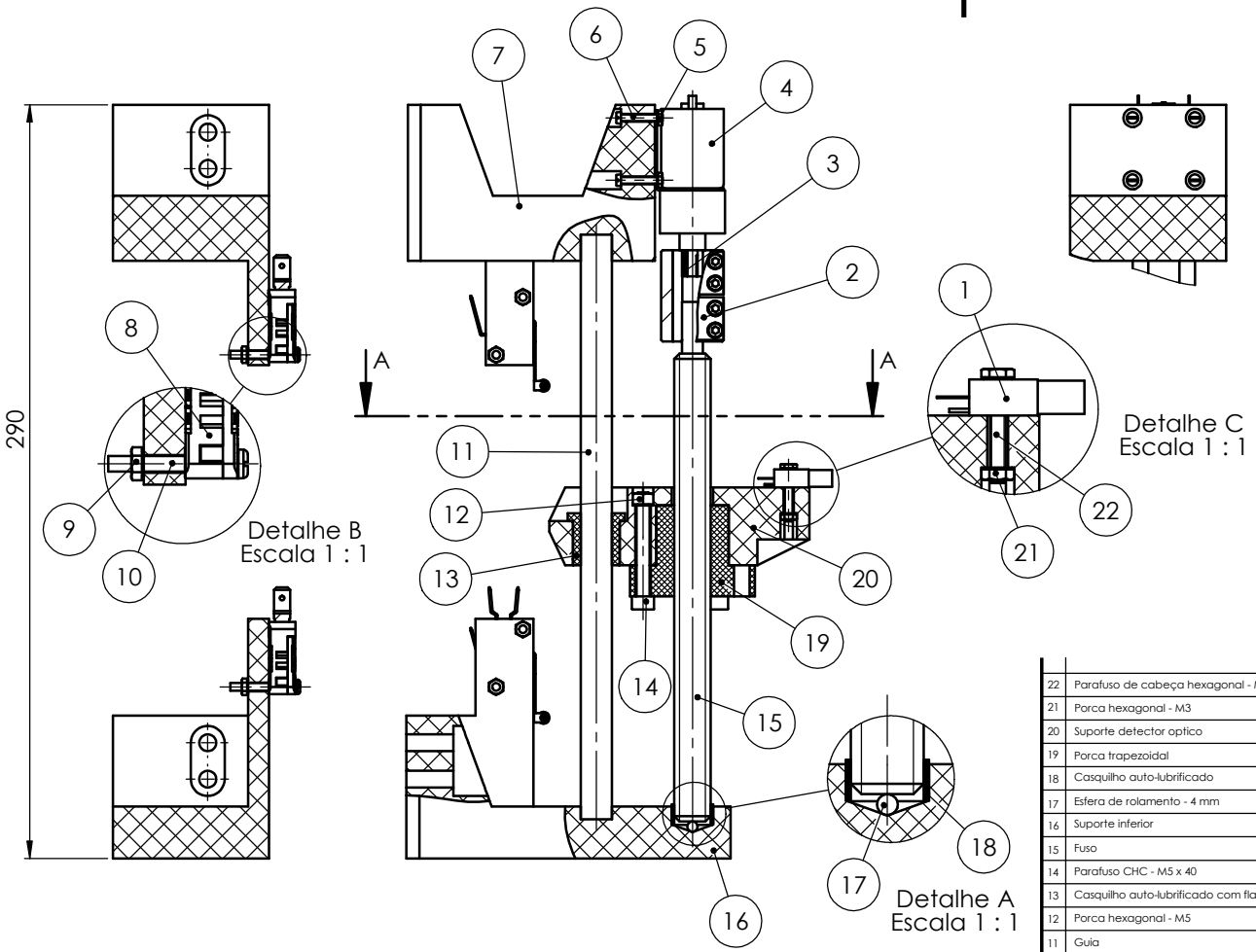

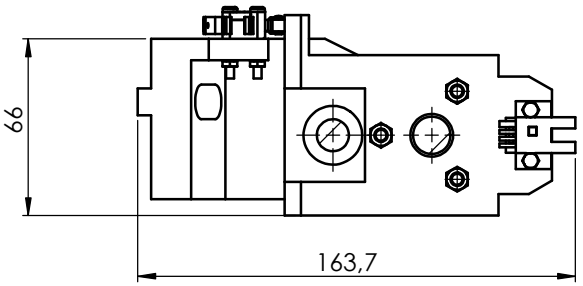

Rf nº	Designação	Norma ou Des Nº	Material	Nº	Massa	Observações
22	Parafuso de cabeça hexagonal - M3 x 20	ISO 4017	Aço 6.8	2		
21	Porca hexagonal - M3	ISO 4032	Aço 6	2	-	
20	Suporte detector optico	-	????	1	????	
19	Porca trapezoidal	-	igus igdur J	1	0,045	igus JFRM-2835TR14x4
18	Casquilho auto-lubrificado	-	igus igdur J	1	-	igus JSM-1416-08
17	Esfera de rolamento - 4 mm	-	-	1	-	
16	Suporte inferior	-	????	1	????	
15	Fuso	-	Aço Inox	1	0,22	igus PTGSG-14x4-01-R-200-Z-20-ES
14	Parafuso CHC - M5 x 40	ISO 4762	Aço 8.8	3	-	
13	Casquilho auto-lubrificado com flange	-	igus igdur J	1	0,005	igus JFM-1218-20
12	Porca hexagonal - M5	-	Aço 8	3	-	
11	Guia	-	Aço CEAX	1	0,198	L=225 mm , D=12 mm
10	Parafuso de cabeça cilíndrica - M3 x 25	DIN 85	Aço Inox A2	4	-	
9	Porca hexagonal - M3	ISO 4032	Aço 6	4	-	
8	Fim de curso	-	-	2	-	Cherry D459-V3RD
7	Suporte superior	-	????	1	????	
6	Parafuso de cabeça cilíndrica - M2,5 x 16	DIN 85	Aço Inox A2	4	-	
5	Porca hexagonal - M2,5	ISO 4032	Aço 6	4	-	
4	Motorredutor	-	-	1	0,077	Como Drills 918D100112
3	Casquilho	V-2	Aço DIN Ck45	1	0,003	
2	Acolpolamento	-	Aço	1	0,1	Ruland MCLX-8-8-F
1	Detector optico	-	-	1	0,019	OMRON EE-SX670-WR 1M

	Nome	Data	Assinatura
Desenho	André Ramos		
Verif.	Inv. Carlos M. Silva		

Revisão: CMS

Número: 0-V

FEUP

Titulo: Aq. Velocidade

A3

ESCALA:1:2

FOLHA 1 de 1

A.2 Technical drawings

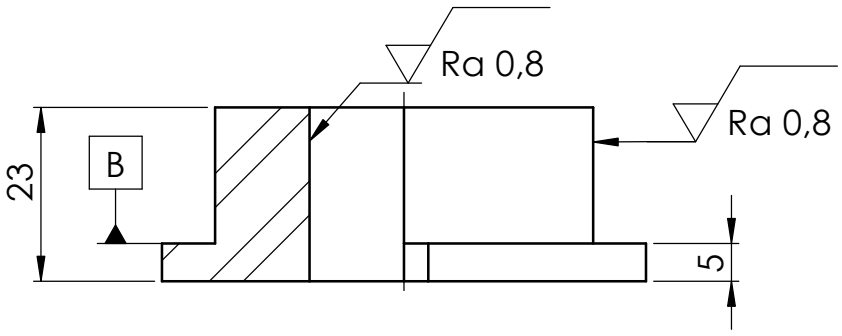

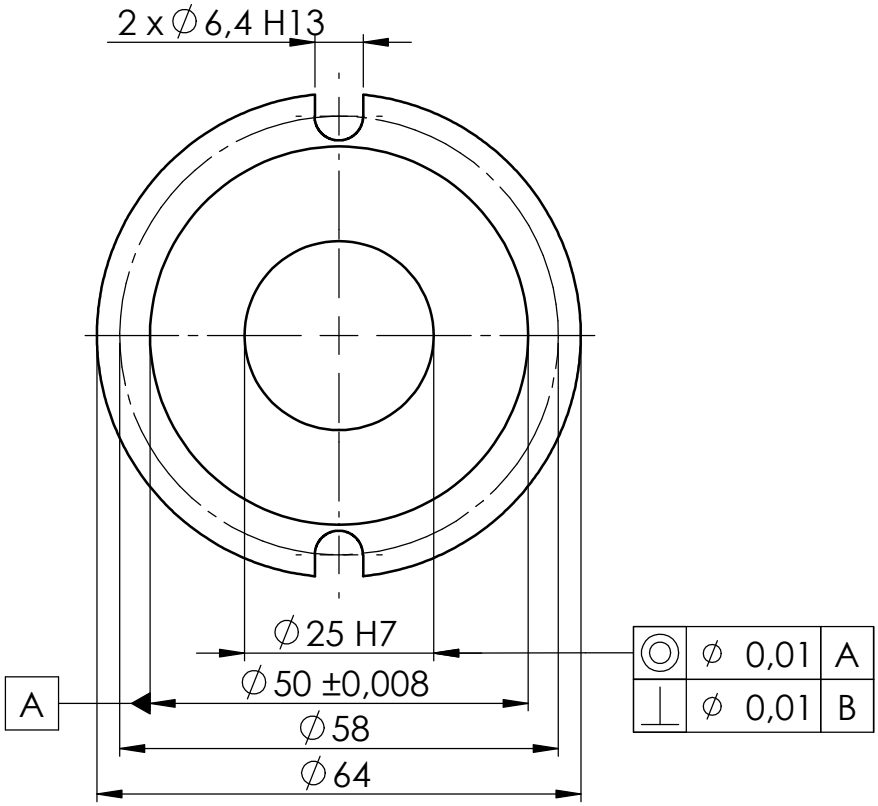

Toleranciamento - ISO 8015 Tolerâncias gerais - ISO 2768 - mK Rugosidades gerais - ISO 1302 Cantos e chanfros gerais - ISO 13715	FEUP	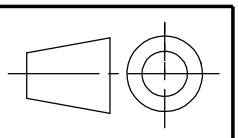		
	NOME	DATA	MATERIAL:	TITLE:
DESENHO	André Ramos		Aço Ck45	Casquilho inferior preso
VERIF.	Inv. Carlos M. Silva			
SOLIDWORKS Student License Academic Use Only		QUANTIDADE 1	Número E-1	Rev. CMS / A4
			ESCALA1:1	

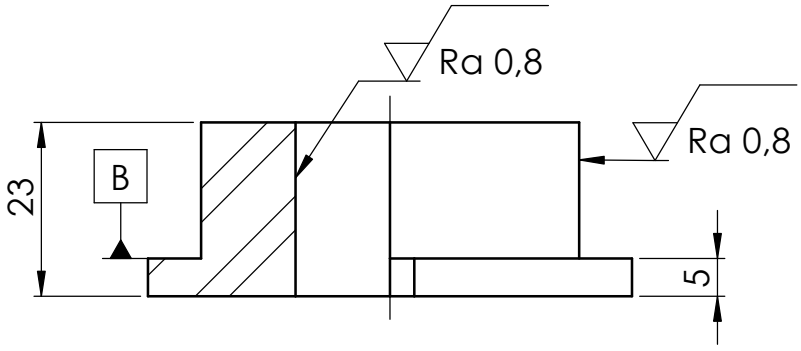

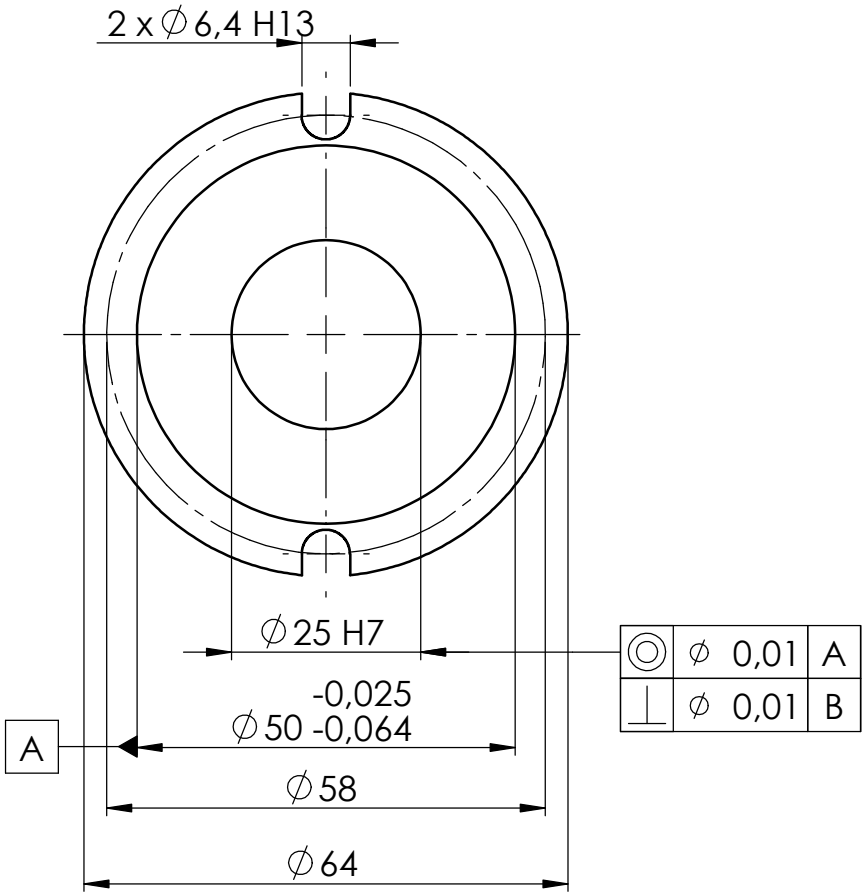

Toleranciamento - ISO 8015 Tolerâncias gerais - ISO 2768 - mK Rugosidades gerais - ISO 1302 Cantos e chanfros gerais - ISO 13715	FEUP			
	NOME	DATA	MATERIAL:	TITLE:
DESENHO	André Ramos		Aço Ck45	Casquilho inferior flutuante
VERIF.	Inv. Carlos M. Silva			
SOLIDWORKS Student License Academic Use Only		QUANTIDADE: 1	Número: E-2	Rev. CMS: A4
			ESCALA1:1	

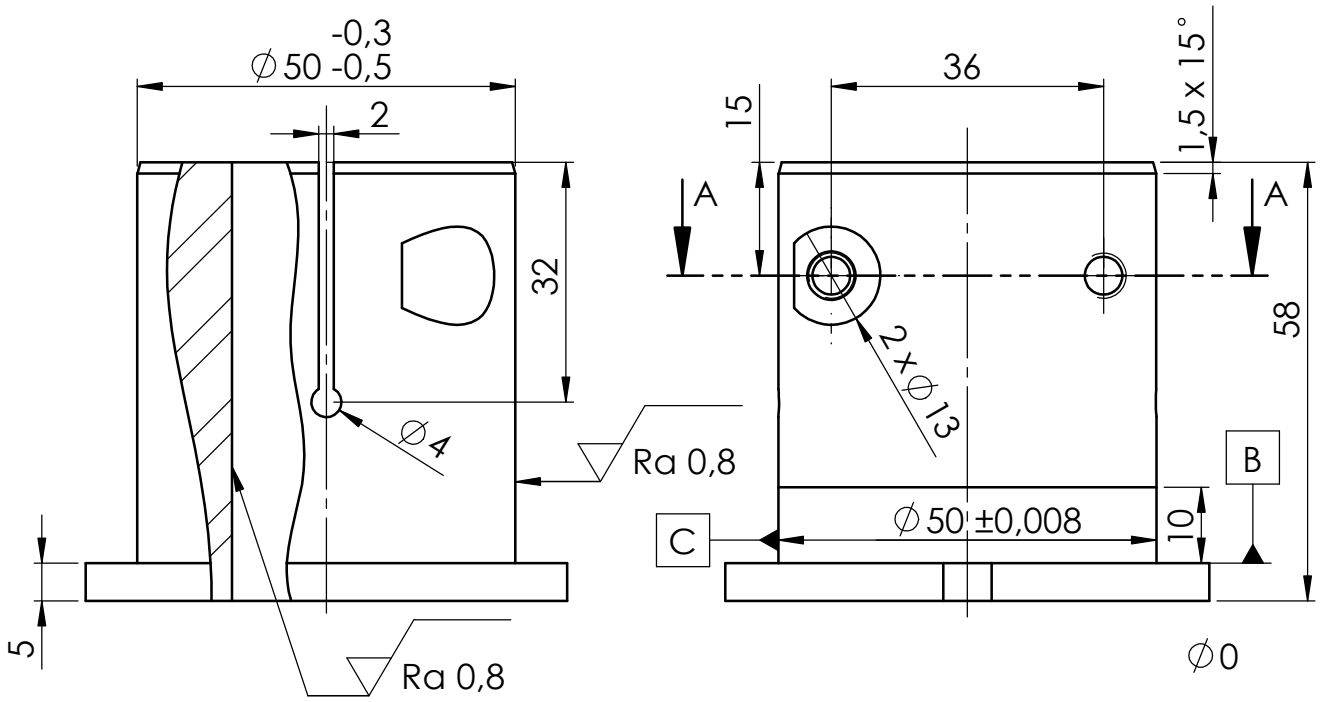

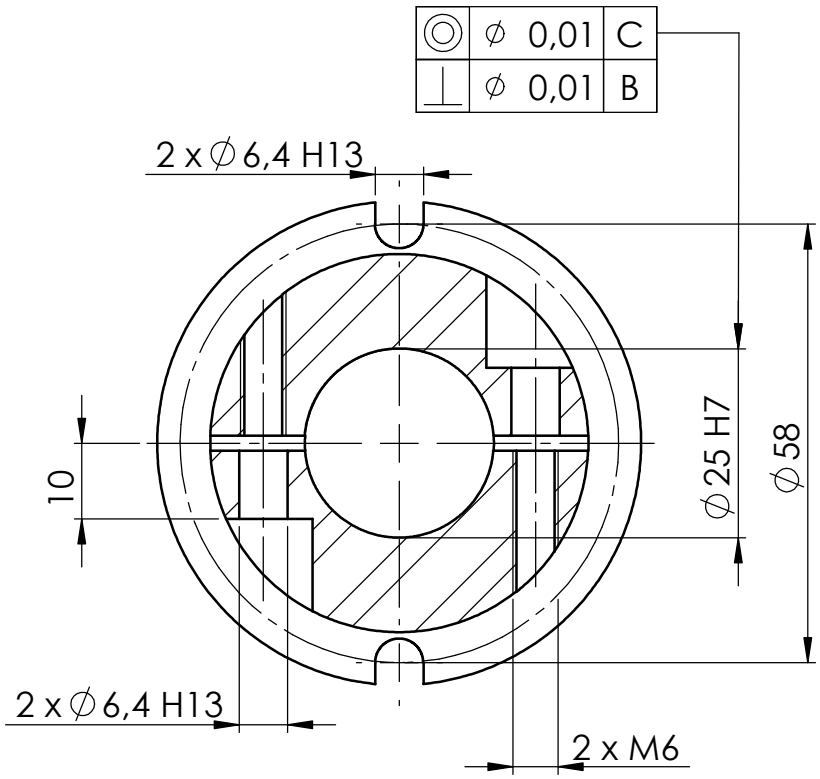

Toleranciamento - ISO 8015 Tolerâncias gerais - ISO 2768 - mK Rugosidades gerais - ISO 1302 Cantos e chanfros gerais - ISO 13715	FEUP			
	NOME	DATA	MATERIAL:	TITLE:
DESENHO	André Ramos		Aço Ck45	Casquilho superior preso
VERIF.	Inv. Carlos M. Silva			
SOLIDWORKS Student License Academic Use Only		QUANTIDADE: 1	Número: E-3	Rev. CMS: A4
			ESCALA1:1	

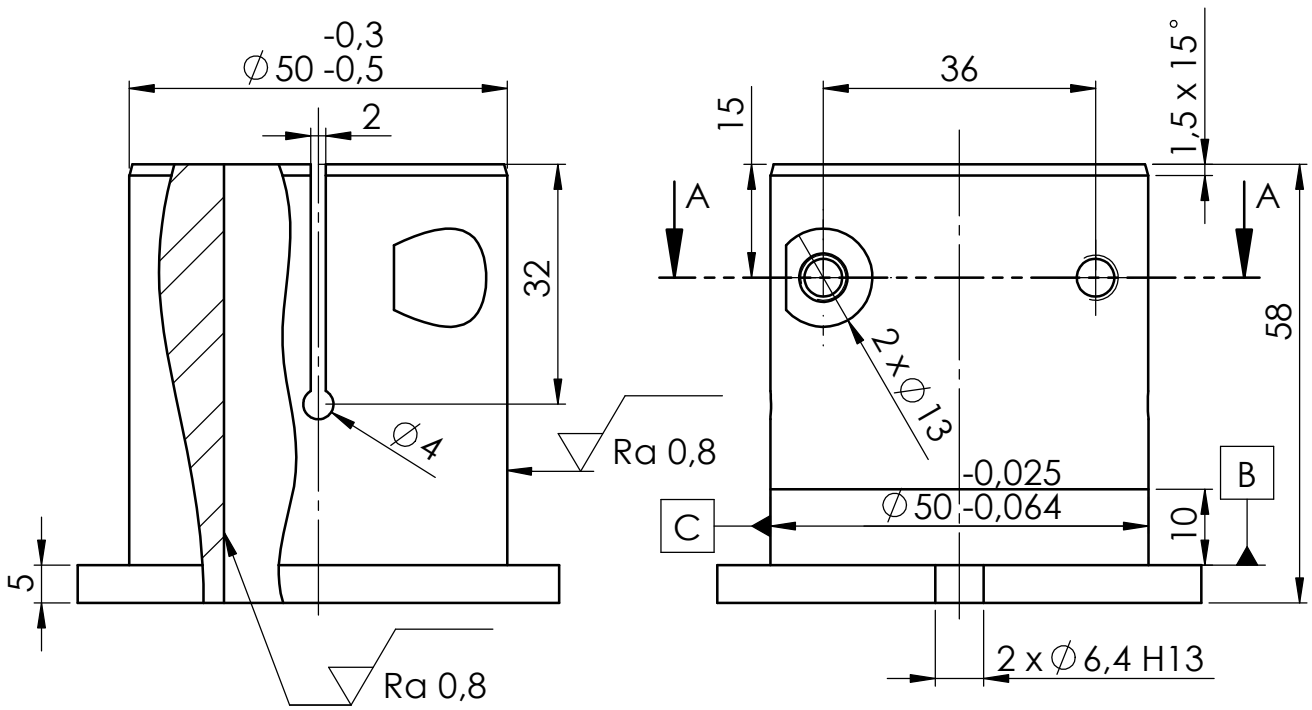

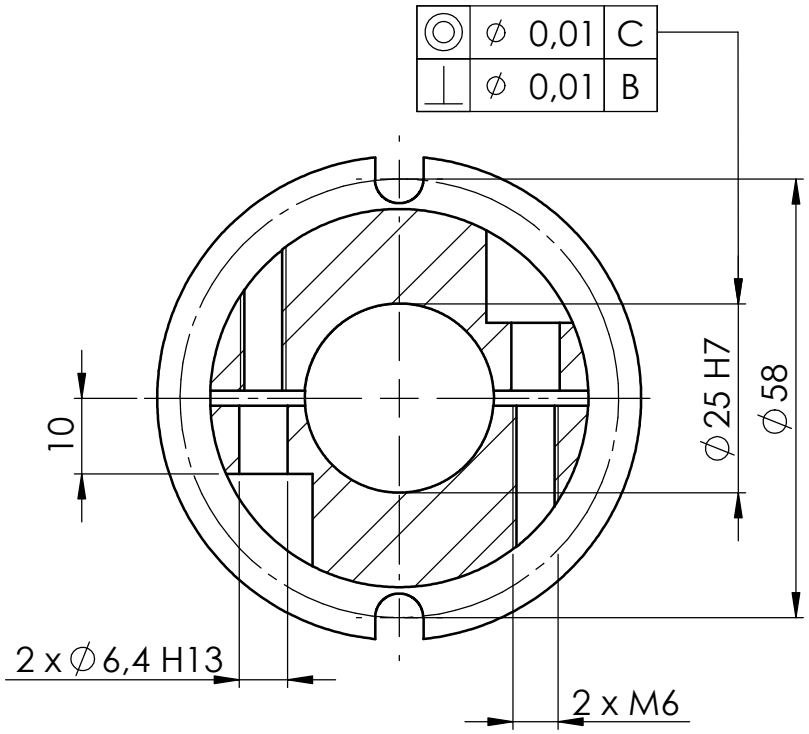

Toleranciamento - ISO 8015 Tolerâncias gerais - ISO 2768 - mK Rugosidades gerais - ISO 1302 Cantos e chanfros gerais - ISO 13715	FEUP			
	NOME	DATA	MATERIAL:	TITLE: Casquilho superior flutuante
DESENHO	André Ramos		Aço Ck45	
VERIF.	Inv. Carlos M. Silva			
SOLIDWORKS Student License Academic Use Only		QUANTIDADE 1	Número E-4	Rev. CMS / A4
			ESCALA1:1	

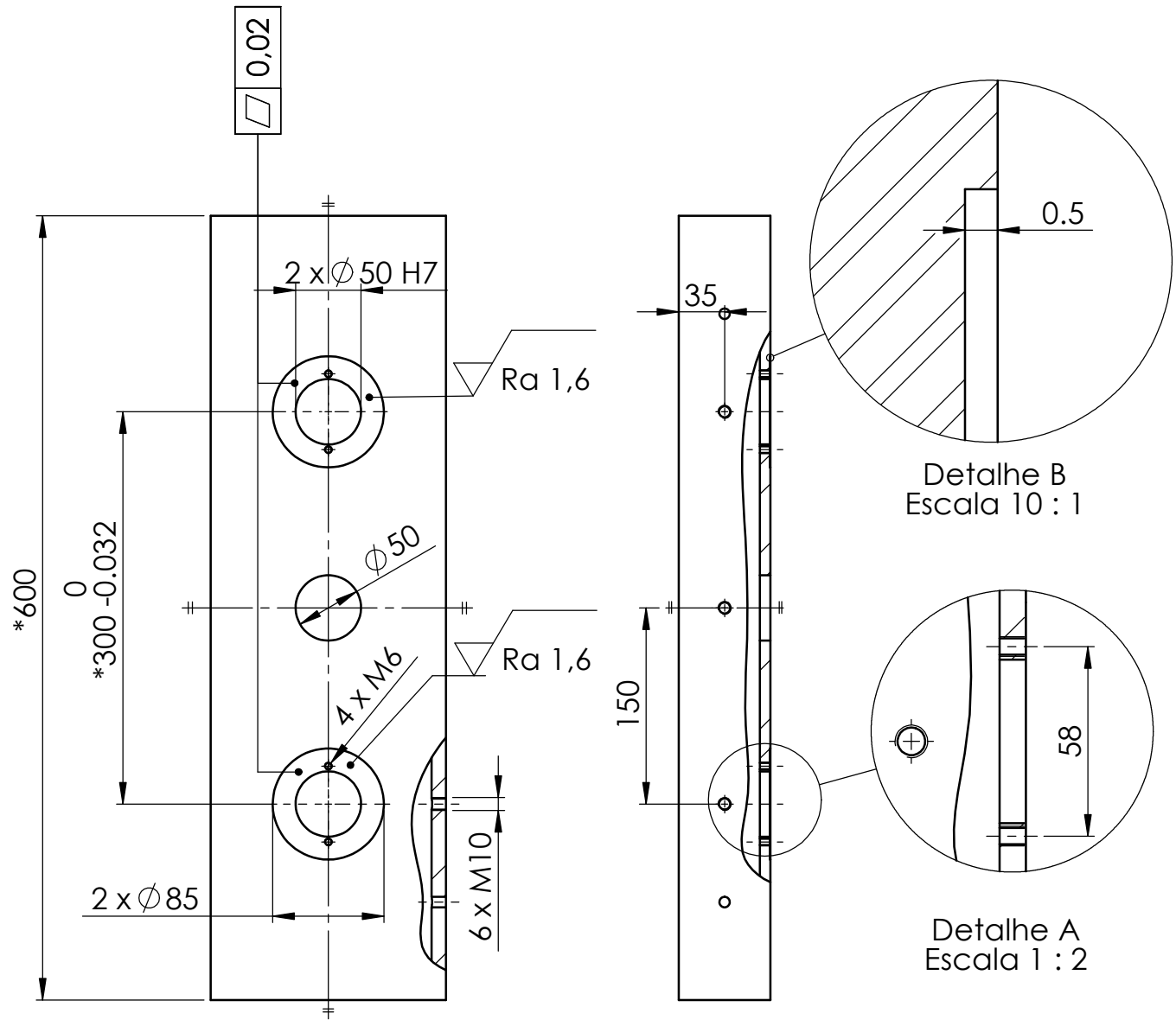

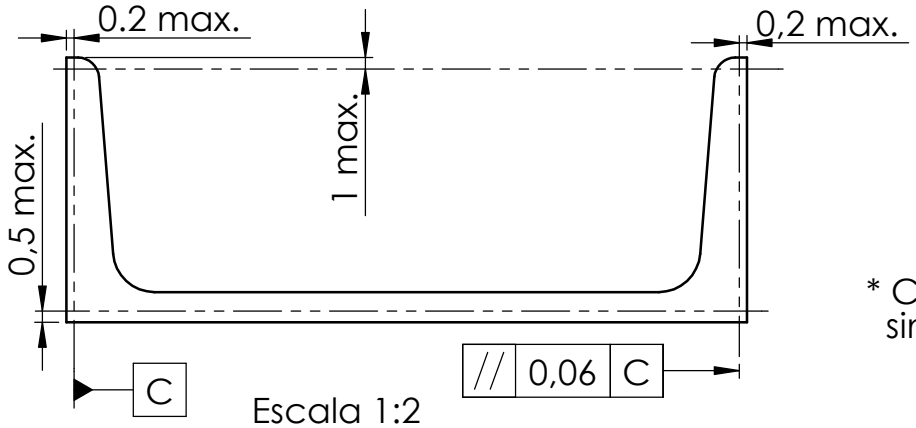

Escala 1:2

* Cotas executadas em simultâneo nas duas peças

Toleranciamento - ISO 8015 Tolerâncias gerais - ISO 2768 - mK Rugosidades gerais - ISO 1302 Cantos e chanfros gerais - ISO 13715	FEUP				
	NOME	DATA	MATERIAL:	TITLE:	
DESENHO	André Ramos		Aço St. 37 UNP180	Mesa Inferior	
VERIF.	Inv. Carlos M. Silva				
SOLIDWORKS Student License Academic Use Only			QUANTIDADE 1	Número E-5	Rev. CMS A4
				ESCALA1:5	

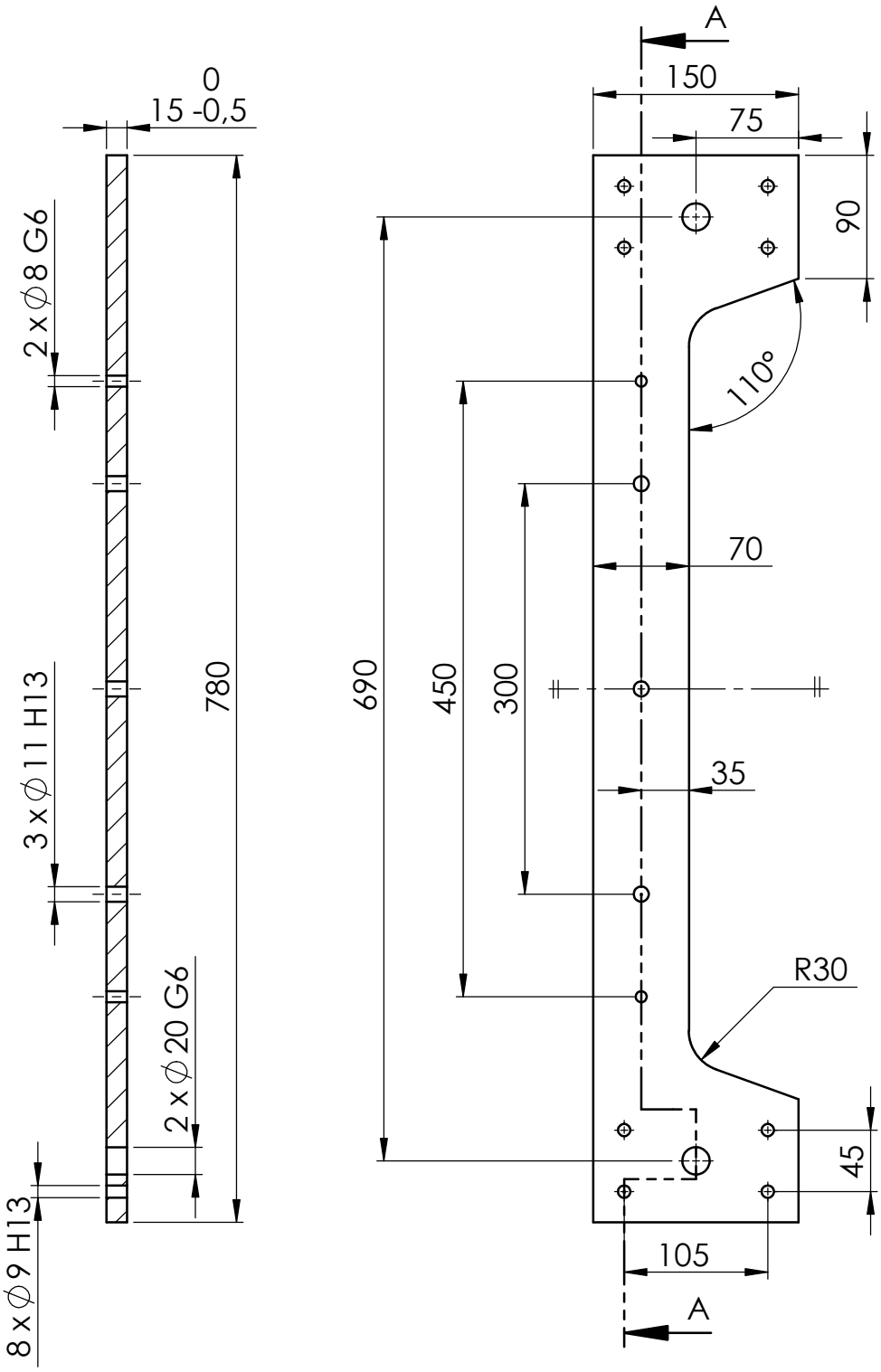

Toleranciamento - ISO 8015 Tolerâncias gerais - ISO 2768 - mK Rugosidades gerais - ISO 1302 Cantos e chanfros gerais - ISO 13715	FEUP			
	NOME	ASSINATURA	MATERIAL:	Título
DESENHO	André Ramos		Aço Ck45	Suporte Lateral
VERIF.	Inv. Carlos M. Silva			
SOLIDWORKS Student License Academic Use Only		QUANTIDADE 2	Número E-6	Rev. A / A4
			ESCALA1:5	

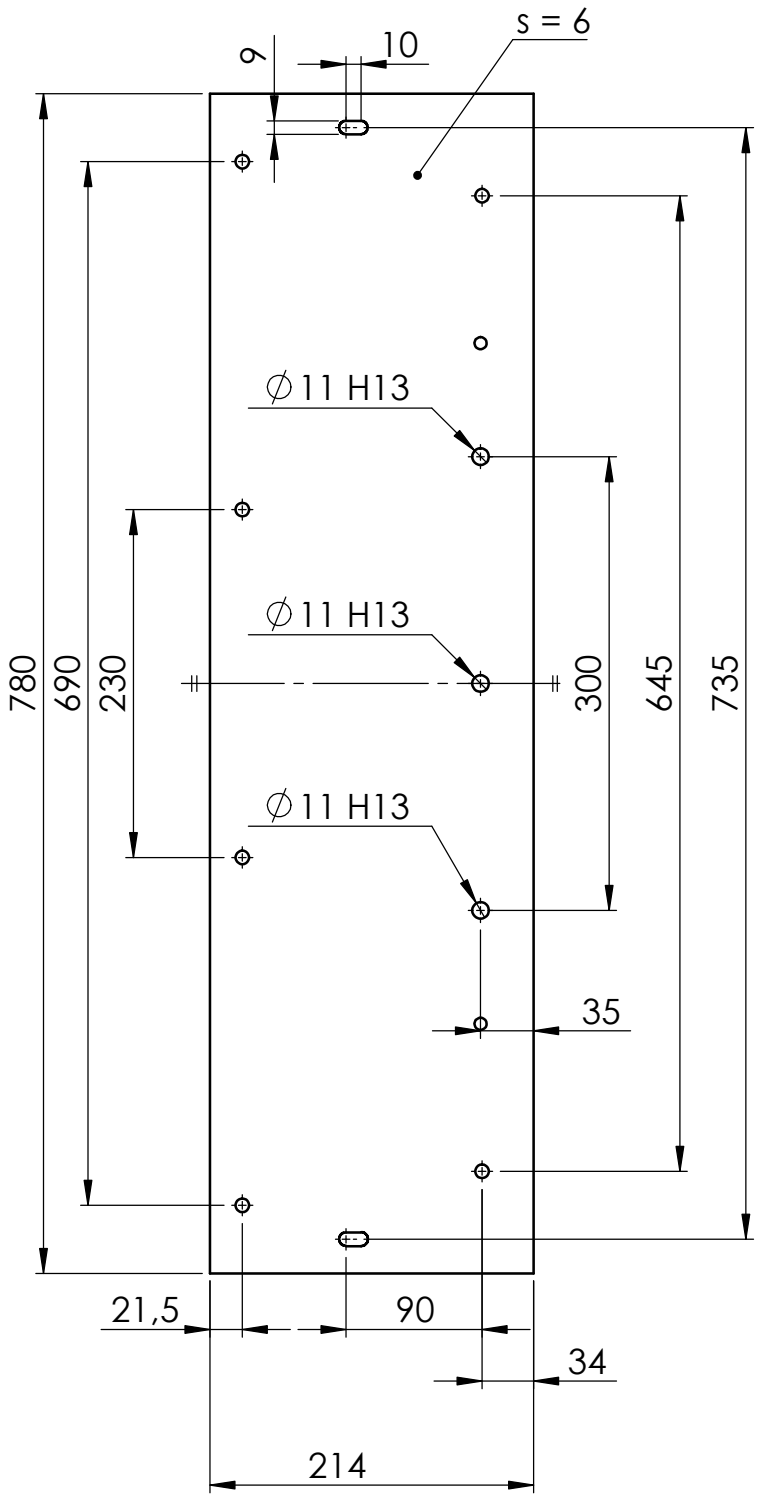

Toleranciamento - ISO 8015 Tolerâncias gerais - ISO 2768 - mK Rugosidades gerais - ISO 1302 Cantos e chanfros gerais - ISO 13715	FEUP				
	NOME	ASSINATURA	MATERIAL:	Título	
DESENHO	André Ramos		Alumínio 2017	Chapa Lateral	
VERIF.	Inv. Carlos M. Silva				
SOLIDWORKS Student License Academic Use Only			QUANTIDADE 2	Número E-7	Rev. CMS A4
				ESCALA1:5	

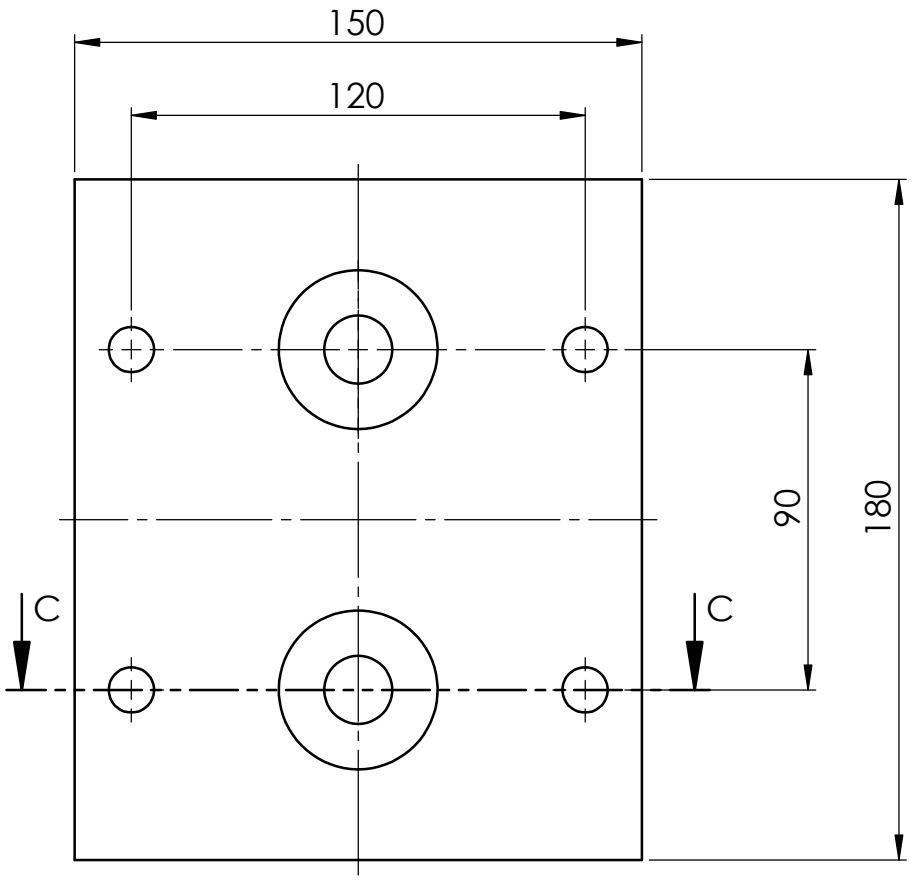

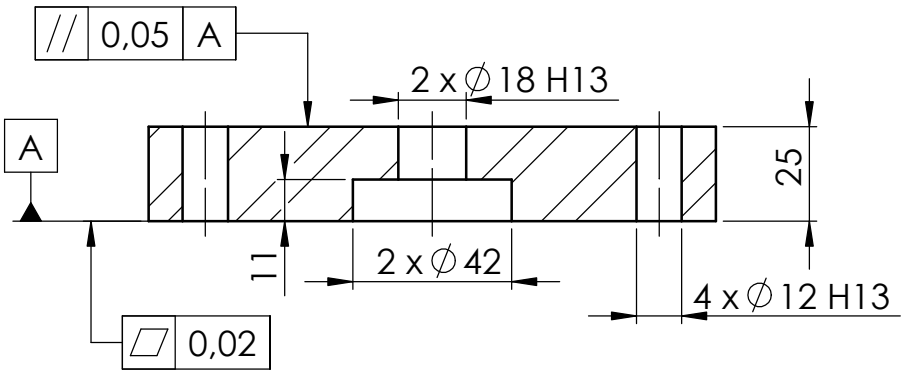

Toleranciamento - ISO 8015 Tolerâncias gerais - ISO 2768 - mK Rugosidades gerais - ISO 1302 Cantos e chanfros gerais - ISO 13715	FEUP			
	NOME	ASSINATURA	MATERIAL:	TITLE:
DESENHO	André Ramos		Aço Ck45	Sapata
VERIF.	Inv. Carlos M. Silva			
SOLIDWORKS Student License Academic Use Only		QUANTIDADE: 2	Número: E-8	Rev. CMS: A4
			ESCALA1:2	

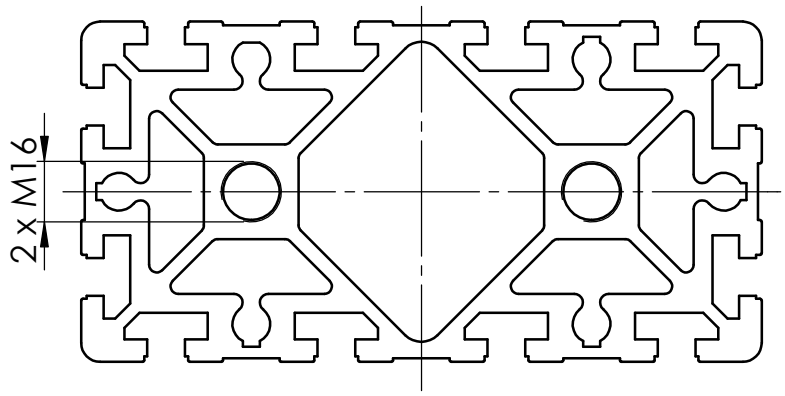

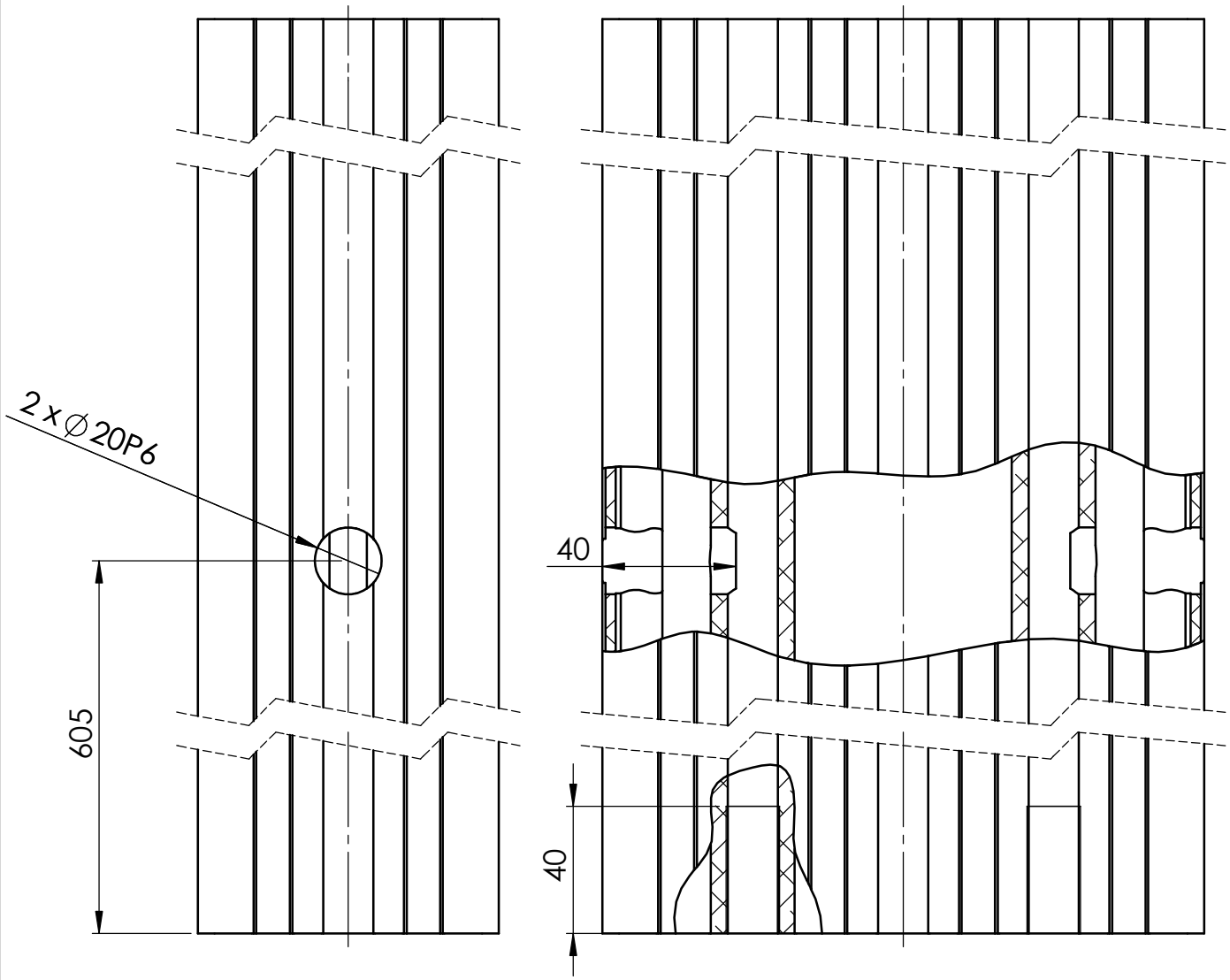

Toleranciamento - ISO 8015 Tolerâncias gerais - ISO 2768 - mK Rugosidades gerais - ISO 1302 Cantos e chanfros gerais - ISO 13715	FEUP			
	NOME	DATA	MATERIAL:	TITLE:
DESENHO	André Ramos		Alumínio 6063-T3	Montante
VERIF.	Inv. Carlos M. Silva			
SOLIDWORKS Student License Academic Use Only		QUANTIDADE 2	Número E-9	Rev. CMS / A4
			ESCALA1:2	

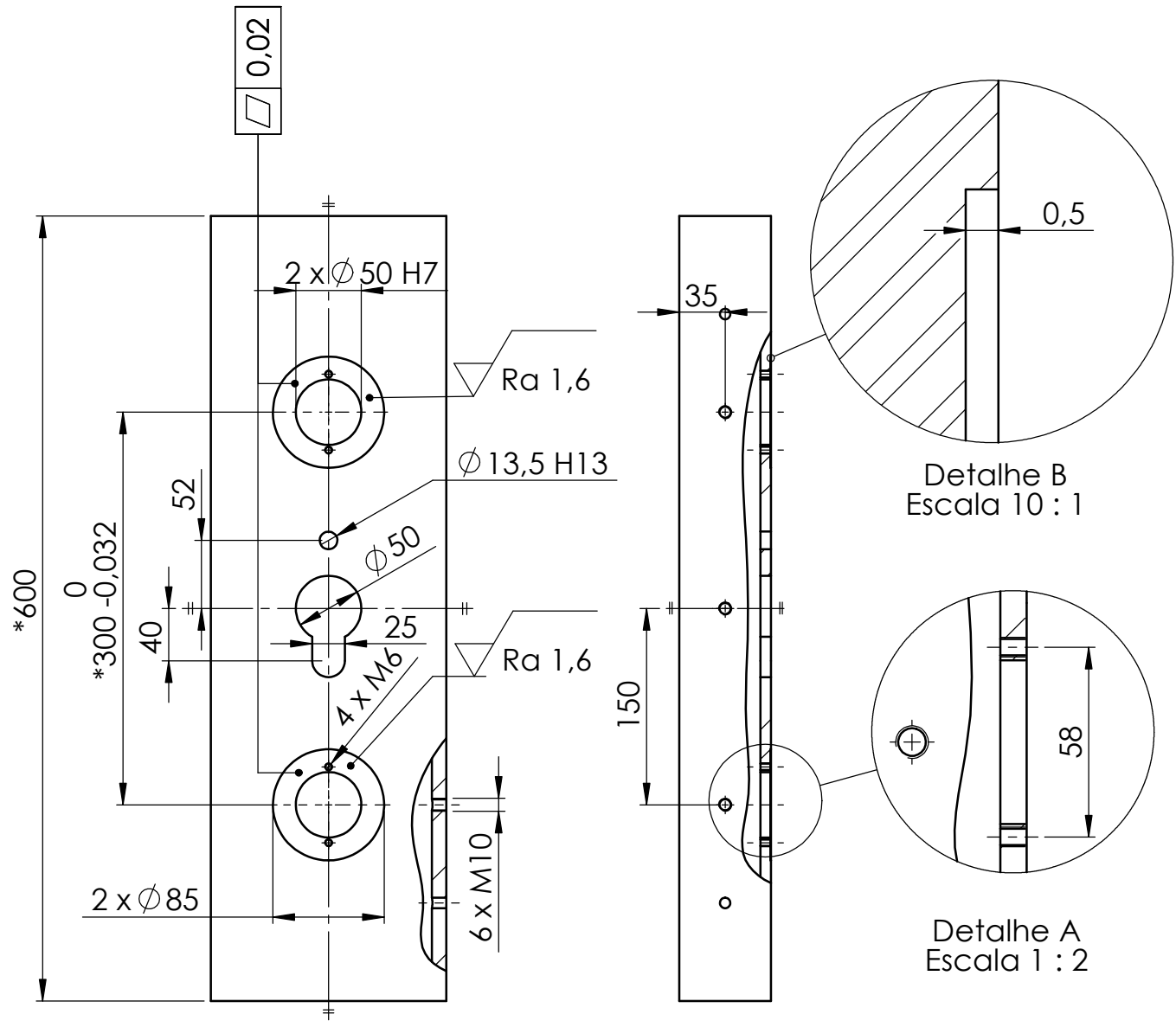

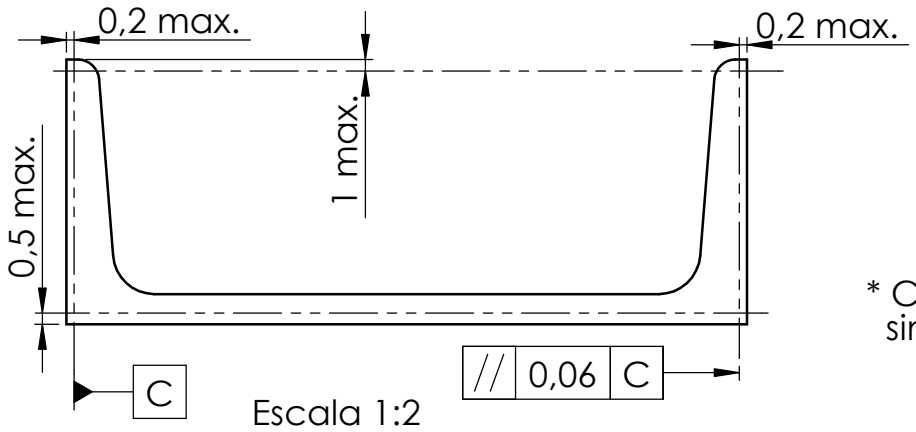

Escala 1:2

* Cotas executadas em simultâneo nas duas peças

Toleranciamento - ISO 8015 Tolerâncias gerais - ISO 2768 - mK Rugosidades gerais - ISO 1302 Cantos e chanfros gerais - ISO 13715	FEUP			
	NOME	ASSINATURA	MATERIAL:	TITLE:
DESENHO	André Ramos		Aço St. 37 UNP180	Mesa Superior
VERIF.	Inv. Carlos M. Silva			
SOLIDWORKS Student License Academic Use Only			QUANTIDADE: 1	Número: E-10 / Rev. CMS / A4
				ESCALA1:5

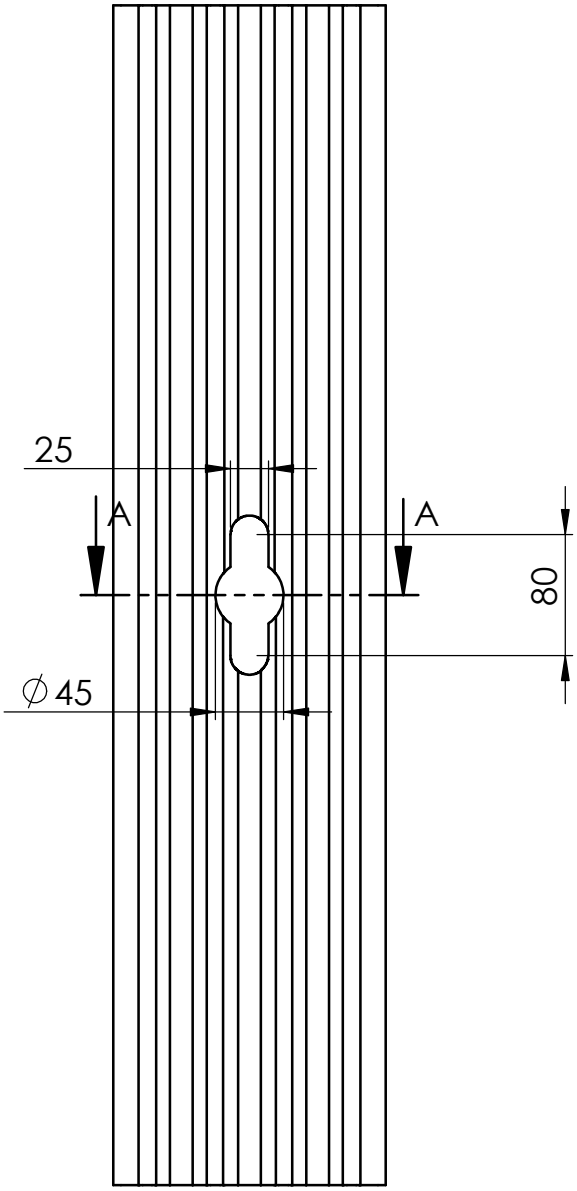

SECTION A-A

Toleranciamento - ISO 8015 Tolerâncias gerais - ISO 2768 - mH Rugosidades gerais - ISO 1302 Cantos e chanfros gerais - ISO 13715	FEUP			
	NOME	Assinatura	MATERIAL:	TITLE:
DESENHO	André Ramos		Alumínio 6063-T3	Topo
VERIF.	Inv. Carlos M. Silva			
SOLIDWORKS Student License Academic Use Only		QUANTIDADE 1	Número E-11	Rev. A / A4
			ESCALA1:5	

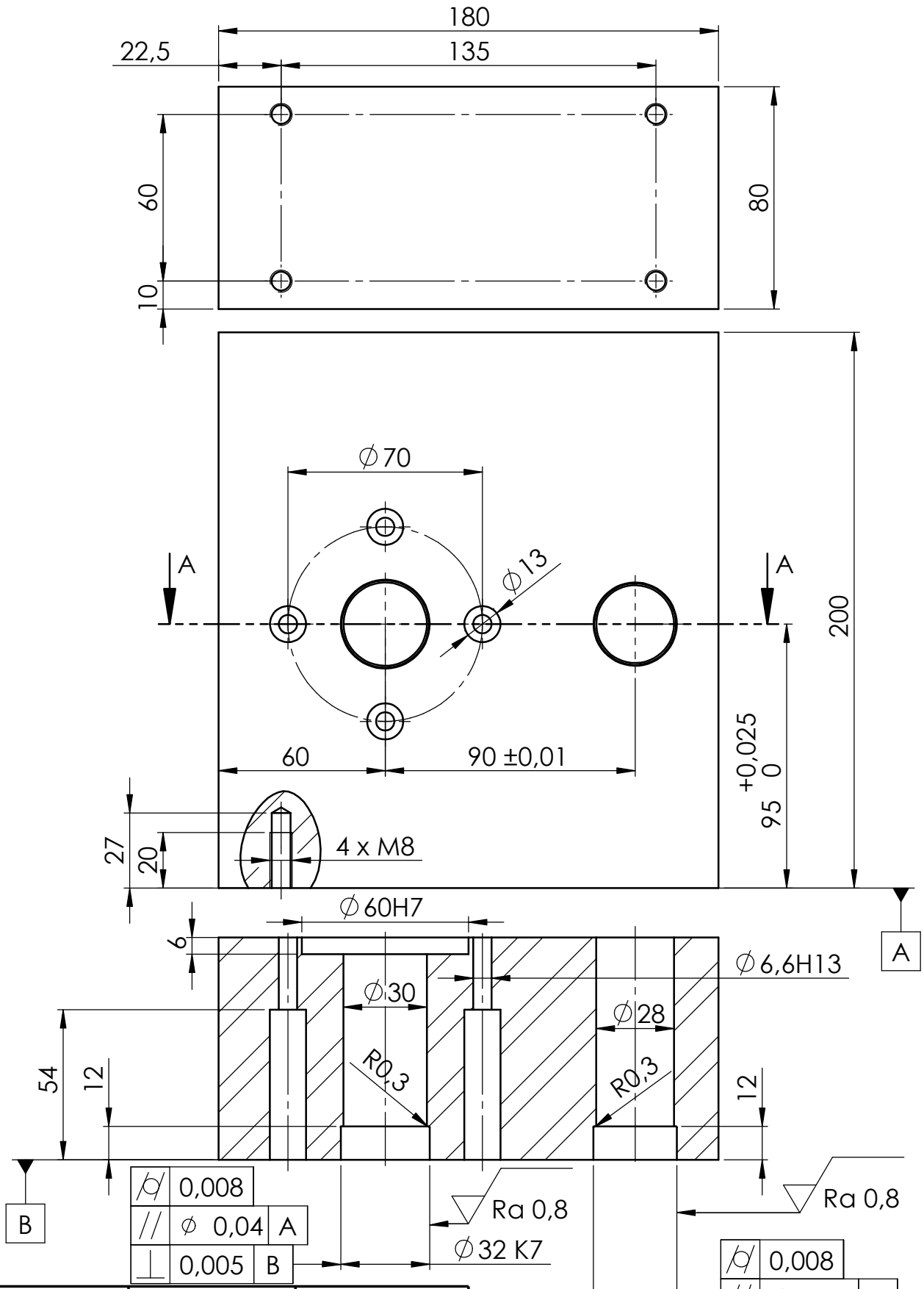

Toleranciamento - ISO 8015 Tolerâncias gerais - ISO 2768 - mK Rugosidades gerais - ISO 1302 Cantos e chanfros gerais - ISO 13715	FEUP				
	NOME	DATA	MATERIAL:	TITLE:	
DESENHO	André Ramos		Aço Ck45	Caixa Anterior	
VERIF.	Inv. Carlos M. Silva				
SOLIDWORKS Student License Academic Use Only		QUANTIDADE 1	Número L-1	Rev. CMS	A4
			ESCALA1:2		

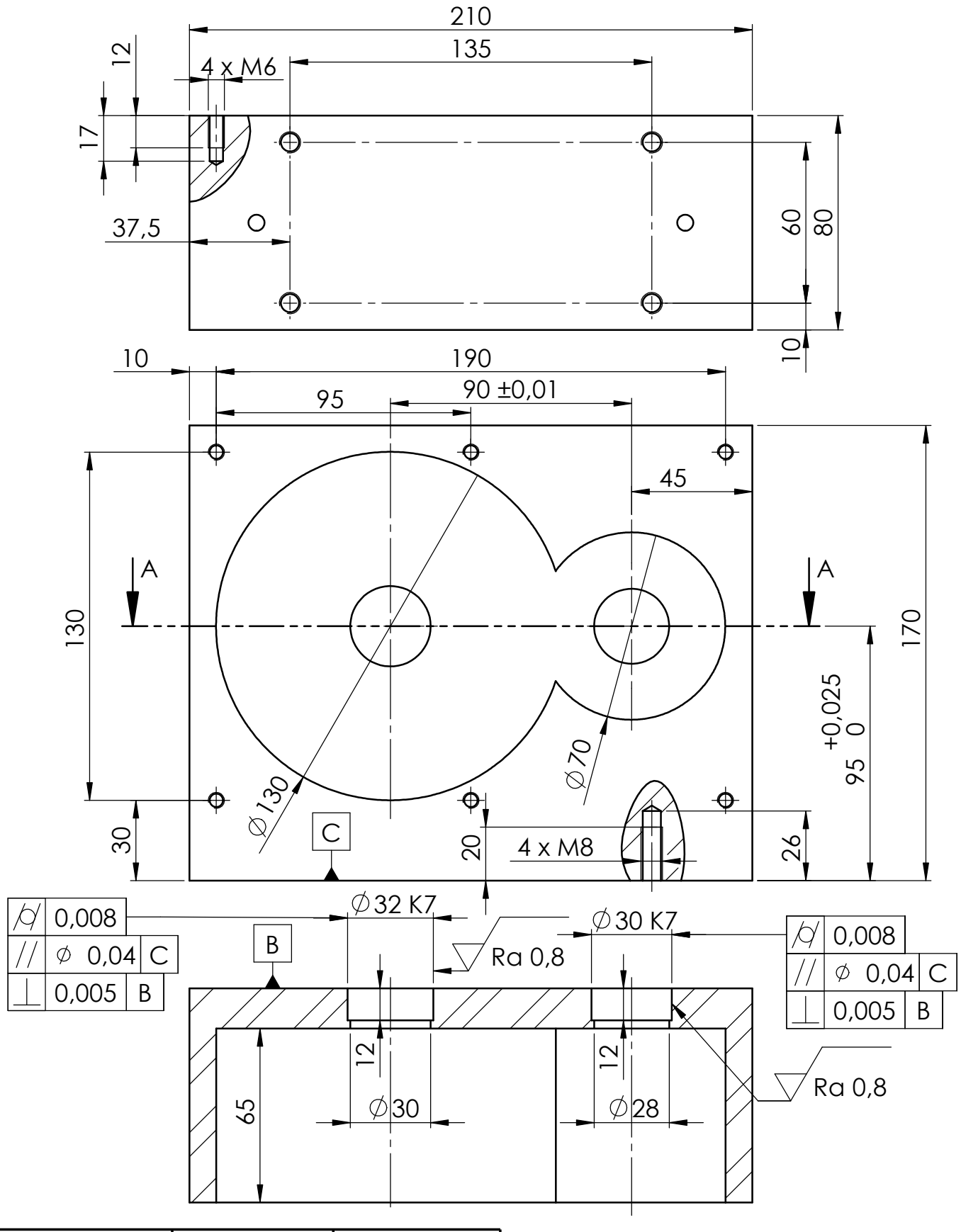

Toleranciamento - ISO 8015 Tolerâncias gerais - ISO 2768 - mK Rugosidades gerais - ISO 1302 Cantos e chanfros gerais - ISO 13715	FEUP			
	NOME	DATA	MATERIAL:	TITLE:
DESENHO	André Ramos		Aço Ck45	Caixa Posterior
VERIF.	Inv. Carlos M. Silva			
SOLIDWORKS Student License Academic Use Only		QUANTIDADE 1	Número L-2	Rev. CMS / A4
			ESCALA1:2	

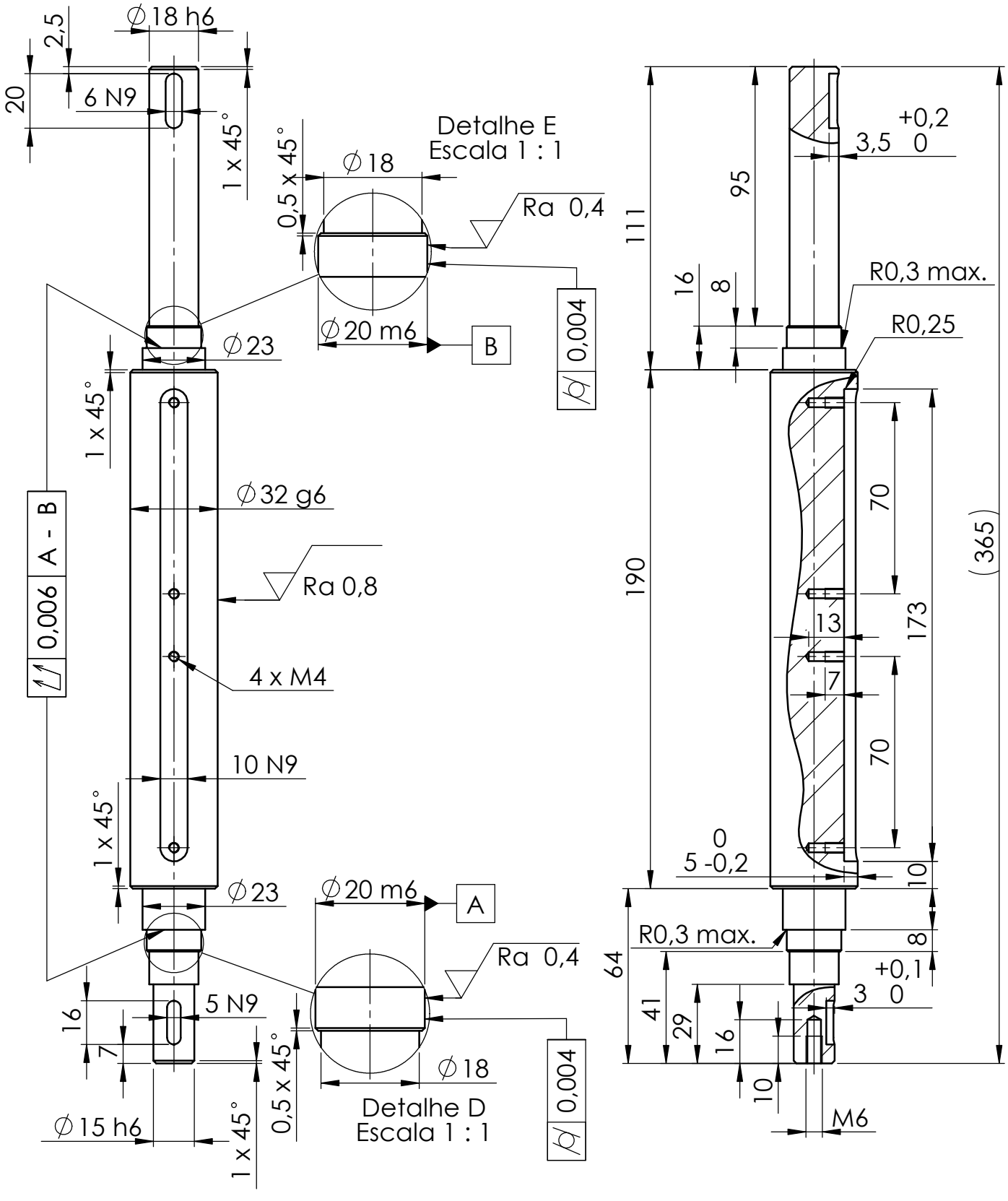

Toleranciamento - ISO 8015 Tolerâncias gerais - ISO 2768 - mK Rugosidades gerais - ISO 1302 Cantos e chanfros gerais - ISO 13715	FEUP			
	NOME	DATA	MATERIAL:	TITLE:
DESENHO	André Ramos		Aço Ck45	Veio Tambor
VERIF.	Inv. Carlos M. Silva			
SOLIDWORKS Student License Academic Use Only		QUANTIDADE 1	Número L-3	Rev. CMS / A4
			ESCALA1:2	

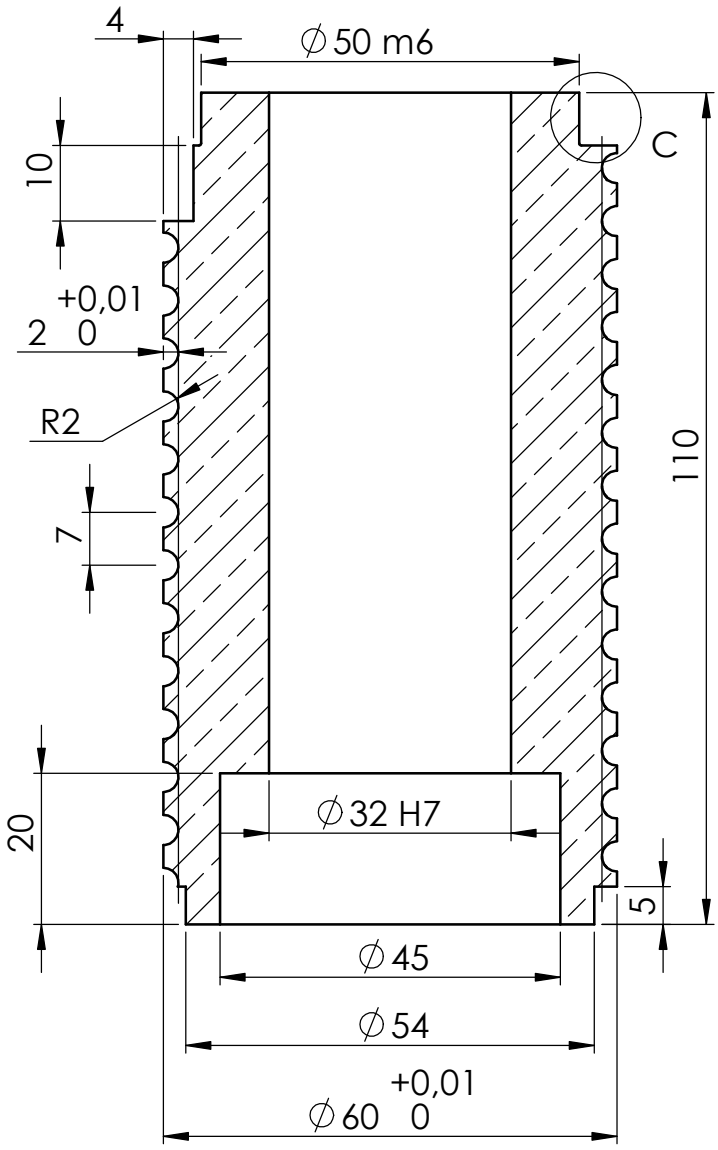

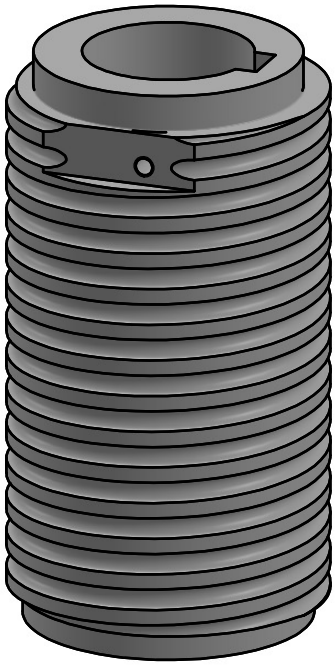

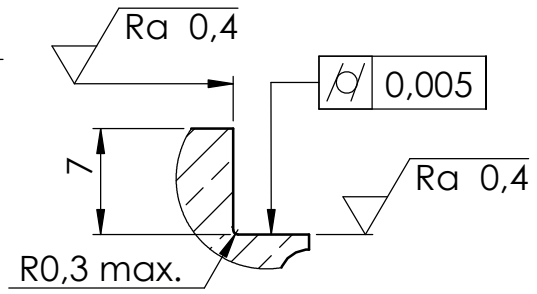

Detalhe C
Escala 2 : 1

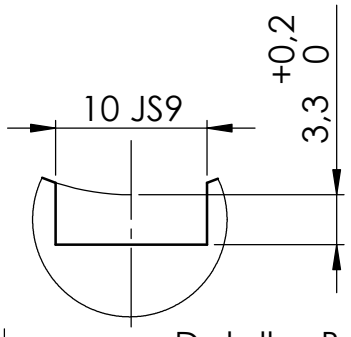

Detalhe B
Escala 2 : 1

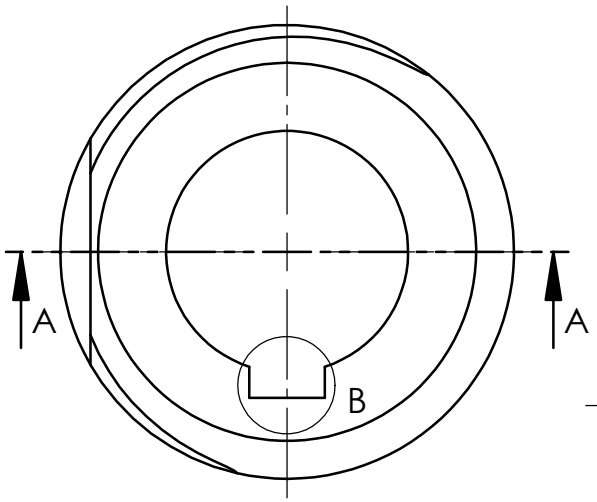

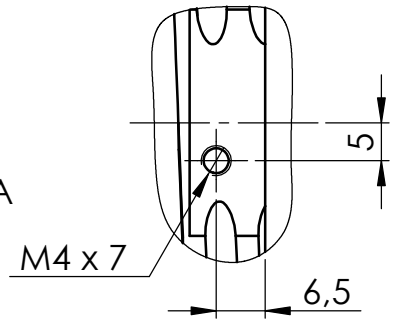

Toleranciamento - ISO 8015 Tolerâncias gerais - ISO 2768 - mK Rugosidades gerais - ISO 1302 Cantos e chanfros gerais - ISO 13715	FEUP			
	NOME	ASSINATURA	MATERIAL:	Título
DESENHO	André Ramos		Bronze DIN CuSn12	Tambor
VERIF.	Inv. Carlos M. Silva			

QUANTIDADE	Número	Rev.	
1	L-4	A	A4
	ESCALA1:1		

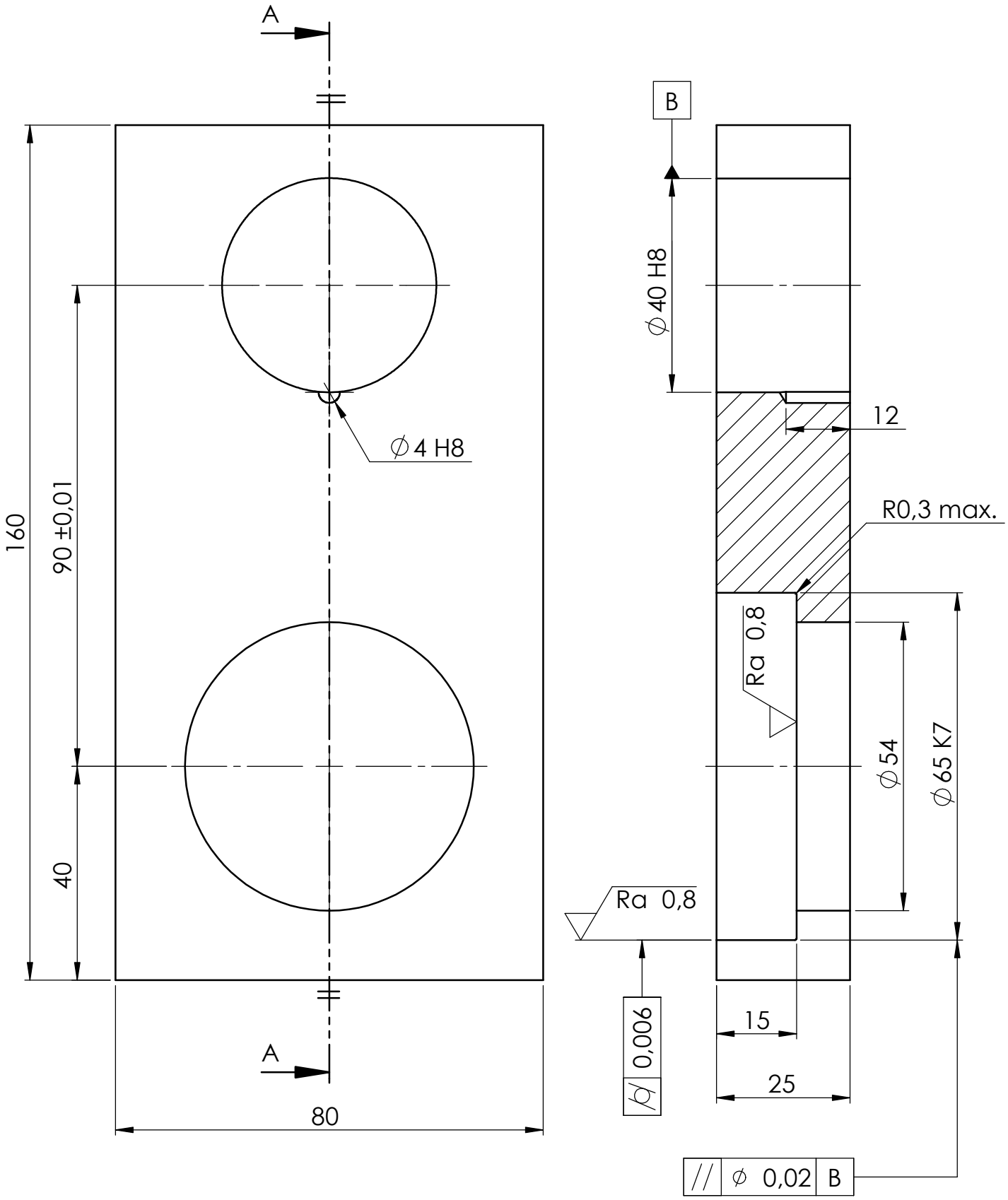

Toleranciamento - ISO 8015 Tolerâncias gerais - ISO 2768 - mK Rugosidades gerais - ISO 1302 Cantos e chanfros gerais - ISO 13715	FEUP			
	NOME	DATA	MATERIAL:	TITLE:
DESENHO	André Ramos		Aço Ck45	Ligação tambor-porca
VERIF.	Inv. Carlos M. Silva			
SOLIDWORKS Student License Academic Use Only		QUANTIDADE 1	Número L-5	Rev. CMS / A4
			ESCALA1:1	

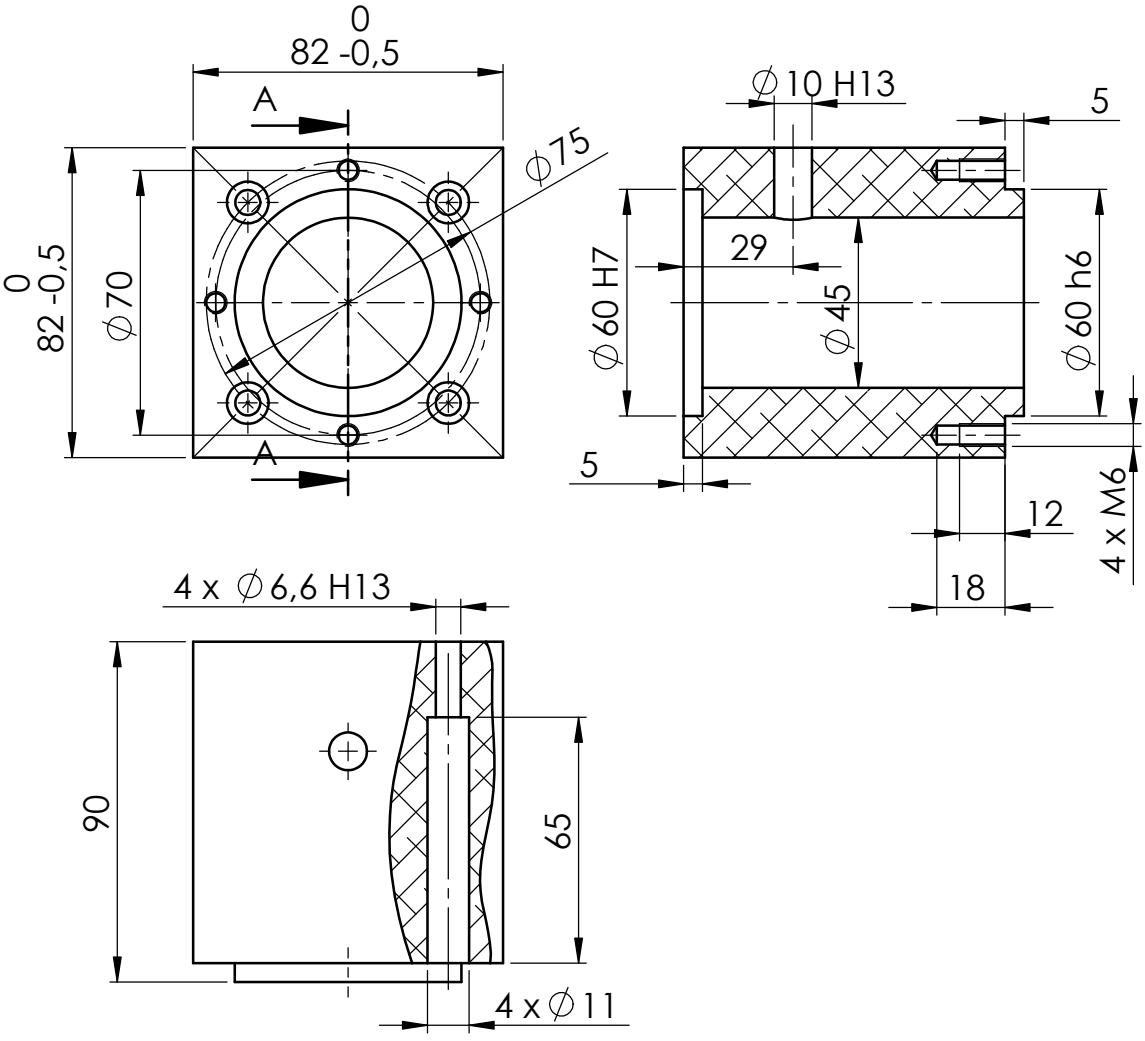

Toleranciamento - ISO 8015 Tolerâncias gerais - ISO 2768 - mK Rugosidades gerais - ISO 1302 Cantos e chanfros gerais - ISO 13715	FEUP			
	NOME	Assinatura	MATERIAL:	TITLE:
DESENHO	André Ramos		Aluminio 7075 T651	Luneta
VERIF.	Inv. Carlos M. Silva			
SOLIDWORKS Student License Academic Use Only		QUANTIDADE 1	Número L-6	Rev. CMS / A4
			ESCALA1:2	

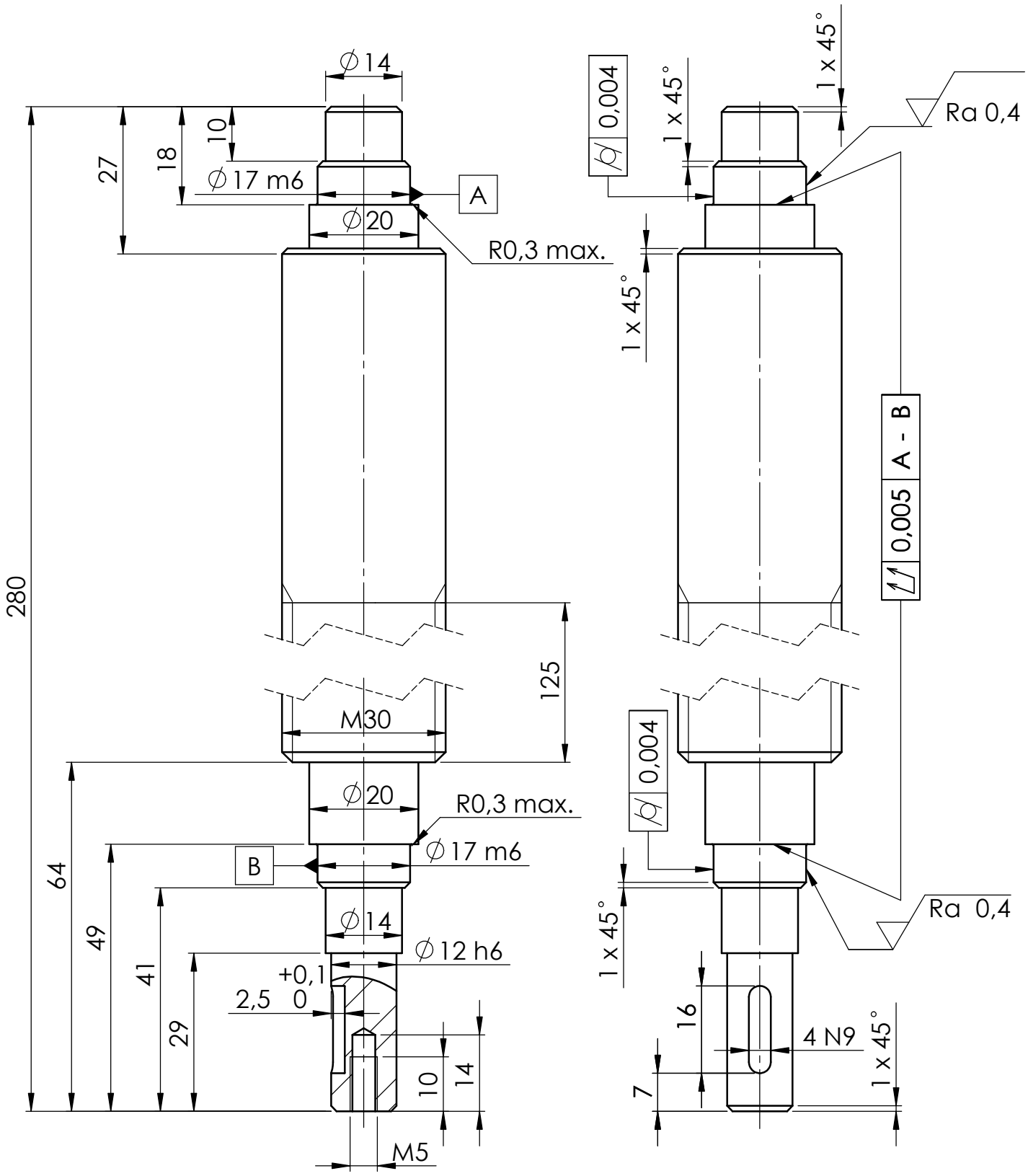

Toleranciamento - ISO 8015 Tolerâncias gerais - ISO 2768 - mK Rugosidades gerais - ISO 1302 Cantos e chanfros gerais - ISO 13715	FEUP			
	NOME	DATA	MATERIAL:	TITLE:
DESENHO	André Ramos		Aço Ck45	Veio de Translação
VERIF.	Inv. Carlos M. Silva			
SOLIDWORKS Student License Academic Use Only		QUANTIDADE: 1	Número: L-7	Rev. A / A4
			ESCALA1:1	

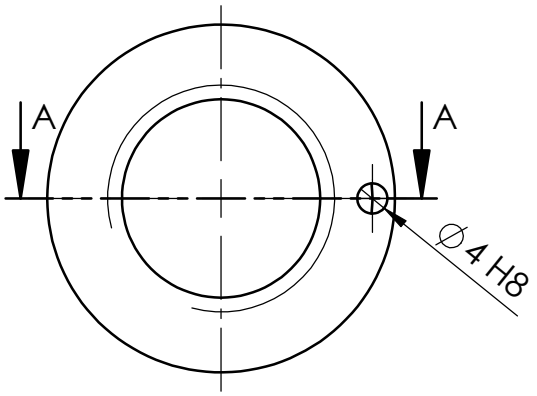

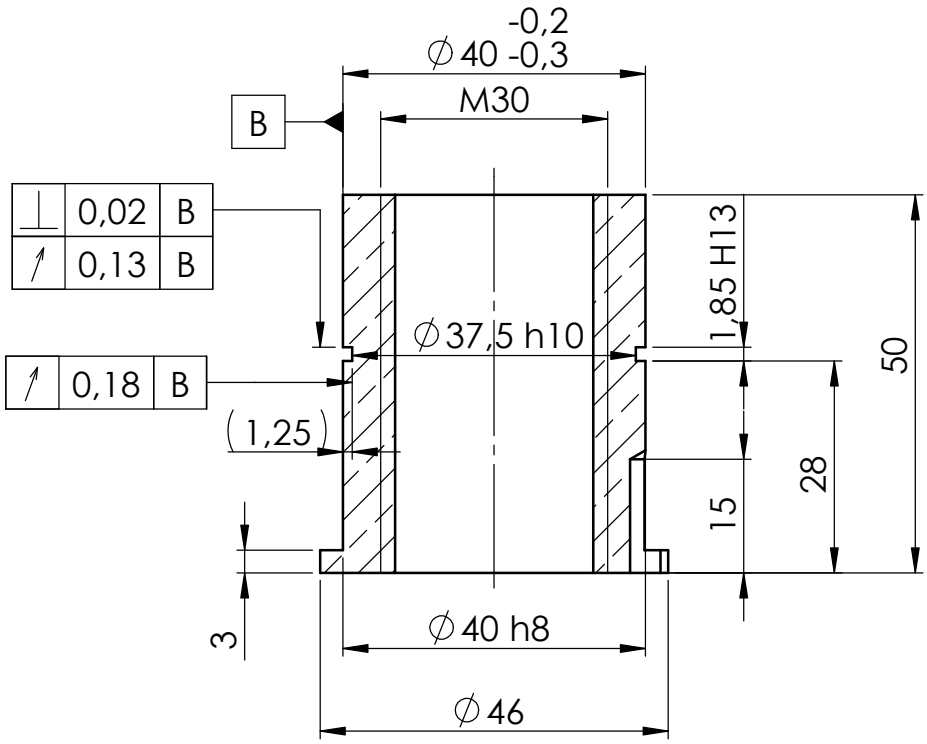

Toleranciamento - ISO 8015 Tolerâncias gerais - ISO 2768 - mK Rugosidades gerais - ISO 1302 Cantos e chanfros gerais - ISO 13715	FEUP				
	NOME	DATA	MATERIAL:	TITLE:	
DESENHO	André Ramos		Bronze DIN CuSn12	Porca Motriz	
VERIF.	Inv. Carlos M. Silva				
SOLIDWORKS Student License Academic Use Only		QUANTIDADE 1	Número L-8	Rev. CMS	A4
			ESCALA1:1		

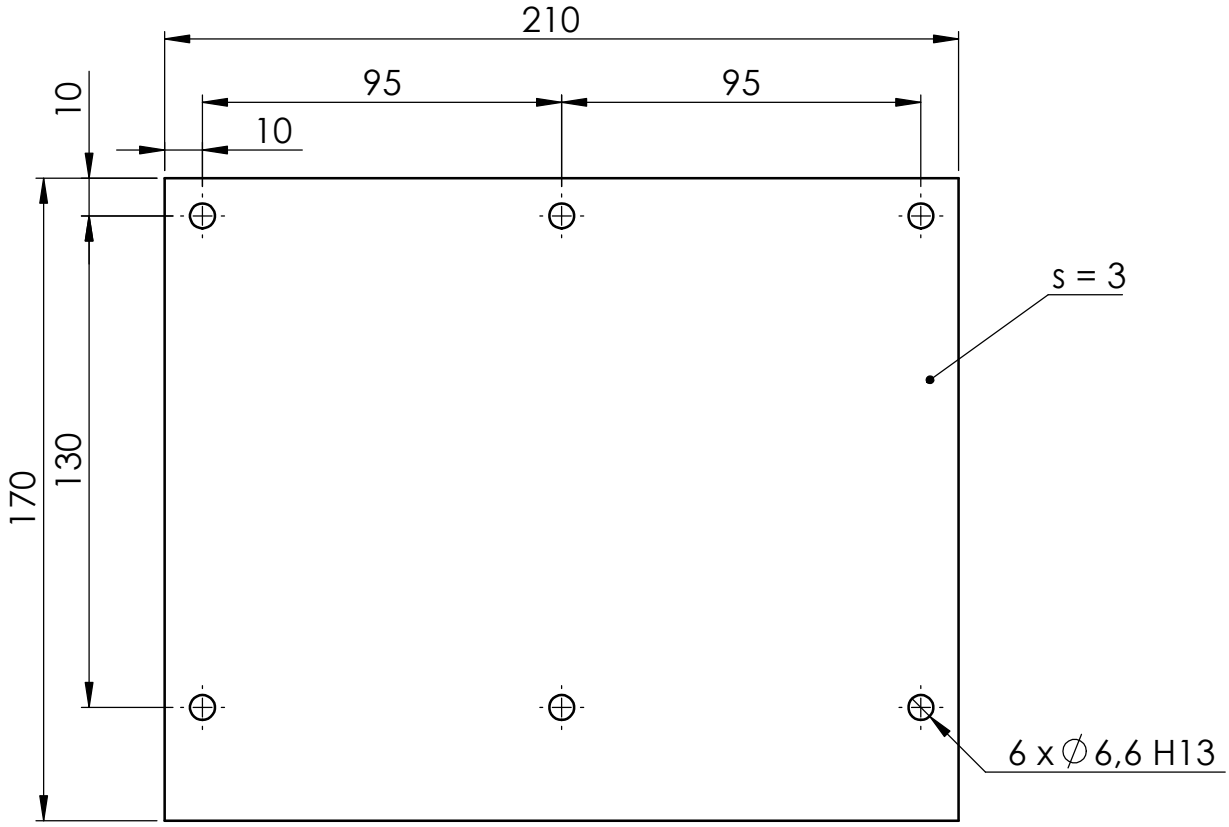

Toleranciamento - ISO 8015 Tolerâncias gerais - ISO 2768 - mK Rugosidades gerais - ISO 1302 Cantos e chanfros gerais - ISO 13715	FEUP			
	NOME	ASSINATURA	MATERIAL:	TITLE:
DESENHO	André Ramos		Al 5754	Tampa engrenagens
VERIF.	Inv. Carlos M. Silva			
SOLIDWORKS Student License Academic Use Only		QUANTIDADE 1	Número L-9	Rev. A / A4
			ESCALA1:2	

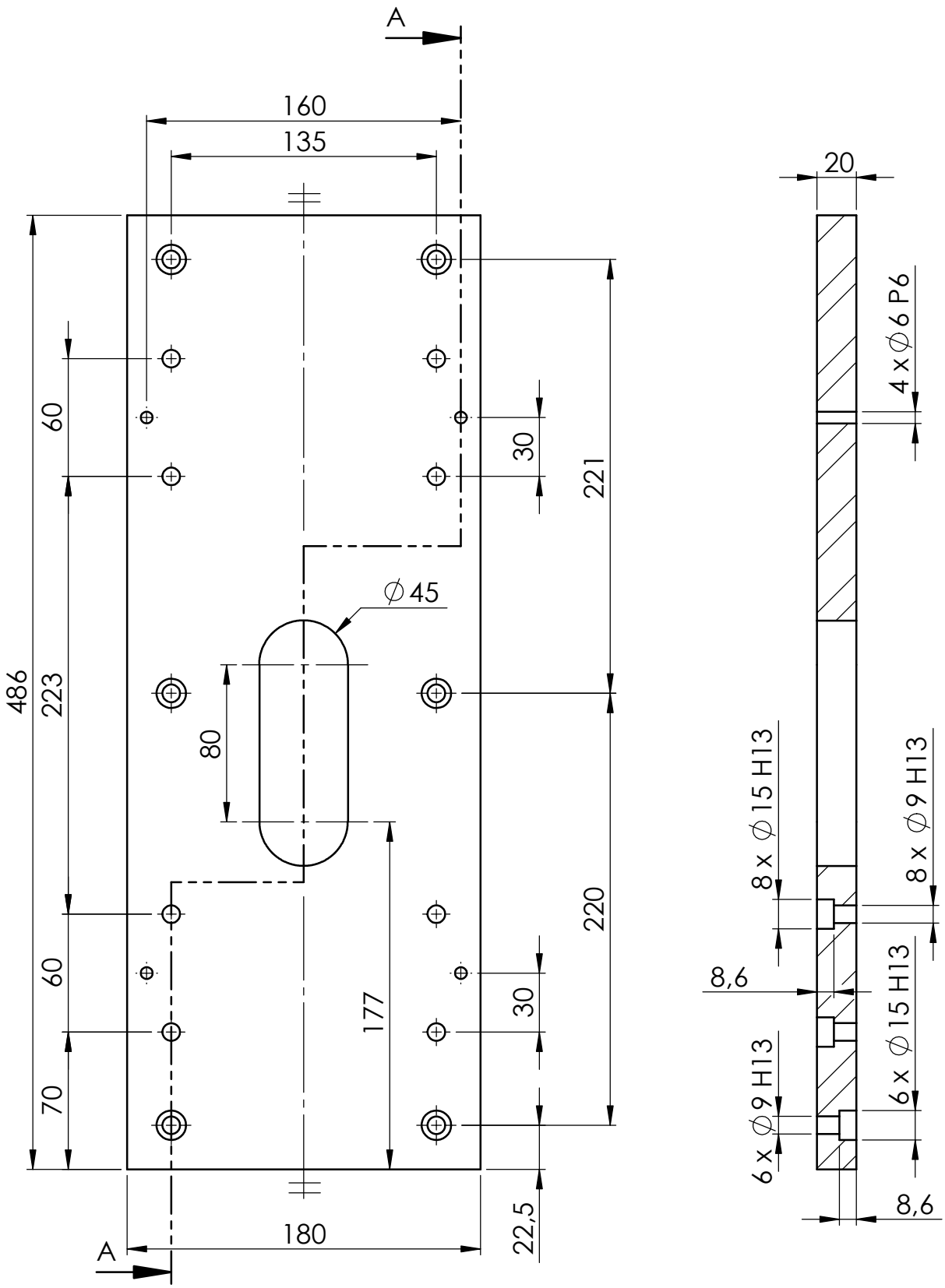

Toleranciamento - ISO 8015 Tolerâncias gerais - ISO 2768 - mK Rugosidades gerais - ISO 1302 Cantos e chanfros gerais - ISO 13715	FEUP			
	NOME	ASSINATURA	MATERIAL:	TITLE:
DESENHO	André Ramos		Al 5083	Base elevação
VERIF.	Inv. Carlos M. Silva			
SOLIDWORKS Student License Academic Use Only		QUANTIDADE 1	Número L-10	Rev. A / A4
			ESCALA1:3	

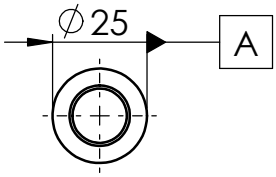

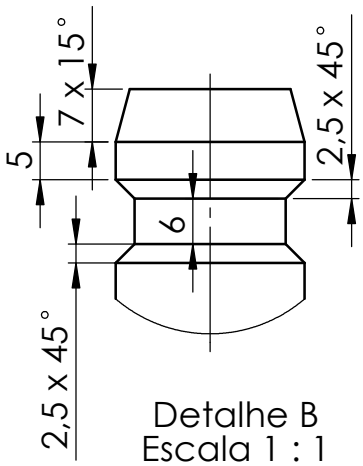

Detalhe B
Escala 1 : 1

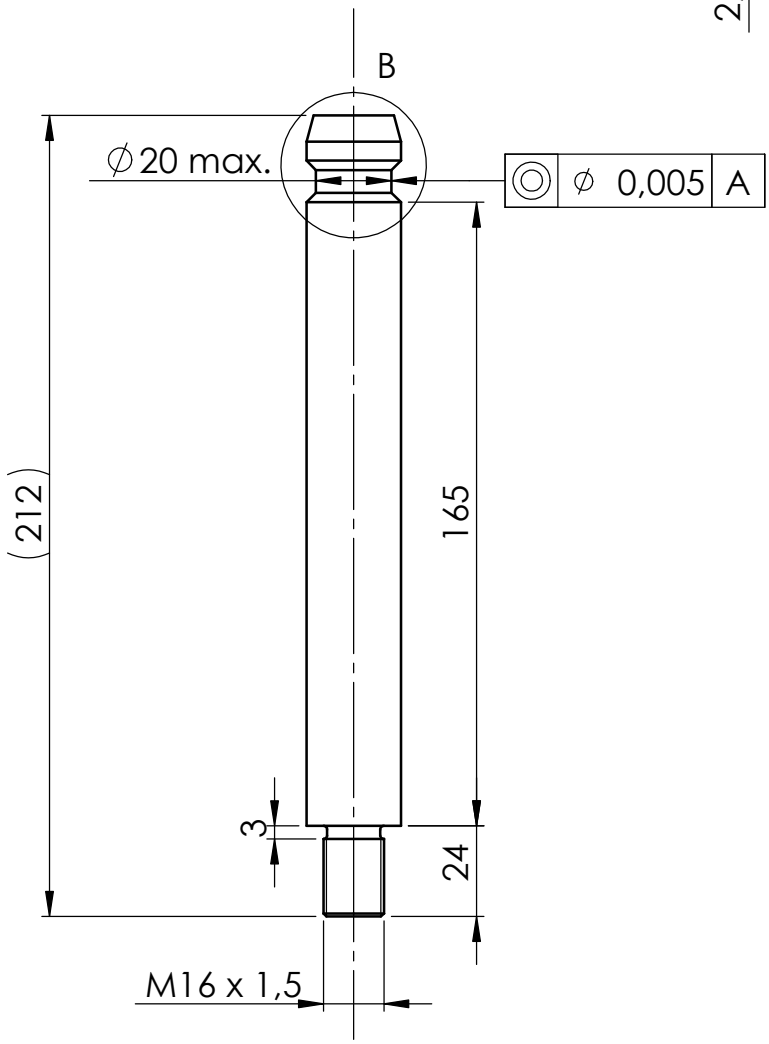

Toleranciamento - ISO 8015 Tolerâncias gerais - ISO 2768 - mH Rugosidades gerais - ISO 1302 Cantos e chanfros gerais - ISO 13715	FEUP	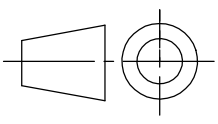		
	NOME	ASSINATURA	MATERIAL:	TITLE:
DESENHO	André Ramos		Varão ⌀25h6 Aço CEAX	Suporte Massa Longo
VERIF.	Inv. Carlos M. Silva			

SOLIDWORKS Student License Academic Use Only	QUANTIDADE 1	Número M-1	Rev. A	A4
		ESCALA1:2		

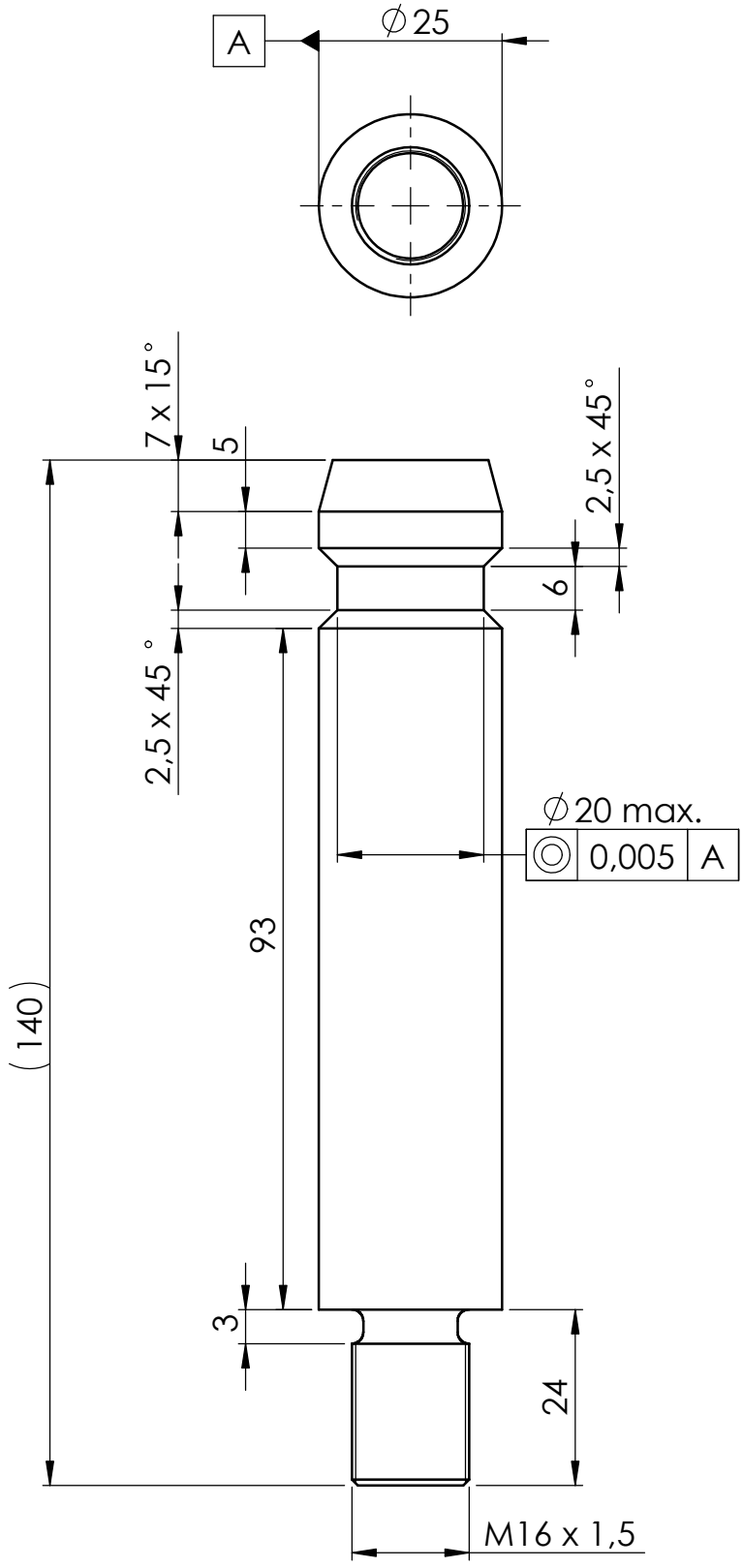

Toleranciamento - ISO 8015 Tolerâncias gerais - ISO 2768 - mH Rugosidades gerais - ISO 1302 Cantos e chanfros gerais - ISO 13715	FEUP			
	NOME	ASSINATURA	MATERIAL:	TITLE:
DESENHO	André Ramos		Varão ∅25h6 Aço CEAX	Suporte Massa Curto
VERIF.	Inv. Carlos M. Silva			
SOLIDWORKS Student License Academic Use Only		QUANTIDADE: 1	Número: M-2	Rev. A / A4
			ESCALA1:1	

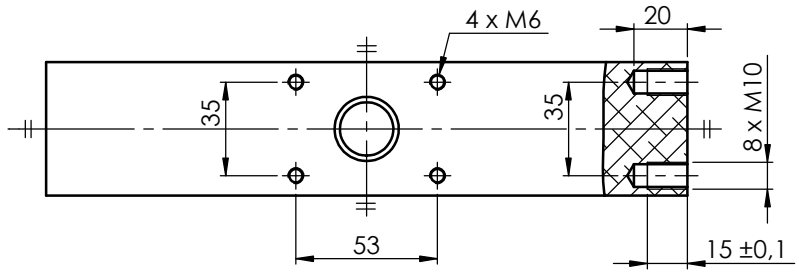

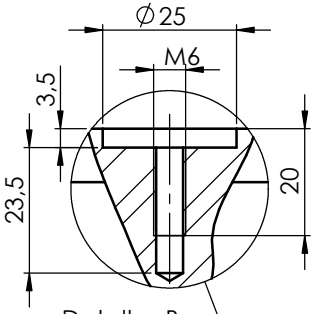

Detalhe B
Escala 1 : 1

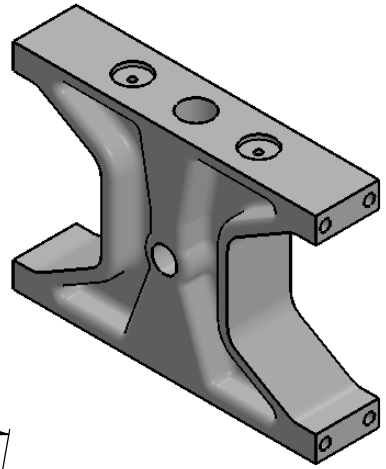

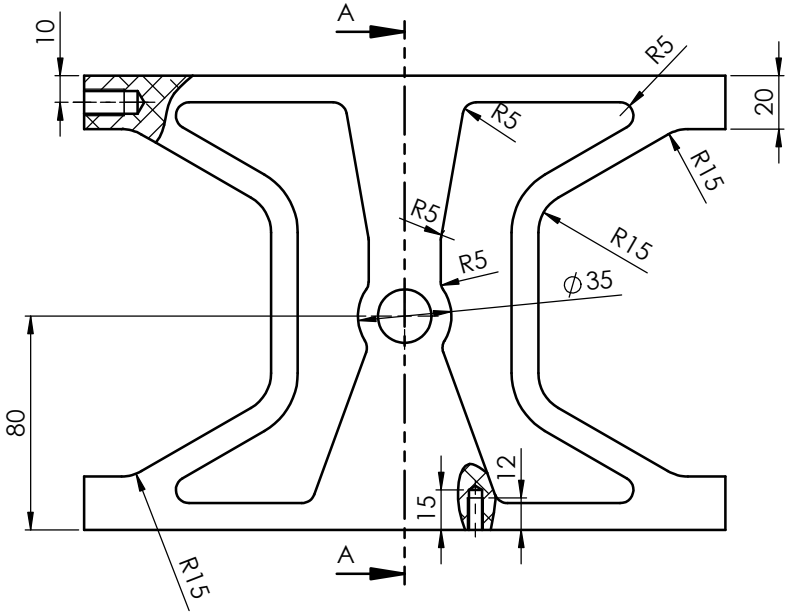

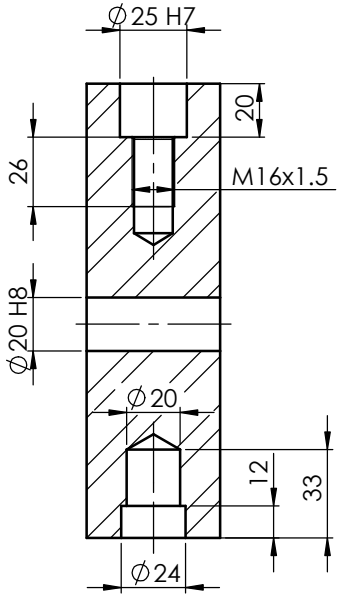

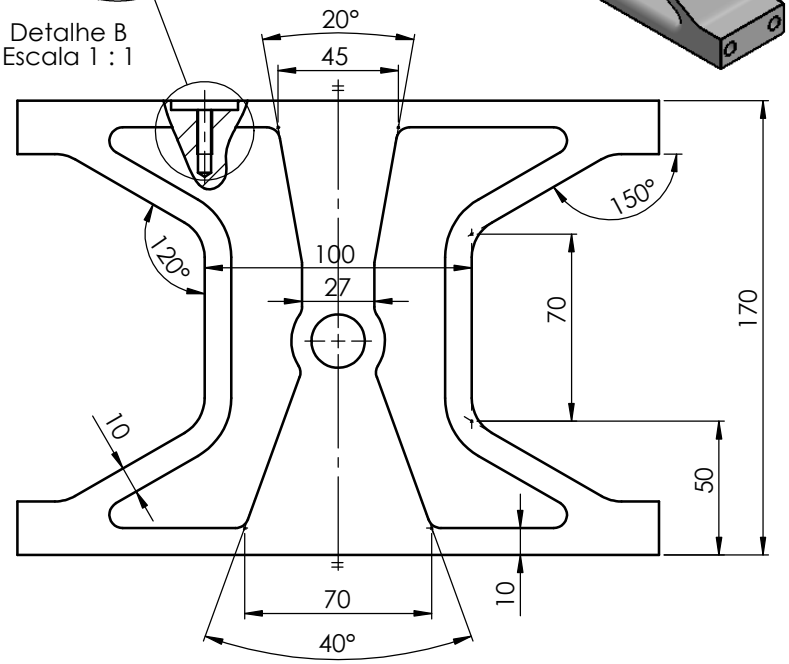

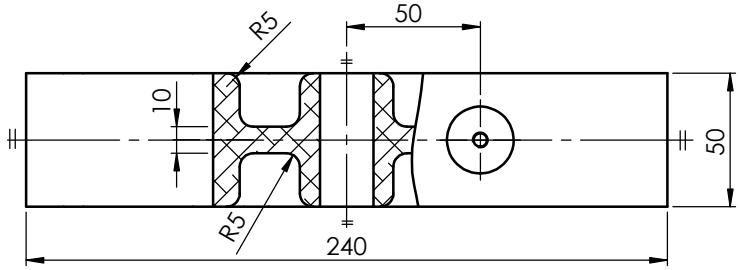

	Nome	Assinatura	
Desenho	André Ramos		
Verif.	Inv. Carlos M. Silva		

Quantidade 1

Número M-3

Toleranciamento - ISO 8015
Tolerâncias gerais - ISO 2768 - mK
Rugosidades gerais - ISO 1302
Cantos e chanfros gerais - ISO 13715

FEUP

MATERIAL: Al 7075 T651

Titulo: Bigorna

A3

ESCALA:1:2

FOLHA 1 de 1

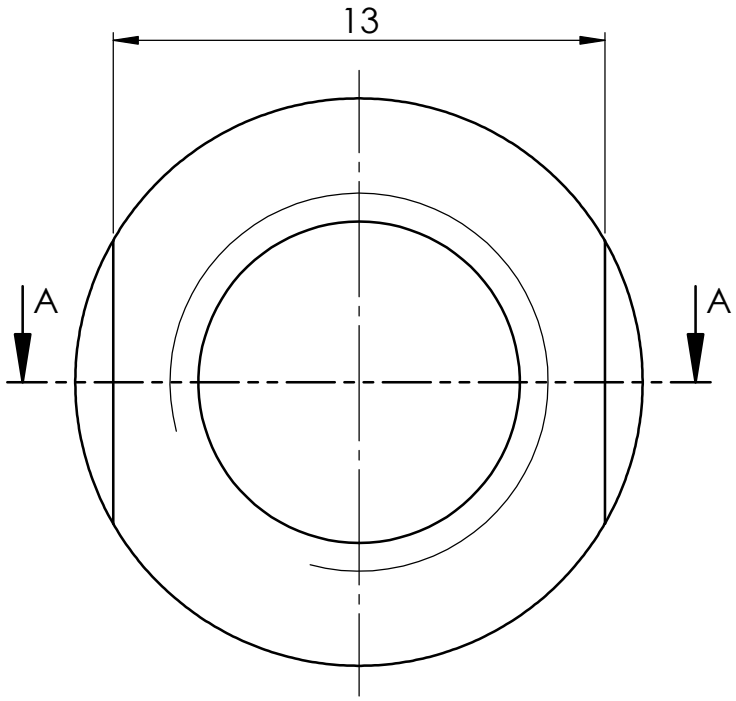

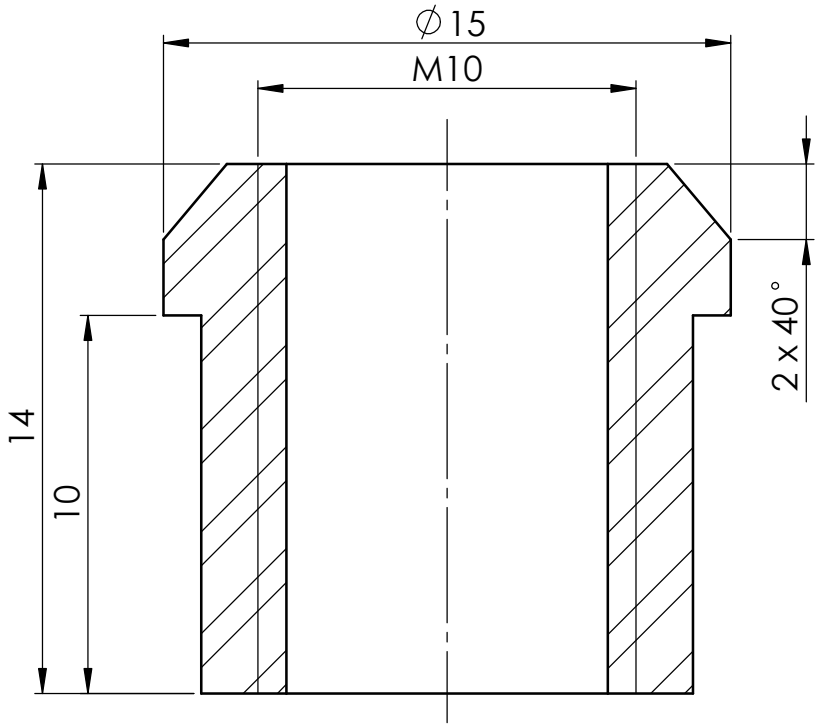

Toleranciamento - ISO 8015 Tolerâncias gerais - ISO 2768 - mK Rugosidades gerais - ISO 1302 Cantos e chanfros gerais - ISO 13715	FEUP	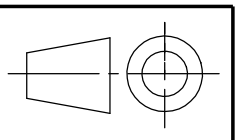		
	NOME	DATA	MATERIAL:	Titulo
DESENHO	André Ramos		Aço Ck45	Controlador de folga
VERIF.	Inv. Carlos M. Silva			
SOLIDWORKS Student License Academic Use Only		QUANTIDADE 8	Número M-4	Rev. CMS A4
			ESCALA5:1	

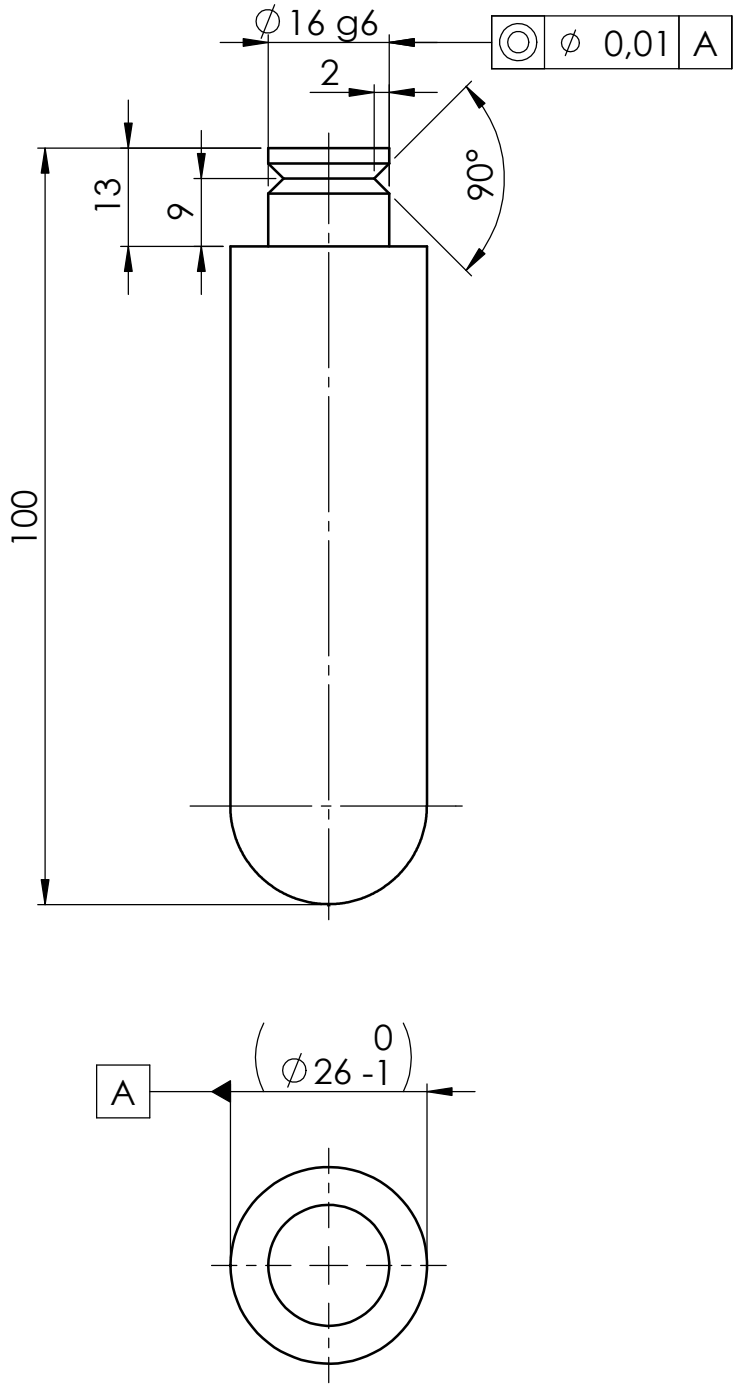

Toleranciamento - ISO 8015 Tolerâncias gerais - ISO 2768 - mK Rugosidades gerais - ISO 1302 Cantos e chanfros gerais - ISO 13715	FEUP			
	NOME	Assinatura	MATERIAL:	Titulo
DESENHO	André Ramos		K600	Impactador
VERIF.	Inv. Carlos M. Silva			
SOLIDWORKS Student License Academic Use Only		QUANTIDADE: 1	Número M-5	Rev. CMS / A4
			ESCALA1:1	

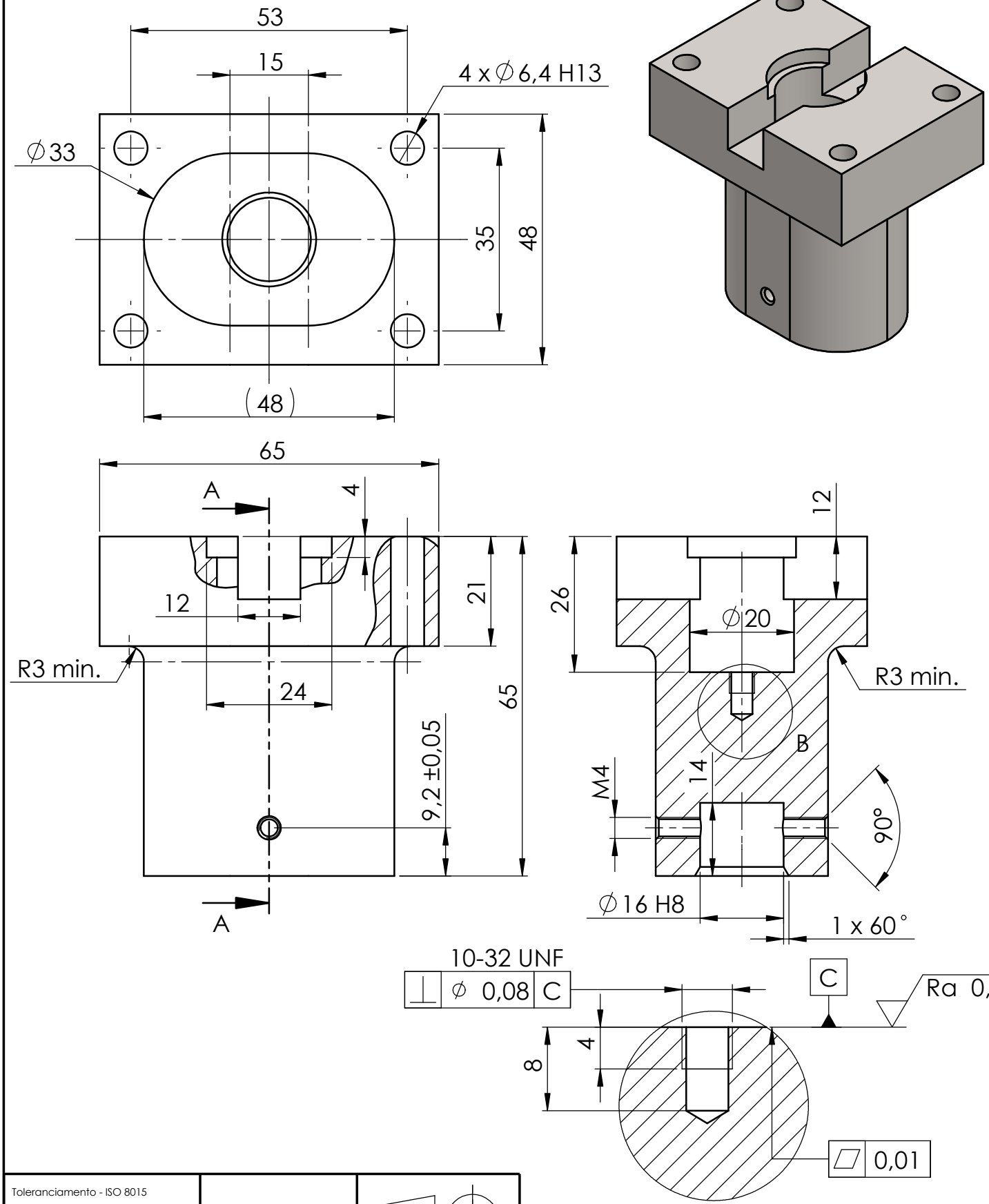

Toleranciamento - ISO 8015 Tolerâncias gerais - ISO 2768 - mK Rugosidades gerais - ISO 1302 Cantos e chanfros gerais - ISO 13715	FEUP			
	NOME	ASSINATURA	MATERIAL:	TITLE:
DESENHO	André Ramos		Aço K600	Ligação acel-impact
VERIF.	Inv. Carlos M. Silva			
SOLIDWORKS Student License Academic Use Only		QUANTIDADE 1	Número M-6	Rev. F / A4
			ESCALA1:1	

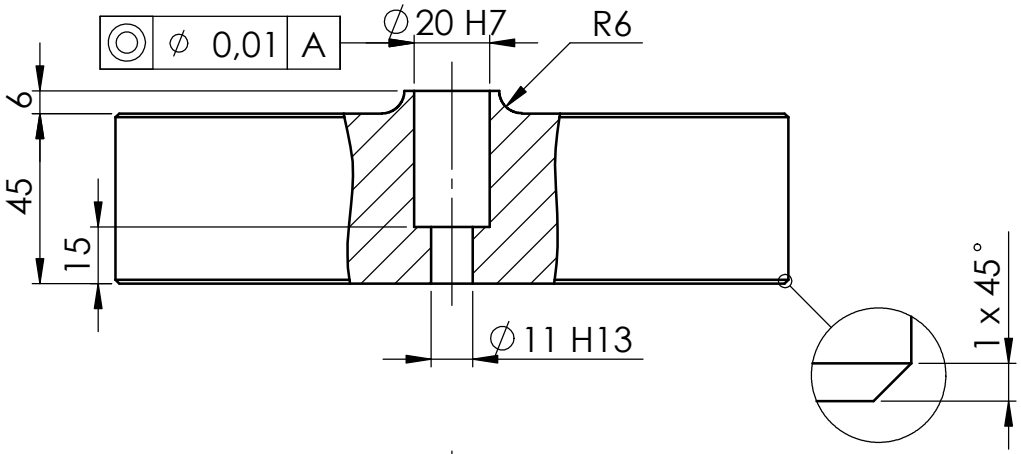

Detalhe A
Escala 5 : 1

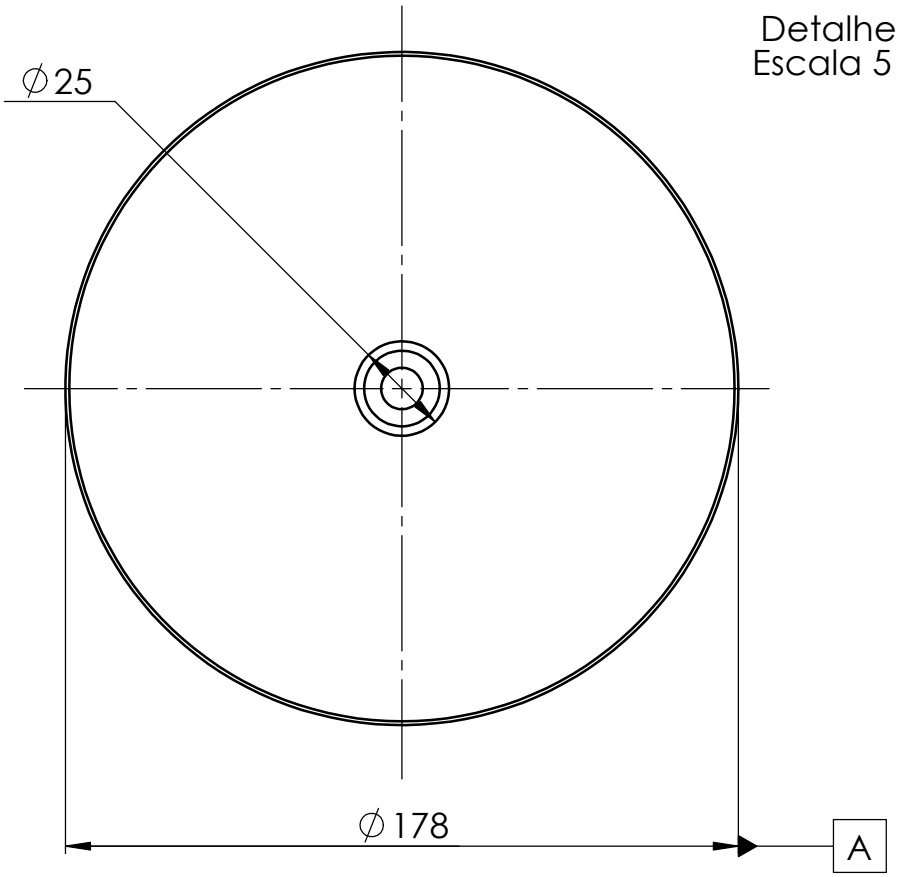

Toleranciamento - ISO 8015 Tolerâncias gerais - ISO 2768 - mH Rugosidades gerais - ISO 1302 Cantos e chanfros gerais - ISO 13715	FEUP			
	NOME	ASSINATURA	MATERIAL:	TITLE:
DESENHO	André Ramos		Aço Ck45	Extensão lateral
VERIF.	Inv. Carlos M. Silva			
SOLIDWORKS Student License Academic Use Only		QUANTIDADE: 2	Número M-7	Rev. A / A4
			ESCALA1:2	

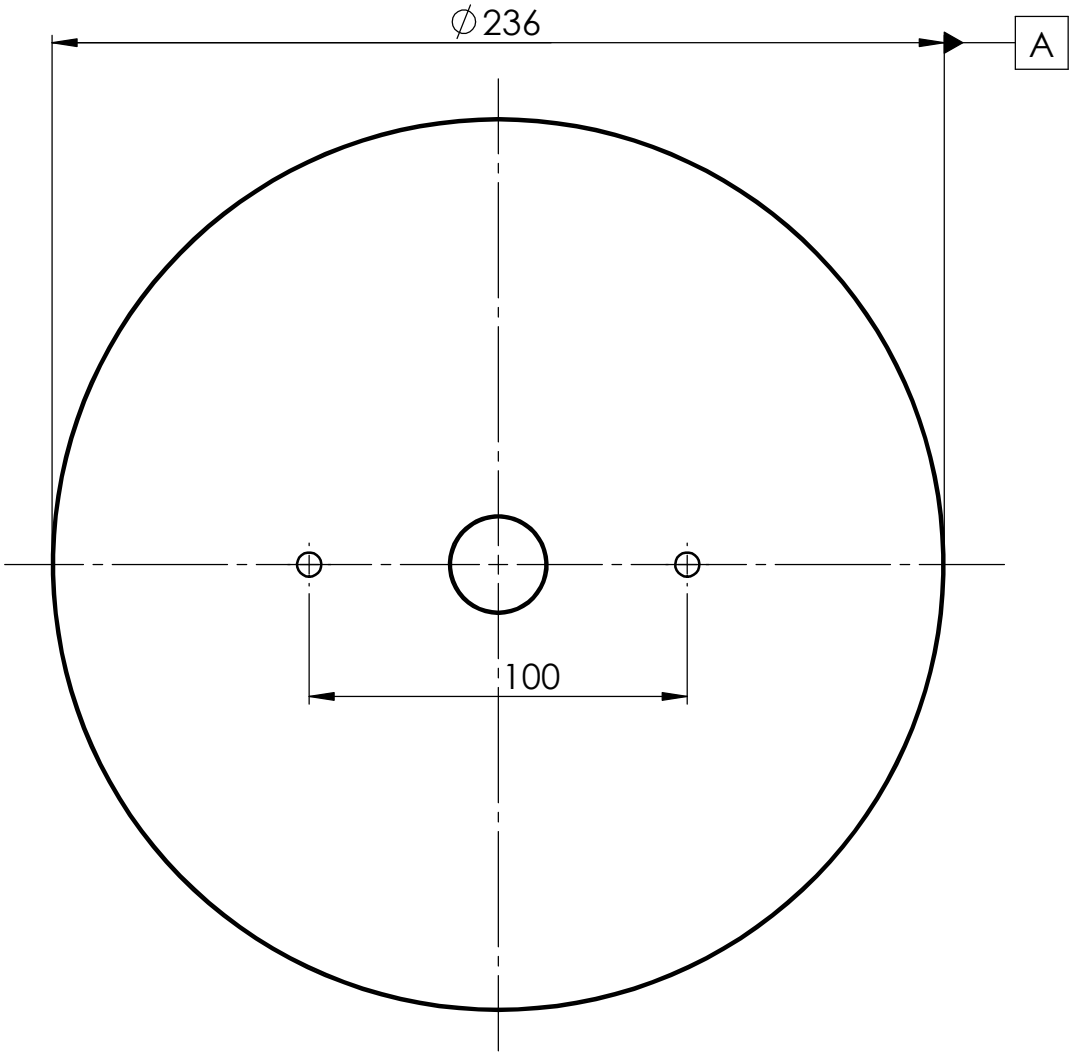

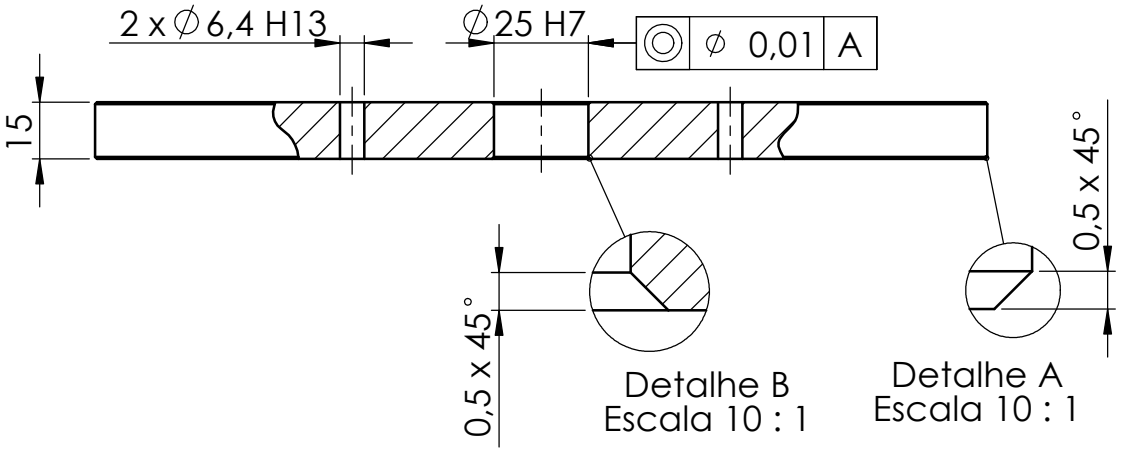

Toleranciamento - ISO 8015 Tolerâncias gerais - ISO 2768 - mK Rugosidades gerais - ISO 1302 Cantos e chanfros gerais - ISO 13715	FEUP			
	NOME	ASSINATURA	MATERIAL:	TÍTULO:
DESENHO	André Ramos		Aço Ck45	Extensão superior 5 kg
VERIF.	Inv. Carlos M. Silva			
SOLIDWORKS Student License Academic Use Only		QUANTIDADE 7	Número M-9	Rev. A / A4
			ESCALA1:2	

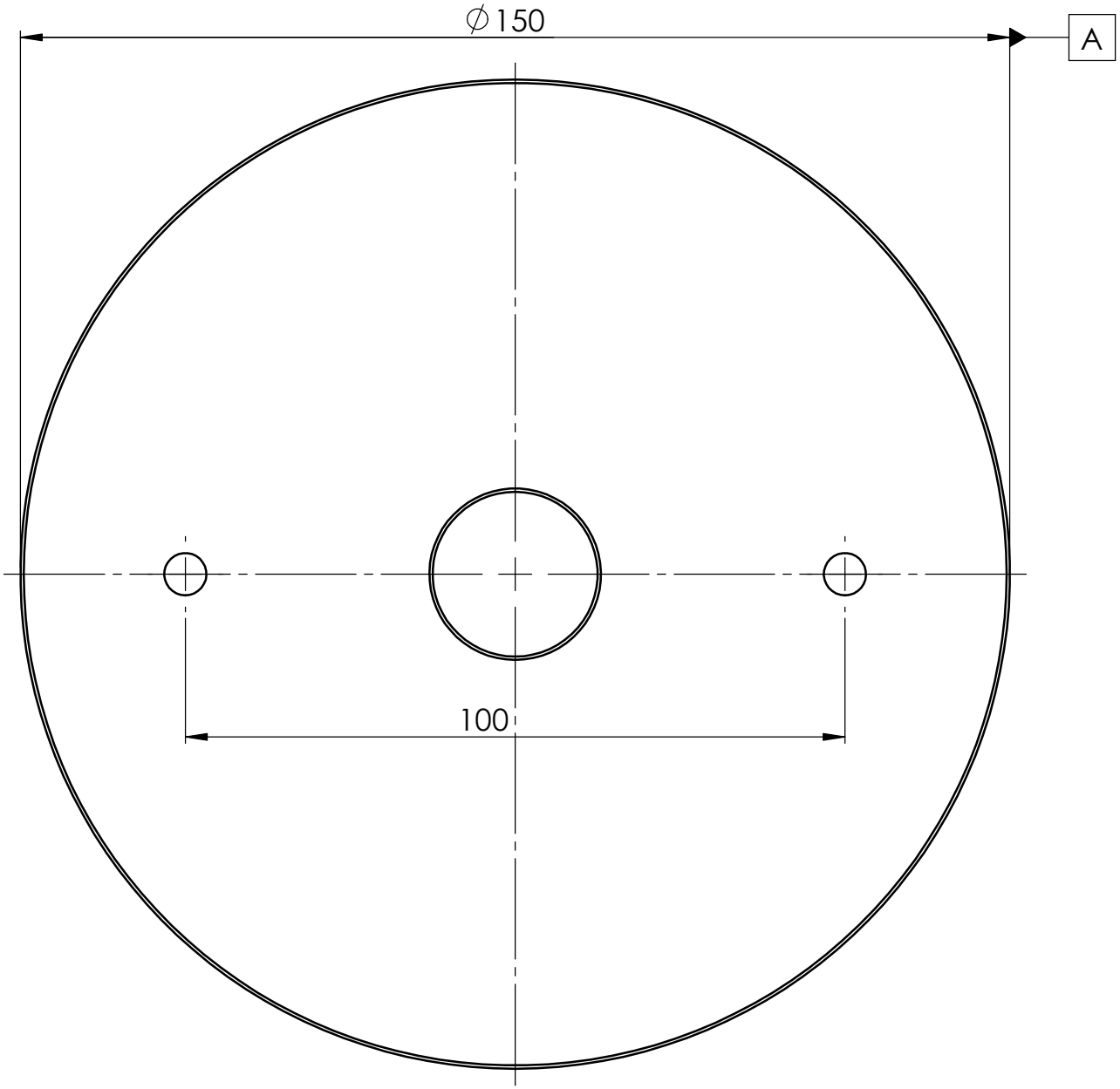

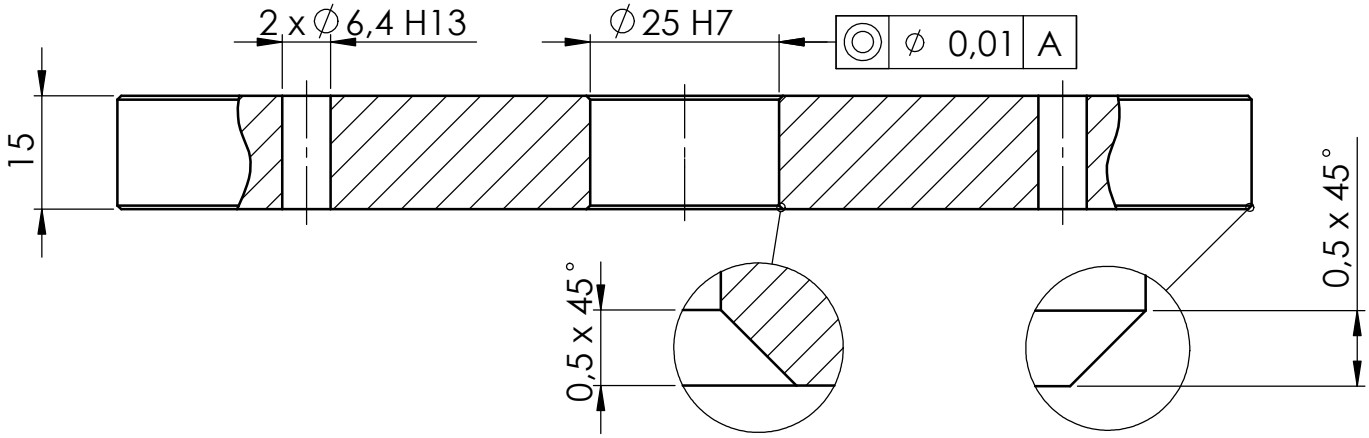

DETAIL A
SCALE 20 : 1

DETAIL B
SCALE 20 : 1

Toleranciamento - ISO 8015
Tolerâncias gerais - ISO 2768 - mK
Rugosidades gerais - ISO 1302
Cantos e chanfros gerais - ISO 13715

FEUP

	NOME	ASSINATURA
DESENHO	André Ramos	
VERIF.	Inv. Carlos M. Silva	

MATERIAL: Aço Ck45

TITLE: Extensão superior 2 kg

SOLIDWORKS Student License
Academic Use Only

QUANTIDADE: 2

Número: M-10

Rev. A

A4

ESCALA1:1

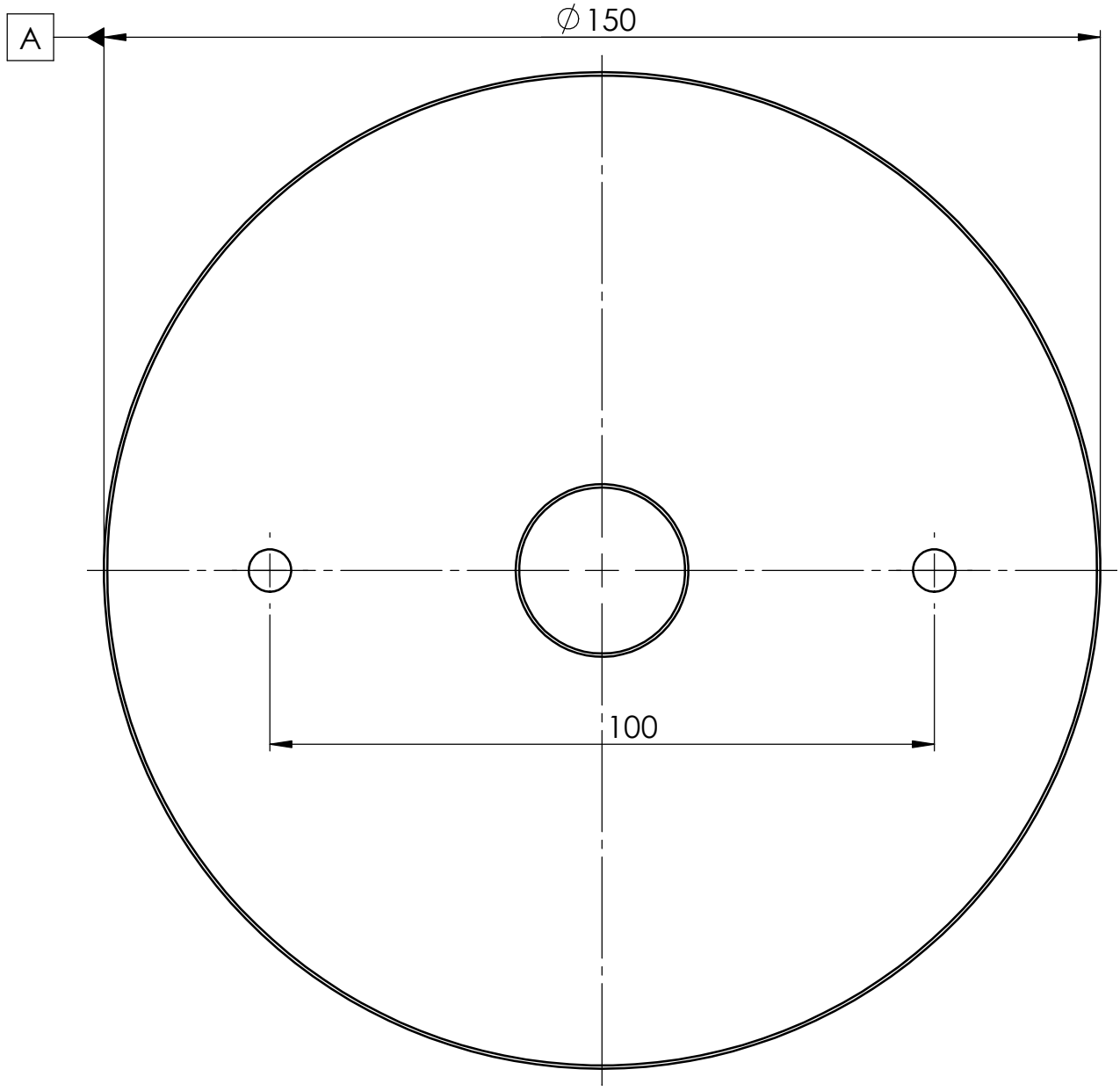

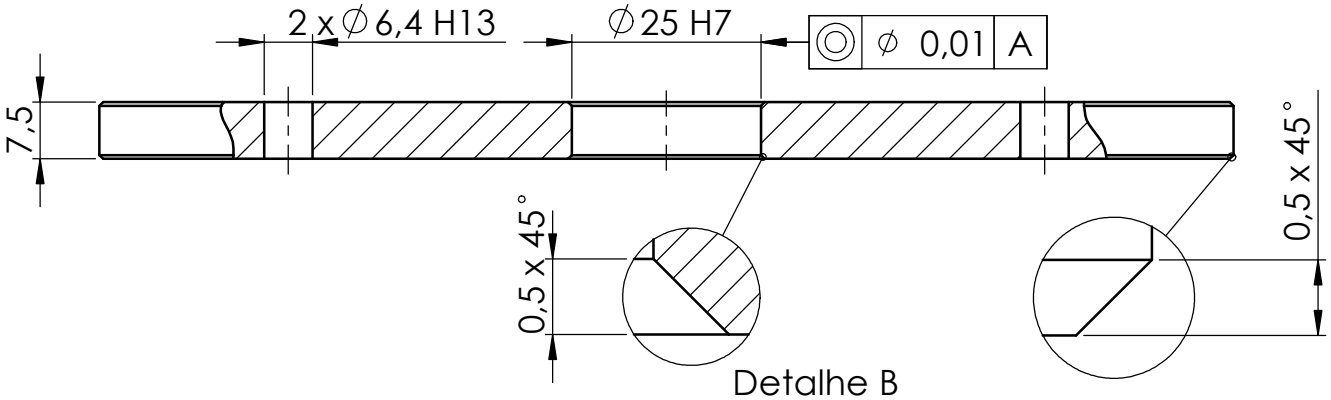

Detalhe B
Escala 20 : 1

Detalhe A
Escala 20 : 1

Toleranciamento - ISO 8015 Tolerâncias gerais - ISO 2768 - mK Rugosidades gerais - ISO 1302 Cantos e chanfros gerais - ISO 13715	FEUP			
	NOME	ASSINATURA	MATERIAL:	TÍTULO
DESENHO	André Ramos		Aço Ck45	Extensão superior 1 kg
VERIF.	Inv. Carlos M. Silva			
SOLIDWORKS Student License Academic Use Only			QUANTIDADE: 1	Número M-11 / Rev. A / A4
				ESCALA1:1

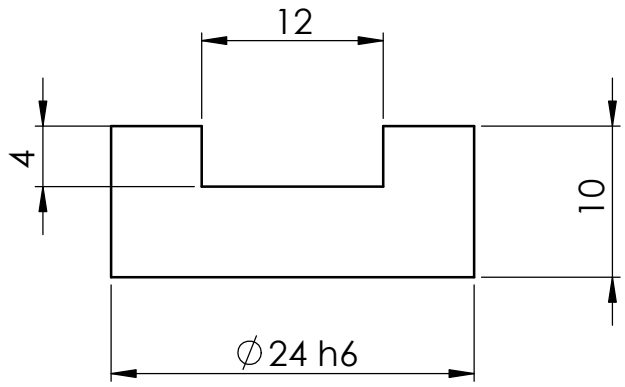

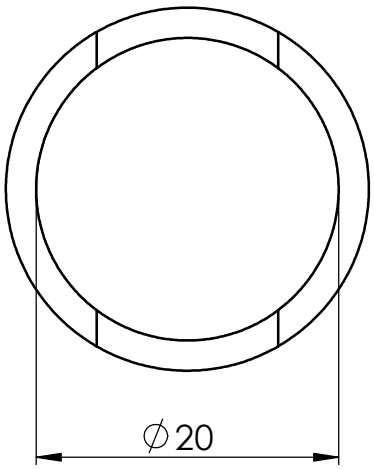

Toleranciamento - ISO 8015 Tolerâncias gerais - ISO 2768 - mH Rugosidades gerais - ISO 1302 Cantos e chanfros gerais - ISO 13715	FEUP			
	NOME	DATA	MATERIAL:	TITLE:
DESENHO	André Ramos		Aço Ck45	Manga Centragem
VERIF.	Inv. Carlos M. Silva			
SOLIDWORKS Student License Academic Use Only		QUANTIDADE: 1	Número M-12	Rev. A / A4
			ESCALA2:1	

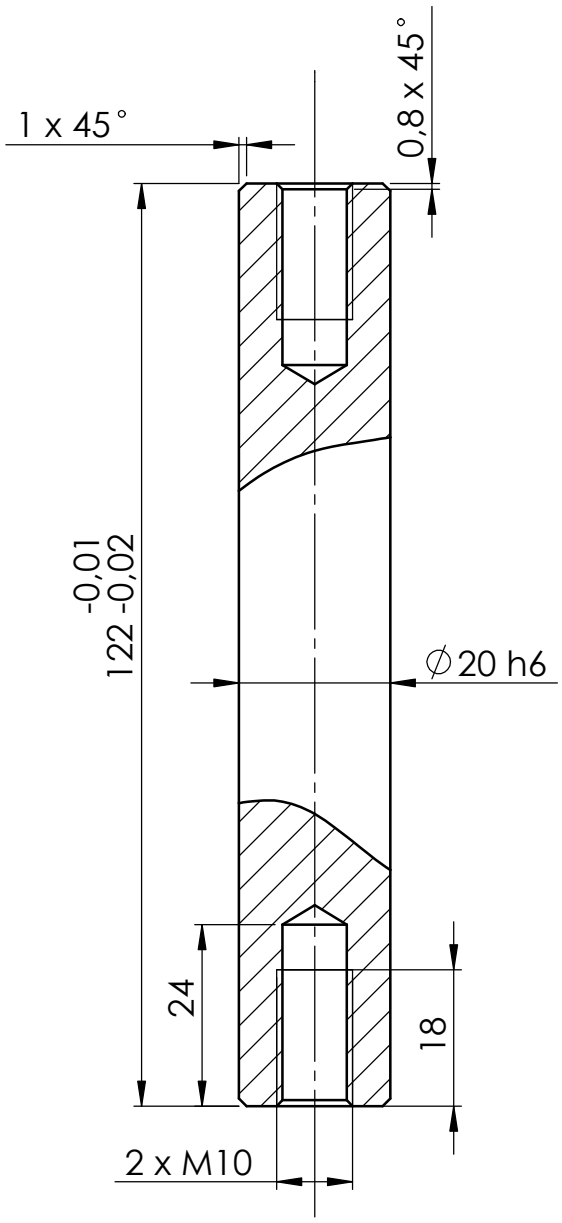

Toleranciamento - ISO 8015 Tolerâncias gerais - ISO 2768 - mH Rugosidades gerais - ISO 1302 Cantos e chanfros gerais - ISO 13715	FEUP			
	NOME	ASSINATURA	MATERIAL:	TITLE:
DESENHO	André Ramos		Aço Ck45	Veio Central
VERIF.	Inv. Carlos M. Silva			
SOLIDWORKS Student License Academic Use Only		QUANTIDADE: 1	Número M-13	Rev. A / A4
			ESCALA1:1	

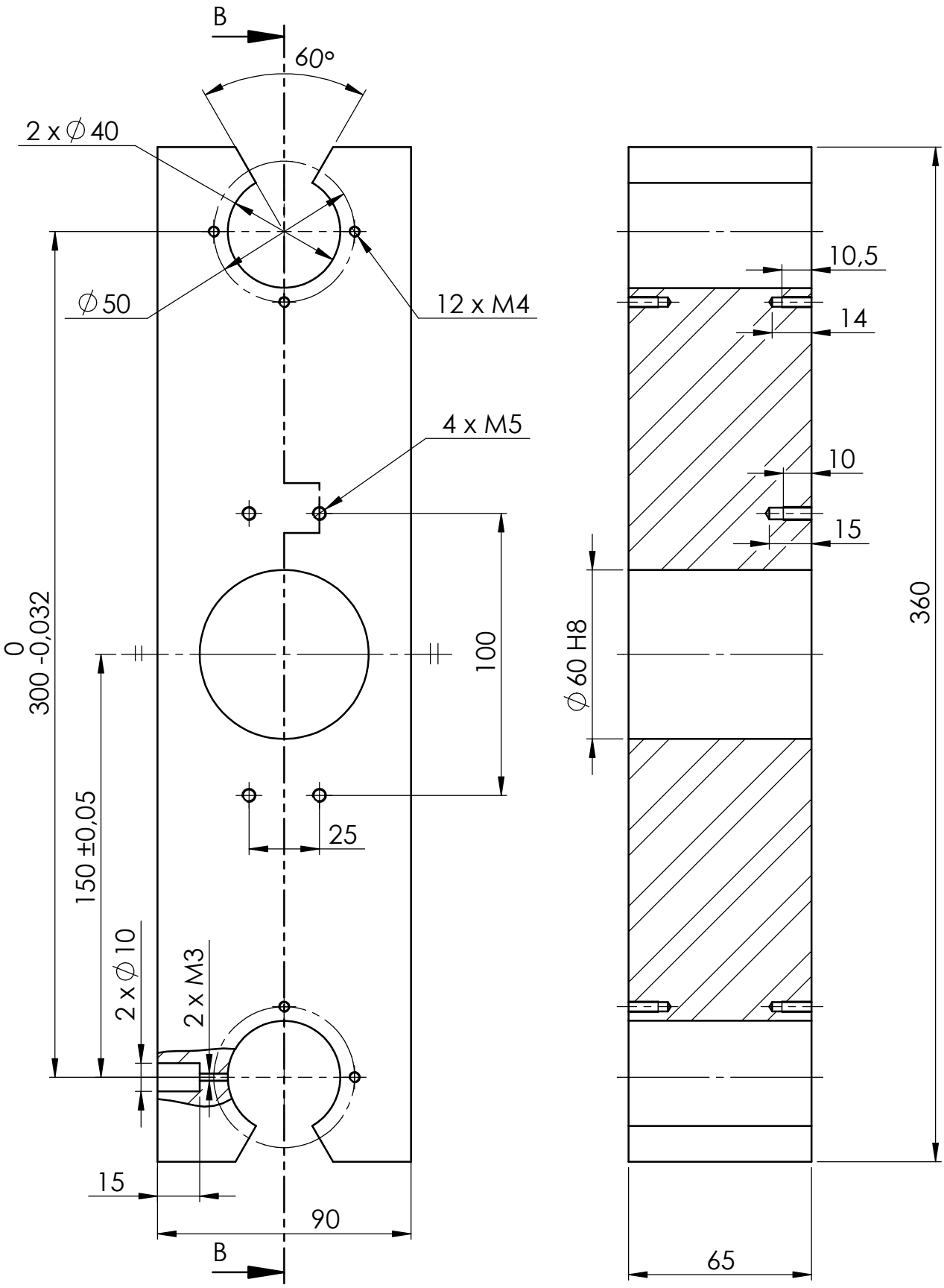

Toleranciamento - ISO 8015 Tolerâncias gerais - ISO 2768 - mK Rugosidades gerais - ISO 1302 Cantos e chanfros gerais - ISO 13715	FEUP			
	NOME	DATA	MATERIAL:	TITLE:
DESENHO	André Ramos		Aluminio 7075	Carro
VERIF.	Inv. Carlos M. Silva			
SOLIDWORKS Student License Academic Use Only		QUANTIDADE 1	Número T-1	Rev. CMS / A4
			ESCALA1:2	

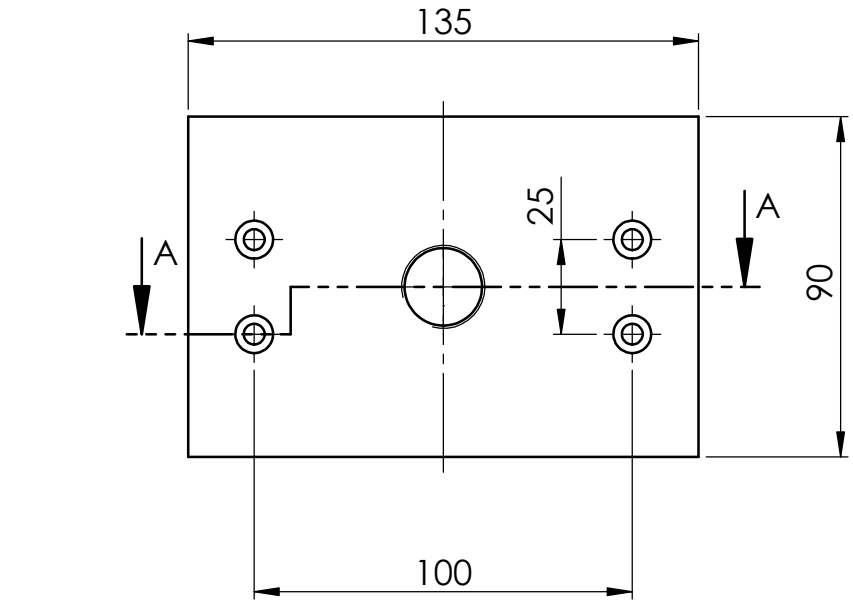

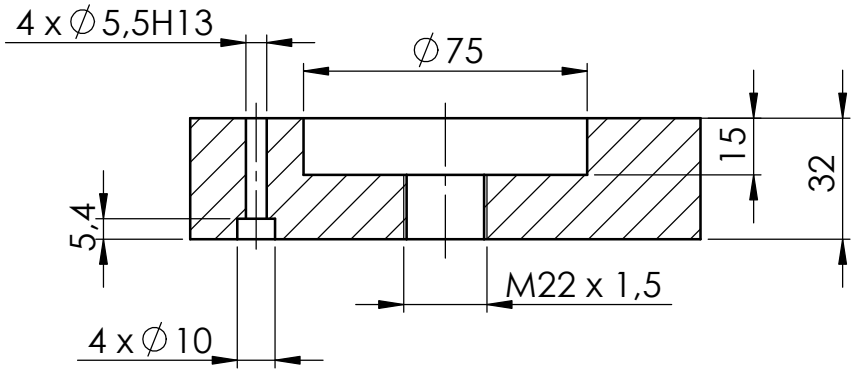

Toleranciamento - ISO 8015 Tolerâncias gerais - ISO 2768 - mK Rugosidades gerais - ISO 1302 Cantos e chanfros gerais - ISO 13715	FEUP			
	NOME	Assinatura	MATERIAL:	TITLE:
DESENHO	André Ramos		Aço Ck45	Ligação carro-cilindro
VERIF.	Inv. Carlos M. Silva			
SOLIDWORKS Student License Academic Use Only		QUANTIDADE: 1	Número T-3	Rev. CMS: A4
			ESCALA1:2	

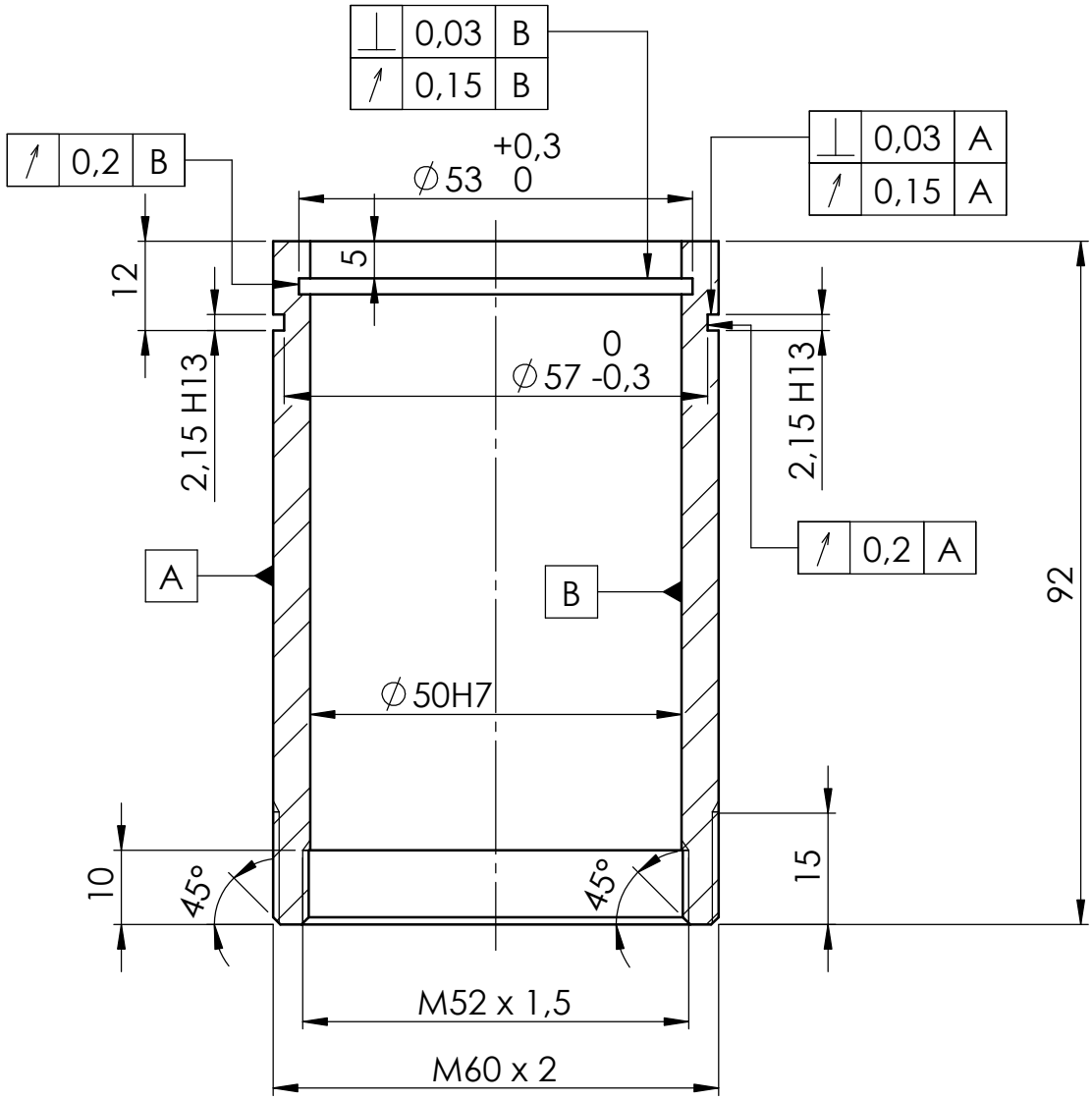

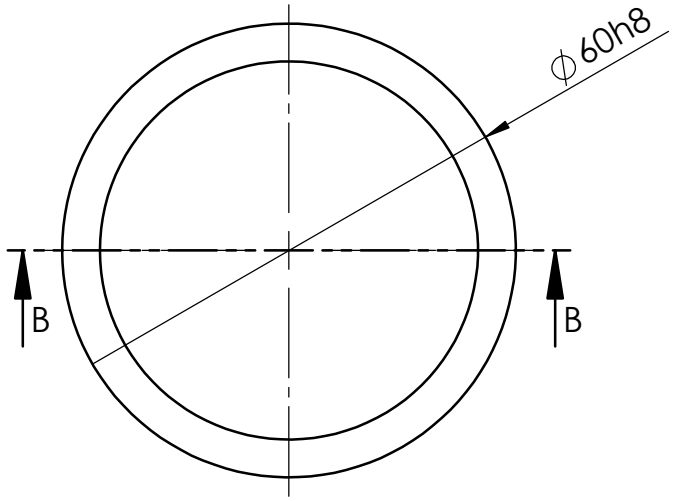

Toleranciamento - ISO 8015 Tolerâncias gerais - ISO 2768 - mK Rugosidades gerais - ISO 1302 Cantos e chanfros gerais - ISO 13715	FEUP			
	NOME	DATA	MATERIAL:	TITLE:
DESENHO	André Ramos		Aço Inox R304	Peça Exterior
VERIF.	Inv. Carlos M. Silva			
SOLIDWORKS Student License Academic Use Only		QUANTIDADE 1	Número T-4	Rev. CMS / A4
			ESCALA1:1	

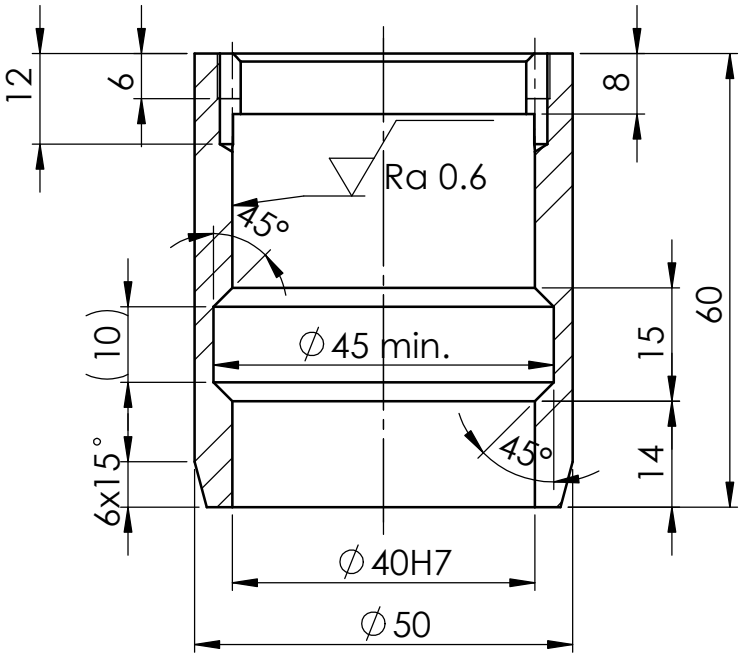

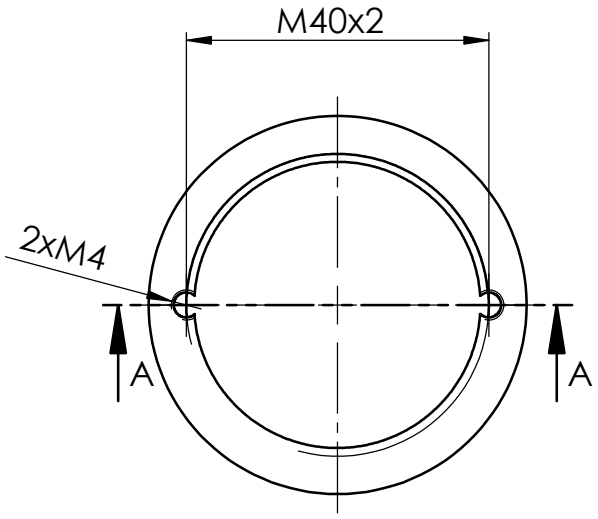

1. Furos M4 a roscar em conjunto com a peça número T-6

Toleranciamento - ISO 8015 Tolerâncias gerais - ISO 2768 - mK Rugosidades gerais - ISO 1302 Cantos e chanfros gerais - ISO 13715	FEUP			
	NOME	ASSINATURA	MATERIAL:	TITLE:
DESENHO	André Ramos		igdur© J	Camisa esferas
VERIF.	Inv. Carlos M. Silva			
SOLIDWORKS Student License Academic Use Only		QUANTIDADE 1	Número T-5	Rev. CMS / A4
			ESCALA1:1	

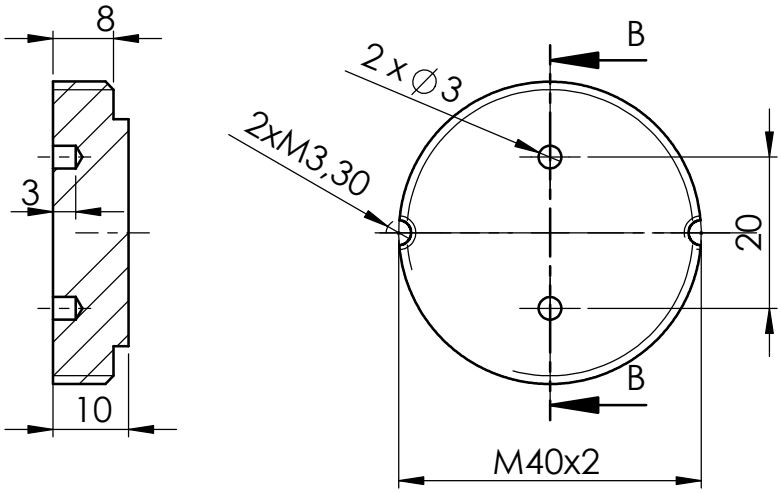

1. Furos M4 a roscar em conjunto com a peça número T-5

Toleranciamento - ISO 8015 Tolerâncias gerais - ISO 2768 - mK Rugosidades gerais - ISO 1302 Cantos e chanfros gerais - ISO 13715	FEUP				
	NOME	ASSINATURA	MATERIAL:	TITLE:	
DESENHO	André Ramos		igdur © J	Tampa camisa esferas	
VERIF.	Inv. Carlos M. Silva				
SOLIDWORKS Student License Academic Use Only			QUANTIDADE 1	Número T-6	Rev. CMS A4
				ESCALA1:1	

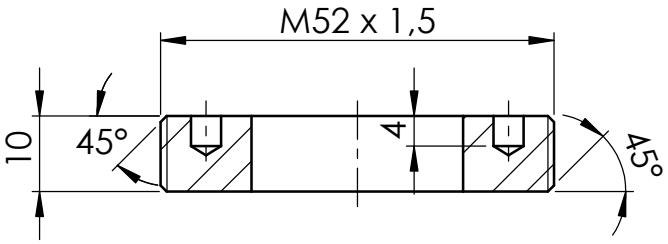

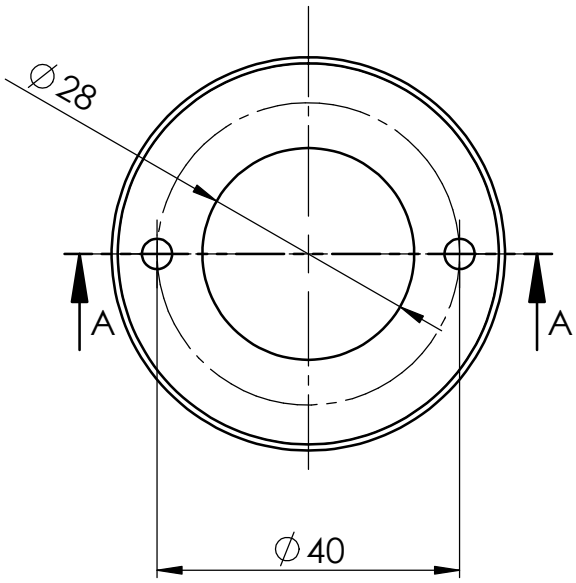

Toleranciamento - ISO 8015 Tolerâncias gerais - ISO 2768 - mK Rugosidades gerais - ISO 1302 Cantos e chanfros gerais - ISO 13715	FEUP			
	NOME	DATA	MATERIAL:	TITLE:
DESENHO	André Ramos		Aço Inox R304	Tampa Interior
VERIF.	Inv. Carlos M. Silva			
SOLIDWORKS Student License Academic Use Only		QUANTIDADE 1	Número T-7	Rev. CMS / A4
			ESCALA1:1	

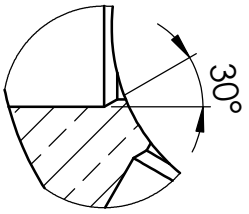

DETALHE E
ESCALA 2 : 1

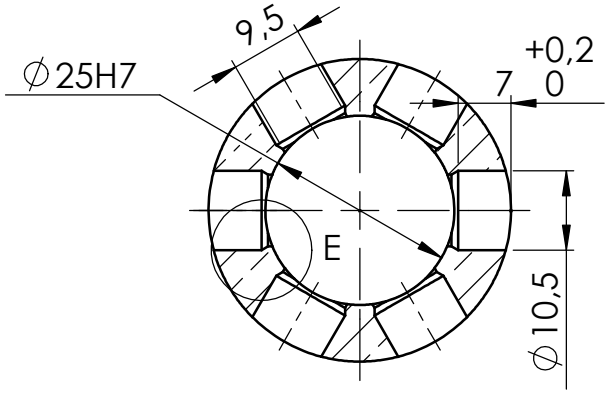

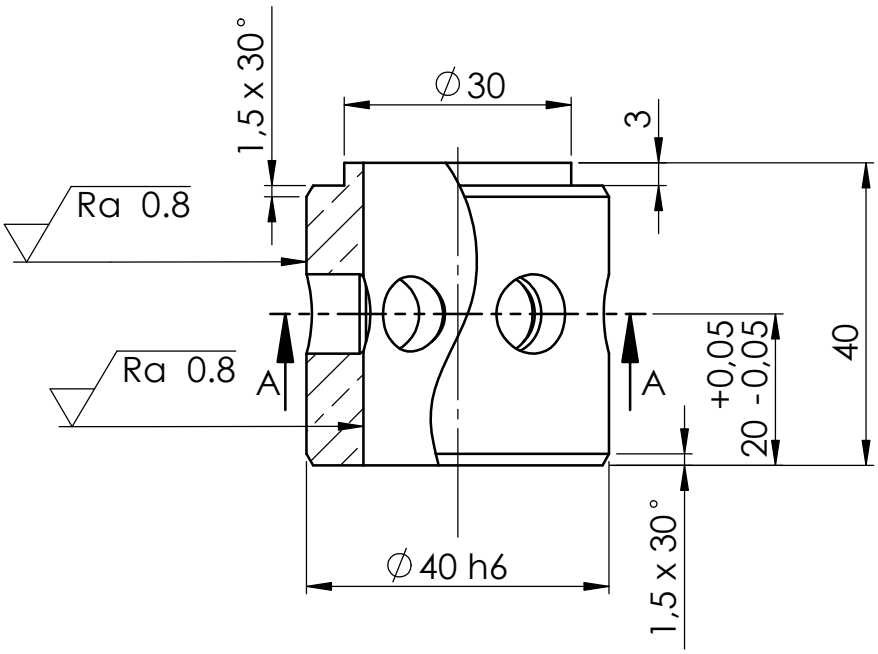

Toleranciamento - ISO 8015 Tolerâncias gerais - ISO 2768 - mK Rugosidades gerais - ISO 1302 Cantos e chanfros gerais - ISO 13715	FEUP				
	NOME	DATA	MATERIAL:	Título	
DESENHO	André Ramos		Bronze DIN CuSn12	Porta esferas	
VERIF.	Inv. Carlos M. Silva				
SOLIDWORKS Student License Academic Use Only			QUANTIDADE 1	Número T-8	Rev. CMS A4
				ESCALA1:1	

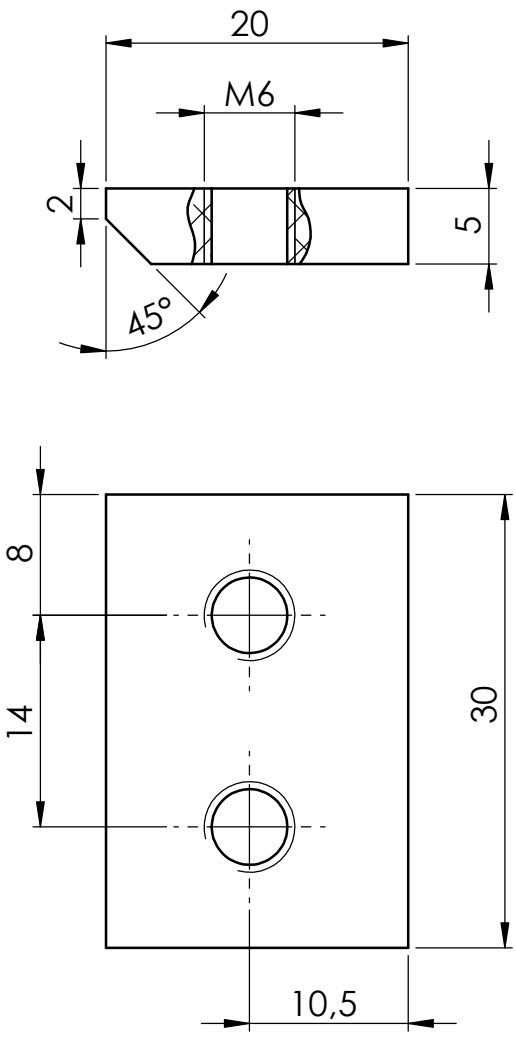

Toleranciamento - ISO 8015 Tolerâncias gerais - ISO 2768 - mK Rugosidades gerais - ISO 1302 Cantos e chanfros gerais - ISO 13715	FEUP			
	NOME	ASSINATURA	MATERIAL:	TÍTULO
DESENHO	André Ramos		Aço Ck45	Porca lig-aqv
VERIF.	Inv. Carlos M. Silva			
SOLIDWORKS Student License Academic Use Only		QUANTIDADE 2	Número V-1	Rev. F / A4
			ESCALA2:1	

Appendix B

MATLAB code

In this Appendix, the code produced in MATLAB [16] used throughout the thesis will be presented and explained.

B.1 Solving a system of differential equations

In Section 3.1.4 it was needed to solve Equation 3.22,

$$\left[m\right]\left\{\ddot{x}\right\}+\left[c\right]\left\{\dot{x}\right\}+\left[k\right]\left\{x\right\}=\left\{f\right\}$$

Which consist in a system of five second order differential equations. This system, in order to be solved by MATLAB numerical solver, `ode45`, had to be represented in the state-space. This was achieved using the following transformation,

$$\begin{aligned} y_1 &= x_1 & y_6 &= \dot{x}_3 \\ y_2 &= \dot{x}_1 & y_7 &= x_4 \\ y_3 &= x_2 & y_8 &= \dot{x}_4 \\ y_4 &= \dot{x}_2 & y_9 &= x_5 \\ y_5 &= x_3 & y_{10} &= \dot{x}_5 \end{aligned}$$

That results in,

$$\begin{aligned} \dot{y}_1 &= y_2 \\ \dot{y}_2 &= -\frac{1}{m_{11}}\left(y_1 \cdot k_{11} + y_3 \cdot k_{12}\right) \\ \dot{y}_3 &= y_4 \\ \dot{y}_4 &= -\frac{1}{m_{22}}\left(y_1 \cdot k_{21} + y_3 \cdot k_{22} + y_5 \cdot k_{23}\right) \\ \dot{y}_5 &= y_6 \\ \dot{y}_6 &= -\frac{1}{m_{33}}\left(y_3 \cdot k_{32} + y_5 \cdot k_{33} + y_7 \cdot k_{23} + y_9 \cdot k_{35}\right) \\ \dot{y}_7 &= y_8 \\ \dot{y}_8 &= -\frac{1}{m_{44}}\left(y_5 \cdot k_{43} + y_7 \cdot k_{44} + y_8 \cdot c_{44}\right) \\ \dot{y}_9 &= y_{10} \\ \dot{y}_{10} &= -\frac{1}{m_{55}}\left(y_5 \cdot k_{53} + y_9 \cdot k_{55}\right) \end{aligned}$$

which in turn can be described in MATLAB code as shown in Listing B.1,

Listing B.1: Differential equation system implementation `dy.m`

```
function dy = dy(t,y)

% Importing constants
var;

% Initializing dy with 0's
dy = zeros(10, 1);

% Implementing the system of equations
dy(1) = y(2);
dy(2) = -1/mdiag(1)*(y(1)*k(1,1)+y(3)*k(1,2));
dy(3) = y(4);
dy(4) = -1/mdiag(2)*(y(1)*k(2,1)+y(3)*k(2,2)+y(5)*k(2,3));
```

```
dy(5) = y(6);
dy(6) = -1/mdiag(3)*(y(3)*k(3,2)+y(5)*k(3,3)+y(7)*k(3,4)+y(9)*k(3,5)
    );
dy(7) = y(8);
dy(8) = -1/mdiag(4)*(y(5)*k(4,3)+y(7)*k(4,4)+y(8)*c(4,4));
dy(9) = y(10);
dy(10)= -1/mdiag(5)*(y(5)*k(5,3)+y(9)*k(5,5));
```

and solved using the code presented in Listing B.2

Listing B.2: Main routine

```
% Importing the constatns
var;

% Time vector generator
tspan = 0:0.000003:.04;

% Initial conditions y0(10)= 7,37 m/s
y0 = [0; 0; 0; 0; 0; 0; 0; 0; 0; 7.37];

% Numerically solves the system
[t,y] = ode45('dy', tspan, y0);

%Calculating f40(t)
f40=.25*(ka*y(:,7) + ca*y(:,8));

plot (t,f40,'k');
xlabel ('$t$','Interpreter','LaTex','FontSize',16);
ylabel ('$f_{13}$','Interpreter','LaTex','FontSize',16);

%Maximum force transmitted
F40=max(f40)+sum(mdiag)*g;
```

`tspan` was chosen to be approximately equal to $\frac{1}{10 \cdot w_N}$ where w_N is the Nyquist frequency. `var.m` contains the constants calculation (Listing B.3)

Listing B.3: Constants declared in `var.m`

```
% Mass matrix
ml=59;
mc=43.4;
mb=246;
ma=2.65*4;
```

```
mt=20;
m=[ml,0,0,0,0;
    0,2*mc,0,0,0;
    0,0,mb,0,0;
    0,0,0,ma,0;
    0,0,0,0,mt];
mdiag=diag(m);

% Stiffness matrix
kc=3.5194e+08;
kb=1.1515e+08;
ka=4*9e6;
kt=3e9;
k=[2*kc,-2*kc,0,0,0;
    -2*kc,4*kc,-2*kc,0,0;
    0,-2*kc, 2*kc+kt+kb, -kb,-kt;
    0,0,-kb,kb+ka,0;
    0,0,-kt,0,kt];

% Damping matrix
ca=3.91e3;
c=zeros(5);
c(4,4)=ca;

%Misc
g=9.81;
```

Running the main routine will return the numerical solution of the position of all degrees of freedom on the odd indexes of vector `y(n,t)` and their velocities on the next even indexes.

It will also return the numerical solution and plot for $f_{40}(t)$, to be later used in Section 3.1.4.

B.2 Computation of [x,F]

The instrumentation implemented provides the acceleration value on the acquired points and the data relevant is force in function of the deformation some computations need to be done.

Since,

$$v = \int_{t_i}^{t_f} a\,dt \tag{B.1}$$

and

$$x = \int_{t_i}^{t_f} v\,dt \tag{B.2}$$

The time at the moment of impact, t_i, must be determined.

Since the acceleration is constant and negative until the moment of impact, the function displayed in Listing B.4 returns the position in the `accel` array immediately before the variation in acceleration.

Listing B.4: Time of impact computation

```
function [ t_i ] = t_i( accel )
    for t_i = 1:length(accel)
        da = accel(t_i+1) - accel(t_i);
        if da > 0
            break
        end
    end
end
```

Using the trapezoidal rule for integration,

$$\int_a^b f(x)\,dx \approx (b-a)\frac{f(a)+f(b)}{2} \tag{B.3}$$

Defining a and b as every consecutive point, the integration can be implemented in MATLAB as shown in Listing B.5

Listing B.5: Numerical integration

```
function [ int ] = int( f, fl0 )
    int = zeros(length(f),1);
    int(1) = fl0;
    for i=2:length(f)
        int(i) = int(i-1) + (f(i)+f(i-1))/2;
    end
end
```

where `fl0` is the initial condition, the velocity of impact for the first integration and 0 for the second.

Using this function twice, with the respective initial conditions and vectors truncated correctly,

```
v=int(accel(t_i:end),vi)
x=int(v,0)
```

The force in newtons can be represented by the vector,

```
F = m*accel(t_i:end)
```

where `m` is the drop-weight mass, input priorly by the user (Section 5.1.3)

Following this methodology, `[x,F]` can be plotted correctly.

Appendix C

Datasheets

C.1 Elesa+ganter leveling foot

LW.A

Vibration-damping levelling elements

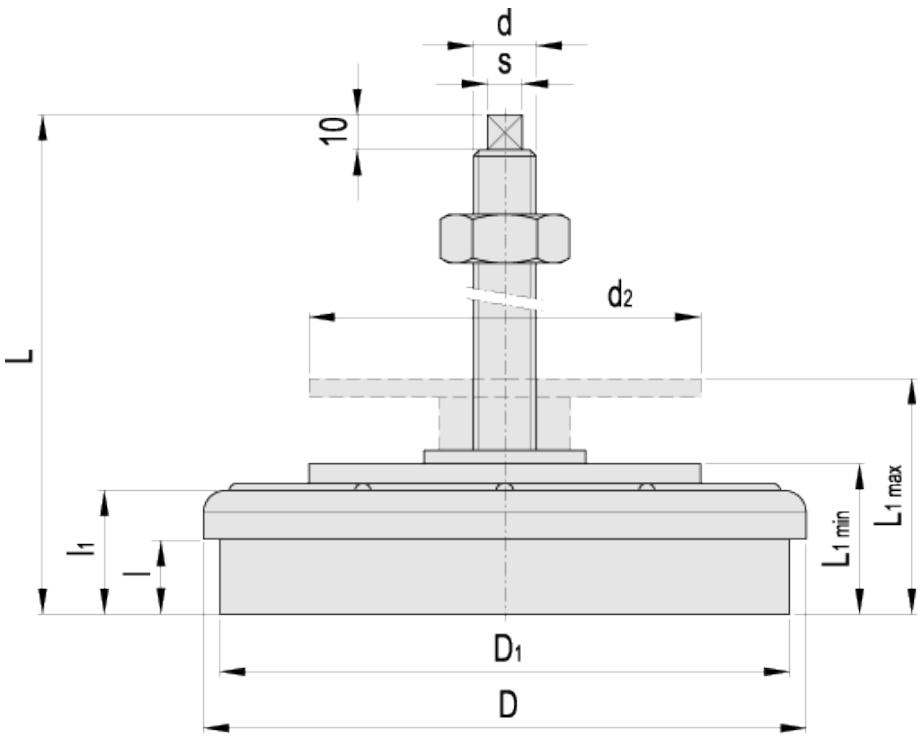

technical informations

Base

Zinc-plated steel.

Vibration-damping disk

Natural rubber NR, hardness 80 Shore A, black colour, matte finish.

Levelling plate

Zinc-plated steel.

Packing ring

OR in NBR synthetic rubber.

Threaded stem

Zinc-plated steel, supplied not assembled.

Nut and washer

Zinc-plated steel.

Assembly instructions

- Put the base of the vibration-damping element under the machine and insert the stem through the hole (not tapped) in the frame of the machine (fig.1)
- Turn the square end of the stem to take the levelling plate in contact with the machine thus obtaining the levelling required. Then lock with nut and washer (fig.2)

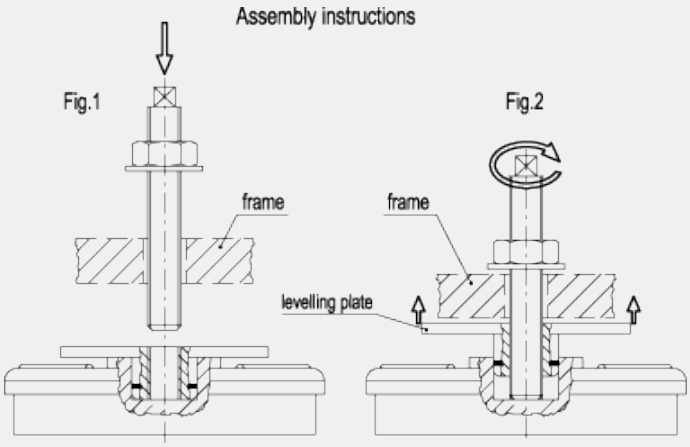

Features and applications

ELESA vibration-damping levelling elements have been designed to damp vibrations, shocks and noises produced by moving bodies or non-balanced vibrating masses of equipment and machines which can cause:
- malfunctioning and reduction of the machine lifespan and/or of the adjacent ones
- damage at men's health
- noise.

Technical data and guidelines for the choice

1) Basic data required:
- disturbing frequency: the frequency of the disturbing vibration produced by a on-duty machine. In general, it coincides with the number of rotations of the engine [rpm]
- the static load applied to every single vibration-damping element [N]
- the isolation degree required [%]
- damping disk deflection value [mm] under a given load
- the stiffness, that is to say the load that applied to the vibration-damping element, produces a deflection of 1mm [N/mm].

2) How to choose the vibration-damping element:
- with reference to the nomograph (Diagram), intersect the disturbing frequency value with the isolation degree required (each isolation degree corresponds to a line on the nomograph) and define the deflection (static deflection mm)
- divide the load applied onto the vibration-damping element by the deflection value to obtain the required rigidity of the vibration-damping element
- compare the rigidity obtained with the rigidity shown in the table and choose the vibration-damping element which presents the nearest value (lower) to the calculated one.

3) Check the values obtained:
- the deflection of the vibration-damping element chosen can be obtained in graphic 2 on the basis of the static load.
- intersect the disturbing frequency value with the vibration-damping element deflection value in the nomograph (Diagram) to obtain the isolation degree offered by the vibration-damping element chosen.
- compare the obtained value with the isolation degree required.

4) Example:
A 80% isolation degree is required.
Conditions of use:
- disturbing frequency = 3,000 rpm;

- load applied to every levelling element = 4,000 N.
- Diagram shows that with a 3,000 rpm disturbing frequency and an isolation degree of 80%, the deflection obtained is 0.6 mm.
- Divide the load applied by the deflection obtained to define the rigidity required, which is 4,000/0.6= 6,666 N/mm.
- Compare the rigidity value obtained (6,666 N/mm) with the values reported in the table. This value is within the rigidity value reported in the table for LW.A-120 (4,000 N/mm) and LW.A-160 (9,000 N/mm). Choose the vibration-damping element with the lower value that is LW.A-120.

For a further check:
- graphic 2 shows that LW.A-120 (4,000 N/mm) deflection is 1mm.
- by intersecting the deflection value with the disturbing frequency of 3,000 rpm in the nomograph, the isolation degree obtained is 90%.

This value is even greater than the required one; your choice has proved correct.

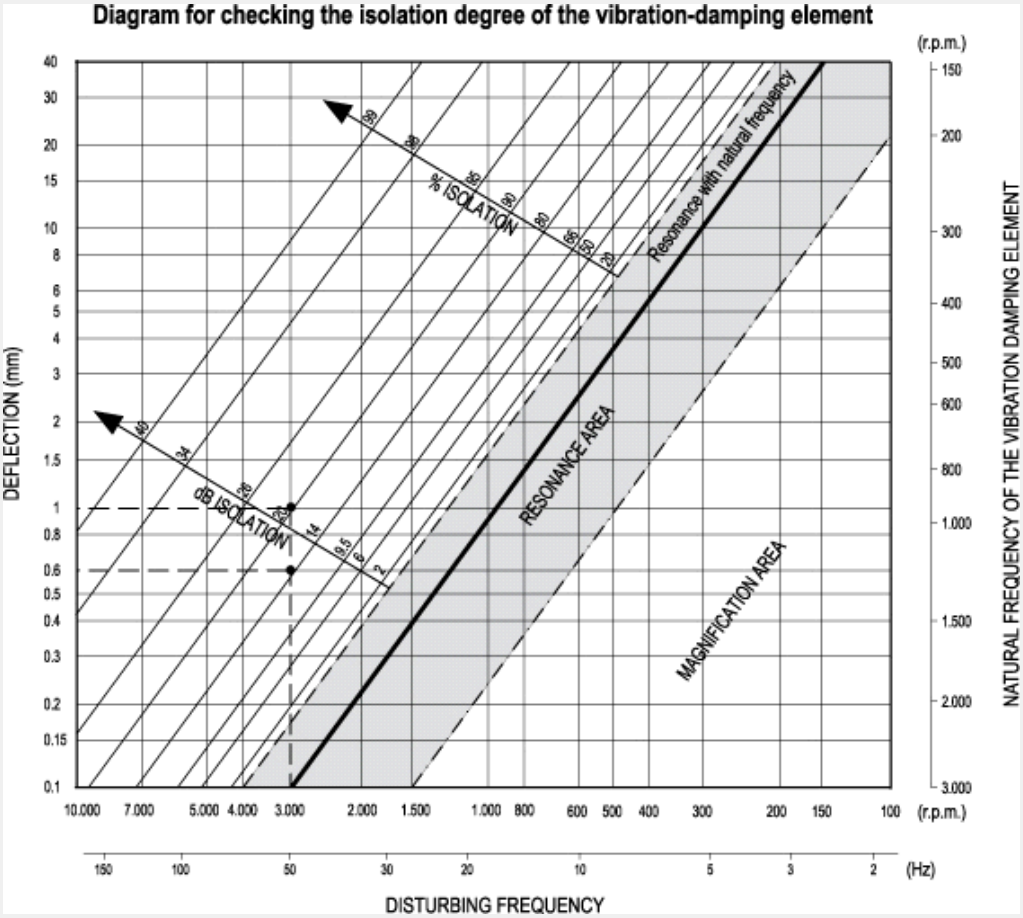

Graphic 2

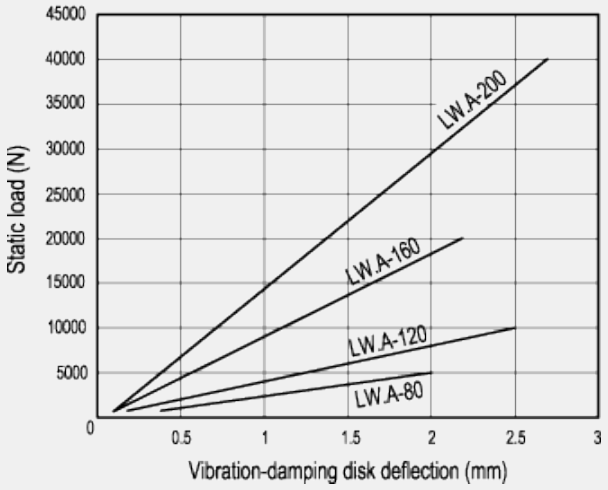

Standard Elements	Main dimensions	Threaded stem	Max load	Max deflection	Stiffness	Weig

Code	Description	D	D_1	L	$L_{1\ min}$	$L_{1\ max}$	l	l_1	d_2	d	s	[N]	[mm]	[N/mm]	g
415111	LW.A-80-M12x1.25x120	80	72	134	38	50	18.5	33	60	M12x1.25	7x7	5000	2	2500	530
415121	LW.A-120-M16x1.5x130	120	109	150	45	58	23	39	80	M16x1.5	9x9	10000	2.5	4000	120
415131	LW.A-160-M20x1.5x170	160	150	192	55	70	29	47	130	M20x1.5	12x12	20000	2.2	9000	265
415141	LW.A-200-M20x1.5x170	200	186	206	65	80	36	58	130	M20x1.5	12x12	40000	2.7	15000	450

C.2 Ball bearings

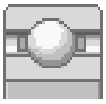

Deep groove ball bearings 61804-2Z (Series 618..-2Z)

main dimensions to DIN 625-1, gap seals on both sides

The datasheet is only an overview of dimensions and basic load ratings of the selected product. Please always observe all the guidelines in these overview pages. Further information is given on many products under the menu item "Description". You can also order comprehensive information via the Catalogue selection system (http://www.fag.de/content.fag.de/en/mediathek/library/library.jsp) or by telephone on +49 (91 32) 82 - 28 97.

d	20	mm	
D	32	mm	
B	7	mm	
d_1	24	mm	
D_2	29,2	mm	
$D_{a\ max}$	30	mm	
$d_{a\ min}$	22	mm	
$r_{a\ max}$	0,3	mm	
r_{min}	0,3	mm	
m	0,018	kg	Mass
C_r	3400	N	Basic dynamic load rating, radial
C_{0r}	2020	N	Basic static load rating, radial
n_G	28000	1/min	Limiting speed
n_B	16600	1/min	Reference speed
C_{ur}	102	N	Fatigue limit load, radial

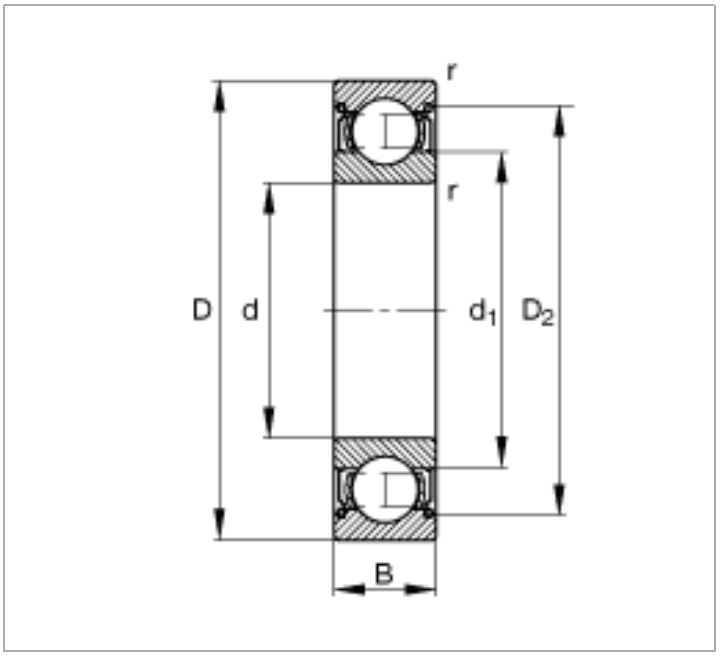
r
r
D
d
d_1
D_2
B

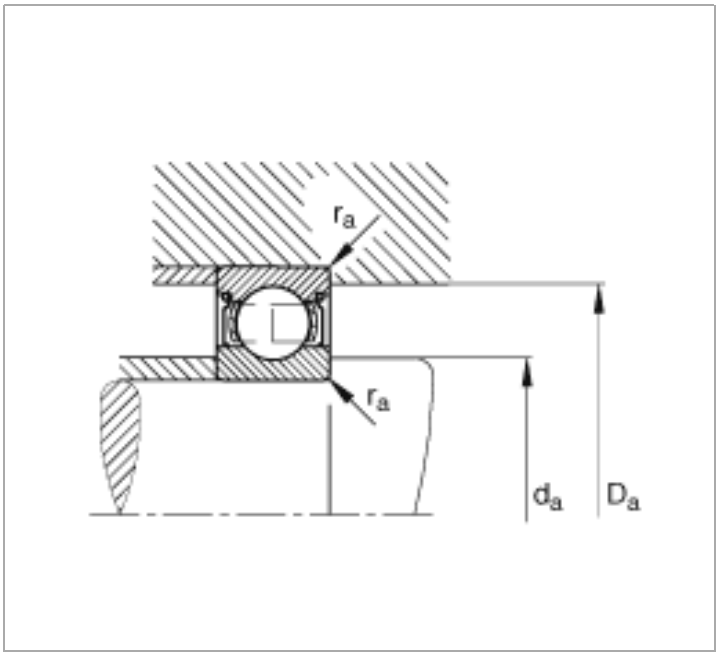
r_a
r_a
d_a
D_a

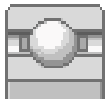

Deep groove ball bearings

61810-2Z-Y (Series 618..-2Z)

main dimensions to DIN 625-1, gap seals on both sides

The datasheet is only an overview of dimensions and basic load ratings of the selected product. Please always observe all the guidelines in these overview pages. Further information is given on many products under the menu item "Description". You can also order comprehensive information via the Catalogue selection system (http://www.fag.de/content.fag.de/en/mediathek/library/library.jsp) or by telephone on +49 (91 32) 82 - 28 97.

d	50	mm	
D	65	mm	
B	7	mm	
d_1	55,1	mm	
D_2	61,8	mm	
$D_{a\ max}$	63	mm	
$d_{a\ min}$	52	mm	
$r_{a\ max}$	0,3	mm	
r_{min}	0,3	mm	
m	0,052	kg	Mass
C_r	7200	N	Basic dynamic load rating, radial
C_{0r}	6300	N	Basic static load rating, radial
n_G	12900	1/min	Limiting speed
n_B	6400	1/min	Reference speed
C_{ur}	425	N	Fatigue limit load, radial

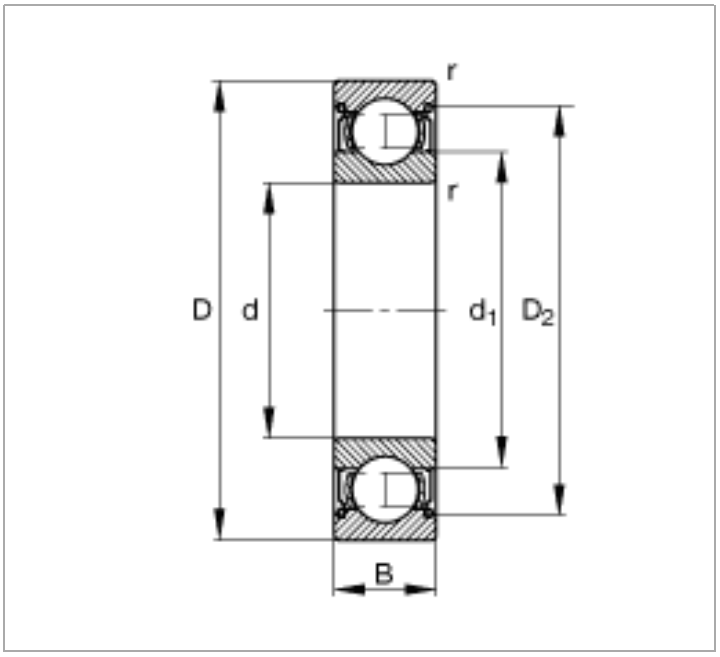
r
r
D
d
d_1
D_2
B

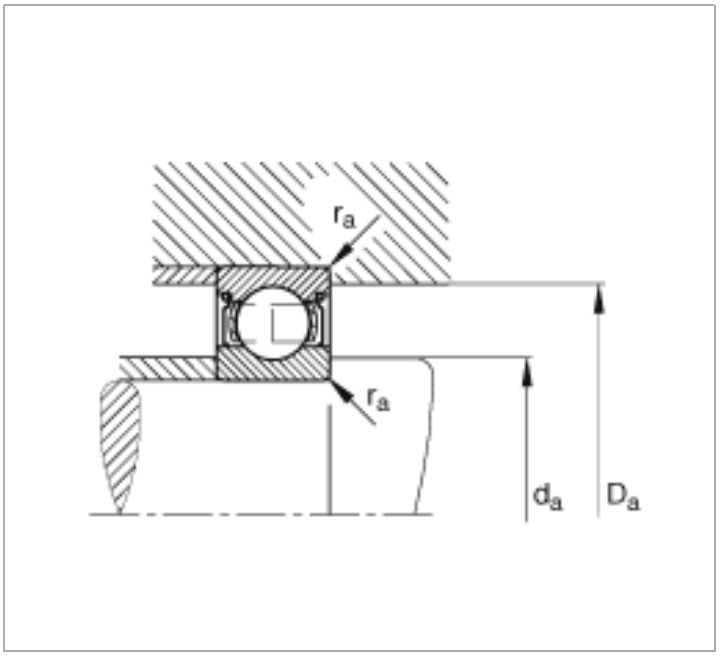
r_a
r_a
d_a
D_a

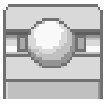

Deep groove ball bearings 61903-2Z (Series 619..-2Z)

main dimensions to DIN 625-1, gap seals on both sides

The datasheet is only an overview of dimensions and basic load ratings of the selected product. Please always observe all the guidelines in these overview pages. Further information is given on many products under the menu item "Description". You can also order comprehensive information via the Catalogue selection system (http://www.fag.de/content.fag.de/en/mediathek/library/library.jsp) or by telephone on +49 (91 32) 82 - 28 97.

d	17	mm	
D	30	mm	
B	7	mm	
d_1	20,8	mm	
D_2	27,5	mm	
$D_{a\ max}$	28	mm	
$d_{a\ min}$	19	mm	
$r_{a\ max}$	0,3	mm	
r_{min}	0,3	mm	
m	0,019	kg	Mass
C_r	4900	N	Basic dynamic load rating, radial
C_{0r}	2550	N	Basic static load rating, radial
n_G	29500	1/min	Limiting speed
n_B	18500	1/min	Reference speed
C_{ur}	129	N	Fatigue limit load, radial

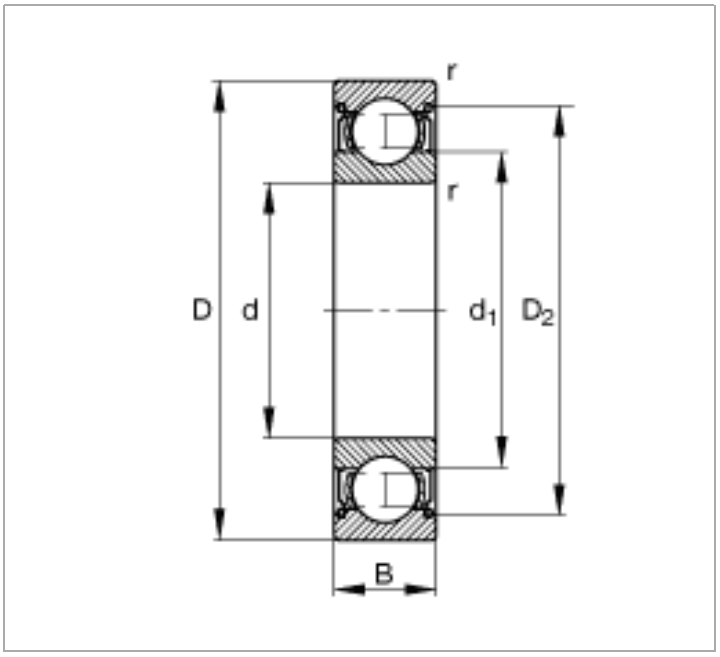
r
r
D
d
d_1
D_2
B

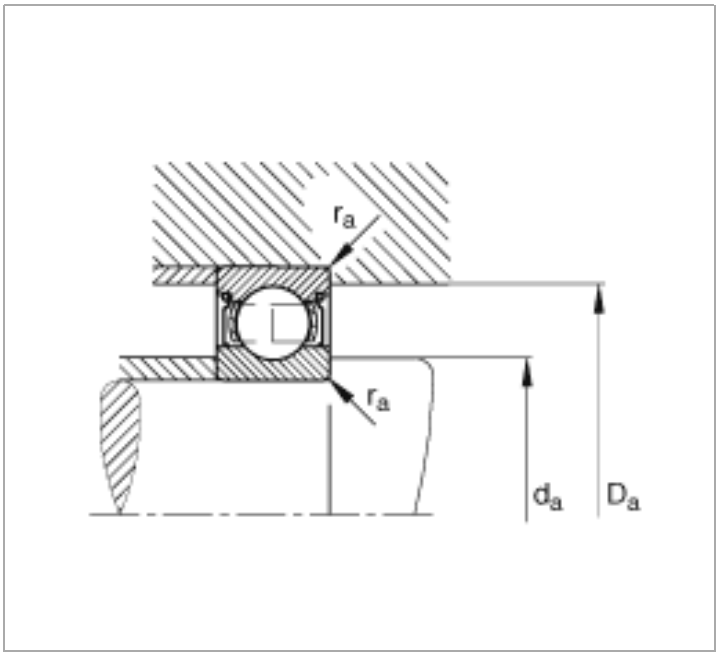
r_a
r_a
d_a
D_a

C.3 Linear ball bearings

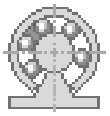

Linear ball bearings KBO25-PP

(Series KBO..-PP)

open design, sealed on all sides; corrosion-resistant design possible

The datasheet is only an overview of dimensions and basic load ratings of the selected product. Please always observe all the guidelines in these overview pages. Further information is given on many products under the menu item "Description". You can also order comprehensive information via the Catalogue ordering system (http://www.ina.de/content.ina.de/en/mediathek/library/library.jsp) or by telephone on +49 (91 32) 82 - 28 97.

F_w	25	mm	
D	40	mm	
L	58	mm	Tolerance: h12
	5		Number of rows of balls
1)			Main load direction
B_2	12,5	mm	Dimension B2 on diameter Fw
B_{L2}	1,85	mm	Slot dimensions suitable for retaining rings to DIN 471.
D_N	37,5	mm	Slot dimensions suitable for retaining rings to DIN 471.
L_2	43,7	mm	Tolerance: H13
N_4	3	mm	Hole position symmetrical to bearing width L
T_4	1,5	mm	
α	60	°	
			Supplied with initial greasing (sealed on both sides)
m	0,15	kg	Mass of bearing
C_{max}	2850	N	Basic load ratings in main load direction The basic load ratings are only valid for hardened (670+170 HV) and ground shaft raceways.
$C_{0\,max}$	2330	N	Basic load ratings in main load direction The basic load ratings are only valid for hardened (670+170 HV) and ground shaft raceways.

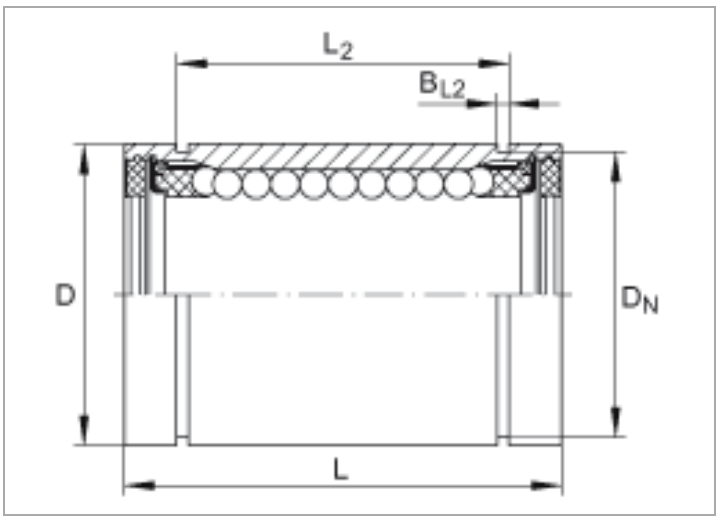
L2
BL2
D
DN
L

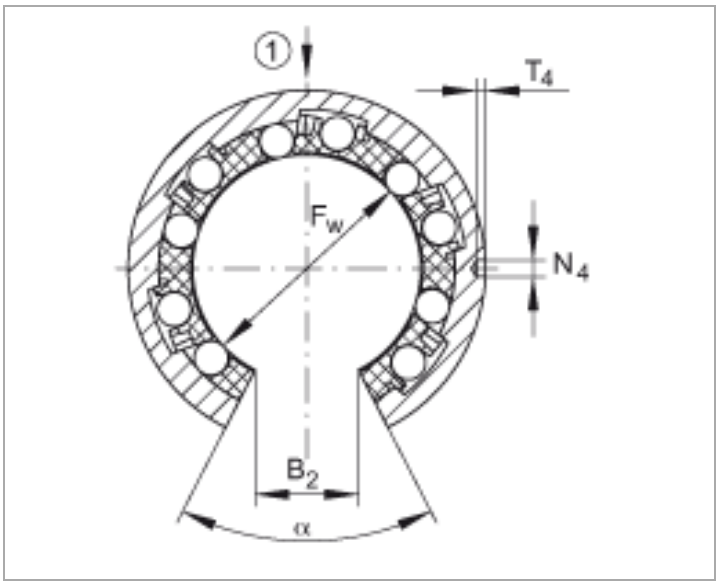
①
T4
Fw
N4
B2
α

C.4 Locknut

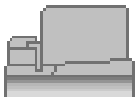

Locknuts KM12 (Series KM)

main dimensions to DIN 981

The datasheet is only an overview of dimensions and basic load ratings of the selected product. Please always observe all the guidelines in these overview pages. Further information is given on many products under the menu item "Description". You can also order comprehensive information via the Catalogue selection system (http://www.fag.de/content.fag.de/en/mediathek/library/library.jsp) or by telephone on +49 (91 32) 82 - 28 97.

d_{2G}	M60X2		Thread
D_m	80	mm	
b_1	11	mm	
	30	°	Chamfer angle
D_a	73	mm	
m	7	mm	
n	3	mm	
m_1	0,18	kg	Mass, nut
	MB12		Designation, retainer

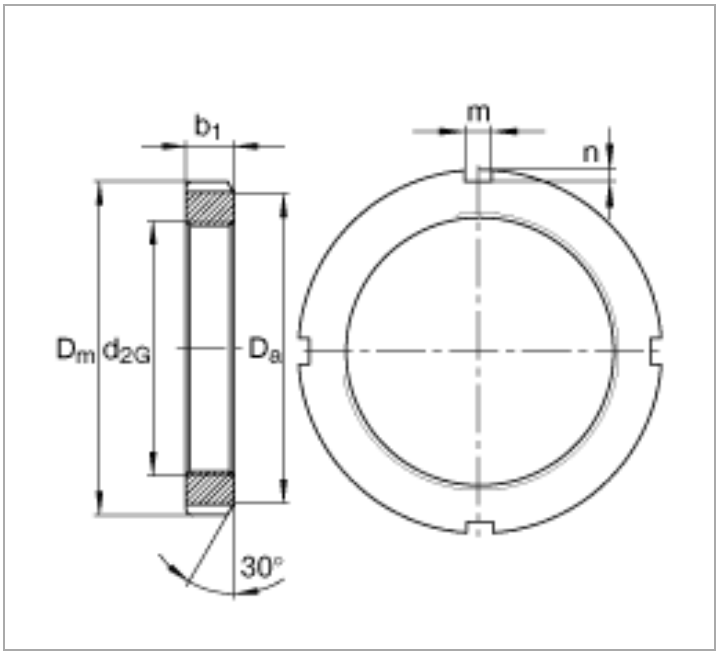

C.5 T-bolt

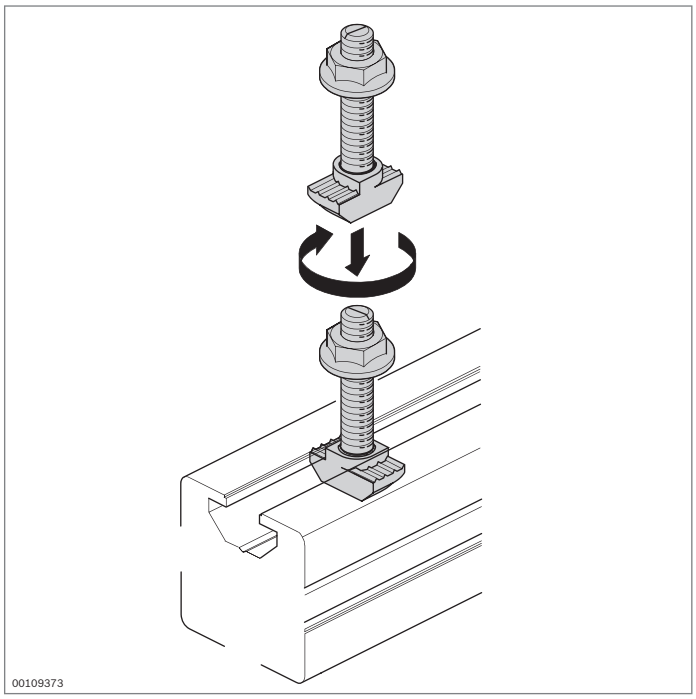

T-bolt
Flange nut

- Secure, conductive connection
- Notch at bolt end as marker for correct position identification
- Profile finishing: not required

Technical data (p. 19-5)

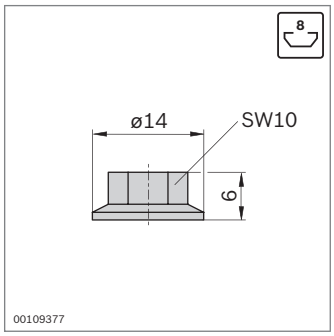

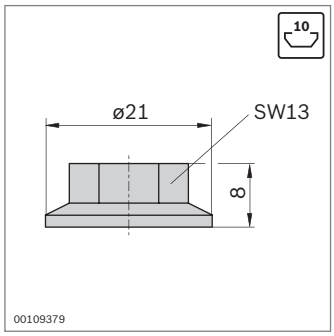

Flange nut	Slot	M	ESD		No.
	8	M6		100	**3 842 523 925**
	10	M8		100	**3 842 345 081**

Material: Steel, galvanized

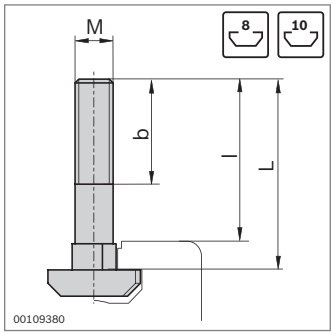

Slot	F_{max}
8	4000 N
10	6000 ... 18,000 N[1)]

1) Depending on profile (p. 19-5)

T-bolt	Slot	MxL	**b** (mm)	**l** (mm)	ESD		No.
	8	M6x16	10	14		100	**3 842 523 920**
		M6x20	14	18		100	**3 842 523 921**
		M6x25	18	23		100	**3 842 523 922**
	10	M8x20	14	14		100	**3 842 528 715**
		M8x25	19	19		100	**3 842 528 718**
		M8x30	24	24		100	**3 842 528 721**
		M8x40	22	34		100	**3 842 528 724**
		M8x50	22	44		100	**3 842 528 727**

Material: Steel, galvanized

C.6 Gears

Spur Gears 2.0MOD - 20° p.a.

Steel EN8, 080M40/080M46 or equivalent

All dimensions in mm

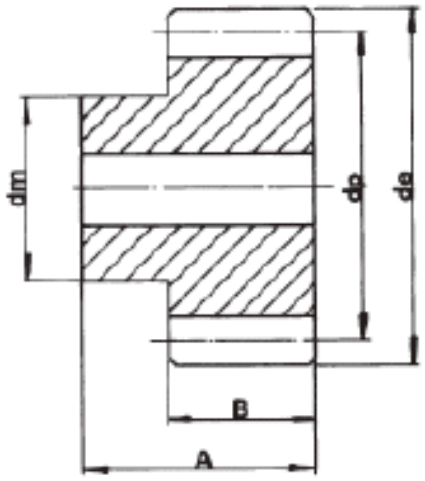

Intermediate sizes &
Special gears to drawing up to 1000mm diameter

Standard : DIN 3962 Grade 8/9

Standard tolerances, unless otherwise stated ±0.25mm.

Code	No. of Teeth	Pitch Ø dp	Bore Ø H7	Hub/Boss Ø dm	Outside Ø da	O/A Width A	Face Width B
SS20/12B	12	24	10	18	28	30	20
SS20/15B	15	30	12	24	34	30	20
SS20/16B	16	32	12	26	36	30	20
SS20/18B	18	36	12	30	40	30	20
SS20/20B	20	40	12	32	44	30	20
SS20/24B	24	48	12	38	52	30	20
SS20/30B	30	60	12	50	64	30	20
SS20/32B	32	64	12	50	68	30	20
SS20/36B	36	72	12	55	76	30	20
SS20/40B	40	80	15	55	84	30	20
SS20/44B	44	88	15	55	92	30	20
SS20/50B	50	100	15	55	104	30	20
SS20/60B	60	120	15	60	124	30	20
SS20/80B	80	160	20	60	164	30	20

SS Gears have a black oxide finish

C.7 Rotex coupling

Properties of standard spiders

Spider type (Shore hardness)	92 Shore-A (T-PUR®)	DZ 92 Shore-A (T-PUR®)	92 Shore-A
	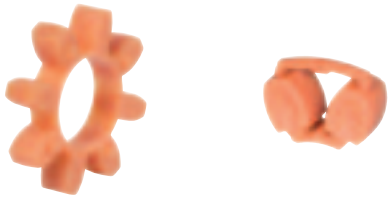 T-PU R®		
Size	14 to 180	100 to 180	14 to 90
Material	T-PUR®		Polyurethane (PUR)
Permissible temperature range Permanent temperature Short-term temperature	 -50 °C to +120 °C -50 °C to +150 °C		 -40 °C to +90 °C -50 °C to +120 °C
Properties	– significantly higher service life expectancy – very good temperature resistance – improved damping of vibrations – good damping, average elasticity – suitable for all hub materials		– good damping, average elasticity – suitable for all hub materials

Spider type (Shore hardness)	98 Shore-A (T-PUR®) 1)	DZ 98 Shore-A (T-PUR®)	98 Shore-A 1)
	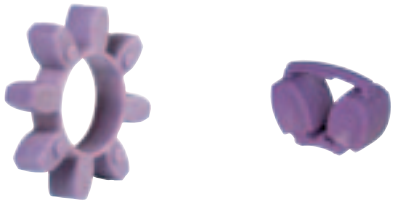 T-PUR®		
Size	14 to 180	100 to 180	14 to 90
Material	T-PUR®		Polyurethane (PUR)
Permissible temperature range Permanent temperature Short-term temperature	 -50 °C to +120 °C -50 °C to +150 °C		 -30 °C to +90 °C -40 °C to +120 °C
Properties	– significantly higher service life expectancy – very good temperature resistance – improved damping of vibrations – transmission of high torques with average damping – recommended hub material: steel, GJL and GJS		– transmission of high torques with average damping – recommended hub material: steel, GJL and GJS

Spider type (Shore hardness)	64 Shore-D (T-PUR®)	DZ 64 Shore-D (T-PUR®)	64 Shore-D
	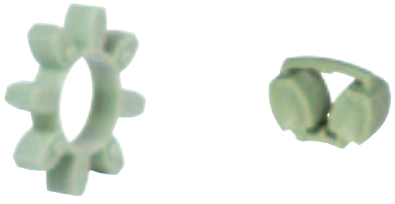 T-PUR®		
Size	14 to 180	100 to 180	14 to 90
Material	T-PUR®		Polyurethane (PUR)
Permissible temperature range Permanent temperature Short-term temperature	 -50 °C to +120 °C -50 °C to +150 °C		 -30 °C to +110 °C -30 °C to +130 °C
Properties	– significantly higher service life expectancy – very good temperature resistance – improved damping of vibrations – transmission of very high torques with low damping – recommended hub material: steel and GJS		– transmission of very high torques with low damping – suitable to shift critical speeds – resistant to hydrolysis – recommended hub material: steel and GJS

ROTEX® 14 ROTEX® 19 ROTEX® 24 - 65 ROTEX® 75 - 160 ROTEX® 180 ROTEX® DZ 100 - 160 ROTEX® DZ 180

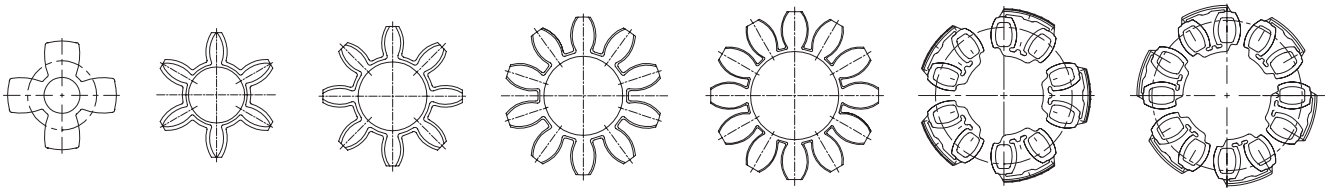

Material steel / UL / marine

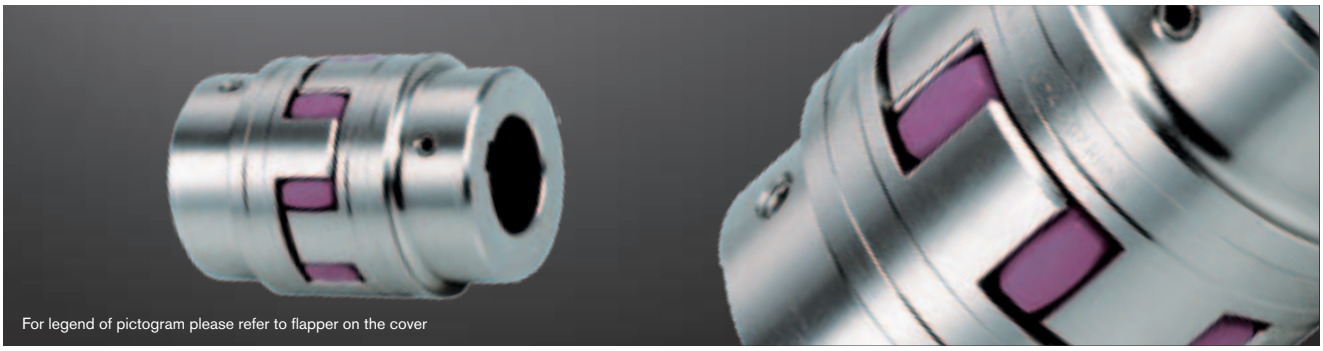

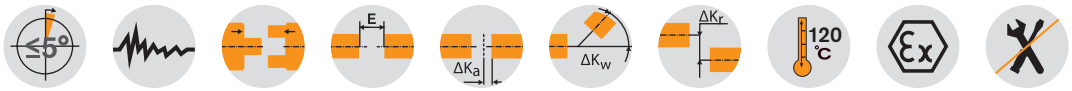

ROTEX® Steel (St)

Size	Compo-nent	Spider (part 2) rated torque [Nm]			Dimensions [mm]												
					Finish bore	General									Thread for setscrew		
		92 Sh-A	98 Sh-A	64 Sh-D	d (min-max)	L	l_1; l_2	E	b	s	D_H	d_H	D	N	G	t	T_A [Nm]
14	1a	7,5	12,5	16	0-16	35	11	13	10	1,5	30	10	30	—	M4	5	1,5
	1b					50	18,5										
19	1a	10	17	21	0-25	66	25	16	12	2	40	18	40	—	M5	10	2
	1b					90	37										
24	1a	35	60	75	0-35	78	30	18	14	2	55	27	55	—	M5	10	2
	1b					118	50										
28	1a	95	160	200	0-40	90	35	20	15	2,5	65	30	65	—	M8	15	10
	1b					140	60										
38	1	190	325	405	0-48	114	45	24	18	3	80	38	70	27	M8	15	10
	1b					164	70						80	—			
42	1	265	450	560	0-55	126	50	26	20	3	95	46	85	28	M8	20	10
	1b					176	75						95	—			
48	1	310	525	655	0-62	140	56	28	21	3,5	105	51	95	32	M8	20	10
	1b					188	80						105	—			
55	1	410	685	825	0-74	160	65	30	22	4	120	60	110	37	M10	20	17
	1b					210	90						120	—			
65	1	625	940	1175	0-80	185	75	35	26	4,5	135	68	115	47	M10	20	17
	1b					235	100						135	—			
75	1	1280	1920	2400	0-95	210	85	40	30	5	160	80	135	53	M10	25	17
	1b					260	110						160	—			
90	1	2400	3600	4500	0-110	245	100	45	34	5,5	200	100	160	62	M12	30	40
	1b					295	125						200	—			
100	1	3300	4950	6185	0-115	270	110	50	38	6	225	113	150	89	M12	30	40
110	1	4800	7200	9000	0-125	295	120	55	42	6,5	255	127	200	96	M16	35	80
125	1	6650	10000	12500	60-145	340	140	60	46	7	290	147	230	112	M16	40	80
140	1	8550	12800	16000	60-160	375	155	65	50	7,5	320	165	255	124	M20	45	140
160	1	12800	19200	24000	80-185	425	175	75	57	9	370	190	290	140	M20	50	140
180	1	18650	28000	35000	85-200	475	195	85	64	10,5	420	220	325	156	M20	50	140

■ = If no material is specified in the order, it is stipulated in the calculation/order.
[1] Maximum torque of coupling $T_{Kmax.}$ = rated torque of coupling $T_{K\ rated}$ x 2. For selection see page 10 et seqq.

Ordering example:

ROTEX® 38	St	92 Sh-A	1 – Ø 45		1 – Ø 25	
Coupling size	Material	Spider hardness	Component	Finish bore	Component	Finish bore

Components

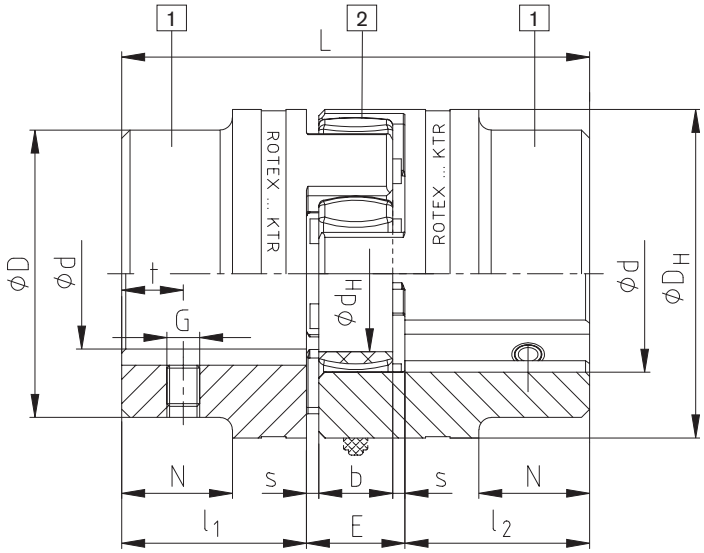

Steel (thread on the keyway)

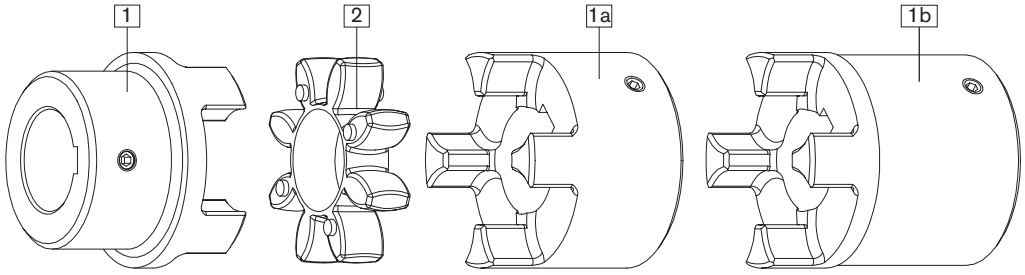

Standard hub | Spider | Large hub | Large hub lengthened

Marine programme:
Hub materials S355J2+N and 42CrMo4+QT acc. to DIN EN10204-3.1+3.2 size 75-180 available from stock.

DNV·GL ABS Lloyd's Register

UL LISTED

Use in fire extinguisher pumps

ROTEX® couplings comply with the specifications of NFPA 20 standard for the installation of stationary pumps for fire protection and on completion of the necessary permanent tests they also comply with the specifications of UL 448A, flexible couplings and connection shafts for stationary fire extinguisher pumps.

Sizes available:

ROTEX® UL-Listed								
Size	Component	Material	Spider (part 2) Rated torque [Nm] 92 Sh-A	Dimensions [mm] Finish bore d (min-max)	L	l_1; l_2	E	D_H
42	1	St	265	18-55	126	50	26	95
55	1	St	410	24-74	160	65	30	120
65	1	St	625	24-80	185	75	35	135
75	1	St	1280	24-95	210	85	40	160
90	1	St	2400	30-110	245	100	45	200

* For complete dimensions see table on page 36

C.8 Aluminum 7075 T651 properties

LIGA 2017 T451 (AL CU MG)

Espessuras em stock permanente de: 5 a 100 mm

PRINCIPAIS CARACTERÍSTICAS

Alta resistência mecânica
Moderada resistência à corrosão

CARACTERÍSTICAS FÍSICAS

Peso específico (g/cm3): 2,80
Módulo de elasticidade (MPa): 72000
Coef. de dilatação térmica linear (20-100 °C): 23,6 .
Condutibilidade térmica (W/mK): 125-140
Condutibilidade eléctrica específica (20 °C) (m/ . mm2): 20
Intervalo de fusão (°C): 585-650

APLICAÇÕES TÍPICAS

Peso específico (g/cm3): 2,80
Módulo de elasticidade (MPa): 72000
Coef. de dilatação térmica linear (20-100 °C): 23,6 .
Condutibilidade térmica (W/mK): 125-140
Condutibilidade eléctrica específica (20 °C) (m/ . mm2): 20
Intervalo de fusão (°C): 585-650

CARACTERÍSTICAS MECÂNICAS

Carga de ruptura Rm (MPa): 430
Limite elástico Rp 0,2 (MPa): 285
Alongamento A 5 (%): 16
Dureza Brinell HB: 105-110

LIGA 7075 T651 (AL MG CU 1,5)

Espessuras em stock permanente de: 15 a 110mm

Espessuras disponíveis sob encomenda de: 3 a 12mm e de 120 a 330mm

PRINCIPAIS CARACTERÍSTICAS

Excelente resistência mecânica
Resistência média à corrosão
Boa apetência para o forjado

CARACTERÍSTICAS FÍSICAS

Peso específico (g/cm3): 2,83
Módulo de elasticidade (MPa): 72000
Coef. de dilatação térmica linear (20-100 °C): 23,4 .
Condutibilidade térmica (W/mK): 130
Condutibilidade eléctrica específica (20 °C) (m/ f . mm2):20
Intervalo de fusão (°C): 480-640

APLICAÇÕES TÍPICAS

Peças de avião e de máquinas submetidas a altas tensões mecânicas; matrizes, suportes; componentes eléctricos e electrónicos; moldes de sopro, termoconformação, vácuo, para todo o tipo de plásticos, borracha e matérias esponjosas

CARACTERÍSTICAS MECÂNICAS

Carga de ruptura Rm (MPa): 525
Limite elástico Rp 0,2 (MPa): 455
Alongamento A 5 (%): 7
Dureza Brinell HB: 130-150

C.9 Kistler K-Shear accelerometer

Outline dimensions used in mounting that vary by series designation are shown in Figure 3. Type designations that include the letter E are sized in metric units.

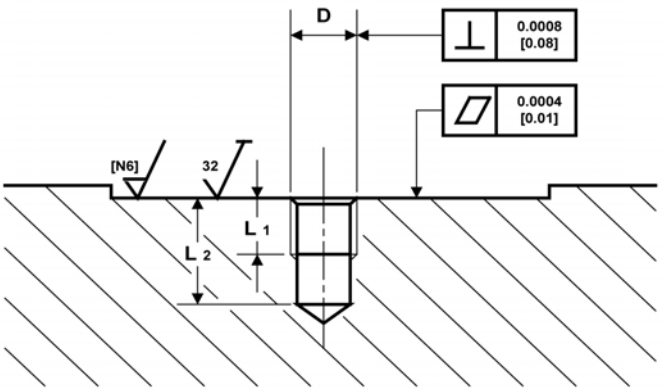

Surface Dia.	D	L1 inch [mm]	L2 inch [mm}
3/8" minimum	10-32 UNF	0.156 [4.0]	0.315 [8.0]
1/2" minimum	¼-28 UNF	0.22 [5.6]	0.42 [10.7]

Table 3: Mounting Surface Preparation

5.4 Securing Cables

Figures 4 and 5 show the correct and incorrect ways for installing cables. Allow a sufficient radius to ensure a proper strain relief. The actual radius will depend on the cables being used. It is recommended that cables be secured to the accelerometer mounting surface to minimize cable and connector fatigue failures. Secure cables with a cable clamp.

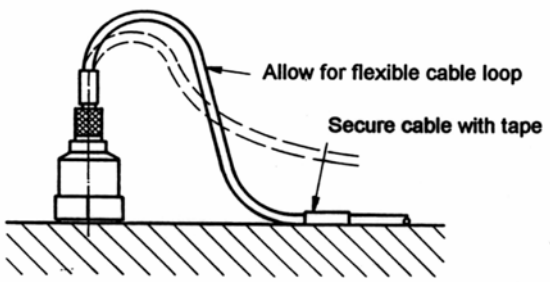

Figure 4: Correct Cable Strain Relief

C.10 Ruland coupling

ONE- AND TWO-PIECE RIGID COUPLINGS

WITHOUT OR WITH KEYWAY • METRIC DIMENSION SERIES

MCLX/MSPX
MCLC/MSPC

MCLX

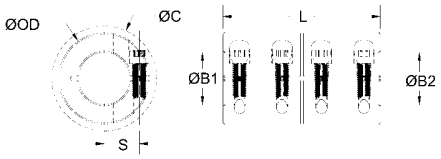

MCLC

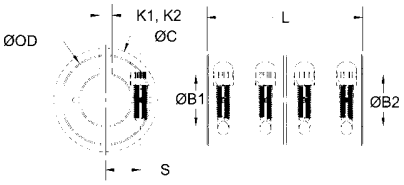

MSPX

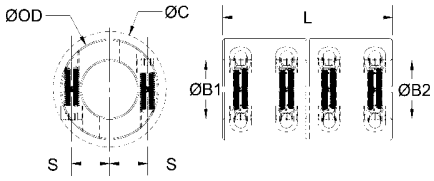

MSPC

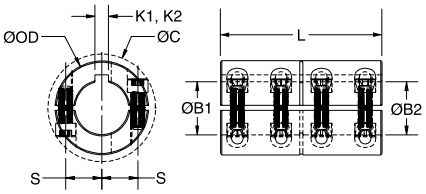

- Does not mar the shaft.
- Precision honed bore on straight bore couplings.
- 3-piece styles available.
- Nypatch® Anti-vibration hardware.
- Opposing hardware on 2-piece styles.
- Additional sizes available.
- Bore tolerance: +.050 mm +.012 mm
- Maximum speed: 4,000 rpm

PART NUMBER | **SPECIFICATIONS**

ONE-PIECE BLACK OXIDE STEEL	ALUMINUM	STAINLESS STEEL	TWO-PIECE BLACK OXIDE STEEL	STAINLESS STEEL	BORES B1, B2 (mm)	OD (mm)	LENGTH L (mm)	SCREW LOC. S (mm)	CLEARANCE DIAM. C (mm) MAX	KEYWAY K1, K2 (mm)	FORGED CLAMP SCREW
MCLX-3-3-F	MCLX-3-3-A	MCLX-3-3-SS	MSPX-3-3-F	MSPX-3-3-SS	3	15	22	4.6	15.0		M2
MCLX-4-4-F	MCLX-4-4-A	MCLX-4-4-SS	MSPX-4-4-F	MSPX-4-4-SS	4	15	22	4.6	15.0		M2
MCLX-5-5-F	MCLX-5-5-A	MCLX-5-5-SS	MSPX-5-5-F	MSPX-5-5-SS	5	15	22	4.6	15.0		M2
MCLX-6-6-F	MCLX-6-6-A	MCLX-6-6-SS	MSPX-6-6-F	MSPX-6-6-SS	6	18	30	5.9	21.5		M3
MCLX-8-8-F	MCLX-8-8-A	MCLX-8-8-SS	MSPX-8-8-F	MSPX-8-8-SS	8	24	35	9.0	27.1		M3
MCLX-10-10-F	MCLX-10-10-A	MCLX-10-10-SS	MSPX-10-10-F	MSPX-10-10-SS	10	29	45	10.6	33.0		M4
MCLX-12-12-F	MCLX-12-12-A	MCLX-12-12-SS	MSPX-12-12-F	MSPX-12-12-SS	12	29	45	10.6	33.0		M4
MCLX-14-14-F		MCLX-14-14-SS	MSPX-14-14-F	MSPX-14-14-SS	14	34	50	12.0	39.4		M5
MCLX-15-15-F		MCLX-15-15-SS	MSPX-15-15-F	MSPX-15-15-SS	15	34	50	12.0	39.4		M5
MCLX-16-16-F		MCLX-16-16-SS	MSPX-16-16-F	MSPX-16-16-SS	16	34	50	12.0	39.4		M5
MCLX-20-20-F		MCLX-20-20-SS	MSPX-20-20-F	MSPX-20-20-SS	20	42	65	15.4	48.9		M6
MCLX-25-25-F		MCLX-25-25-SS	MSPX-25-25-F	MSPX-25-25-SS	25	45	75	16.9	51.5		M6
MCLX-30-30-F		MCLX-30-30-SS	MSPX-30-30-F	MSPX-30-30-SS	30	53	83	20.9	58.7		M6
MCLX-35-35-F		MCLX-35-35-SS	MSPX-35-35-F	MSPX-35-35-SS	35	67	95	26.7	74.7		M8
MCLX-40-40-F		MCLX-40-40-SS	MSPX-40-40-F	MSPX-40-40-SS	40	77	108	31.8	84.0		M8
MCLX-50-50-F		MCLX-50-50-SS	MSPX-50-50-F	MSPX-50-50-SS	50	85	124	34.1	94.2		M10
MCLC-6-6-F		MCLC-6-6-SS	MSPC-6-6-F	MSPC-6-6-SS	6	18	30	5.9	21.5	2	M3
MCLC-8-8-F		MCLC-8-8-SS	MSPC-8-8-F	MSPC-8-8-SS	8	24	35	9.0	27.1	2	M3
MCLC-10-10-F		MCLC-10-10-SS	MSPC-10-10-F	MSPC-10-10-SS	10	29	45	10.6	33.0	3	M4
MCLC-12-12-F		MCLC-12-12-SS	MSPC-12-12-F	MSPC-12-12-SS	12	29	45	10.6	33.0	4	M4
MCLC-14-14-F		MCLC-14-14-SS	MSPC-14-14-F	MSPC-14-14-SS	14	34	50	12.0	39.4	5	M5
MCLC-15-15-F		MCLC-15-15-SS	MSPC-15-15-F	MSPC-15-15-SS	15	34	50	12.0	39.4	5	M5
MCLC-16-16-F		MCLC-16-16-SS	MSPC-16-16-F	MSPC-16-16-SS	16	34	50	12.0	39.4	5	M5
MCLC-20-20-F		MCLC-20-20-SS	MSPC-20-20-F	MSPC-20-20-SS	20	42	65	15.4	48.9	6	M6
MCLC-25-25-F		MCLC-25-25-SS	MSPC-25-25-F	MSPC-25-25-SS	25	45	75	16.9	51.5	8	M6
MCLC-30-30-F		MCLC-30-30-SS	MSPC-30-30-F	MSPC-30-30-SS	30	53	83	20.9	58.7	8	M6
MCLC-35-35-F		MCLC-35-35-SS	MSPC-35-35-F	MSPC-35-35-SS	35	67	95	26.7	74.7	10	M8
MCLC-40-40-F		MCLC-40-40-SS	MSPC-40-40-F	MSPC-40-40-SS	40	77	108	31.8	84.0	12	M8
MCLC-50-50-F		MCLC-50-50-SS	MSPC-50-50-F	MSPC-50-50-SS	50	85	124	34.1	94.2	14	M10

FOR ENGINEERING AND WARRANTY INFORMATION SEE WWW.RULAND.COM

C.11 Transtecno Gearmotor ECM-100/040

EC100.120 - EC100.240 - EC100.24E

Caratteristiche / *Features*

Costruzione	Tubolare, senza ventilazione
Grandezza	Ø 80 mm
Potenza	140 W S2 (100 W S1)
Magneti	2
Supporti	Cuscinetti a sfera
Fori di montaggio	4
Alimentazione	Bassa tensione, 12 o 24 Vcc
Spazzole	N° 2 di composto grafite-rame
Dimensione spazzole	LxPxH = 17.1 x 6.5 x 16.7 mm
Cavo di alimentazione	Lunghezza: 1000 mm
Bisporgenza	Standard solo EC100.24E

Construction	*Tubular, without fan*
Size	*Ø 80 mm*
Power	*140 W S2 (100 W S1)*
Magnets	*2*
Bearings	*Ball bearings*
Mounting holes	*4*
Power supply	*Low voltage, 12 or 24 Vdc*
Brushes	*2 inside brushes made of graphite/copper composite*
Brushes size	*LxWxH = 17.1 x 6.5 x 16.7 mm*
Electric cable	*Length: 1000 mm*
Rear shaft	*Standard only EC100.24E*

Tipo *Type*	S	Pn [W]	V [V]	I [A]	IC	FF	Mn [Nm]	n_1 [min^{-1}]	IP	Kg
EC100.120	**S1**	100	12	12	F	1	0.31	3000	40	2.7
	S2 25'	140		16.8			0.43			
EC100.240	**S1**	100	24	6			0.31			
	S2 25'	140		8.4			0.43			
EC100.24E	**S1**	100		6			0.31		20	
	S2 25'	140		8.4			0.43			

Dimensioni / *Dimensions*

EC100.120
EC100.240

56 B14	
L	153
D	80
S	65
C (-0.03 / -0.01)	50
63B14*	
L	155
D	90
S	75
C (-0.03 / -0.01)	60

* Usare boccola 9/11
** Use sleeve 9/11*

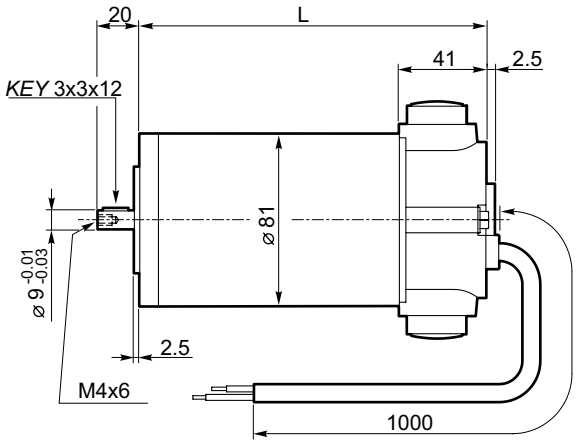

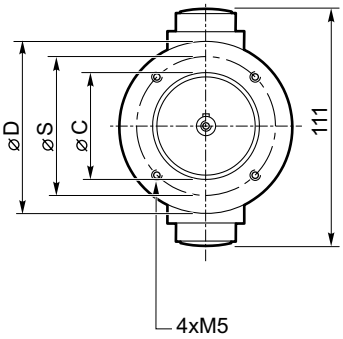

Freno / *Brake* → H23

Encoder → H24

EC100.24E

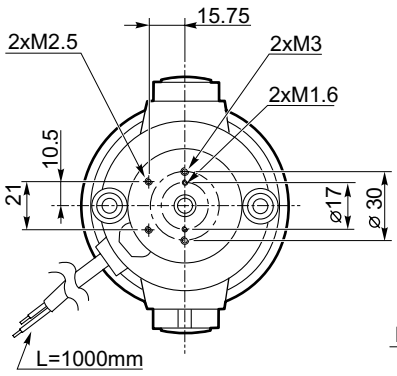

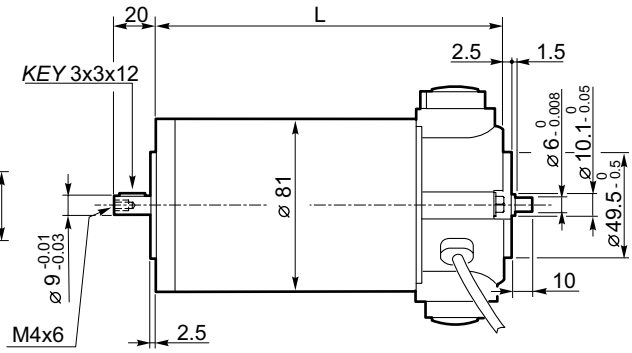

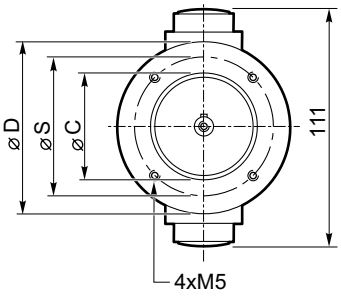

EC100.120 - EC100.240 - EC100.24E

Prestazioni ***Performances***

EC100.120

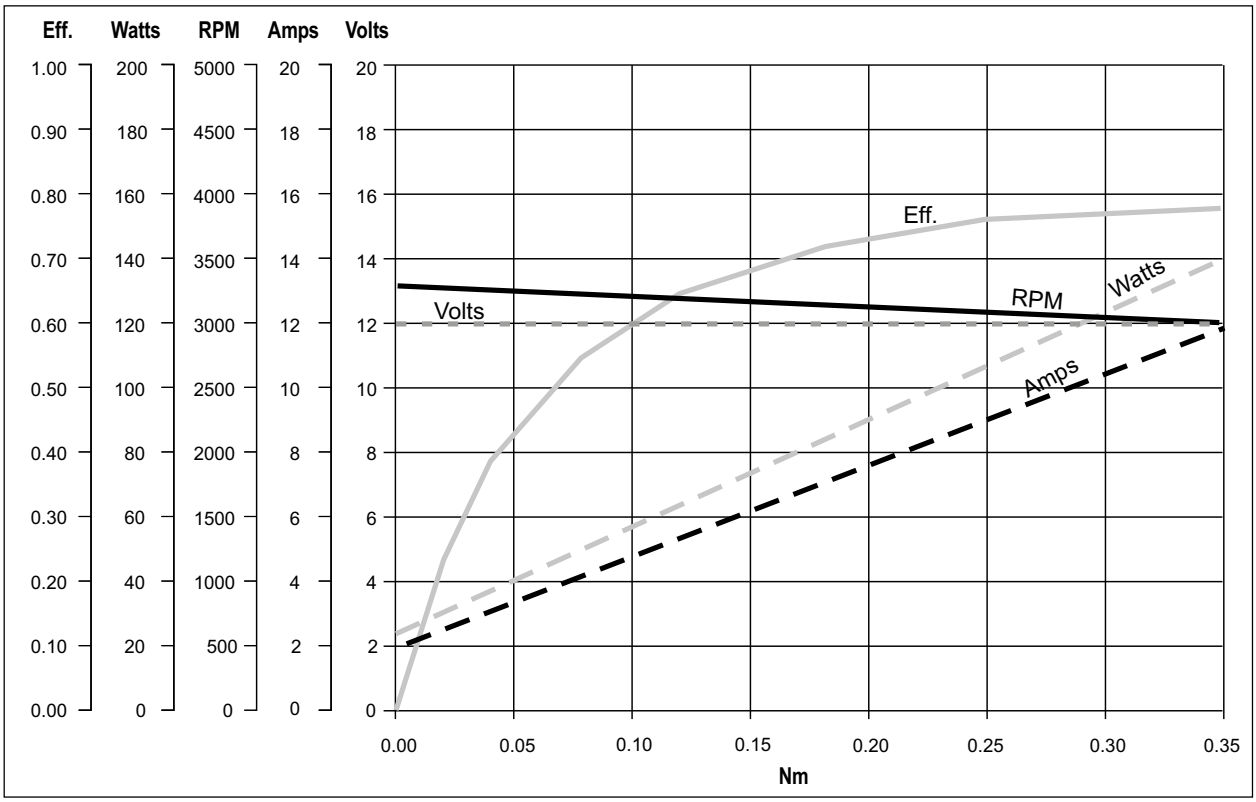

EC100.240 - EC100.24E

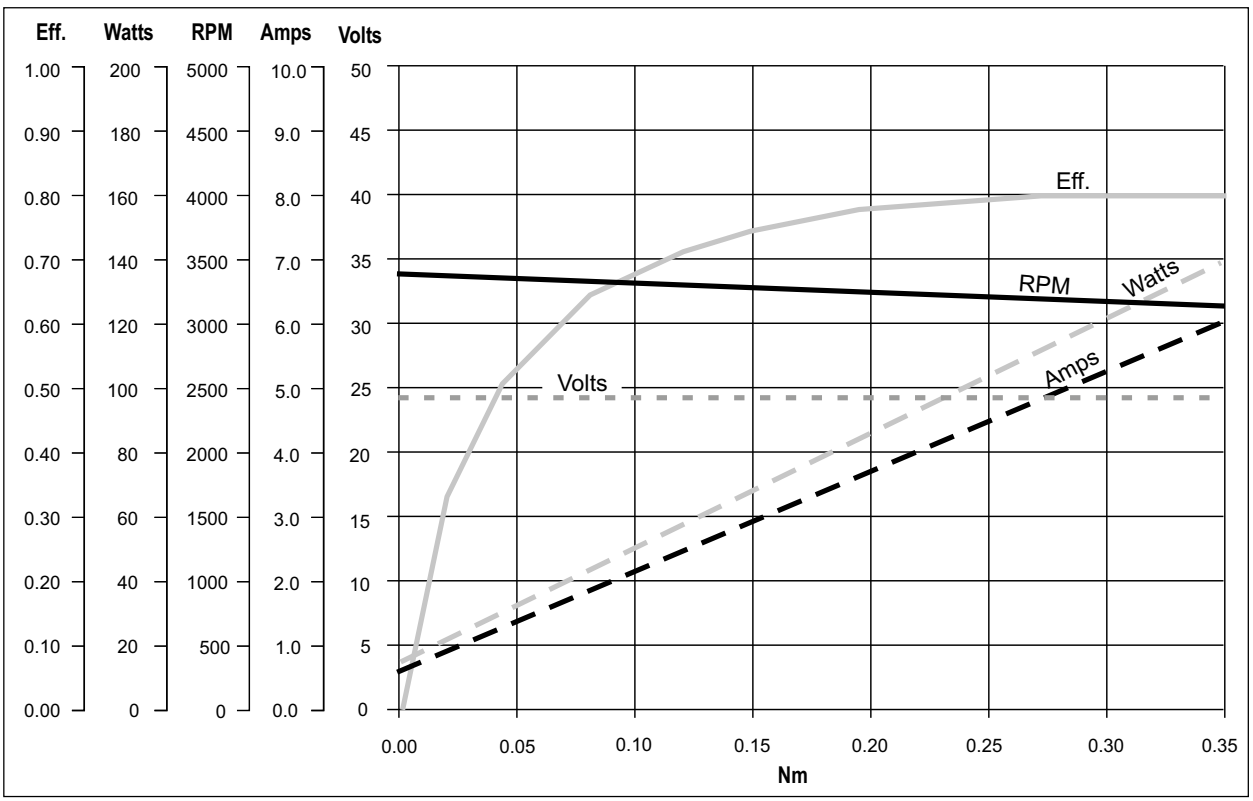

Encoder ***Encoder***

EC020.24E ME22

EC050.12E ME22
EC050.24E ME22

EC070.12E ME22
EC070.24E ME22

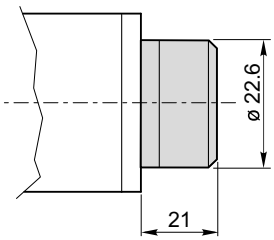

EC100.24E ME22
EC180.24E ME22

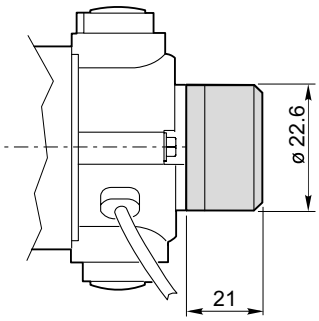

Risoluzione Encoder (CPR) / *Encoder Resolution (CPR)*	Numero di canali / *Number of channels*	Tensione d'alimentazione / *Power supply*
001	2	5 VdC - TTL
100		
300		

Per risoluzioni encoder non standard, si prega di contattare il nostro Servizio Tecnico.

For non-standard encoder resolution, please contact our Technical Department.

Caratteristiche tecniche — *Technical features*

Le caratteristiche principali dei motoriduttori CC a vite senza fine a magneti permanenti in ferrite serie ECM sono:

- Alimentazione in bassa tensione 12/24 Vcc
- Possibilità di montaggio encoder
- Potenze motore disponibili da 100 a 800W S2
- Magneti in ferrite
- Carcasse dei riduttori in pressofusione di alluminio
- Lubrificazione permanente con olio sintetico.

The main features of ECM ferrite permanent magnets DC wormgearmotors range are:

- *Low voltage power supply 12/24 Vdc*
- *Suitable for encoder assembly*
- *Motor power ratings available from 100 to 800W S2*
- *Ferrite magnets*
- *Die-cast aluminum housing*
- *Permanent synthetic oil long-life lubrication.*

Designazione — *Classification*

MOTORIDUTTORE / *GEARMOTOR*

ECM	070/026	U	10	SZDX	BRSX	90	240	VS
Tipo *Type*	Grandezza *Size*	Versione Riduttore *Gearbox Version*	Rapporto *Ratio*	Albero di uscita *Output shaft*	Braccio di reazione *Torque arm*	Angolo *Angle*	Versione Motore *Motor Version*	Opzioni *Options*
ECM 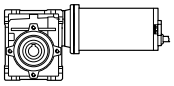	**070/026** **070/030** **100/026** **100/030** **100/040** **180/026** **180/030** **180/040** **180/050** **250/030** **250/040** **250/050** **250/063** **350/030** **350/040** **350/050** **350/063** **350/070** **600/040** **600/050** **600/063** **600/070**	**U** **FD** **FS** **FLD** **FLS** **FBD** **FBS**	Vedere tabella *See tables*	**SZDX** **SZSX** **DZ**	**BRDX** **BRSX**	**0°** **90°** **180°** **270°**	**120** **240** **24E**	**VS**

Versione Riduttore *Gearbox Version*

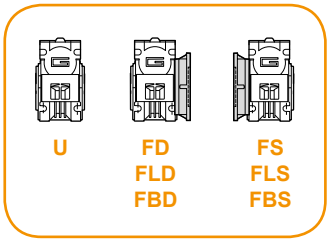

Albero di uscita *Output shaft*

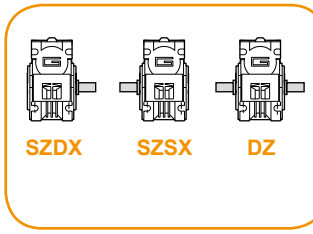

Braccio di reazione *Torque arm*

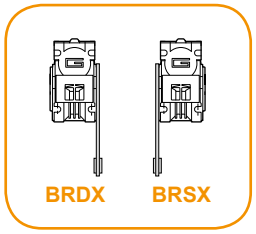

Angolo *Angle*

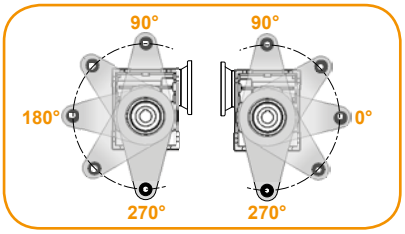

Simbologia — *Symbols*

n_1	[min^{-1}]	Velocità in ingresso / *Input speed*	Rd	%	Rendimento dinamico / *Dynamic efficiency*
n_2	[min^{-1}]	Velocità in uscita / *Output speed*	A_2	N]	Carico assiale ammissibile in uscita / *Permitted output axial load*
i		Rapporto di riduzione / *Ratio*	Rs	%	Rendimento statico / *Static efficiency*
P_1	[kW]	Potenza in entrata / *Input power*	R_2	[N]	Carico radiale ammissibile in uscita / *Permitted output radial load*
M_2	[Nm]	Coppia in uscita in funzione di P_1 / *Output torque referred to* P_1	Z		Numero di principi della vite / *Worm starts*
sf		Fattore di servizio / *Service factor*	β		Angolo d'elica / *Helix angle*

Dati di dentatura — *Toothing data*

	Dati della coppia vite-corona Worm wheel data	Rapporto / *Ratio*											
		5	7.5	10	15	20	25	30	40	50	60	80	100
CM026	Z	6	4	3	2	2		1	1	1	1		
	β	34° 35'	24° 41'	19° 1'	12° 57 '	10° 30'		6° 33'	5° 17'	4° 26'	3°49'		
CM030	Z	6	4	3	2	2	2	1	1	1	1	1	1
	β	27° 4'	24° 28'	18° 50'	12° 49'	10° 23'	8° 43'	6° 29'	5° 14'	4° 23'	3° 46'	2° 57'	2° 25'
CM040	Z	6	4	3	2	2	2	1	1	1	1	1	1
	β	34° 19'	24° 28'	18° 50'	12° 49'	10° 23'	8° 43'	6° 29'	5° 14'	4° 23'	3°46'	2° 57'	2° 25'
CM050	Z	6	4	3	2	2	2	1	1	1	1	1	1
	β	33° 37'	23° 54'	18° 23'	12° 29'	10° 6'	8° 28'	6° 19'	5° 5'	4° 15'	3° 39'	2°51'	2° 20'
CM063	Z	6	4	3	2	2	2	1	1	1	1	1	1
	β	34° 23'	24° 31'	18° 53'	12° 50'	10° 24'	8° 44'	6° 30'	5° 14'	4° 23'	3° 47'	2° 57'	2° 25'
CM070	Z		4	3	2	2	2	1	1	1	1	1	1
	β		26°12'	20°15'	13°49'	11°15'	9°29'	7°0'	5°41'	4°46'	4°7'	3°13'	2°39'

Rendimento — *Efficiency*

	n_1 [min^{-1}]	Rendimento Efficiency	Rapporto / *Ratio*											
			5	7.5	10	15	20	25	30	40	50	60	80	100
CM026	2800	Rd	89	87	85	83	80		73	68	64	60		
	1400		87	84	83	78	74		66	61	57	53		
	900		84	83	80	75	71		61	57	52	48		
		Rs	72	71	68	61	56		46	41	36	34		
CM030	2800	Rd	89	88	86	84	81	78	74	70	65	62	57	52
	1400		86	85	84	79	75	72	67	62	58	55	48	43
	900		84	83	81	75	71	68	62	58	53	49	43	39
		Rs	72	67	63	55	50	43	39	35	31	27	23	21
CM040	2800	Rd	90	89	87	84	83	80	77	73	69	66	60	56
	1400		88	86	84	81	78	74	70	65	60	58	52	46
	900		86	84	82	77	74	70	66	60	57	53	46	41
		Rs	74	71	67	60	55	51	45	40	36	32	28	24
CM050	2800	Rd	91	90	88	86	84	82	78	74	71	68	62	58
	1400		89	87	85	82	79	76	72	67	63	60	54	49
	900		87	85	84	79	75	72	68	62	59	55	48	43
		Rs	73	70	66	59	55	51	44	39	35	32	27	23
CM063	2800	Rd	91	90	88	86	84	83	79	76	73	70	65	60
	1400		90	88	86	84	81	78	75	70	66	63	57	52
	900		89	86	84	81	78	75	70	65	61	58	52	47
		Rs	73	71	67	60	55	51	45	40	36	33	28	24
CM070	2800	Rd		90	89	87	85	84	80	77	74	72	67	62
	1400			89	87	84	82	80	76	72	68	65	60	53
	900			87	85	82	79	77	72	67	63	60	54	49
		Rs		72	69	62	60	55	48	43	38	36	31	26

Rendimento teorico del riduttore dopo il rodaggio
Theoretical efficiency of the gearbox after the first running period

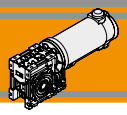

Dati tecnici per servizio S2

Technical data for S2 duty

P_1 [W]	n_2 [min^{-1}]	M_2 [Nm]	sf	i	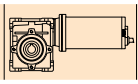	Versione motore *Motor version*
100						
(3000 min^{-1})	**600**	1.4	7.1	5	**ECM070/026**	12E/24E
	400	2.1	5.3	7.5		
	300	2.7	4.1	10		
	200	4.0	2.8	15		
	150	5.1	2.2	20		
	100	7.0	1.7	30		
	75	8.7	1.3	40		
	60	10	1.0	50		
	50	11	0.8	60		
	600	1.4	9.2	5	**ECM070/030**	12E/24E
	400	2.1	7.1	7.5		
	300	2.7	5.8	10		
	200	4.0	4.0	15		
	150	5.2	2.7	20		
	120	6.2	2.4	25		
	100	7.1	2.5	30		
	75	8.9	1.8	40		
	60	10	1.4	50		
	50	12	1.2	60		
	38	15	0.8	80		
	30	17	0.7	100		
140						
(3000 min^{-1})	**600**	2.0	5.0	5	**ECM100/026**	120/240/24E
	400	2.9	3.8	7.5		
	300	3.8	2.9	10		
	200	5.5	2.0	15		
	150	7.1	1.5	20		
	100	10	1.2	30		
	75	12	0.9	40		
	60	14	0.7	50		
	50	13	0.7	60		
	200	5.6	2.8	15	**ECM100/030**	120/240/24E
	150	7.2	1.9	20		
	120	8.7	1.7	25		
	100	10	1.8	30		
	75	12	1.3	40		
	60	14	1.0	50		
	50	17	0.8	60		
	38	17	0.7	80		
	30	16	0.7	100		
	100	10	3.7	30	**ECM100/040**	120/240/24E
	75	13	2.6	40		
	60	15	2.1	50		
	50	18	1.6	60		
	38	21	1.3	80		
	30	25	1.0	100		
250						
(3000 min^{-1})	**600**	3.5	2.8	5	**ECM180/026**	120/240
	400	5.2	2.1	7.5		
	300	6.8	1.6	10		
	200	10	1.1	15		
	150	13	0.9	20		
	100	17	0.7	30		
	75	16	0.7	40		
	60	14	0.7	50		
	50	13	0.7	60		
	600	3.5	3.7	5	**ECM180/030**	120/240/24E
	400	5.3	2.9	7.5		
	300	6.8	2.3	10		
	200	10	1.6	15		
	150	13	1.1	20		
	120	16	1.0	25		
	100	18	1.0	30		
	75	22	0.7	40		
	60	21	0.7	50		
	50	20	0.7	60		120/240
	38	17	0.7	80		
	30	16	0.7	100		

P_1 [W]	n_2 [min^{-1}]	M_2 [Nm]	sf	i	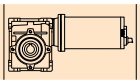	Versione motore *Motor version*
250						
(3000 min^{-1})	**200**	10	3.5	15	**ECM180/040**	120/240/24E
	150	13	2.3	20		
	120	16	1.8	25		
	100	18	2.1	30		
	75	23	1.5	40		
	60	27	1.2	50		
	50	32	0.9	60		
	38	38	0.7	80		
	30	34	0.7	100		
	75	24	2.5	40	**ECM180/050**	120/240/24E
	60	28	2.0	50		
	50	32	1.6	60		
	38	39	1.2	80		
	30	46	0.9	100		
350						
(3000 min^{-1})	**600**	5.0	2.6	5	**ECM250/030**	120/240
	400	7.4	2.0	7.5		
	300	10	1.7	10		
	200	14	1.1	15		
	150	18	0.8	20		
	120	22	0.7	25		
	100	25	0.7	30		
	75	22	0.7	40		
	60	21	0.7	50		
	200	14	2.5	15	**ECM250/040**	120/240
	150	18	1.7	20		
	120	22	1.3	25		
	100	26	1.5	30		
	75	33	1.0	40		
	60	38	0.8	50		
	50	44	0.7	60		
	38	38	0.7	80		
	30	35	0.7	100		
	150	19	2.9	20	**ECM250/050**	120/240
	120	23	2.2	25		
	100	26	2.6	30		
	75	33	1.8	40		
	60	40	1.4	50		
	50	45	1.1	60		
	38	55	0.8	80		
	30	65	0.7	100		
	75	34	3.3	40	**ECM250/063**	120/240
	60	41	2.5	50		
	50	47	2.1	60		
	38	58	1.5	80		
	30	67	1.2	100		
500						
(3000 min^{-1})	**600**	7.1	1.8	5	**ECM350/030**	120/240
	400	11	1.4	7.5		
	300	14	1.2	10		
	200	20	0.8	15		
	150	20	0.7	20		
	120	21	0.7	25		
	100	26	0.7	30		
	75	23	0.7	40		
	60	21	0.7	50		

N.B.
Verificare sempre che la coppia M2 utilizzata non ecceda il valore indicato nelle caselle in grigio
N.B.
Please check that the output torque M2 does not exceed the value in the grey areas

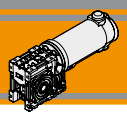

Dimensioni ***Dimensions***

ECM100/040 U

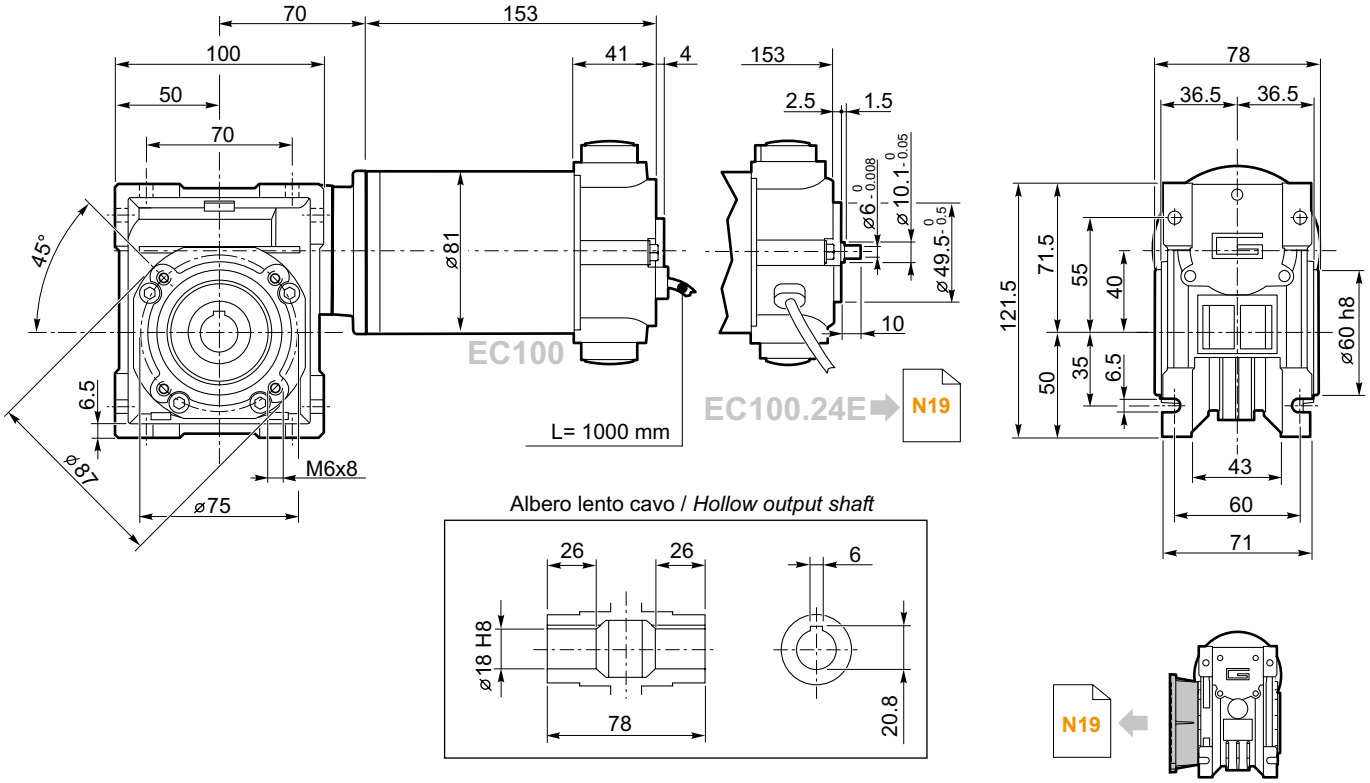

Albero lento cavo / *Hollow output shaft*

ECM100/040 F
ECM100/040 FL
ECM100/040 FB

Freno / *Brake* → H23

Encoder → H24

C.12 Drive Electromen EM-12A

EM-12A PWM DC-MOTOR CONTROL UNIT 24V 8A 200W

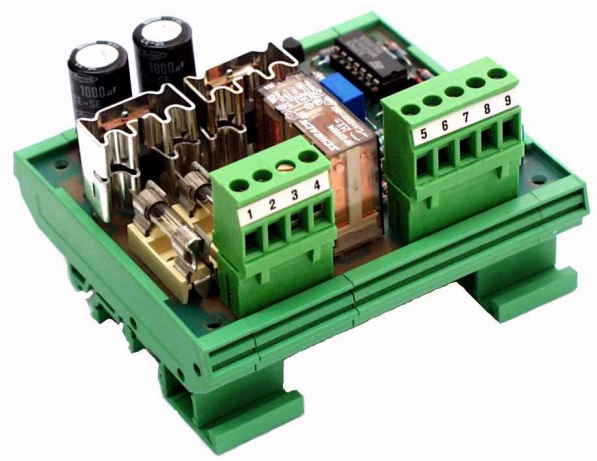

FEATURES:

- **Continuous power regulation and controlled direction change**
- **Adjustable current limit, acceleration ramp and max. power limit**
- **Load short circuit protected**
- **CB-mode for increased starting torque**
- **High efficiency, small size**
- **Controllable with potentiometer, switch or voltage signal**
- **Rail mounting base available**

EM-12A DC-motor control unit is designed for use in industry and automation applications in power range of 0...200 W. With EM-12A DC-motor can be controlled easily and economically.
EM-12A includes many adjustments and various connection choices. Inbuilt protection features increase the reliability of use. CB-function (current boost) eliminates motor rushing if started with load.
EM-12A can be controlled continuously with one potentiometer forward/stop/reverse or the control can be divided to switch and potentiometer or just for switch. EM-12A can be controlled with ±10 V signal as well.

TECHNICAL DATA:

Operating voltage	18...30 Vdc
Idle current	50mA
Load capacity	8A (RMS) mom. 15A (5s)
Operating frequency	approx. 22 kHz
Control pot.meter	10k or 25k 0.25W lin.
Recommended fuses (F1,F2)	max. 8A, slow
Operating temp.	0...50 °C
Dimensions	87*72*28 mm

Adjustments:	
Acceleration ramp (0...100%)	0.5 ... 5 s
Current limit	0.5 ... 20 A
Max. power limit	0 ... 100 %

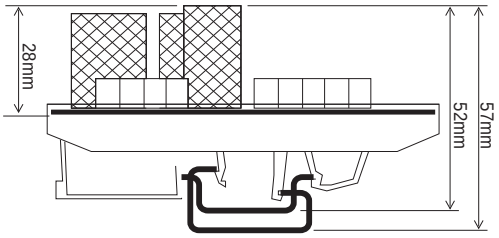

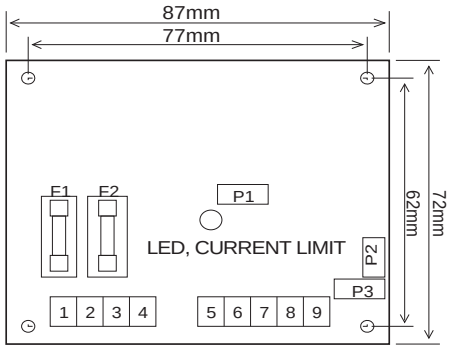

FUSES (8A, SLOW)
F1, SUPPLY
F2, MOTOR

ADJUSTMENTS
P1, CURRENT LIMIT
P2, ACCELERATION RAMP
P3, MAX. POWER LIMIT

EM-12A INSTRUCTIONS

CONNECTIONS

Connection choices are displayed in figures 2a, 2b, 2c and 2d. If the operating direction of the connected potentiometer is not as desired, the outer wires should be switched. If the rotating direction of the motor is not as wanted, the motor wires should be switched.
CAUTION. When the card is supplied from a transformer, capacitor should be added as shown in figures. With battery supply the capacitor is needed only if supply leads are extensive (over 5m).

INTRODUCTION

Adjust the max. power limit to 100 % (P3 clockwise), acceleration ramp to 5 s position (P2 counterclockwise) and the current limit to 20 A (P1 clockwise).

CONTROL LIMIT

Drive the motor full forward or full reverse. If the maximum running speed of the motor needs to be restricted, adjust P3 counter-clockwise until the running speed of the motor is acceptable.

ACCELERATION RAMP

With the preset ramp length of 5 s and maximum power, reversing the motor (full forward <=> full reverse) takes approximately 10 s. If the application can be stopped faster, the acceleration ramp can be set to shorter value by turning the P2 clockwise. DO NOT ADJUST THE RAMP TO SO SHORT VALUE THAT THE REVERSING OCCURS WHILE THE MOTOR IS STILL RUNNING.

CURRENT LIMIT

The purpose of the current limit is to protect the motor from overloading. Adjust the current limit so that the red led on the card is not lit during normal load conditions. NOTE: by adjusting the current limit too low, the torque of the motor is decreased. The operation of the current limit can be checked by overloading the motor.
CAUTION: Do not use the control card in applications with high inertia (eg. flywheel drive) or where the load rotates the motor (eg. automotive devices going downhill).

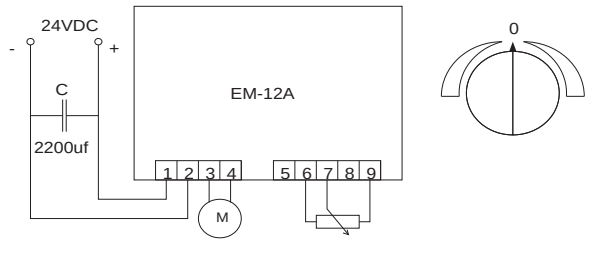

FIGURE 2a. POTENTIOMETER CONTROL. MIDDLE POSITION OF POT.METER FUNCTION STOP. CONTINUOS CONTROL IN BOTH DIRECTIONS

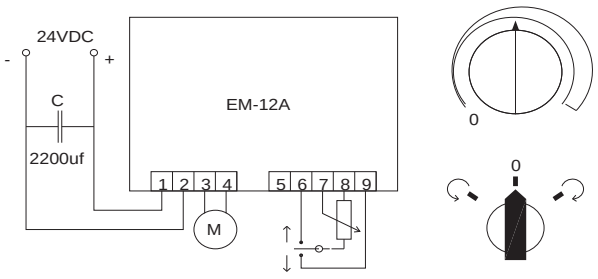

FIGURE 2b. SPEED CONTROL WITH POT.METER, DIRECTION WITH SWITCH. STOP FUNCTION IS ACHIEVED WITH THREE POSITION SWITCH.

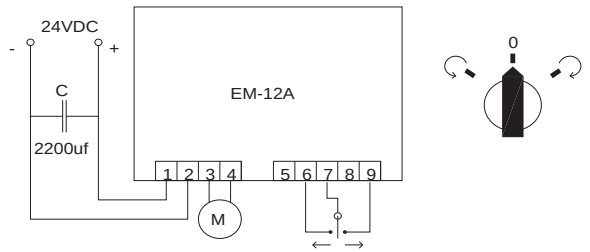

FIGURE 2c. CONTROL WITH SWITCH. FUNCTIONS FORWARD/STOP/REVERSE.

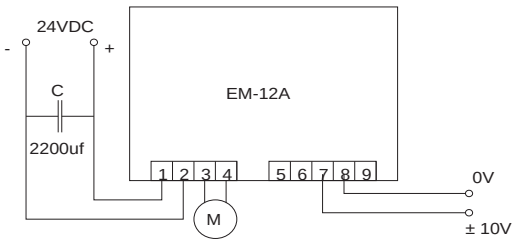

FIGURE 2d. VOLTAGE CONTROL. VOLTAGE SHOULD BE GALVANICALLY ISOLATED FROM DRIVER VOLTAGE.

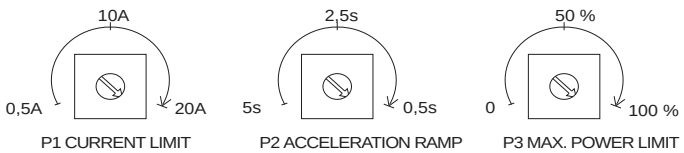

FIGURE 3. EM-12A ADJUSTMENTS.

ELECTROMEN Oy Vähäheikkiläntie 56B, 20810 Turku, FINLAND Tel. +358-2-4693050 Fax. +358-2-4693052

C.13 Directional valve Parker B3R5BXXXXH

Flow characteristics

Flow capacities in accordance with ISO6358
All pressures = effective pressure
The curves in the diagram below are typical only

Technical Data B3

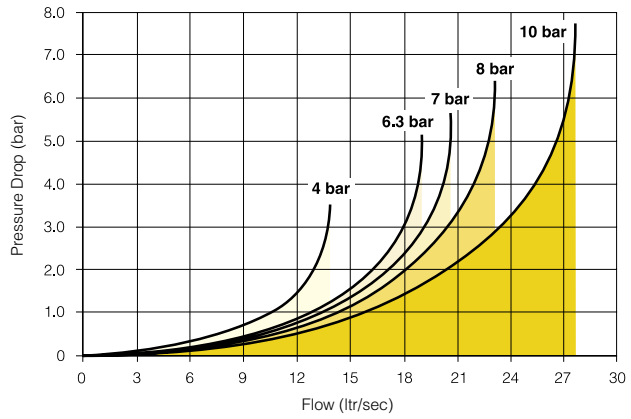

Port size	G1/8
Operating pressure.	Vacuum - 10 bar
Working temperature.	
Pneumatically operated valves.	-10°C to + 50°C
Solenoid operated valves.	-10°C to + 50°C
Response times:	
Single sol spring return	
Single sol air spring return	24/26ms
Double solenoid operated	13/15ms
Flow (acc. to ISO 6358)	c = 2.3
	b = 0.45
	Qn = 13 l/s
	Qmax = 16 l/s
	Cv = 0.75

Technical Data B4

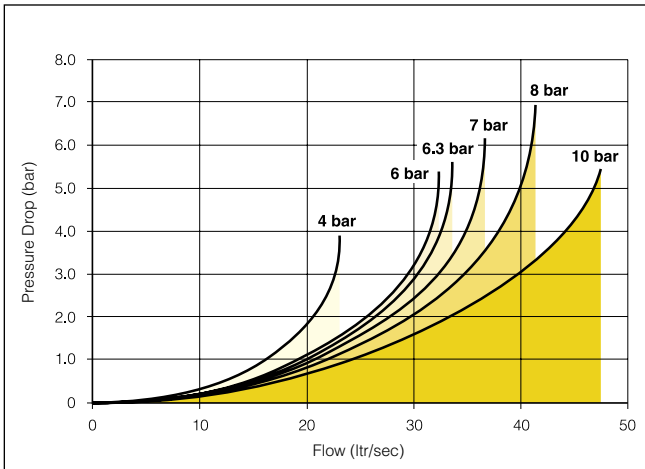

Port size	G1/4
Operating pressure.	Vacuum - 10 bar
Working temperature.	
Pneumatically operated valves.	-10°C to + 50°C
Solenoid operated valves.	-10°C to + 50°C
Response times:	
Single sol spring return	
Single sol air spring return	38/38ms
Double solenoid operated	23/24ms
Flow (acc. to ISO 6358)	c = 4.56
	b = 0.30
	Qn = 19.5 l/s
	Qmax = 32 l/s
	Cv = 1.2

Technical Data B5

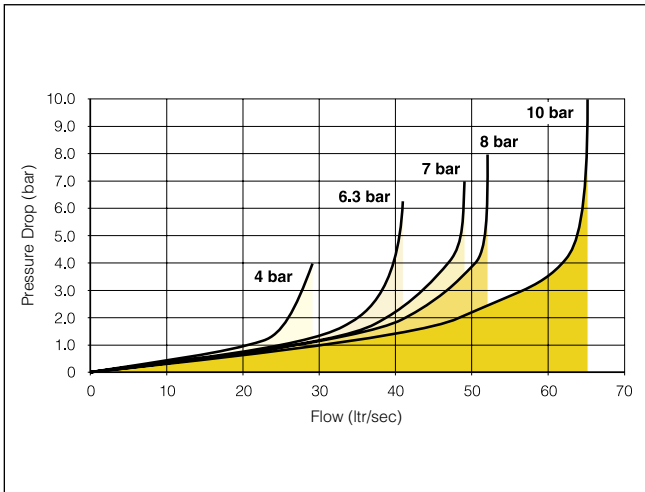

Port size	G1/4
Operating pressure.	Vacuum - 10 bar
Working temperature.	
Pneumatically operated valves.	-10°C to + 50°C
Solenoid operated valves.	-10°C to + 50°C
Response times:	
Single sol spring return	
Single sol air spring return	38/40ms
Double solenoid operated	16/18ms
Flow (acc. to ISO 6358)	Qn = 24 l/s
	Qmax = 37 l/s
	Cv = 1.4

- G1/8 ports, 3/2, 5/2 and 5/3 functions
- Inlet-exhaust manifold facility
- DIN rail mounting
- Integral mounting holes
- 1.2 watt solenoid actuators
- FormC/ISO15217 connector

Operating information

Working pressure	Vacuum - 10 bar	Flow (3/2) and (5/2) (acc. to ISO 6358)	C = 2,3
Working temperature;			b = 0,45
Pneumatically actuated	-10°C to +60°C		Qn = 13 l/s
Electrically actuated	-10°C to +50°C		Qmax = 16 l/s
			Cv = 0,6

B 3 | 2 | 5 | B | B | 5 | 49 | H

	Basic series
B3	Ported valve

	Port size
5	G1/8

Operator function		
3 Port		
G		3/2 N/C Single sol - air differential return
J		3/2 Double solenoid
K		3/2 N/C Remote air pilot - air differential return
M		3/2 Double remote air pilot
R		3/2 N/C Single sol - spring return
S		3/2 N/C Single sol - remote air pilot return
U		3/2 N/C Remote air pilot - spring return
5 Port		
1		5/2 Single sol - air differential return
2		5/2 Double solenoid
3		5/2 Remote air pilot - air differential return
4		5/2 Double remote air pilot
5		5/3 Double solenoid - all ports blocked (APB)
6		5/3 Double solenoid - cyl to exhaust ports (CE)
7		5/3 Double solenoid - press to cylinder ports (PC)
8		5/3 Double remote operated - all ports blocked (APB)
9		5/3 Double remote operated - (CE) ①
0		5/3 Double remote operated - (PC) ②
A		5/2 Single sol - remote air pilot return
P		5/2 Remote air pilot - spring return
T		5/2 Single sol - spring return

Shaded part numbers are standard

Pilot source / Exh / Pilot exhaust	
0	None (Air pilot only)
B	Port 1 / Vented / Side

	Solenoid overrides / Lights
0	None (Air pilot only)
B	Spring return, flush without light
C	Locking, flush without light
X	None (Solenoid valve less solenoid)

	Solenoid Enclosures
0	None (Air pilot only)
5	15mm connector
X	None

	Pilot operator / Coil voltage
39	12V 50Hz
43	24V 50Hz
44	48V 50Hz
45	12V DC
49	24V DC
53	110V 50Hz
57	220V 50Hz
XX	Valve less solenoid operator

Engineering level H

① Cyl to exhaust ports (CE)
② Press to cylinder ports (PC)

Main data for Directional control valves, B3 Series

	Symbol	Actuator	Return	Signal pressure min, bar at 6 bar actua./return	Changeover time, ms at 6 bar actua./return	Weight Kg	Voltage	Order code	Qty
Pneumatically actuated 3/2 valves									
	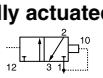	Air	Differential air	1,4/-	16/17	0,07		**B3K5000XXH**	1
		Air	Spring return	3,0/-	20/18	0,07		**B3U5000XXH**	1
		Air	Air	1,4/-	2/2	0,08		**B3M5000XXH**	1
Pneumatically actuated 5/2 and 5/3 valves									
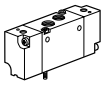	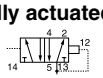	Air	Differential air	1,4/-	16/17	0,09		**B335000XXH**	1
		Air	Spring return	3,0/-	20/18	0,09		**B3P5000XXH**	1
		Air	Air	1,4/1,4	2/2	0,10		**B345000XXH**	1
	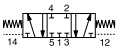	Air Closed centre position	Air Self centring	3,0/3,0	12/12	0,10		**B385000XXH**	1
		Air Vented centre position	Air Self centring	3,0/3,0	12/12	0,10		**B395000XXH**	1
	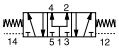	Air Pressurised centre position	Air Self centring	3,0/3,0	12/12	0,10		**B305000XXH**	1
Electrically actuated 3/2 valves									
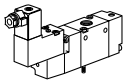		Electric	Differential air	1,4/-	12/14	0,12 0,08	24 VDC Less solenoid	**B3G5BB549H** **B3G5BXXXXH**	1 1
		Electric	Spring return	3,0/-	22/28	0,12 0,08	24 VDC Less solenoid	**B3R5BB549H** **B3R5BXXXXH**	1 1
		Electric	Air	1,4/1/4	9/3	0,13 0,09	24 VDC Less solenoid	**B3S5BB549H** **B3S5BXXXXH**	1 1
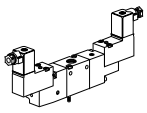		Electric	Electric	1,4/1/4	8/8	0,13 0,09	24 VDC Less solenoid	**B3J5BB549H** **B3J5BXXXXH**	1 1
Electrically actuated 5/2 valves									
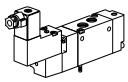		Electric Air	Differential Air	1,4/-	12/14	0,12 0,09	24 VDC Less solenoid	**B315BB549H** **B315BXXXXH**	1 1
		Electric	Spring return	3,0/-	22/28	0,12 0,09	24 VDC Less solenoid	**B3T5BB549H** **B3T5BXXXXH**	1 1
		Electric	Air	1,4/1/4	9/3	0,14 0,10	24 VDC Less solenoid	**B3A5BB549H** **B3A5BXXXXH**	1 1
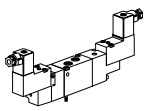		Electric	Electric	1,4/1/4	8/8	0,19 0,10	24 VDC Less solenoid	**B325BB549H** **B325BXXXXH**	1 1

C.14 Barrel inductive proximity sensor RS Pro 701-8253

Sensing range 4 mm

Inductive sensor

- Short-circuit protection (pulsed)
- Robust brass housing, nickel-plated with fine thread M12 x 1 mm
- Enclosure rating IP 67
- Installation non-flush

Dimensional drawing

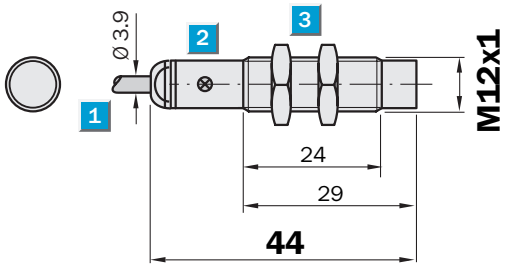

1 Connection
2 Display LED
3 Fastening nuts (2 x); width across 17, metal

Connection type

IME12-04NNSZW2KF38
IME12-04NPSZW2KF38

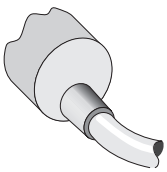

3 x 0.25 mm²

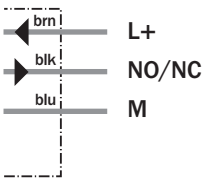

Accessories

Mounting systems

Technical specifications	IME12-	04NNS ZW2K F38	04NPS ZW2K F38								
Sensing range S_n	4 mm										
Electrical configuration	DC3-wire										
Supply voltage V_s	DC 10 ... 30 V										
Ripple U_{pp}	≤ 10 %										
Voltage drop U_d	≤ 2 V[1]										
Power consumption	≤ 10 mA[2]										
Continuous current I_a	≤ 200 mA										
Time delay before availability t_v	≤ 100 ms										
Hysteresis H, of s_r	5 ... 15 %										
Repeatability R	≤ 2 % (U_b and T_a constant)[3]										
Temperature drift, of s_r	± 10 %										
EMC	According to EN 60947-5-2										
Switching output	NPN										
	PNP										
Output function	Normally open										
Installation	Non-flush										
Connection type	Cable, PVC, 2 m										
Enclosure rating	IP 67[4]										
Max. switching frequency	2000 Hz										
Dimensions	M12 x 1[5]										
Short-circuit protection	✓[6]										
Reverse polarity protection	✓										
Power-up pulse suppression	✓										
Shock/vibration stress	30 g, 11 ms/10 ... 55 Hz, 1 mm										
Ambient temperature T_a	–25 °C ... +75 °C										
Housing material	Brass nickel-plated, plastic (PA6)										
Tightening torque	Typ. 12 Nm										
Approvals											
Protection class	⧈										
UL approval	cULus Listed										

[1] At I_a max
[2] Without load
[3] Of s_r
[4] According to EN 60529
[5] Thread diameter x pitch (mm)
[6] (Pulsed)

Reduction factor R_M

The following are reference values, which may vary from type to type:	
St37 (Fe)	1
Stainless steal (V2A)	Approx. 0.8
Aluminum (solid)	Approx. 0.45
Copper (Cu)	Approx. 0.4

Ordering information	
Type	**Part Number**
IME12-04NNSZW2KF38	7018250
IME12-04NPSZW2KF38	7018253

C.15 Photoelectric sensor by diffuse reflection Omron E3FA-DN23

Ordering Information

Sensors [Refer to *Dimensions on page* 18.]

Red light

Sensor type	Sensing distance	Connection method	Model	
			NPN output	PNP output
Through-beam *1. 	20 m	pre-wired	**set E3FA-TN11 2M** Emitter E3FA-TN11-L 2M Receiver E3FA-TN11-D 2M	**set E3FA-TP11 2M** Emitter E3FA-TP11-L 2M Receiver E3FA-TP11-D 2M
		M12 connector	**set E3FA-TN21** Emitter E3FA-TN21-L Receiver E3FA-TN21-D	**set E3FA-TP21** Emitter E3FA-TP21-L Receiver E3FA-TP21-D
Retro-reflective *2. 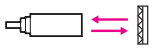	0.1 to 4 m with E39-R1S	pre-wired	**E3FA-RN11 2M**	**E3FA-RP11 2M**
		M12 connector	**E3FA-RN21**	**E3FA-RP21**
Coaxial Retro-reflective *2. 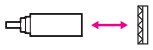	0 to 500 mm with E39-R1S	pre-wired	**E3FA-RN12 2M**	**E3FA-RP12 2M**
		M12 connector	**E3FA-RN22**	**E3FA-RP22**
Diffuse-reflective 	100 mm	pre-wired	**E3FA-DN11 2M**	**E3FA-DP11 2M**
		M12 connector	**E3FA-DN21**	**E3FA-DP21**
	300 mm	pre-wired	**E3FA-DN12 2M**	**E3FA-DP12 2M**
		M12 connector	**E3FA-DN22**	**E3FA-DP22**
	1 m	pre-wired	**E3FA-DN13 2M**	**E3FA-DP13 2M**
		M12 connector	**E3FA-DN23**	**E3FA-DP23**
BGS (background suppression) 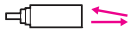	100 mm	pre-wired	**E3FA-LN11 2M**	**E3FA-LP11 2M**
		M12 connector	**E3FA-LN21**	**E3FA-LP21**
	200 mm	pre-wired	**E3FA-LN12 2M**	**E3FA-LP12 2M**
		M12 connector	**E3FA-LN22**	**E3FA-LP22**
Limited distance reflective 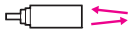	10 to 50 mm	pre-wired	**E3FA-VN11 2M**	**E3FA-VP11 2M**
		M12 connector	**E3FA-VN21**	**E3FA-VP21**
Transparent detected with P-opaquing function *2. 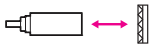	100 to 500 mm with E39-RP1	pre-wired	**E3FA-BN11 2M**	**E3FA-BP11 2M**
		M12 connector	**E3FA-BN21**	**E3FA-BP21**
Transparent detected with P-opaquing function *2. 	0.1 to 2 m with E39-RP1	pre-wired	**E3FA-BN12 2M**	**E3FA-BP12 2M**
		M12 connector	**E3FA-BN22**	**E3FA-BP22**
Through-beam *1. 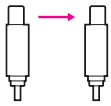	15 m	pre-wired	**set E3RA-TN11 2M** Emitter E3RA-TN11-L 2M Receiver E3RA-TN11-D 2M	**set E3RA-TP11 2M** Emitter E3RA-TP11-L 2M Receiver E3RA-TP11-D 2M
		M12 connector	**set E3RA-TN21** Emitter E3RA-TN21-L Receiver E3RA-TN21-D	**set E3RA-TP21** Emitter E3RA-TP21-L Receiver E3RA-TP21-D
Retro-reflective *2. 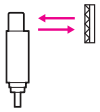	0.1 to 3 m with E39-R1S	pre-wired	**E3RA-RN11 2M**	**E3RA-RP11 2M**
		M12 connector	**E3RA-RN21**	**E3RA-RP21**
Diffuse reflective 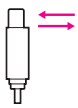	100 mm	pre-wired	**E3RA-DN11 2M**	**E3RA-DP11 2M**
		M12 connector	**E3RA-DN21**	**E3RA-DP21**
	300 mm	pre-wired	**E3RA-DN12 2M**	**E3RA-DP12 2M**
		M12 connector	**E3RA-DN22**	**E3RA-DP22**
	700 mm	pre-wired	**E3RA-DN13 2M**	**E3RA-DP13 2M**
		M12 connector	**E3RA-DN23**	**E3RA-DP23**

*1. The set type includes the emitter and receiver.
*2. The Reflector is sold separately. Select the Reflector model most suited to the application.

Specifications

Straight type

Model / Item	Sensing method		Through-beam	Retro-reflective	Coaxial Retro-reflective	Diffuse-reflective		
	NPN output	Pre-wired	E3FA-TN11 2M	E3FA-RN11 2M	E3FA-RN12 2M	E3FA-DN11 2M	E3FA-DN12 2M	E3FA-DN13 2M
		M12 Connector	E3FA-TN21	E3FA-RN21	E3FA-RN22	E3FA-DN21	E3FA-DN22	E3FA-DN23
	PNP output	Pre-wired	E3FA-TP11 2M	E3FA-RP11 2M	E3FA-RP12 2M	E3FA-DP11 2M	E3FA-DP12 2M	E3FA-DP13 2M
		M12 Connector	E3FA-TP21	E3FA-RP21	E3FA-RP22	E3FA-DP21	E3FA-DP22	E3FA-DP23
Sensing distance			20 m	0.1 to 4 m (with E39-R1S)	0 to 500 mm (with E39-R1S)	100 mm (white paper: 300 × 300 mm)	300 mm (white paper: 300 × 300 mm)	1 m (white paper: 300 × 300 mm)
Spot diameter (typical)			—	—	—	40 × 45 mm Sensing distance of 100 mm	40 × 50 mm Sensing distance of 300 mm	120 × 150 mm Sensing distance of 1 m
Standard sensing object			Opaque: 7 mm dia.min.	Opaque: 75 mm dia.min.	Opaque: 75 mm dia.min.	—	—	—
Differential travel			—	—	—	20% max.	—	—
Directional angle			2° min.	2° min.	2° min.	—	—	—
Light source (wavelength)			Red LED (624 nm)					
Power supply voltage			10 to 30 VDC (include voltage ripple of 10%(p-p) max.)					
Current consumption			40 mA max. (Emitter 25 mA max. Receiver 15 mA max.)	25 mA max.				
Control output			NPN/PNP (open collector) Load current: 100 mA max. (Residual voltage: 3 V max.), Load power supply voltage: 30 VDC max.					
Operation mode			Light-ON/Dark-ON selectable by wiring					
Indicator			Operation indicator (orange) Stability indicator (green) Power indicator (green): only Emitter of Through-beam					
Protection circuits			Reversed power supply polarity protection, Output short-circuit protection and Reversed output polarity protection					
Response time			0.5 ms					
Sensitivity adjustment			One-turn adjuster					
Ambient illumination (Receiver side)			Incandescent lamp: 3,000 lx max./ Sunlight: 10,000 lx max.					
Ambient temperature range			Operating: -25 to 55°C/ Storage: -30 to 70°C (with no icing or condensation)					
Ambient humidity range			Operating: 35 to 85%RH/ Storage: 35 to 95%RH (with no condensation)					
Insulation resistance			20 MΩ min. at 500 VDC					
Dielectric strength			1,000 VAC at 50/60 Hz for 1 min. between current-carrying parts and case					
Vibration resistance			Destruction: 10 to 55 Hz, 1.5 mm double amplitude for 2 hours each in X, Y and Z directions					
Shock resistance			Destruction: 500 m/s^2 3 times each in X, Y and Z directions					
Degree of protection			IEC: IP67, DIN 40050-9: IP69K *					
Weight (packed state/only sensor)	**Pre-wired cable (2M)**		Approx. 110 g/ Approx. 50 g, respectively	Approx. 60 g/ Approx. 50 g				
	Connector		Approx. 30 g/ Approx. 10 g, respectively	Approx. 20 g/ Approx. 10 g				
Material	**Case**		ABS					
	Lens and Display		PMMA					
	Adjuster		POM					
	Nut		ABS					
Accessories			Instruction sheet M18 nuts (4 pcs)	Instruction sheet M18 nuts (2 pcs)				

* IP69K Degree of Protection Specifications
IP69K is a protection specification stipulated by DIN 40050 Part 9 of the German standards.
The test item is sprayed with 80°C water from a nozzle of a specified shape at a water pressure of 80 to 100 bar. The amount of water is 14 to 16 liters per minute.
The distance between the test item and the nozzle is 10 to 15 cm. The water is discharged at angles of 0°, 30°, 60°, and 90° from the horizontal plane for 30 seconds at each angle while the test item is rotated horizontally.

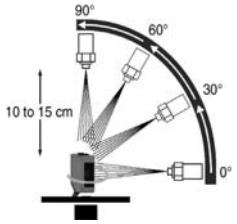

C.16 Kistler K-Shear Shock Accelerometer 5000g

KISTLER
measure. analyze. innovate.

K-Shear® Accelerometer

Type 8742A...

High Resonant Frequency, Shock Accelerometer

Quartz shock accelerometer for measuring short duration impulse and impact shocks. Type 8742A… shock accelerometers have a rugged welded construction, integral stud and are available in four measuring ranges.

- Low impedance, voltage mode
- Unique quartz shear sensing element
- Ranges 5,000 ... 50,000 g
- Low transverse sensitivity
- Rugged connector for repeated connections
- Wide bandwidth, high resonant frequency
- Conforming to CE

Description

The sensing element contained within this shock accelerometer series features a unique, shear mode four quartz crystal configuration combined with an annular preload sleeve and seismic mass. The element design provides over 100 kHz resonance frequency ensuring accurate measurement of high speed events with zero shift and internal amplifier saturation virtually eliminated. These shock sensors exhibit insensitivity to thermal transients, and have extremely low transverse and base strain sensitivity. Using quartz as the sensing material adds another performance benefit in that quartz will not depolarize if exposed to high shock.

Poor connector pin continuity resulting from an applied shock can momentarily interrupt a measured event. To ensure reliable shock measurements, Type 8742A… accelerometer contains an improved spring insert made of a gold plated Beryllium-Copper. Beryllium Copper provides the elastic physical properties that promote positive contact and resists aging.

An internal microelectronic Piezotron® signal conditioning circuit converts the charge developed in the quartz element as a result of the accelerometer being subjected to shock, into a useable high level voltage output signal at a low impedance level. The low impedance output provides high immunity to noise and insensitivity to cable motion.

Dimensions

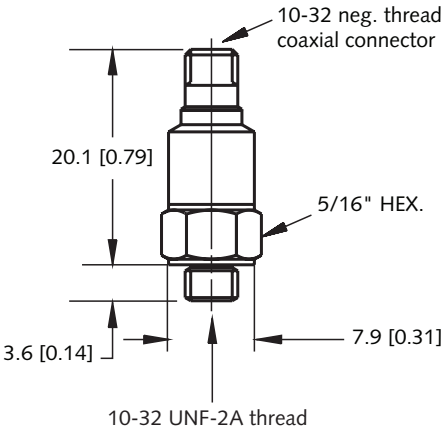

Application

Type 8742A… accelerometer is ideally suited for impact and impulse shock measurements where metal-to-metal impact occurs; where package and product survivability drop shock tests are of interest and where vehicle crash data is collected.

Mounting

Type 8742A… is attached to the test structure by its integral 10-32 UNF stud. Reliable and accurate measurements require that the mounting surface be clean and flat. The instruction manual for the shock accelero-meter series provides detailed information regarding mounting surface preparation.

Usage of the base Type 8466K06 can allow for ground isolation while stud mounted.

KISTLER
measure. analyze. innovate.

Technical Data

Type	Unit	8742A5	8742A10	8742A20	8742A50
Acceleration range	g	±5,000	±10,000	±20,000	±50,000
Acceleration limit	gpk	±6,000	±12,000	±24,000	±60,000
Threshold (noise ≤130 μV_{rms}), nom.	g_{rms}	0.13	0.25	0.5	1.3
Sensitivity, 5 %	mV/g	1	0.5	0.25	0.1
Resonant frequency mounted, nom.	kHz	100			
Frequency response, ±7 %	Hz	1 ... 10,000			
Amplitude linearity	%FSO	±1			
Time constant, nom.	s	≥0.5			
Transverse sensitivity	%	1.5 typ.; 5 max.			

Environmental					
Base strain sensitivity @250 με	g/με	0.005			
Shock limit	gpk	50,000	50,000	50,000	100,000
Temperature coeff. of sensitivity,	%/°C [%/°F]	–0.06 [–0.03]			
Operating temperature range	°C [°F]	–55 ... 120 [–67 … 250]			

Output		
Bias, nom.	VDC	11
Impedance	Ω	<100
Voltage, full-scale	V	±5

Source		
Voltage	VDC	18 ... 30
Constant current	mA	2 ... 20*

Construction		
Sensing element	type	quartz-shear
Housing/Base	material	stainless steel
Sealing housing/connector (EN 60529)		Hermetic
Connector	type	10-32 neg.
Ground isolation		with pad (Type 8466K06 when stud mounted) (Type 8436 when adhesive mounted)
Mass	grams	4.5
Mounting stud	type	10-32 UNF-2A
Mounting torque	N·m [in-lbf]	2 [18]

1 g = 9.80665 m/s², 1 in = 25.4 mm, 1 Gram = 0.03527 oz, 1 lbf-in = 0.113 N·m

*Recommended min. 4 mA

8742A_000-250e-10.15

KISTLER
measure. analyze. innovate.

Measuring Chain		Type
1	Low impedance sensor	8742A...
2	Sensor cable, 10-32 pos. to BNC pos.	1761B...
3	Power supply/signal conditioner	51...
4	Output cable BNC pos. to BNC pos.	1511

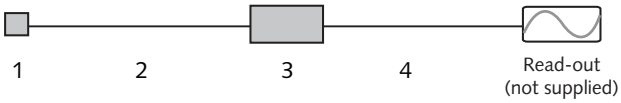

Ordering Key

Type 8742A

Range	
±5,000 g	**5**
±10,000 g	**10**
±20,000 g	**20**
±50,000 g	**50**

8742A_000-250e-10.15

C.17 Charge amplifier and data acquisition unit Kistler LabAmp

KISTLER
measure. analyze. innovate.

Kistler LabAmp

Type 5165A...

Charge Amplifier and Data Acquisition Unit for Dynamic Measurements

This universal laboratory charge amplifier can be used wherever dynamic signals of mechanical quantities are measured with piezoelectric sensors, Piezotron® sensors (IEPE) or sensors with voltage output. Piezoelectric sensors produce an electric charge which varies in direct proportion with the load acting on the sensor. The amplifier converts this charge directly into digital values or a proportional output voltage.

- 1 or 4 channel amplifier for piezoelectric sensors (charge), Piezotron sensors (IEPE) and voltage
- Integrated 24-bit data acquisition with up to 200 kSps per channel
- Continuous digital signal processing at minimal latency
- Fully flexible low-pass, high-pass and notch filter adjustment
- Low-noise design
- TEDS (IEEE 1541.4) for Piezotron sensors
- 1 or 4 analog outputs with fully flexible 2-point scaling and internal routing
- Status indication per channel via LED
- Configuration and control in a standard web-browser
- Virtual instrument driver for LabVIEW™
- Two Ethernet interfaces with included switch functionality

Description

The Kistler LabAmp Type 5165A... is not only an outstanding low-noise charge amplifier for dynamic signals but also a powerful data acquisition device delivering the digitized measurement values directly to a host computer for further analysis. It is configured and operated in a web-interface, conveniently accessible by a standard web-browser.

Thanks to advanced signal processing technology, the Kistler LabAmp Type 5165A... offers impressive flexibility. The frequencies of the highpass, low-pass and notch filters can be directly entered as numeric values in Hertz. The input signals can be flexibly routed to the analog outputs.

The graphical user interface not only offers a simple and intuitive way to configure the device but also displays different measurement values (e.g. live value, peak value, root mean square). Furthermore, the browser-based data download allows the acquired data to be processed in an analysis software. For more advanced tasks or direct analysis, the amplifier can be integrated directly into LabVIEW™ thanks to the provided Virtual Instruments Driver.

5165A_003-146e-06.15

KISTLER
measure. analyze. innovate.

Technical Data

Connections

Number of channels		
Type 5165A1		1
Type 5165A4		4
Input connector type		BNC neg.
Analog output connector type		BNC neg.
Ethernet interface		2xRJ45

Charge Input

Measuring range	pC	±100 … 1 000 000
Frequency range (–3dB)	Hz	0,1 … 100 000
Input noise (typ.)		
1 Hz ... 100 kHz		
100 pC	pC_{rms}	0,006
1 000 pC	pC_{rms}	0,008
10 000 pC	pC_{rms}	0,048
100 000 pC	pC_{rms}	0,67
1 000 000 pC	pC_{rms}	4,6
1 Hz ... 10 kHz		
100 pC	pC_{rms}	0,006
1 000 pC	pC_{rms}	0,007
10 000 pC	pC_{rms}	0,03
100 000 pC	pC_{rms}	0,35
1 000 000 pC	pC_{rms}	2,8
Maximum input voltage	V	±30
Measuring error		
Measuring range <100 pC	%	<1
Measuring range ≥100 pC	%	<0,5
Crosstalk between channels	dB	≤–80
Sensor impedance	MΩ	>10

Piezotron Input

Gain		1/10
Sensor supply voltage	V	22
Power supply	mA	4/10
Frequency range (–3dB)	Hz	0,1 … 100 000
Input noise (typ., 0 Ω shunt at input)		
1 Hz ... 100 kHz		
Gain 10	μV_{rms}	6
Gain 1	μV_{rms}	45
1 Hz ... 10 kHz		
Gain 10	μV_{rms}	3,5
Gain 1	μV_{rms}	28
Maximum input voltage	V	±30
Measuring error		
Gain 10	%	<1
Gain 1	%	<0,5
Crosstalk between channels	dB	≤–80

Voltage Input

Input type		single-ended
Measuring range	V	±1 … 10
Input impedance	MΩ	10
Frequency range (–3dB)	Hz	0 … 100 000
Input noise (typ.)		
1 Hz ... 100 kHz		
Measuring range 1 V	μV_{rms}	6
Measuring range 10 V	μV_{rms}	45
1 Hz ... 10 kHz		
Measuring range 1 V	μV_{rms}	3,5
Measuring range 10 V	μV_{rms}	28
Max. input voltage	V	±30
Measuring error		
Measuring range <1 V	%	<1
Measuring range ≥1 V	%	<0,5
Crosstalk between channels	dB	≤–80

Voltage Output

Nominal output range	V	±10
Output impedance	Ω	10
Max. common mode voltage between input and output ground	V	±14
Output noise (all ranges)		
1 Hz ... 100 kHz, typ.	mV_{rms}	0,046
1 Hz ... 10 kHz, typ.	mV_{rms}	0,041
Frequency range (–3dB)	Hz	0 … 100 000
Group delay (input to output, filters off)	µs	≤12
Zero error	mV	<±2
DAC resolution (analog out)	Bit	16

KISTLER
measure. analyze. innovate.

Technical Data (Continuation)

Data Acquisition

ADC resolution	Bit	24
ADC sampling rate	kSps	625
Output update rate per channel (adjustable)	kSps	≤200

Note: For the data acquisition an anti-aliasing filter is automatically set with a corner frequency of 0,3 x selected output update rate.

Digital High-Pass Filter

Order		1.
Cutoff-frequency (–3dB) selection in 0,1 Hz steps	Hz	≥0,1 ... 10 000
Tolerance (typ.)	%	<1

Digital Low-Pass Filter

Filter type		Bessel or Butterworth
Order		2./4.
Cutoff-frequency (–3dB) selection in 1 Hz steps	Hz	≥10
Tolerance (typ.)	%	<1

Digital Notch Filter

Center frequency selection in 1 Hz steps	Hz	≥10
Tolerance (typ.)	%	<1
Q factor		0,8 ... 1 000

Ethernet Interface

Data rate	MBit	100

Power Supply Requirements

Supply voltage range	VDC	18 ... 30
Power consumption	W	<15
Socket for barrel jack plug (IEC 60130-10 Type A)	mm	5,5x2,5x9,5
Power supply requirements		– galvanic isolation – PE and GND not connected

General Data

Operating temperature range	°C	0 ... 60
Storage temperature range	°C	–10 ... 70
Rel. humidity, not condensing	%	≤90
Degree of protection (EN 60529)		IP20
Outer dimensions incl. feet and connectors (WxHxD)	mm	≈218x50x223
Weight	kg	1,2

Application

The instrument has been designed for use in research, development and the laboratory. The Kistler LabAmp Type 5165A... is the perfect choice wherever dynamic signals need to be measured precisely and with high resolution. Acceleration and vibration measurements, pulsating pressure applications or force measurements of fast machining procedures are just a few examples where the Kistler LabAmp Type 5165A... can demonstrate his strengths.

Operation

All settings are configured in a standard web-browser through the graphical user interface. Simply connect to the Kistler LabAmp Type 5165A... by its network name and start working. A simple data acquisition is also implemented, offering a data download controlled by a start/stop button. In addition, an API is available to perform automated measuring tasks PC-based.

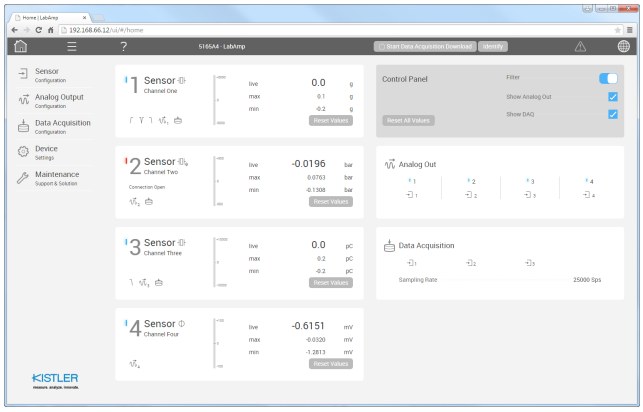

KISTLER
measure. analyze. innovate.

Block Diagram

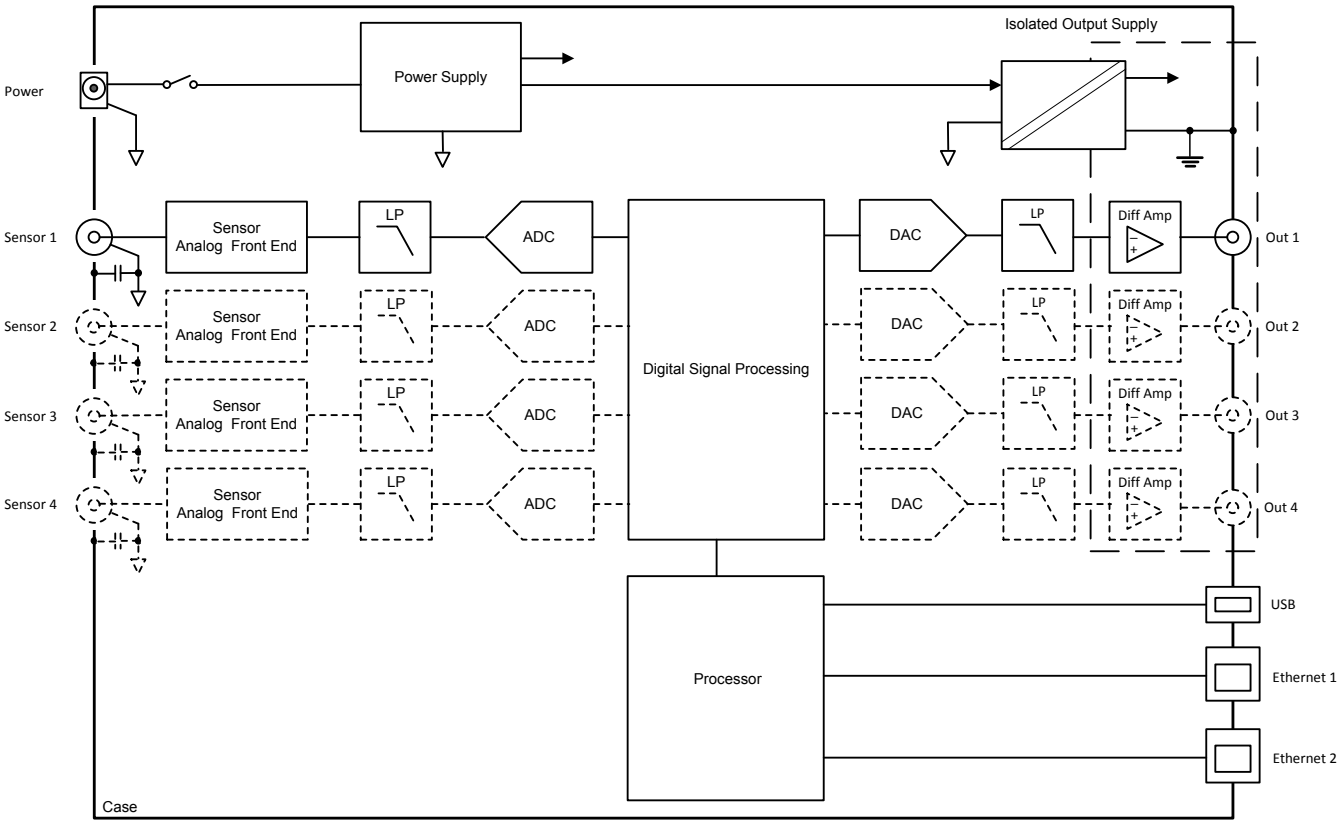

Fig. 1: Block diagram of the Kistler LabAmp Type 5165A...

5165A_003-146e-06.15

KISTLER
measure. analyze. innovate.

Dimensions

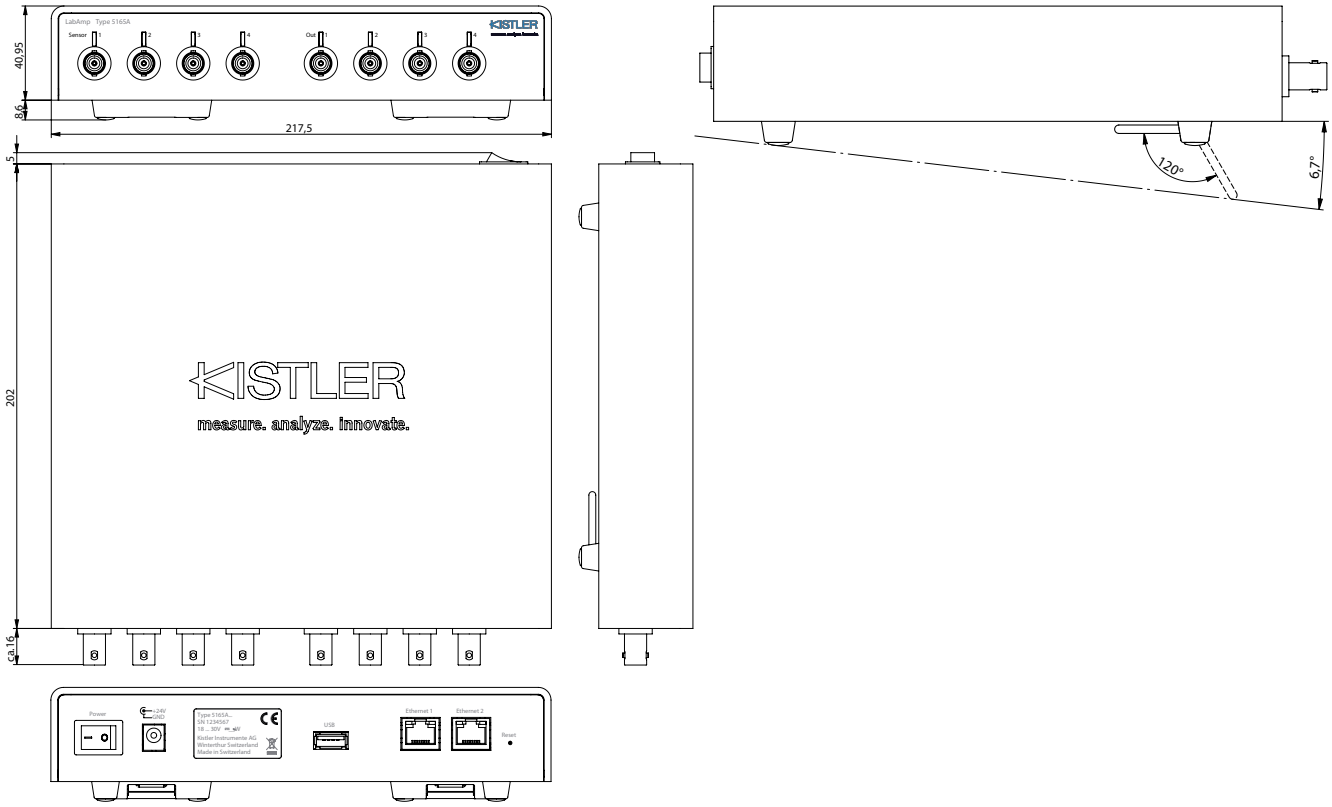

Fig. 2: Dimensions of Kistler LabAmp Type 5165A4

Included Accessories	Type/Mat. No.
• Calibration sheet	–
• Quick-start guide	–

Optional Accessories	Type/Mat. No.
• Power supply* 24 V incl. country-specific plug	5779A2
• Ethernet cable, l = 2 m*	tbd
• 19" rack mounting tablet	5748A1
• Dummy panel for empty 19" position	5748A2

* Available as combined kit together with the amplifier

Ordering Key

Type 5165A ☐ ☐

LabAmp	
Single-channel	**1**
4 channels	**4**

Amplifier only	**–**
Kit with amplifier, 24 V power supply, 2 m Ethernet cable	**K**

5165A_003-146e-06.15

LabVIEW™ is a registered trade mark of National Instruments Corporation.

C.18 Photoelectric sensor through beam Omron EE-SX670-WR 1M

Pre-wired Models

Infrared light

Appearance	Sensing method	Sensing distance		Output configuration	Indicator mode	Connecting method	Model	
							NPN output	PNP output
Standard 	Through-beam type (with slot)		5 mm (slot width)	Dark-ON/ Light-ON (selectable) *	Incident light	Pre-wired Models (1m)	**EE-SX670-WR 1M**	**EE-SX670P-WR 1M**
L-shaped 							**EE-SX671-WR 1M**	**EE-SX671P-WR 1M**
T-shaped, slot center 7 mm 							**EE-SX672-WR 1M**	**EE-SX672P-WR 1M**
Close-mounting 							**EE-SX673-WR 1M**	**EE-SX673P-WR 1M**
Close-mounting 							**EE-SX674-WR 1M**	**EE-SX674P-WR 1M**
T-shaped, slot center 10 mm 							**EE-SX675-WR 1M**	**EE-SX675P-WR 1M**
F-shaped 							**EE-SX676-WR 1M**	**EE-SX676P-WR 1M**
R-shaped 							**EE-SX677-WR 1M**	**EE-SX677P-WR 1M**

* Dark-ON operation can be used when the L terminal is left unconnected or Light-ON operation can be used when the L terminal and positive (+) terminal are connected to each other. Do not connect the L terminal to 0 V when using dark-ON operation.

Accessories (Order Separately) Connector Models

Type		Cable length	Model	Remarks
Connector			**EE-1001**	
			EE-1001-1	L terminal and positive (+) terminal are already short-circuited.
			EE-1009	
	Connector with Cable	1 m	**EE-1006**	
			EE-1010	
		2 m	**EE-1006**	
			EE-1010	
	Connector with Robot Cable	1 m	**EE-1010-R**	
		2 m	**EE-1010-R**	
Connector Hold-down Clip			**EE-1006A**	For EE-1006 only.

* Refer to *Accessories* for details.

Ratings and Specifications

Item		Type	Standard	L-shaped	T-shaped, slot center 7 mm	Close-mounting		T-shaped, slot center 10 mm	F-shaped	R-shaped
	NPN models	Connector models	EE-SX670 EE-SX670A EE-SX470	EE-SX671 EE-SX671A EE-SX471	EE-SX672 EE-SX672A EE-SX472	EE-SX673 EE-SX673A EE-SX473	EE-SX674 EE-SX674A EE-SX474	EE-SX675	EE-SX676	EE-SX677
		Pre-wired models	EE-SX670-WR	EE-SX671-WR	EE-SX672-WR	EE-SX673-WR	EE-SX674-WR	EE-SX675-WR	EE-SX676-WR	EE-SX677-WR
	PNP models	Connector models	EE-SX670P EE-SX670R EE-SX470P	EE-SX671P EE-SX671R EE-SX471P	EE-SX672P EE-SX672R EE-SX472P	EE-SX673P EE-SX673R EE-SX473P	EE-SX674P EE-SX674R EE-SX474P	EE-SX675P	EE-SX676P	EE-SX677P
		Pre-wired models	EE-SX670P-WR	EE-SX671P-WR	EE-SX672P-WR	EE-SX673P-WR	EE-SX674P-WR	EE-SX675P-WR	EE-SX676P-WR	EE-SX677P-WR
Sensing distance			5 mm (slot width)							
Sensing object			Opaque: 2 × 0.8 mm min.							
Differential distance			0.025 mm							
Light source			GaAs infrared LED with a peak wavelength of 940 nm							
Indicator *1			Light indicator (red) (turns ON when light is interrupted for models with A or R suffix)							
Supply voltage			5 to 24 VDC ±10%, ripple (p-p): 10% max.							
Current consumption			35 mA max. (NPN models), 30 mA max. (PNP models)							
Control output			NPN open collector: 5 to 24 VDC, 100 mA max. 100 mA load current with a residual voltage of 0.8 V max. 40 mA load current with a residual voltage of 0.4 V max. OFF current (leakage current): 0.5 mA max. PNP open collector: 5 to 24 VDC, 50 mA max. 50 mA load current with a residual voltage of 1.3 V max. OFF current (leakage current): 0.5 mA max.							
Response frequency *2			1 kHz min. (3 kHz average)							
Ambient illumination			1,000 lx max. with fluorescent light on the surface of the receiver.							
Ambient temperature range			Operating: −25 to +55°C, Storage: −30 to +80°C (with no icing or condensation)							
Ambient humidity range			Operating: 5% to 85%, Storage: 5% to 95% (with no icing or condensation)							
Vibration resistance			Destruction: 20 to 2,000 Hz (peak acceleration: 100 m/s^2) 1.5-mm double amplitude for 2 h (4-min periods) each in X, Y, and Z directions							
Shock resistance			Destruction: 500 m/s^2 for 3 times each in X, Y, and Z directions							
Degree of protection			IEC60529 IP50							
Connecting method			Connector Models (direct soldering possible), Pre-wired Models (Standard cable length: 1 m), Models with Connectors (Standard cable length: 0.1 m)							
Weight	Connector models		Approx. 3.1 g	Approx. 3 g	Approx. 2.4 g	Approx. 2.3 g	Approx. 3 g	Approx. 2.7 g	Approx. 2.2 g	Approx. 2.2 g
	Pre-wired models		Approx. 18.9 g	Approx. 17.3 g	Approx. 17.8 g	Approx. 16.8 g	Approx. 17.1 g	Approx. 18.3 g	Approx. 16.9 g	Approx. 16.9 g
Material	Case		Polybutylene phthalate (PBT)							
	Cover		Polycarbonate							
	Emitter/receiver									

*1. The indicator is a GaP red LED (peak wavelength: 690 nm).
*2. The response frequency was measured by detecting the rotating disk shown at the right.

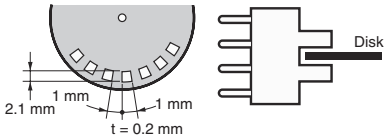

EE-SX47/67

Engineering Data (Typical)

Sensing Position Characteristics

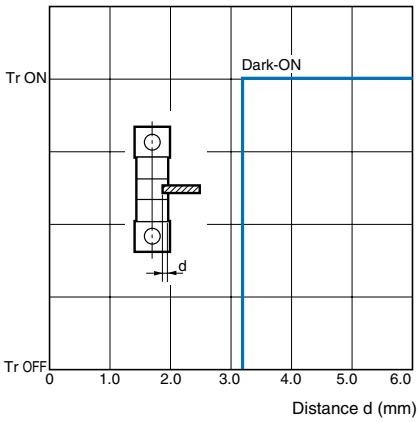

Sensing Position Characteristics

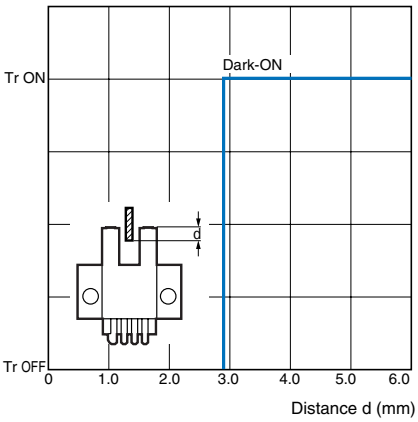

Repeated Sensing Position Characteristics

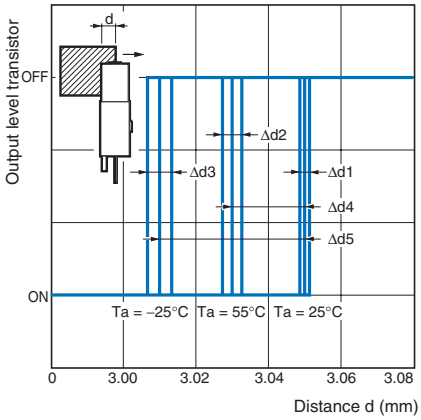

Vcc =12 V, No. of repetitions: 20, Δd1 = 0.002 mm, Δd2 = 0.004 mm, Δd3 = 0.005 mm, Δd4 = 0.02 mm, Δd5 = 0.04 mm

Note: The data applies to dark status. Operation may be affected by external light interference or light coming through the sensing object.

I/O Circuit Diagrams

NPN Output

Model	Output configuration	Timing charts	Terminal connections	Output circuit
EE-SX67□ EE-SX67□-WR	Light-ON	Incident / Interrupted Light indicator (red): ON / OFF Output transistor: ON / OFF Load (e.g., relay): Operates / Releases	Short-circuited between Ⓛ terminal and positive ⊕ terminal	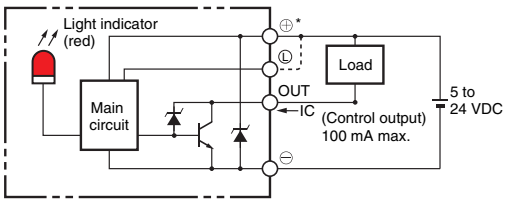
	Dark-ON	Incident / Interrupted Light indicator (red): ON / OFF Output transistor: ON / OFF Load (e.g., relay): Operates / Releases	Open between Ⓛ terminal and positive ⊕ terminal *1	
EE-SX670A EE-SX671A EE-SX672A EE-SX673A EE-SX674A	Light-ON	Incident / Interrupted Light indicator (red): ON / OFF Output transistor: ON / OFF Load (e.g., relay): Operates / Releases	Short-circuited between Ⓛ terminal and positive ⊕ terminal	
	Dark-ON	Incident / Interrupted Light indicator (red): ON / OFF Output transistor: ON / OFF Load (e.g., relay): Operates / Releases	Open between Ⓛ terminal and positive ⊕ terminal *1	
EE-SX470 EE-SX471 EE-SX472 EE-SX473 EE-SX474	Light-ON	Incident / Interrupted Light indicator (red): ON / OFF Output transistor: ON / OFF Load (relay): Operates / Releases	---	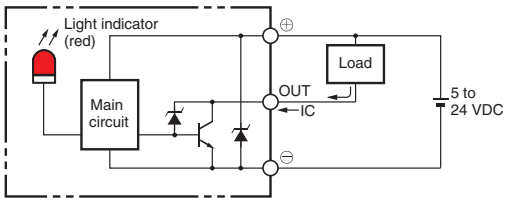

*The terminal arrangement depends on the model. Check the dimensional diagrams.

*1. Do not connect the L terminal to 0 V when using dark-ON operation.

PNP Output

Model	Output configuration	Timing charts	Terminal connections	Output circuit
EE-SX67□P EE-SX67□P-WR	Light-ON	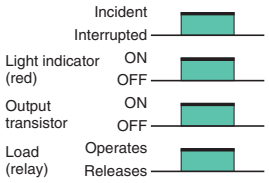	Short-circuited between Ⓛ terminal and positive ⊕ terminal	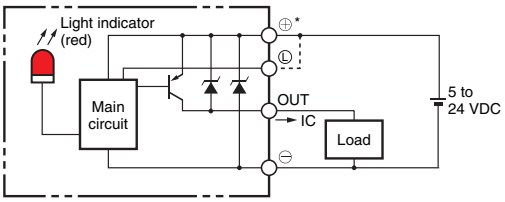
	Dark-ON	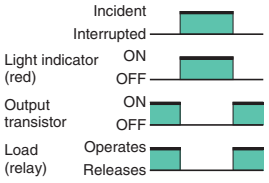	Open between Ⓛ terminal and positive ⊕ terminal *1	
EE-SX670R EE-SX671R EE-SX672R EE-SX673R EE-SX674R	Light-ON	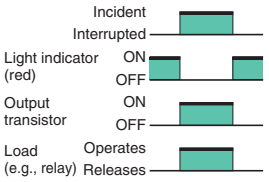	Short-circuited between Ⓛ terminal and positive ⊕ terminal	*The terminal arrangement depends on the model. Check the dimensional diagrams.
	Dark-ON	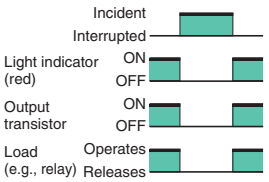	Open between Ⓛ terminal and positive ⊕ terminal *1	
EE-SX470P EE-SX471P EE-SX472P EE-SX473P EE-SX474P	Light-ON	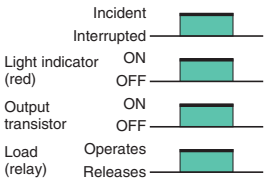	---	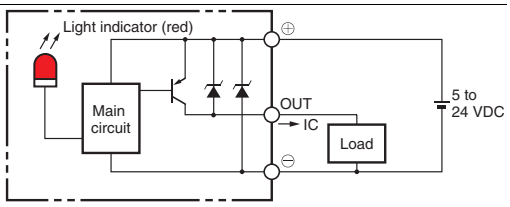

*1. Do not connect the L terminal to 0 V when using dark-ON operation.

Safety Precautions

Refer to *Warranty and Limitations of Liability*.

⚠ WARNING

This product is not designed or rated for ensuring safety of persons either directly or indirectly. Do not use it for such purposes.

Precautions for Safe Use

● Operating Environment

These Photomicrosensors have an IP50 (conforms to IEC) enclosure and do not have a water-proof or dust-proof structure. Therefore, do not use them in applications in which the sensor will be subjected to splashes from water, oil, or any other liquid. Liquid entering the Sensor may result in malfunction.

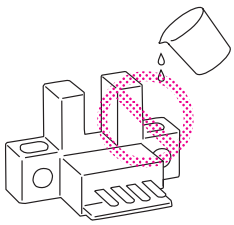

Precautions for Correct Use

Make sure that this product is used within the rated ambient environment conditions.

● Installation

- When direct soldering to the terminals, use the following guidelines.

Soldering Conditions

Item	Temperature	Permissible time	Remarks
Soldering iron	350°C max.	3 s max.	The portion between the base of the terminals and the position 1.5 mm from the terminal base must not be soldered.

- The terminal base uses a polycarbonate resin, which could be deformed by excessive soldering heat, resulting in damage to the product's functionality.

● Lot Number and Model Number Legend

In the following diagrams, 376d indicates the lot number and factory where the product was manufactured. Do not include this code with the model number when ordering.

EE-SX□70□

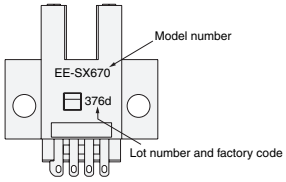

EE-SX670-WR/670P-WR

Terminal Arrangement

Brown	Vcc
Pink	L
Blue	GND (0 V)
Black	OUTPUT

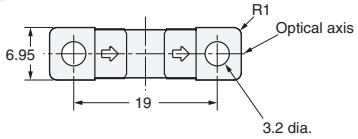

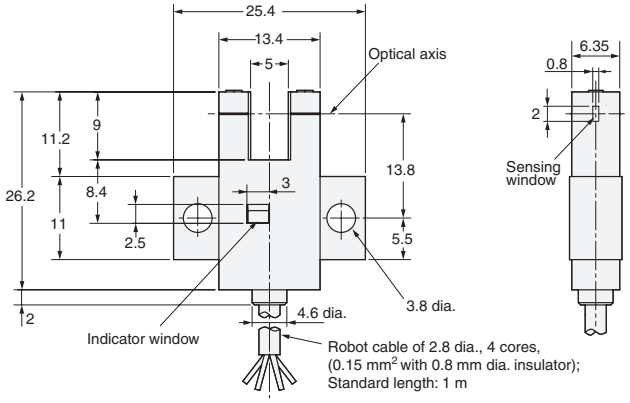

EE-SX671-WR/671P-WR

Terminal Arrangement

Brown	Vcc
Pink	L
Blue	GND (0 V)
Black	OUTPUT

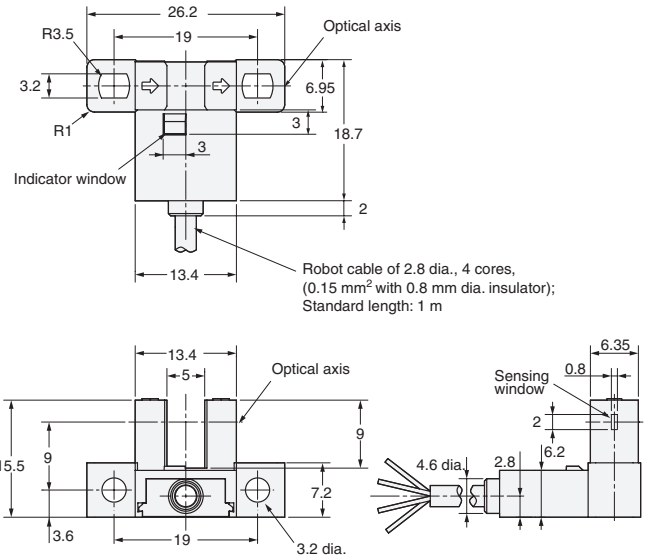

EE-SX672-WR/672P-WR

Terminal Arrangement

Brown	Vcc
Pink	L
Blue	GND (0 V)
Black	OUTPUT

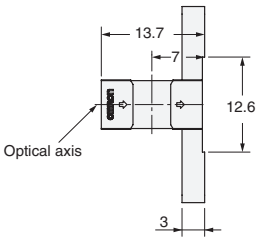

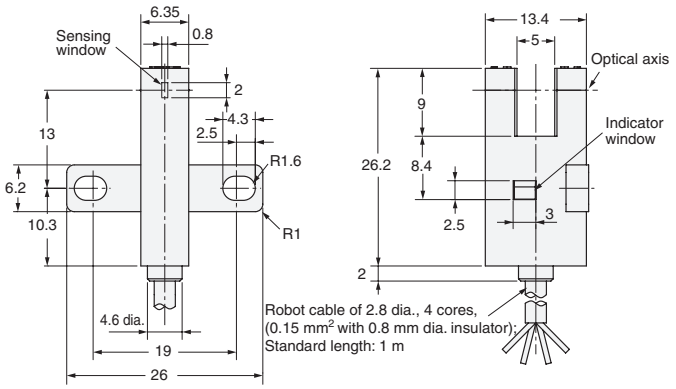

EE-SX673-WR/673P-WR

Terminal Arrangement

Brown	Vcc
Pink	L
Blue	GND (0 V)
Black	OUTPUT

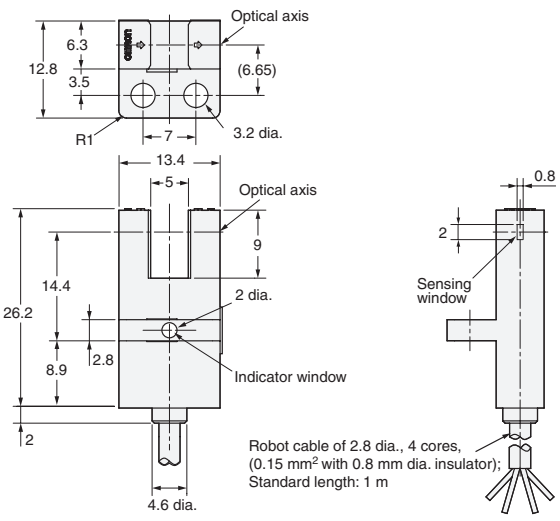

C.19 DC gearmotor Como Drills 918D100112

MFA/COMO DRILLS

918D SERIES 25mm SINGLE RATIO METAL GEARBOX (RE280 MOTOR/RE 280/1 MOTOR)

WITH 2mm OUTPUT SHAFT (15:1 ONLY)

WITH 4mm OUTPUT SHAFT (ALL RATIOS)

RATIOS NOW AVAILABLE AS EX-STOCK ITEMS.

918D151 (1.5v - 3v) WITH RE 280 MOTOR (RATIO 15:1). 2mm SHAFT
918D151/1 (1.5v - 3v) WITH RE 280 MOTOR (RATIO 15:1). 4mm SHAFT
918D301/1 (1.5v - 3v) WITH RE 280 MOTOR (RATIO 30:1). 4mm SHAFT
918D1001/1 (1.5v - 3v) WITH RE 280 MOTOR (RATIO 100:1). 4mm SHAFT
918D2501/1 (1.5v - 3v) WITH RE 280 MOTOR (RATIO 250:1). 4mm SHAFT
918D3601/1 (1.5v - 3v) WITH RE280/3 MOTOR (RATIO 360:1). 4mm SHAFT
918D5001/1 (1.5v - 3v) WITH RE280 MOTOR (RATIO 500:1). 4mm SHAFT

918D15112 (12v - 24v) WITH RE 280/1 MOTOR (RATIO 15:1). 2mm SHAFT
918D15112/1 (12v - 24v) WITH RE 280/1 MOTOR (RATIO 15:1). 4mm SHAFT
918D30112/1 (12v - 24v) WITH RE 280/1 MOTOR (RATIO 30:1). 4mm SHAFT
918D100112/1 (12v - 24v) WITH RE 280/1 MOTOR (RATIO 100:1). 4mm SHAFT
918D250112/1 (12v - 24V) WITH RE280/1 MOTOR (RATIO 250:1). 4mm SHAFT
918D360112/1 (12v - 24v) WITH RE280/4 MOTOR (RATIO 360:1). 4mm SHAFT
918D500112/1 (12v - 24v) WITH RE280 MOTOR (RATIO 500:1). 4mm SHAFT
918D10241/1 (12v - 24v) WITH RE280/1 MOTOR (RATIO 1024:1). 4mm SHAFT

This miniature gearbox is of steel and brass construction with brass gears and is mounted on a 1mm thickness steel bracket. It incorporates a high quality three pole motor with sleeved bearings. The design and construction of the unit make it suitable for a host of model and light industrial applications.

MOTOR DATA. (RE-280 & RE-280/1)

MODEL	VOLTAGE		NO LOAD		AT MAXIMUM EFFICIENCY					STALL TORQUE	
	OPERATING RANGE	NOMINAL	SPEED	CURRENT	SPEED	CURRENT	TORQUE		OUTPUT	EFF	
			R.P.M.	A	R.P.M.	A	oz - in	g - cm	W	%	oz - in	g - cm
RE - 280	1.5 - 3 .0	1.5v CONSTANT	4600	0.120	3750	0.53	0.160	11.53	0.44	56.2	0.86	62.0
RE - 280	1.5 - 3.0	3.0v CONSTANT	9200	0.155	7800	0.85	0.278	20.00	1.60	62.3	1.81	130.0
RE - 280/1	12 - 24	12v CONSTANT	8400	0.10	6300	0.30	0.347	25.0	1.62	44.87	1.389	100
RE - 280/3	1.5 - 3	3v CONSTANT	8800	0.24	7200	1.06		23.2	1.71	53.8		126
RE - 280/4	12 - 24	12v CONSTANT	8224	0.046	6636	0.194		19.2		56.1		99.3

REDUCTION TABLE. R.P.M.

Stall Current RE280 at 1.5v = 2.41A

SUPPLY VOLTAGE	1.5v	3.0v	6v	12v	18v	24v
918D61	730	1409				
918D6112			476	1158	1974	2684
918D151	319	604				
918D15112			193	472	778	1086
918D301	159	296				
918D30112			96	238	405	543
918D1001	43	87				
918D100112			30	74	124	166
918D2501	18	34				
918D250112			12	29	50	67
918D3601	11	23				
918D360112			10	23	35	48
918D5001	8	15				
918D500112			7.5	16	25	33
918D10241	4.5	8.75				
918D1024112			2.8	7.25	12	16.75

WEIGHT	
918D61	75g
918D6112	75g
918D151	75g
918D15112	72g
918D301	75g
918D30112	75g
918D1001	77g
918D100112	77g
918D2501	78g
918D250112	78g
918D3601	87g
918D360112	87g
918D5001	g
918D500112	g
918D10241	89g
918D1024112	89g

GEARBOX RATINGS

RATED TOLERANCE TORQUE (g.cm)		MAX. MOMENTARY TOLERANCE TORQUE
6:1	300	900
15:1	400	1200
30:1	600	1800
100:1	1000	3000
250:1	1200	3600
360:1	1200	3600
500:1	1200	3600
1024:1	1500	4500

Note: Motor speeds may vary by (+) or (-) 12.5%

IMPORTANT NOTICE
At very low ratios the torque produced by this geared motor combination may exceed the maximum permissible torque of the gearbox. In this situation the unit must not be allowed to stall as this may damage the gears. Please refer to the table of the gearbox ratings to ascertain the appropriate geared motor combination.

IMPORTANT NOTICE
Due to the wide range of applications for this product it is the users responsibility to establish the products suitability for their individual purpose(s).

NOTE: To establish Torque Rating in nM, divide g.cm by 10,197.0

MFA/COMO DRILLS FELDERLAND LANE. WORTH. DEAL. KENT. CT14 OBT
TEL: 01304 612132. FAX: 01304 614696
E-MAIL: info@mfacomo.com www.mfacomodrills.com

918D SERIES 25mm SINGLE RATIO METAL GEARBOX

GEARBOX DIMENSIONS.

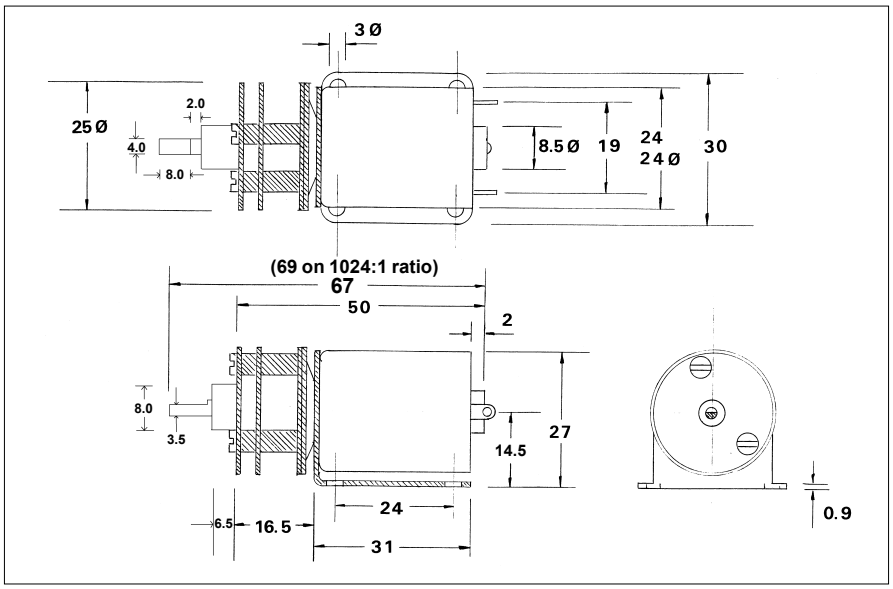

Part No. 1071. Anti vibration mount. M3

Part No. 918D8. Stainless Steel Shaft. 4mm OD x 150mm

Part No. 918D10. Bearing Blocks. 4mm I.D. (20 x 20 x 12.5mm)

Part No. 1105/61 Universal Coupling. 4mm - 4mm

ACCESSORIES FOR 918D SERIES GEARBOX.

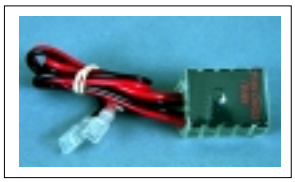

Part No. 917D9. Voltage Regulator. (6-15v DC Input, 3v, 1.5amp output)
Part No. 917D10. Voltage Regulator. (6-15v DC Input. 1.5v, 1.5amp output)
Part No. 917D11. Voltage Regulator. (6-15v DC Input. 4.5v, 1.5amp output)
(Above for 280 motor only)

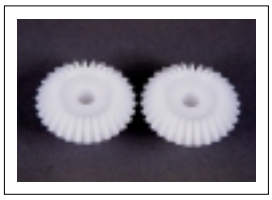

Part No. 918D7. Nylon Bevel Gears (1:1). O.D. 17.2mm. 4mm I.D.

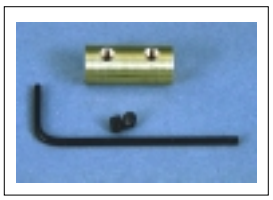

Part No. 918D1. In-Line Coupling. 2mm - 3mm. (Dia. 8mm x 18.4mm)
Part No. 918D1/1. In-Line Coupling 4mm - 4mm. (Dia. 8mm x 18.4mm)

Part No. 918D4. Gear Adapter. 2mm I.D. Shaft Dia 6mm.
Part No. 918D4/1 Gear Adapter. 4mm I.D. Shaft Dia 6mm.

Part No. 917D2458. Pinions (Plastic) 12 tooth. 1.9mm I.D.

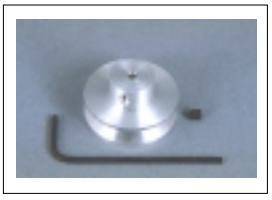

Part No. 918D2. Pulley. 2mm I.D. (25mm dia. x 14.75mm) (Aluminium)
Part No. 918D2/1. Pulley 4mm I.D. (25mm dia. x 14.75mm) (Aluminium)

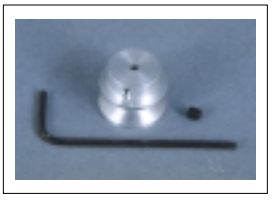

Part No. 918D3. Pulley. 2mm I.D. (16mm dia. x 13.6mm) (Aluminium)
Part No. 918D3/1. Pulley 4mm I.D. (16mm dia x 13.6mm((Aluminium)

Part No. 917D2515. "O" Ring 70mm x 5mm Dia.

Subject to minimum order quantities of 250 units, the following ratios are also available with a six week lead-time.
The physical dimensions of these other gearboxes may vary from the data as illustrated above. Details of individual gearboxes are available upon request.

GEARBOX 6:1 with RE280 motor (1.5v - 3v)	GEARBOX 6:1 with RE280/1 motor (12v - 24v)
GEARBOX 10:1 with RE280 motor (1.5v - 3v)	GEARBOX 10:1 with RE280/1 motor (12v - 24v)
GEARBOX 21:1 with RE280 motor (1.5v - 3v)	GEARBOX 21:1 with RE280/1 motor (12v - 24v)
GEARBOX 44:1 with RE280 motor (1.5v - 3v)	GEARBOX 44:1 with RE280/1 motor (12v - 24v)
GEARBOX 60:1 with RE280 motor (1.5v - 3v)	GEARBOX 60:1 with RE280/1 motor (12v - 24v)
GEARBOX 77:1 with RE280 motor (1.5v - 3v)	GEARBOX 77:1 with RE280/1 motor (12v - 24v)
GEARBOX 112:1 with RE280 motor (1.5v - 3v)	GEARBOX 112:1 with RE280/1 motor (12v - 24v)
GEARBOX 150:1 with RE280 motor (1.5v - 3v)	GEARBOX 150:1 with RE280/1 motor (12v - 24v)
GEARBOX 170:1 with RE280 motor (1.5v - 3v)	GEARBOX 170:1 with RE280/1 motor (12v - 24v)
GEARBOX 200:1 with RE280 motor (1.5v - 3v)	GEARBOX 200:1 with RE280/1 motor (12v - 24v)
GEARBOX 250:1 with RE280 motor (1.5v - 3v)	GEARBOX 250:1 with RE280/1 motor (12v - 24v)
GEARBOX 320:1 with RE280 motor (1.5v - 3v)	GEARBOX 320:1 with RE280/1 motor (12v - 24v)
GEARBOX 360:1 with RE280 motor (1.5v - 3v)	GEARBOX 360:1 with RE280/1 motor (12v - 24v)
GEARBOX 400:1 with RE280 motor (1.5v - 3V)	GEARBOX 400:1 with RE280/1 motor (12v - 24v)
GEARBOX 500:1 with RE280 motor (1.5v - 3v)	GEARBOX 500:1 with RE280/1 motor (12v - 24v)
GEARBOX 700:1 with RE280 motor (1.5v - 3v)	GEARBOX 700:1 with RE280/1 motor (12v - 24v)
GEARBOX 800:1 with RE280 motor (1.5v - 3v)	GEARBOX 800:1 with RE280/1 motor (12v - 24v)
GEARBOX 900:1 with RE280 motor (1.5v - 3v)	GEARBOX 900:1 with RE280/1 motor (12v - 24v)
GEARBOX 1153:1 with RE280 motor (1.5v - 3v)	GEARBOX 1153:1 with RE280/1 motor (12v - 24v)

MFA/COMO DRILLS FELDERLAND LANE. WORTH. DEAL. KENT. CT14 OBT
TEL: 01304 612132. FAX: 01304 614696
E-MAIL: info@mfacomo.com www.mfacomodrills.com

C.20 Roller lever microswitch Cherry D459-V3RD

Miniature Snap Switch

Single and Double Pole
D4 Series

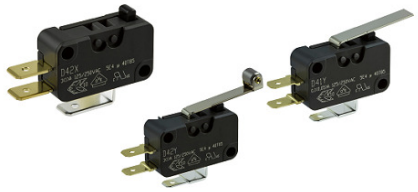

Features
- Choice of standard or light operating force
- Long life coil spring mechanism
- RoHS compliant
- Cadmium free
- Various aux actuators
- Various terminal types
- Agency approved extended life versions available

Standard Parts[1]

D413-R1AA-G2	D429-R1TD-G2	D433-R1AA-G2	D443-R1LD-G2	D449-R1LL-G2	D453-R1RA-G2
D413-R1LA-G2	D429-R1AA-G2	D433-R1LD-G2	D443-R1MD-G2	D449-R1MD-G2	D453-R1RD-G2
D413-R1LD-G2	D429-R1LD-G2	D433-R1RA-G2	D443-R1RA-G2	D449-R1ML-G2	D459-R1AA-G2
D413-R1RA-G2	D429-R1LL-G2	D433-R1RD-G2	D443-R1RD-G2	D449-R1RA-G2	D459-R1LD-G2
D419-R1AA-G2	D429-R1MD-G2	D439-R1LL-G2	D449-R1AA-G2	D449-R1RD-G2	D459-R1LL-G2
D423-R1RA-G2	D429-R1ML-G2	D439-V1ML-G2	D449-R1LD-G2	D453-B8AA-G2	D459-R1ML-G2
D423-R1RD-G2		D443-R1AA-G2		D453-R1AA-G2	

[1]The part number configuration matrix below provides details to the part numbers above.
For configurable part numbers that are not listed above, not listed in your region, or for custom part numbers, contact the factory or your distributor.
For information on crossing discontinued U.S. only part numbers, see D4 cross-reference chart at www.cherryswitches.com.

Part Number Breakdown

D413-R1AA-G2 (most part numbers end in –G2; see D4 cross-reference chart for exceptions)

Series

D4

Contact Rating[2]

1	0.1 A
2	3 A
3	5 A
4	10 A
5	15 A
8	21 A

Configuration[3]

85 °C			125 °C		150 °C		
1	SPST – NO	Standard Op. Force	G	SPST – NO	S	SPST – NO	Light Op. Force
2	SPST – NC		H	SPST – NC	T	SPST – NC	
3	SPDT		M	SPDT	U	SPDT	
7	SPST – NO	Light Op. Force	N	SPST – NO			
8	SPST – NC		P	SPST – NC			
9	SPDT		R	SPDT			

[2]UL AC current rating; see table on reverse for complete details
[3]D48 only available with light operating force

Terminal Type mm (inches)

A1	Welding
B8	Short solder
P4	1.2 x 0.5 (0.047 x 0.020) PCB, underside*
P5	1.2 x 0.5 (0.047 x 0.020) PCB, rear*
PA	1.2 x 0.5 (0.047 x 0.020) PCB, housing side*
PB	1.2 x 0.5 (0.047 x 0.020) PCB, cover side*
Q1	4.8 x 0.8 (0.187 x 0.032) QC, straight*
Q3	4.8 x 0.8 (0.187 x 0.032) QC, dog leg*

*not available for D48 **not available for D45 or D48

R1	4.8 x 0.5 (0.187 x 0.020) QC, straight**
R3	4.8 x 0.5 (0.187 x 0.020) QC, dog leg**
S1	Solder with temp stop
V1	6.3 x 0.8 (0.250 x 0.032) QC, straight
V3	6.3 x 0.8 (0.250 x 0.032) QC, dog leg
W9	Screw*
X5	1.5 x 0.8 (0.059 x 0.032) QC, 2.5 mm grid
Y5	6.3 x 0.8 (0.250 x 0.032) QC, 5 mm grid

Actuator Type mm (inches)

		Actuation length
AA	Button	N/A
JA	SS lever, standard ratio	21.2 (0.835)
JD	SS lever, standard ratio	35.6 (1.4)
JL	SS lever, standard ratio	69.9 (2.75)
KA	SS lever, high ratio	25.7 (1.01)
KD	SS lever, high ratio	40.1 (1.58)
KL	SS lever, high ratio	74.4 (2.93)
LA	Lever, standard ratio	21.2 (0.835)
LD	Lever, standard ratio	35.6 (1.4)
LL	Lever, standard ratio	69.9 (2.75)

		Actuation length
MA	Lever, high ratio	25.7 (1.01)
MD	Lever, standard ratio	40.1 (1.58)
ML	Lever, high ratio	74.4 (2.93)
RA	Roller, standard ratio	20.6 (0.811)
RD	Roller, standard ratio	34.1 (1.34)
SA	Roller, simulated, rear mount	20.6 (0.811)
TA	Roller, high ratio	25.1 (0.988)
TD	Roller, high ratio	38.6 (1.52)
UA	Roller, simulated, front mount	25.1 (0.988)

For actuator details, see D4 actuator reference sheet at www.cherryswitches.com

Electrical Specifications – Contact Ratings

Contact	EN61058	UL1054
1	0.1 (0.5) A, 250 VAC; 0.5 A, 30 VDC; 1 (1) A, 250 VAC	0.1 A, 125/250 VAC; 0.5 A, 30 VDC; 1 A, 125 VAC
2	3 (1) A, 250 VAC	3 A, 125/250 VAC; 1/10 HP, 250 VAC
3	6 (2) A, 250 VAC	5 A, 125/250 VAC; ¼ HP, 250 VAC
4	10 (3) A, 250 VAC	10 A, 125/250 VAC; 6 A, 30 VDC; ½ HP, 125/250 VAC
5	16 (4) A, 250 VAC	15 A, 125/250 VAC; ½ HP, 125-250 VAC
8	21 (8) A, 250 VAC	21 A, 250 VAC; 1 HP, 125 VAC; 2 HP, 250 VAC

UL file number E314201

Environmental and Mechanical Specifications

Operating Temperature	-40 °C to 85, 125 or 150 °C (-40 °F to 185 , 257 or 302 °F)
Flammability Rating	UL 94V-0

Operating life – electrical life at rated load, 85 °C

Contact	EN61058	UL1054[4]
1	50,000	6,000
2	50,000	6,000
3	50,000	6,000
4	50,000	6,000
5	50,000	6,000
7	10,000	6,000

[4]Extended life available

Material Specifications

Case	Thermoplastic Polyester PET
Cover	Thermoplastic Polyester PET
Actuating Button	Thermoplastic Acetyl (POM) 85 °C, Thermoplastic Polyester (PET) 125 or 150 °C
Contacts	Gold Cross Point (D41), Silver (D42), Silver Alloy (D43-D48)
Terminals	Brass
Auxiliary Actuator	Stainless Steel or Cold-Rolled Steel (Nickel Plated)
Moving Blade	Silver Plated Brass

Environmental Specifications

Ambient Temperature	-40 °C to 85 °C/120 °C (-40 °F to 185 °F/248 °F)
Operating Force	70 – 280 cN (model dependent, without actuator)
Total Travel	1.6 mm
Ingress Protection	IP50

Dimensions mm (inches) and terminal configurations

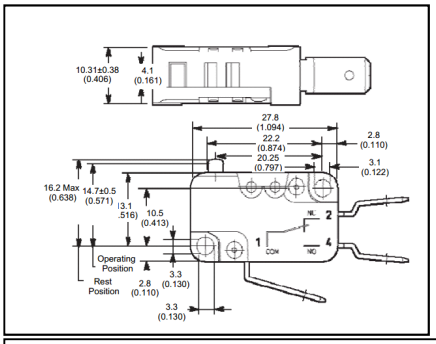

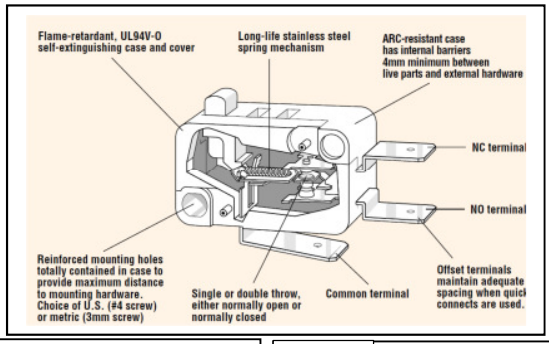

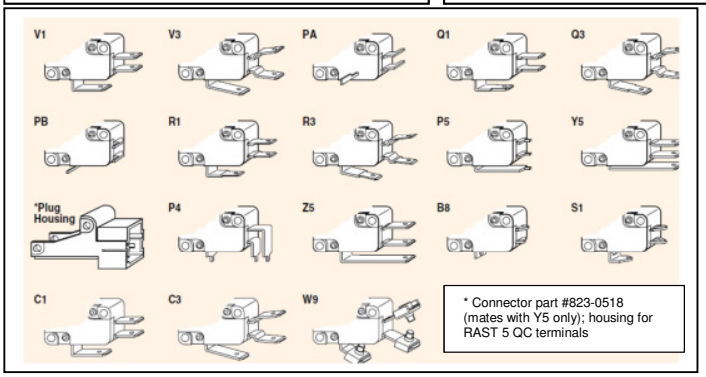

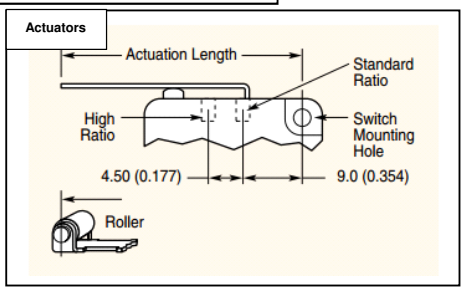

References

[1] Rui Barbosa. Conceção e automatização de um dispositivo para medir a resistência ao impacto de ligações adesivas. Master's thesis, Faculdade de Engenharia da Universidade do Porto, 2014.

[2] Carlos Castro. Desenvolvimento de um dispositivo experimental para medir a resistência ao impacto de ligações adesivas. Master's thesis, Faculdade de Engenharia da Universidade do Porto, 2014.

[3] Lucas F.M. da Silva, David A. Dillard, Bamber R.K. Blackman, and Robert D. Adams. *Testing Adhesive Joints: Best Practices*. Wiley VCH, 2012.

[4] J A Harris and R D Adams. An assessment of the impact performance of bonded joints for use in high energy absorbing structures. *Proceedings of the Institution of Mechanical Engineers, Part C: Journal of Mechanical Engineering Science*, 199(2):121–131, 1985.

[5] Lijuan Liao, Toshiyuki Sawa, and Chenguang Huang. Experimental and fem studies on mechanical properties of single-lap adhesive joint with dissimilar adherends subjected to impact tensile loadings. *International Journal of Adhesion & Adhesives*, February 2013.

[6] Thomas Carlberger, Anders Biel, and Ulf Stigh. Influence of temperature and strain rate on cohesive properties of a structural epoxy adhesive. *Springer*, March 2009.

[7] B. R. K. Blackman, A. J. Kinloch, A. C. Taylor, and Y. Wang. The impact wedge-peel performance of structural adhesives. *Journal of Materials Science*, August 1999.

[8] Instron. Impact Performance of Adhesive Bonds under Impact – ISO 11343, 2007.

[9] Dassault Systemes SolidWorks Corporation. SolidWorks.

[10] Farrat. Detailed vibration isolation theory, from. http://www.farrat.com/resources/detailed-vibration-isolation-theory, April 2016.

[11] Elesa+Ganter. LW.A – Vibration-Damping Leveling Elements, from. http://www.elesa-ganter.com/en/2/sp/7954/4/88/vibration-damping-levelling-elements/lw.a/eg/, April 2016.

[12] José Simões Morais. *Desenho Técnico Básico*. Gráficos Reunidos, Lda, 27th edition, 2007.

[13] Luiz Fernando Martha, Associate Professor PUC-Rio. Ftool.

[14] Richard G. Budynas and J. Keith Nisbett. *Shigley's Mechanical Engineering Design*. McGraw-Hill, 9th edition edition, 2008.

[15] Singiresu S. Rao. *Mechanical Vibrations*. Prentice Hall, 5th edition edition, 2011.

[16] Mathworks. MATLAB.

[17] Shaeffler Technologies AG & Co. KG. Features linear bearings and linear bearing and housing units KBO..-PP. http://medias.schaeffler.com/medias/en!hp.info/KBO..-PP, April 2016.

[18] igus GmbH. igus - fusos drylin - visão geral dos produtos. http://www.igus.pt/wpck/2371/-drylin _trapezgewindemutter, May 2016.

[19] Parvalux. Permanent magnet catalog, 2009.

[20] Transtecno Group. Motoredutor de rosca sem fim com motor em continua | Transtecno. http://www.transtecno.com/pt-br/redutores-motoredutores/12v-24v-cc/motoredutor-de-rosca-sem-fim-motor/, May 2016.

[21] Electromen. Electromen :: EM-12A PWM DC-MOTOR CONTROL UNIT 24V 8A 200W. http://electromen.com/en/products/item/motor-controllers/dc-motor-below-10A/EM-12A, June 2016.

[22] RS Components Ltd. Rs components | electronic and electrical components. http://uk.rs-online.com/, June 2016.

[23] Parker Hannifin Ltd. Parker Legris Connectic Low Pressure, technical components for industrial fluids. http://http://www.parkerlegris.com/, June 2016.

[24] Kistler Holding AG. Kistler | measuring systems and sensors. https://www.kistler.com/ls/en/, June 2016.